

April 2015

A Decision Support System for Assessing the Ecohydrological Response of Toolibin Lake

J. Z. Coletti, R. Vogwill, B. Busch, J.N. Callow & M.R. Hipsey

Report prepared for:
Department of Parks and Wildlife
Government of Western Australia



THE UNIVERSITY OF
WESTERN AUSTRALIA



Executive Summary

Overview

The sustainable management of the Toolibin Lake wetland system requires a quantitative understanding of ecosystem processes sufficient to guide management activities. Given the complexity of the hydrological processes throughout the Toolibin Lake catchment, it was identified that a comprehensive model framework was required to guide decision making by predicting the effect of hydrologic engineering, land use changes and climate variability on wetland vegetation. This report documents in detail the integrated model system developed for the Department of Parks and Wildlife (DPaW) under the project "Decision Tools for Managing Hydrological Threats to Biodiversity Assets". This project started in 2010 with the aim of improving our understanding of the hydrology of the Toolibin Catchment following on from previous work in Lake Bryde Natural Diversity Recovery Catchment.

The scope of the study was to:

- a) develop an integrated model system to be used for decision support to maximize wetland vegetation health. This model system needs to be suited to provide practical guidance to DPaW on the operation of the surface water diversion and groundwater pumping infrastructure, in addition to being able to assess catchment and lake bed re-vegetation practices;
- b) validate the model against available hydrological and vegetation data, ranging from event scale to decadal scale dynamics;
- c) demonstrate the utility of the model for answering a number of management questions on how to best protect high value biodiversity assets through an application of re-vegetation and/or engineering interventions.

An Integrated Model System

Following a review of the available data and previous studies, three distinct zones of hydrological function were identified in the catchment: the upland region, the valley floor and the wetland itself. We concluded that each one of these hydrological zones requires a different modelling approach. The main focus of the model system was to capture the water and salt balance of the lake-bed and associated response of the high conservation value tree species, in particular *Melaleuca strobophylla* and *Casuarina obesa*, to changes in hydrology. These hydrological changes have been brought about by historic land clearing and catchment management activities, we therefore integrated a custom wetland ecohydrology model setup for Toolibin Lake within a semi-distributed catchment hydrology model able to predict salt export, including long-term regional change in surface and groundwater dynamics. Additional local scale issues were assessed through implementation of a hydraulic model to answer high-resolution drainage related questions in the valley floor.

Considering that a single numerical tool for managing the catchment would be more appropriate for testing scenarios, summarizing hydrological behaviours and communicating results, the collection of models were integrated via an automated coupling process, to test and quantify the ecohydrological benefit of management interventions. It is envisioned that this will assist DPaW to allocate resources in the most effective manner whilst achieving the desired outcome of minimising wetland salinisation and maximising vegetation health.

Within the wetland system itself the lake and groundwater levels, including salinity, showed a good agreement between the observed and modelled values. Vegetation dynamics were not as straightforward to validate due to poor data availability, however, biomass predictions and growth trends were predicted within the range described by the literature and available field data. A sensitivity analysis of key vegetation parameters was also undertaken. In the upland and valley floor domains, the model predictions were assessed against available flow gauging, surface water salinities and sub-catchment scale average groundwater levels. The lack of long-term data limited our ability to complete a comprehensive model calibration (e.g., in some gauges only one flow event was recorded in 5 years), however, manual adjustments of soil and vegetation parameters allowed us to confidently simulate the magnitude and behavior of surface runoff and salt export in accordance with field measurements. A further hydrological 'process validation' was undertaken by comparing predicted water fluxes with those described in the literature as typical of the WA wheatbelt, and used to build confidence in the model predictions. In particular, values for the major water pathways, such as recharge and evapotranspiration were in agreement with the literature. Whilst some questions remain about the model calibration and several limitations to its ability exist, overall the model system was suitable for assessing lake-bed vegetation response to environmental changes.

Assessment of Management Interventions

Specifically, this model was developed in order to answer management questions on how to best protect the lake-bed vegetation through re-vegetation and engineering activities. Scenarios were used to assess the benefit of various levels of interventions that could improve the condition of the Toolibin lake-bed vegetation assemblage, including:

- lake-bed specific interventions (e.g., groundwater pumping);
- operation rules for the diversion gate;
- re-vegetation in the wetland, nearby sub-catchments, and in the wider catchment region;
- improved conveyance of surface water through Dulbinning Natural Reserve, via the construction of a waterway;
- a combination of surface water diversion and groundwater pumping.

Modelling results suggest that vegetation persistence, let alone recovery, in the lake-bed is unlikely without ongoing hydrological intervention. Results showed that under the current climate the most efficient engineering intervention was groundwater pumping, which not only reduced groundwater heads (and the degree of overlap between the root zone and the underlying saline groundwater), but also significantly decreased the wetland hydroperiod. When the distance of the water table from the lowest point of the lake bed reaches 2.5 meters below ground level (mBGL), we recommend the monitoring of salt concentration in the shallow groundwater as well as surface water quality at the diversion. At 2.5 mBGL, root zone salinity is controlled by shallow groundwater salinity so water table levels should be kept lower than this threshold. It is not until the water table is ~4 mBGL that surface water should be allowed to enter the lake. Once surface water is present in the lake shallow groundwater levels and salinity should be measured frequently (weekly) and surface water pumping (through the sump pump) should begin immediately for vegetation protection as benefits in terms of flushing the root zone occur quickly.

Once groundwater and surface water are connected through a saturated soil zone, upward export of salt occurs to the surface water body through diffusion and the benefits of the initial soil flushing are reversed. The long term management (20+ years) target for groundwater should be 4 mBGL and pumping of 800 m³ per day. Groundwater pumping of 800 m³ per day can achieve groundwater depths of 4 mBGL this assuming that a return to a wetter climate period does not occur. Surface water runoff events that are likely to reach the lake are also likely to present low EC thus having capacity to flush the salt from the soil. Relaxing the current inflow criteria of <1,000 mg/l is considered appropriate, assuming the depth the water table is greater the 4 mBGL and sump pumping is present.

Results suggest that retention of surface water in the lake for longer than 60% of the year (7 months) will be severely detrimental for vegetation biomass. However, Toolibin Lake is also being managed for waterbirds as a breeding site so this needs to be considered but that has not been addressed specifically in this report. This could be undertaken as a future exercise with the model. Waterbirds require surface water to provide suitable breeding habitat. Given these distinct and somewhat contradictory management objectives, we have determined that there is a possibility of providing an appropriate ecological niche for both native vegetation and waterbirds, with the condition that the latter rely on less than 7 months of open water per year to complete a breeding cycle (i.e. fledglings need to be able to fly).

In terms of re-vegetation priority, it was found that a rainfall event with an Annual Exceedance Probability of 20% (1 in 5 years) can generate runoff that connects the upland, valley floor and reaches the wetland. We identified the western sub-catchments as producing higher runoff than the eastern ones under the recent climatic regime. We recommend re-vegetation efforts be focused on the valley floor and preferentially on the western side of the catchment. As a rough measure, the re-vegetated area in the sub-catchments tested, needs to exceed 8% of the entire sub-catchment area. Other levels of re-vegetation (20, 40 and 60% of the entire catchment) have been previously assessed as being more effective, but these levels of treatment were considered unrealistic in the current funding climate and so haven't been presented herein. Given the current situation for re-vegetation in terms of conservation funding and Mallee commercialization prospects, re-vegetation at levels that would allow the engineering to be decommissioned seems unlikely. Further work on testing the benefit of Mallees combined with surface water management (contour banks) is recommended as there are still questions that need to be resolved with respect to this practice. The hydrological benefit of this combined management approach to catchment re-vegetation may be considerably greater than agroforestry practices focuses on Mallee belts alone.



CONTRIBUTORS AND DOCUMENT DETAILS:

AUTHORS:

Janaine Zanella Coletti
 Ryan Vogwill
 Brendan D. Busch
 J. Nikolas Callow
 Matthew R. Hipsey

DOCUMENT AND PROJECT DETAILS:

Document title:	<i>A Decision Support System for Assessing the Ecohydrological Response of Toolibin Lake</i>
Document authors:	<i>Janaine Z. Coletti, Ryan Vogwill, Matthew R. Hipsey, Brendan D. Busch and Nik Callow</i>
Project title:	Decision tools for managing hydrological threats to biodiversity assets
Project investigators:	Matthew Hipsey and Ryan Vogwill
Client organisation:	Department of Parks and Wildlife - WA
Client contact:	Jasmine Rutherford

REVISION AND DISTRIBUTION HISTORY:

Issue	Issued to	Qty	Date	Reviewed	Approved
V1 DRAFT FINAL REPORT	Jasmine Rutherford	e	28/08/2014	RV MH	
FINAL REPORT	Jasmine Rutherford	e	10/12/2014	MH	
REVIWED FINAL REPORT	Jasmine Rutherford	e	16/02/2015		

Acknowledgements

This project has been developed by the Aquatic EcoDynamics Research Group team at UWA (<http://aed.see.uwa.edu.au>) and was funded by the Department of Parks and Wildlife (DPaW). The authors acknowledge the contribution of Paul Drake for providing insights into the vegetation physiology and vegetation data.

Citing this report: Coletti, J. Z., Vogwill, R., Busch, B. Callow, J.N & Hipsey, M.R. 2015. A Decision Support System for Assessing the Ecohydrological Response of Toolibin Lake. AED Report #R27, The University of Western Australia, Perth, Australia. 143pp

Release Status: FINAL

Copyright © 2015. The University of Western Australia.

Contents

Executive Summary	3
Overview	3
An Integrated Model System	3
Assessment of Management Interventions	4
Contents	6
List of Figures	8
List of Tables	12
1. Introduction	13
1.1 Background	13
1.2 Objectives and Scope	14
2. Toolibin Lake Catchment Overview – Conceptual Basis for the Model Approach	15
2.1 The Upland Hydrological Landscape	17
2.2 The Valley Floor Hydrological Landscape	18
2.3 The Wetland Hydrological Landscape	19
3. Decision Support System Approach	23
3.1 Hydrological Regions & Model Domains	23
3.2 Model Parameterization	26
3.2.1 LASCAM-S.....	26
3.2.2 LASCAM-R.....	27
3.2.3 LASCAM-Q.....	28
3.2.4 TUFLOW.....	29
3.2.5 WET-0D.....	29
4. Model Verification and Performance Assessment	33
4.1 Comparison Against Literature Values	33
4.2 Comparison Against Field Data	34
4.2.1 Surface Runoff.....	34
4.2.2 Salt Load.....	39
4.2.2 Groundwater.....	42
4.3 Wetland Ecohydrology	47
4.3.1 Groundwater and Surface Water.....	47
4.3.2 Salinity.....	49
4.3.3 Vegetation Biomass.....	49
4.3.4 Sensitivity Analyses of Vegetation Parameters.....	50
5. Management Scenarios	53
5.1 Scenario Settings	53
5.2 Vegetation Change Scenarios	54
5.2.1 Rainfall Decrease and Vegetation Clearing in the Valley Floor.....	54
5.2.2 Re-vegetation with Woody Perennials and Saltland Pasture in the Valley Floor.....	56
5.2.3 Re-vegetation of the Lake Surroundings and Gate Operation.....	57
5.2.4 Vegetation Clearing in the Upland and Priority Catchments for Re-vegetation.....	58
5.3 Engineering Scenarios	59
5.3.1 Groundwater Pumping.....	59
5.3.2 Combined Effect of Pumping and Surface Water Diversion- Recommendation for Future Management.....	61
5.3.3 Lake Bed Re-vegetation.....	65
5.3.4 Implementation of Dulbinning Channel.....	65
5.3.5 Channel Implementation at Canal Road.....	68
5.3.6 Mallee Plantation in the Valley Floor.....	70
5.3.7 Culverts Implementation along Brown Rd and Toolibin Rd North.....	73

5.4 The Combined Effect of Groundwater Pumping and Surface Water Diversion	74
6. Conclusions and Recommendations	77
6.1 Model Validation, Limitations and Suitability	77
6.2 Future Studies	78
6.3 Application of the Model System to Management Scenario Assessment	78
6.3.1 Lake-Bed Interventions	78
6.3.2 Flow Management in the Valley Floor	79
6.3.3 Re-vegetation Effort	80
7. References	81
Appendix A: Model Overview - LASCAM-S	86
Appendix B: Model Overview - LASCAM-R	89
Appendix C: Model Overview - LASCAM-Q	90
Appendix D: Model Overview - WET-0D	91
Water budget	91
Standing Water Storage	92
Soil Water Storage	93
Biomass Budget	95
Salinity Budget	97
Salt in the Soil Surface	97
Salt in the Vadose Zone	98
Salt in the Groundwater	100
Salt in the Lake	101
Appendix E: Model Overview - TUFLOW	102
Validation	102
Appendix F: Model Performance Indices	106
Appendix G: Summary of Water Storages and Fluxes	107
Sub-catchment 7 (SC7)	107
Sub-catchment 10 (SC10)	110
Sub-catchment 12 (SC12)	113
Sub-catchment 22 (SC22)	116
Sub-catchment 28 (SC28)	119
Sub-catchment 32 (SC32)	122
Appendix H: Monthly Comparison of Surface Flows	125
Appendix I: Operation Summary of the Integrated Model	128
Domain and Sub-catchment Selection	131
Soil	132
Surface Water Storage	132
Land Use	133
Rainfall	134
Evaporation	135
Time Settings	136
Specific Settings	136
LASCAM Post Processing Results	137
Appendix J: Example of Input Files	141
Future Climate	141
Re-vegetation	141
Appendix K: Surface Flow (Dis)connection	142
Appendix L: List of Acronyms	143

List of Figures

Figure 1: The “Flow-Fill-Flood” conceptual model. Note that in the setup and analysis of the Toolibin Catchment model, those areas are referred to as upland, valley floor and wetland landscapes. Adapted from [Callow, in prep.].....	15
Figure 2: Catchment DEM and landscape partitioning.....	16
Figure 3: The decline in precipitation observed between 1980 and 2012 in the Toolibin Catchment. Blue line and left axis refer to the daily rainfall, red line and right axis refer to the total annual rainfall. The decline is significant with $p < 0.01$	16
Figure 4: Remnant vegetation coverage in Toolibin Catchment, used as an indicator for deep rooted vegetation.....	17
Figure 5: Schematic representation of the hydrological processes typical of the upland hydrological landscape in Toolibin Catchment, indicating the soil layering and relevant hillslope hydrological processes.....	17
Figure 6: Schematic representation of the landscape and hydrological processes typical of the valley floor....	18
Figure 7: Schematic representation of landscape and hydrological processes typical of the wetland.	19
Figure 8: Biomass density map - Toolibin Lake as at January, 2005 [Ecoscape, 2005].	20
Figure 9: Map of root zone salinity in Toolibin Lake as at January, 2005 [Ecoscape, 2005].	21
Figure 10: The integrated model system conceptualization showing the landscape partitioned into three major regions of distinct hydrological function resolved by a different modelling approach (red font) and the major engineering interventions tested (black font). Note that flow routing behaviour was also informed by simulations of the high-resolution TUFLOW model.....	24
Figure 11: The distribution of the sub-catchments (numbered from 0 to 34) within the Toolibin Catchment map. The domain of each landscape and model is differentiated by colours.	25
Figure 12: Summary of the decision support system. Possible testing scenarios are depicted in blue, hydrological models are depicted in black and the major outputs are depicted in red.	25
Figure 13: LASCAM-S - Upland hydrological zone model stores and simulated pathways. Refer to Appendix A for model equations.	27
Figure 14: Weekly LAI variation in an example sub-catchment (SC02), as derived from the MODIS LAI products.	27
Figure 15: LASCAM-R - Valley floor hydrological stores and pathways. Refer to Appendix B for model equations.	28
Figure 16: The DEM of Toolibin Lake (a). The wetland hydrological zones represented in WET-0D (U, S and L) and the vegetation species resolved by the model (b). Refer to Appendix D for model equations.....	29
Figure 17: The location of each sub-catchment (SC0 to SC34) and surface gauges in the Upland (squares) and in the Valley Floor (triangles).	35
Figure 18: Sub-catchment 7 (SC7) and gauge station HAL001 surface runoff time-series.	36
Figure 19: Sub-catchment 10 (SC10) and gauge station WDR001 surface runoff time-series.	36
Figure 20: Sub-catchment 12 (SC12) and gauge station EDR001 surface runoff time-series.	36
Figure 21: Sub-catchment 22 (SC22) and gauge station 03TIN001 surface runoff time-series.....	37
Figure 22: Sub-catchment 28 (SC28) and gauge station HAR002 surface runoff time-series.	37
Figure 23: Sub-catchment 32 (SC32) and gauge station HC001 surface runoff time-series.	37
Figure 24: Sub-catchment 2 (SC2) and gauge station DUL006 surface runoff time-series (note the small magnitude of the Y scale).....	38
Figure 25: Sub-catchment 3 (SC3) and gauge station DOW609038 surface runoff time-series.	38
Figure 26: Sub-catchment 1 (SC1 – end-of-catchment) and gauge station DOW609010 surface runoff time-series.	38
Figure 27: Sub-catchment 1 (SC1) and gauge station DOW609010 flow duration curve (from 1979 to 2013). Note the very small window of exceedance time periods (<2%) on the x-axis.	39
Figure 28: Sub-catchment 7 (SC7) and gauge station HAL001 salt load time-series.....	40
Figure 29: Sub-catchment 12 (SC12) and gauge station EDR001 salt load time-series.....	40
Figure 30: Sub-catchment 28 (SC28) and gauge station HAR002 salt load time-series.....	40
Figure 31: Sub-catchment 1 (SC1) and gauge station DOW609010 water temperature (a), salt concentration (b), flow (c) and salt load (d) time-series from 1989-2013.....	41
Figure 32: Inflow versus salinity at the gauge DOW609010 predicted by the model (blue stars) and reported (red stars)by [Muirden and Coleman, 2014]. The insert shows the original graph by Muirden and Coleman [2014], where summer (red squares) and winter (blue diamonds) were separated. The dash line shows the extension of the insert.....	42
Figure 33: The location of each LASCAM sub-catchment and bores in the upland (blue triangles) and valley floor (red dots).	43
Figure 34: Groundwater variation observed at the reference bore (blue diamond) and predicted by the model at SC7 (black line).....	44
Figure 35: Groundwater variation observed at the reference bore (blue diamond) and predicted by the model at SC10 (black line).....	44

Figure 36: Groundwater variation observed at the reference bore (blue diamond) and predicted by the model at SC12 (black line).	44
Figure 37: Groundwater variation observed at the reference bore (blue diamond) and predicted by the model at SC22 (black line).	45
Figure 38: Groundwater variation observed at the reference bore (blue diamond) and predicted by the model at SC28 (black line).	45
Figure 39: Groundwater variation observed at the reference bore (blue diamond) and predicted by the model at SC32 (black line).	45
Figure 40: Groundwater variation observed by the reference group of bores (statistical distribution represented by the whisker plot, in black) and predicted by the model at SC1 (red line).	46
Figure 41: Groundwater variation observed by the reference group of bores (statistical distribution represented by the whisker plot, in black) and predicted by the model at SC2 (red line).	46
Figure 42: Groundwater variation observed by the reference group of bores (statistical distribution represented by the whisker plot, in black) and predicted by the model at SC3 (red line).	47
Figure 43: Bores and pumps location within the wetland domain.	48
Figure 44: The observed and modelled lake level (a) and water table depth from the surface (b).	48
Figure 45: The predicted EC in the lake (a), in the vadose zone (b) and in the groundwater (c), compared to the range observed in the field by various authors (in red and blue).	49
Figure 46: Predicted biomass density (kg m ⁻²) for grasses (a) and for <i>M. strobophylla</i> and <i>C. obesa</i> (b), compared to the values observed by <i>Ecoscape</i> [2005].	50
Figure 47: The range of <i>M. strobophylla</i> biomass predicted by the parameters distribution tested. The red line prior and the black line represents the median of the posterior.	51
Figure 48: The range of <i>C. obesa</i> biomass predicted by the parameters distribution tested. The red line prior and the black line represents the median of the posterior.	51
Figure 49: Posterior probability distribution (grey bars) in relation to the prior (red stars).	51
Figure 50: Hydroperiod in Toolibin Lake given vegetation clearing and rainfall decline for the total period of simulation.	55
Figure 51: Rainfall forcing for Scenarios D2SC3R7, D2SC3R20 and Observed (control). The blue line marks the starting of the driest period. Coincidentally, the factors for decline rainfall are applied until year 2000.	55
Figure 52: Toolibin Lake's dynamic ecohydrological response to rainfall decline and vegetation clearing in the catchment. All variables are relative to the Observed (control) scenario.	56
Figure 53: The effect of re-vegetation and surface water diversion on ground water level (a), salinity at the root zone (b), groundwater salinity (c) and total biomass (d) in the wetland.	58
Figure 54: Map of the relative runoff generation between 2007 and 2010. Values represent percentage of the total flow for the period. Brighter areas represent higher runoff. In general, the western side presents infiltration excess runoff and the eastern side presents saturation excess runoff.	59
Figure 55: Root zone (a), groundwater salinity (b) and groundwater depth (c) in Toolibin Lake as a result of different volumes of water extracted by pumping.	60
Figure 56: Vegetation biomass in response to pumping operation.	61
Figure 57: Hydrological response to different pumping schedule (from 400 to 1200 m ³ d ⁻¹) and no contribution of surface runoff from the catchment.	62
Figure 58: Hydrological response to different pumping schedule (from 400 to 1200 m ³ d ⁻¹). Surface water was allowed in the lake.	63
Figure 59: Summary of the ecohydrological response to pumping schedule with the diversion channel closed (in blue) and with the diversion channel opened (in black). In panel (c), diamonds represent <i>C. obesa</i> , squares represent <i>M. strobophylla</i> and triangles represent grasses. Panel (d) represents the total biomass.	64
Figure 60: Salinity at the root zone (dots) as a function of depth to the groundwater and salinity in the groundwater. Channel opened scenarios are depicted in red, channel closed scenarios are depicted in blue.	64
Figure 61: Influence of pumping schedule (from 400 to 1200 m ³ d ⁻¹) on hydroperiod.	65
Figure 62: Vegetation response in relation to the Observed (control) scenario after attempt to re-vegetate the lake bed without hydrological intervention.	65
Figure 63: The rainfall event observed in January 1990 and the gauges response predicted by LASCAM.	66
Figure 64: The flood extension on 29/01/1990, 3 days after the beginning of the simulation, for a scenario without channel in the Dulbinning Reserve.	66
Figure 65: The flood extension on 29/01/1990, 3 days after the beginning of the simulation, for a scenario where the channel in the Dulbinning Reserve was built.	67
Figure 66: The changes in the hydrograph at the catchment outlet with and without the Dulbinning Channel implementation.	67
Figure 67: Location of the observation point at the catchment outlet.	67
Figure 68: Flood extension after 2 days of simulation, no channel implemented along Canal Rd.	68
Figure 69: Flood extension after 2 days of simulation, a 0.4m deep channel is implemented along Canal Rd in this simulation.	68

Figure 70: The changes in the hydrograph that the implementation of a 0.4 m deep channel along Canal Rd generated.	69
Figure 71: Location of the observation point.	69
Figure 72: Simulation with a further 0.2m excavation in the channel along the Canal Rd.	69
Figure 73: Land coverage map defining the spatial distribution of the hypothetical Mallee plantation.	70
Figure 74: The extension of flooding after 2 days of simulation for a scenario without Mallee plantation.....	70
Figure 75: The extension of flooding after 2 days of simulation for a scenario with Mallee plantation.....	71
Figure 76: The hydrograph at the beginning of the Dulbinning Channel for a scenario without Mallee plantation (Observed scenario) and a scenario with the Mallee plantation.	71
Figure 77: The hydrograph at the catchment outlet for scenarios with and without the Mallee plantation.	71
Figure 78: Observation point at the beginning of Dulbinning Channel.	72
Figure 79: Reduced scattered ponding areas 5 and a half days after the beginning of the simulation for a scenario with the Mallee plantation.....	72
Figure 80: Remaining scattered ponding areas 5 and a half after the beginning of the simulation for a scenario without the Mallee plantation.	72
Figure 81: The extensive area of ponding waters at the corner of Brown Rd and Toolibin Rd North.	73
Figure 82: The position of the two extra culverts, under Brown Rd and under Toolibin Rd North (red dots).	73
Figure 83: The hydrograph at the outlet of the catchment before and after the implementation of the culverts at Brown Rd and Toolibin Rd North.	73
Figure 84: Groundwater level (a) and total vegetation biomass (b) as determined by the level of SW and GW interventions.	75
Figure 85: <i>C. obesa</i> 's (a) and <i>M. strobophylla</i> 's (b) biomass as determined by the level of SW and GW interventions.	75
Figure 86: Root zone (a) and groundwater salinity (b) as a function of SW and GW interventions.	76
Figure 87: The relative abundance of <i>M. strobophylla</i> as a function of SW and GW interventions.	76
Figure 88: <i>M. strobophylla</i> 's biomass (a) and root zone salinity (b) in response to SW and GW interventions if <i>C. obesa</i> was not present.....	76
Figure 89: Conceptual water fluxes (in blue) and water storages (in black) resolved by LASCAM-S.	86
Figure 90: Conceptual diagram of LASCAM-R showing the use of two stores and relevant processes.....	89
Figure 91: The three storage cells or environments with distinct hydrological function (U, S and L) and their correspondent surface areas (A_U , A_S and A_L).....	91
Figure 92: Water fluxes through the three storage cells and their relative areas.	92
Figure 93: The main salt pathways within the wetland domain.....	99
Figure 94: TUFLOW domain. The red dot indicates the observation point (Gauge ASWTLB13DUL006) used in the model assessment. Blue dots indicate the inflow gauges from the upland area used to drive the model.	102
Figure 95: Observed water flow between 15/07/2008 and 20/08/2008 at the 6 monitoring gauge stations that intercept the main water pathways of the catchment.	103
Figure 96: Observed rainfall between 15/07/2008 and 20/08/2008 at the BoM Station # 10654.	103
Figure 97: Land coverage map defining the spatial distribution of two Manning's Roughness Coefficients....	104
Figure 98: Roads and culvert location.....	104
Figure 99: Drainage built from Rd Canal at the point that crosses Brown Rd (Google Maps, 2008)	104
Figure 100: The water level observed in the gauge ASWTLB13DUL006 and the level predicted by TUFLOW at that location. Note the small range on the y-axis indicating flows during the initial rain period <5cm deep.	105
Figure 101: Long term trend groundwater and soil water content - SC7. Note the rising trend in the observed bore height data during the drying period from 2004-2011, in contrast to the model predictions.....	107
Figure 102: Long term trend surface water, recharge and evapotranspiration - SC7.....	108
Figure 103: Long term trend vegetation - SC7.....	109
Figure 104: Long term trend groundwater and soil water content – SC10.....	110
Figure 105: Long term trend surface water, recharge and evapotranspiration – SC10.	111
Figure 106: Long term trend vegetation – SC10.	112
Figure 107: Long term trend groundwater and soil water content – SC12.....	113
Figure 108: Long term trend surface water, recharge and evapotranspiration – S12.	114
Figure 109: Long term trend vegetation – SC12.	115
Figure 110: Long term trend groundwater and soil water content – SC22.....	116
Figure 111: Long term trend surface water, recharge and evapotranspiration – SC22.	117
Figure 112: Long term trend vegetation – SC22.	118
Figure 113: Long term trend groundwater and soil water content – S28. Note the observed groundwater levels increase during the driest year of the simulation period, in contrast to the models predicted drying of the stores.	119
Figure 114: Long term trend surface water, recharge and evapotranspiration – SC28.	120
Figure 115: Long term trend vegetation – SC28.	121
Figure 116: Long term trend groundwater and soil water content – SC32.....	122
Figure 117: Long term trend surface water, recharge and evapotranspiration – S32.	123
Figure 118: Long term trend vegetation – SC32.	124

Figure 119: Monthly totals of surface runoff measured versus predicted at SC7.	125
Figure 120: Monthly totals of surface runoff measured versus predicted at SC10.	125
Figure 121: Monthly totals of surface runoff measured versus predicted at SC12.	126
Figure 122: Monthly totals of surface runoff measured versus predicted at SC22.	126
Figure 123: Monthly totals of surface runoff measured versus predicted at SC28.	127
Figure 124: Monthly totals of surface runoff measured versus predicted at SC32.	127
Figure 125: The integrated model system configuration.....	128
Figure 126: Data necessary for the catchment input file.	129
Figure 127: Data necessary for the climate input file.	129
Figure 128: Data necessary for the vegetation input file.	130
Figure 129: SWWAN-DSS folders creation.....	131
Figure 130: Example of soil parameters file.....	132
Figure 131: Example of "lake"/storage parameters file.	133
Figure 132: Example of remnant vegetation parameter file.	133
Figure 133: Example of percentage of impervious area vegetation parameter file.	134
Figure 134: Example of percentage of deep and riparian vegetation parameter file.	134
Figure 135: Example rainfall input file.....	135
Figure 136: Example rainfall gauge location input file.	135
Figure 137: Example rainfall gauge location input file.	136
Figure 138: Example master input file.	136
Figure 139: Example configuration input file.	137
Figure 140: MatLab command window.....	138
Figure 141: Example of an output file showing monthly averages of relevant hydrological processes.	138
Figure 142: Example of output chart (daily values).	139
Figure 143: Additional output files.	139
Figure 144: Example of output chart (monthly values).	140
Figure 145: Example climate input csv files.	141
Figure 146: Re-vegetation input file showing how a user can set rate and extent of revegetation.	141
Figure 147: Surface flow (dis)connection in Toolibin catchment.	142

List of Tables

Table 1: Summary of the landscape regions and models domains.	23
Table 2: Summary of typical parameters used in LASCAM-S and their justification. Refer to Appendix A for model equations.	26
Table 3: Summary of parameters used in LASCAM-R. Refer to Appendix B for model equations.	27
Table 4: Summary of parameters used in LASCAM-Q, and their justification.	28
Table 5: Summary of parameters used in TUFLOW.	29
Table 6: Summary of parameters used in WET-0D and their justification. Refer to Appendix D for details of model equations.	30
Table 7: Vegetation parameters used in WET-0D and their justification.	31
Table 8: Summary of the major hydrological processes and average values predicted by the model (based on 1979-2013 simulation) and values reported in the literature for similar sites.	34
Table 9: List of representative surface gauge for each sub-catchment.	35
Table 10: List of representative bore(s) for each sub-catchment.	43
Table 11: Target parameters tested to explore their effect on vegetation biomass.	50
Table 12: Summary of scenarios as requested by DPaW.	53
Table 13: Summary of the hydrological changes caused by rainfall decrease and vegetation clearing in the valley floor (SC3) in relation to the Observed (control) scenario.	54
Table 14: Summary of the hydrological changes caused by re-vegetation in SC2 in relation to the Observed (control) scenario.	57
Table 15: Summary of the ecohydrological changes in the wetland caused by re-vegetation in the lake surroundings and gate operation in relation to the Observed (control) scenario.	57
Table 16: Summary of the ecohydrological changes during pumping in relation to the Observed (control) scenario.	60
Table 17: Summary of additional groundwater pumping scenarios.	61
Table 18: Notional level of intervention for SW and GW.	75
Table 19: List of the major equations of LASCAM-S.	87
Table 20: List of variables in LASCAM-S.	87
Table 21: List of the major equations of LASCAM-R.	89
Table 22: List of the major equations of LASCAM-Q.	90
Table 23: List of parameters required for LASCAM-Q.	90
Table 24: Example of values for the water uptake strategy compatibility parameter.	97

1. Introduction

1.1 Background

Wetlands found in regions with Mediterranean or semi-arid climates, such as south-west Western Australia (SWWA), are known to be particularly sensitive to changes in climate and land-use. In this region, most rainfall occurs in winter, when temperatures are at their lowest, so a higher conversion of rainfall to runoff and recharge occurs [CSIRO, 2009]. Conversely, the dry season happens during periods with high evaporation rates [CSIRO, 2009], leading to prolonged periods of water deficits in the soil [Petroni *et al.*, 2010]. In addition to having a highly variable water delivery pattern [Humphries *et al.*, 2011; Tooth and McCarthy, 2007], semi-arid wetlands are prone to salinisation [Crosbie *et al.*, 2009; Laurance *et al.*, 2011]. To date, increased salinisation has already caused negative impact on wetland plant communities in SWWA [Davis *et al.*, 2003; Froend *et al.*, 1987; Halse, 2004; Halse and Massenbauer, 2005], with more under risk, including many rare and endemic species [Myers *et al.*, 2000].

This is well exemplified in the case of Toolibin Lake (34°20'44.92'' S/ 115°08'16.82'' E), a 300 ha wetland listed under the RAMSAR Convention as a Wetland of International Importance [Wetlands, 2013]. Toolibin Lake sits at the base of a 480 km² (48,000 ha) catchment, and has been adversely impacted by land clearing and an altered hydrological regime. As a result of salinity development in the catchment, stands of *Casuarina obesa* and *Melaleuca strobophylla* across the lake and within the nearby remnants are dying [George *et al.*, 2004]. These deaths have been caused by increased soil salinity and waterlogging within the root zone. Halse *et al.* [2000] further documented the impact that increased lake salinity was having on waterbirds and aquatic macro-invertebrates.

The Toolibin Lake catchment contains distinctive landform zones that have different hydrological functions. These zones are 1) the upland area, 2) the low-gradient valley floors and 3) the wetland, near the catchment outflow. Runoff is generated in most years from the uplands but typically this only flows as far as the valley floor region where it ponds, along with in-situ runoff. It is only during the heaviest of rainfall years or most intense events that the valley floor truly fills and surface flows occur throughout the catchment. During most years, substantial amounts of internal catchment surface water redistribution occurs, this has been identified as a critical driver of the altered hydrology that causes dryland salinisation [Callow, in prep.]. The conceptual basis for hydrological flows in the Toolibin Lake catchment is discussed further below.

In 2003, secondary salinisation had already affected 8% of Toolibin catchment and 24% was at risk [Dogramaci *et al.*, 2003]. Included in the salt-affected and high risk areas within the valley floor of the catchment are two large nature reserves (Toolibin and Dulbinning), which together are important habitat for 41 species of waterbirds and other local fauna. Airborne data interpretations from the eastern part of the catchment showed that salinisation risk areas are located around the drainage system [Pracilio *et al.*, 1998; Street *et al.*, 2002]. There has been much discussion around the exact mechanisms driving the degradation of the wheatbelt catchments. Clarke *et al.* [1998] argue that geological features such as major faults affected the development of dryland salinity in the wheatbelt of Western Australia. George and Conacher [1993] identified the four mechanisms for the further development of modern salinity: 1) increased overland flow; 2) increased throughflow and the development of perched aquifers; 3) increased infiltration to deep aquifers leading to rising water-tables; 4) increased throughflow and infiltration to deep groundwater, leading to a mixing of perched and deeper aquifer systems in saline seeps. It was proposed that mechanism three was the dominant causal process leading to secondary salinity in dryland areas [George and Conacher, 1993]. Finally, [George *et al.*, 2008a] conclude that the modern salinity appears to be reoccupying landscapes made saline by previous changes in climate. The advance of watertable and salinity into areas containing stranded playas is salutary evidence of persistent processes.

With this in mind, the Northern Arthur River Wetlands Rehabilitation Committee (NARWRC) was established to investigate and develop recommendations for the conservation of Toolibin Lake. In 1987, the Committee produced a report: "*The Status and Future of Toolibin Lake as a Wildlife Reserve*". This report outlined previous studies and listed management recommendations for the lake. The recommendations included works such as re-vegetation of the western buffer zone, groundwater control via pumping and diversion of saline surface flow, whose results have been evaluated [George *et al.*, 2004; Vogwill *et al.*, 2010]. To date, those efforts have caused some improvement in vegetation health, especially for *C. obesa*, in some parts of the wetland [Drake *et al.*, 2012b; Vogwill *et al.*, 2010]. Many of the subsequent interventions in Toolibin Lake were based on these recommendations [Ludwig *et al.*, 1997]. However, despite regional and catchment-scale investigations into the groundwater dynamics and surface-water hydrology, few studies to date have addressed the interaction of surface and groundwater over time-scales relevant to restoration of vegetation, and there has been limited effort to link the physiological dynamics of the vegetation with the surface and subsurface hydrological processes that shape ecosystem dynamics. Making this connection is ultimately necessary if we are to successfully forecast vegetation responses to management efforts and changes to rainfall regimes.

1.2 Objectives and Scope

The sustainable management of wetlands such as Toolibin Lake requires a quantitative understanding of ecosystem processes sufficient to guide management activities. Given the complexity of the hydrological processes throughout the Toolibin Lake catchment, a comprehensive model framework is required to be used as a decision support system able to predict the effect of land use and climate change on valley floor and wetland vegetation. In particular, this model framework needs to be able to test potential management interventions such as altering surface drainage and groundwater pumping, as well as the effect of predicted impacts of landscape revegetation and alterations to rainfall patterns.

The overarching aim of this study was to provide an integrated model system to be used for decision support for maximizing wetland vegetation health, and able to provide practical guidance for the operation of the surface water diversion and groundwater pumping infrastructure. In addition, the model system was developed with the intention of exploring catchment and lake bed re-vegetation as a long-term sustainable management option. The model framework that has been developed simulates the water and salt balance of the lake-bed and associated response of the high conservation value tree species, whilst being integrated within a semi-distributed catchment hydrology model able to predict salt export and long-term regional change in surface and groundwater dynamics.

Whilst the primary objective of this report is to document the development and validation of the model system, various requested management scenarios were explored to demonstrate the utility of the model for supporting management effort. Examples of questions that first motivated the development of the model platform and the guided the scenarios reported here include:

1. What are the most efficient management actions to control the groundwater level?
2. Can we manage surface water salinity and hydroperiod to support the Threatened Ecological Communities (TEC) of plants, specifically *Casuarina obesa* and *Melaleuca strobophylla* as well as waterbirds?
3. What is a significant rainfall event likely to generate catchment scale flow, i.e., an event that connects the upland to the wetland, without being stored in the microtopography of the valley floor?
4. What are the monitoring triggers (e.g., salinity of inflow) that can be used to lead to a management response (e.g., stop pumping or close gate)?
5. What is the relationship between groundwater level and root zone salinity?
6. What has been the benefit of pumping at current rate and what are the effects of pumping rate decrease or increase?
7. When should the surface water inlet gate be open/closed?
8. What hydrological monitoring needs to be conducted pre/during/post significant rainfall events?
9. Which management actions in the catchment can bring positive impact to the wetland vegetation?

Due to the diversity of spatial and temporal scales being covered by the above questions and patchy data availability, various technical challenges were required to be overcome in order to make the model operate as an integrated system. The report outlines the validation of the model against available ecohydrological data for the region and uses the model system to explore the relative sensitivity of the wetland vegetation response to the level of remediation efforts.

2. Toolibin Lake Catchment Overview - Conceptual Basis for the Model Approach

Toolibin Catchment is situated within a semi-arid climate and it is spatially heterogeneous in its hydrology. These factors, typical of SWWA wheatbelt catchments, make modelling a challenge [Viney *et al.*, 2007] and therefore requires an appropriate conceptual model on which the numerical model can be based. Specifically, Toolibin Catchment has distinctive landforms, related to soil/regolith type, geomorphology and topographic gradient, differentiating the low-gradient valley floor from the more hydrologically connected, upland areas. These landforms are recognised as having distinct runoff characteristics and water transport pathways [Cattlin, 2006; Cattlin and Farmer, 2004].

Previous projects that monitored surface water flows and salt export in the Toolibin Catchment over the period 2007-2012 [Callow *et al.*, 2007] provided insight into the complex nature of the surface hydrology relative to “textbook” catchment rainfall-runoff conceptual models. Callow [in prep.], have interpreted this data to suggest that there are three landscape “components” (upland, valley floor and wetland) and that each of them behave in different ways, depending on the volume of rainfall. In drier years, there is runoff from the upland (termed “flow” landscapes) to the valley floor regions (termed “fill” landscapes). Fill landscapes have a significant internal storage capacity due to their low gradient and microtopography/detention storage (Figure 1). In dry years, small amounts of runoff are generated from the upland areas but the volume of internal catchment water redistribution is less than that sufficient to generate catchment scale flow. Consequently the water from upland areas (as well as in-situ rainfall and runoff) pools in the valley floors where it recharges groundwater and evapoconcentrates, driving salinisation. During large rainfall events (often summer) and in wetter (winter/spring rainfall) years, the runoff from the upland exceeds the internal storage capacity of the valley floors and allows for hydrological connection through to the wetland.

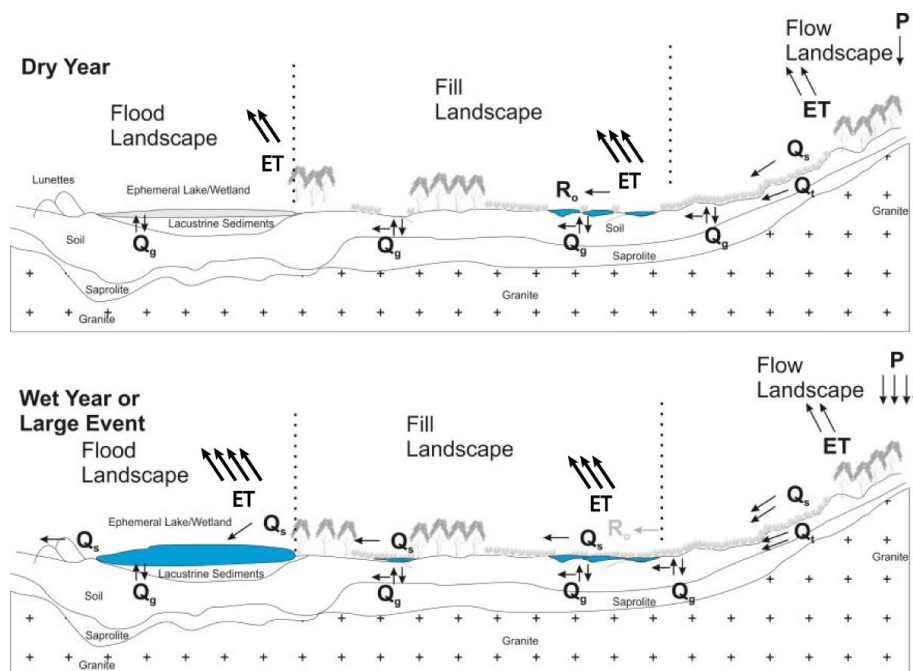


Figure 1: The “Flow-Fill-Flood” conceptual model. Note that in the setup and analysis of the Toolibin Catchment model, those areas are referred to as upland, valley floor and wetland landscapes. Adapted from [Callow, in prep.].

As a consequence, the characteristic hydrological processes throughout the landscape in Toolibin Catchment can be conceptually divided into three hydrological zones of distinct functionality: the upland, the valley floor and the wetland, in the terminal part of the catchment. The distinction between the upland and valley-floor regions is based on a working definition for where the slope varies significantly from <1% to >1% [Dogramaci *et al.*, 2003] as can be seen in the Digital Elevation Model (DEM) presented in Figure 2.

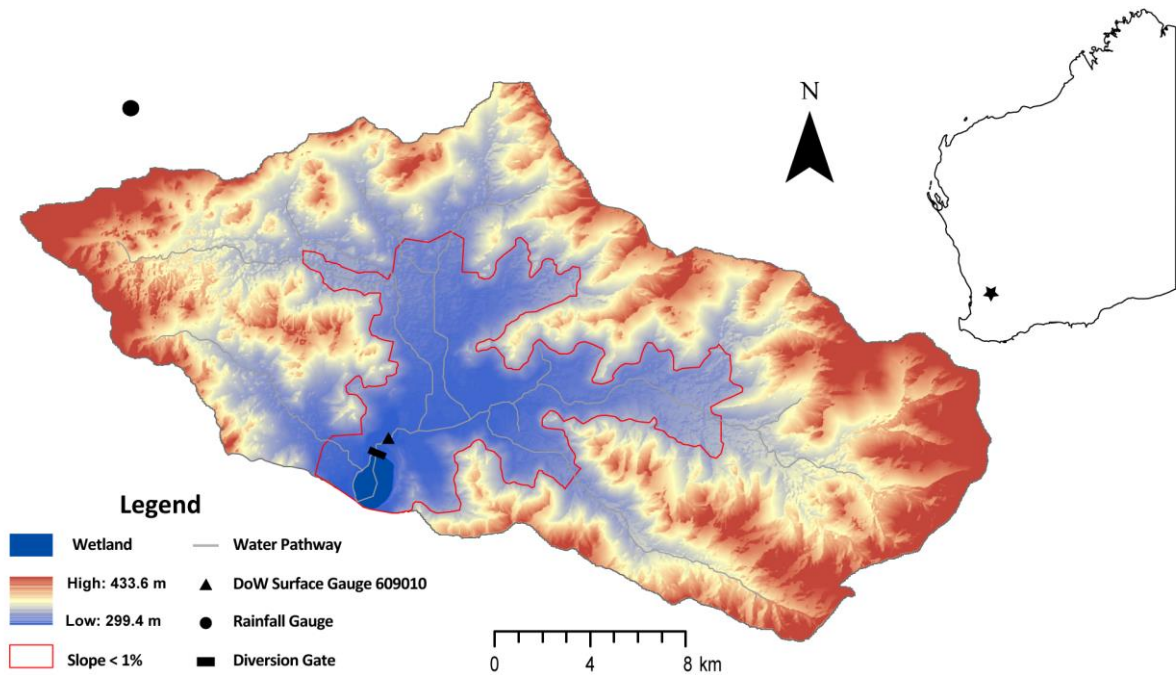


Figure 2: Catchment DEM and landscape partitioning.

Toolibin catchment is located in an area of temperate climate with mean annual rainfall of 420 mm and pan evaporation of 1900 mm. In the middle 1970's, a decline in precipitation was observed in the SWWA [CSIRO, 2007] and the Toolibin Lake catchment is no exception (Figure 3). This considerable decline in precipitation has reduced runoff and recharge in the catchment, an important context when analysing model predictions for the validation period. Variation in rainfall across the catchment is unclear due to the lack of long-term data sets at multiple stations. Also, many rainfall events are highly localised (particularly during episodic events), creating a further challenge for modelling assessments due to a lack of distributed rainfall data (refer to Appendix K for an example that illustrates flow asynchrony within the catchment).

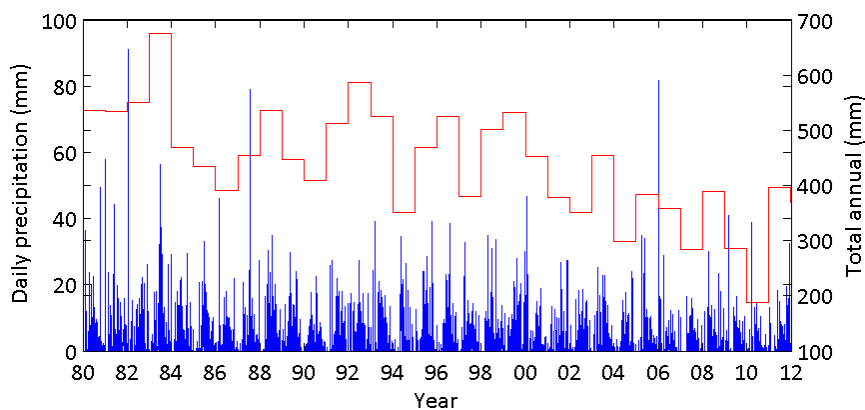


Figure 3: The decline in precipitation observed between 1980 and 2012 in the Toolibin Catchment. Blue line and left axis refer to the daily rainfall, red line and right axis refer to the total annual rainfall. The decline is significant with $p < 0.01$.

Aside from different landscape and climate elements that shape the catchment hydrology and flow delivery to Toolibin Lake, the clearing of native vegetation has been extensive and ubiquitous throughout most of the catchment (Figure 4). Whilst there is limited information on the rate of land clearing specifically for the catchment, analysis conducted by [Allison and Hobbs, 2004] has indicated that most clearing was completed by the 1970's and has not varied substantially since, except for relatively small revegetation efforts.

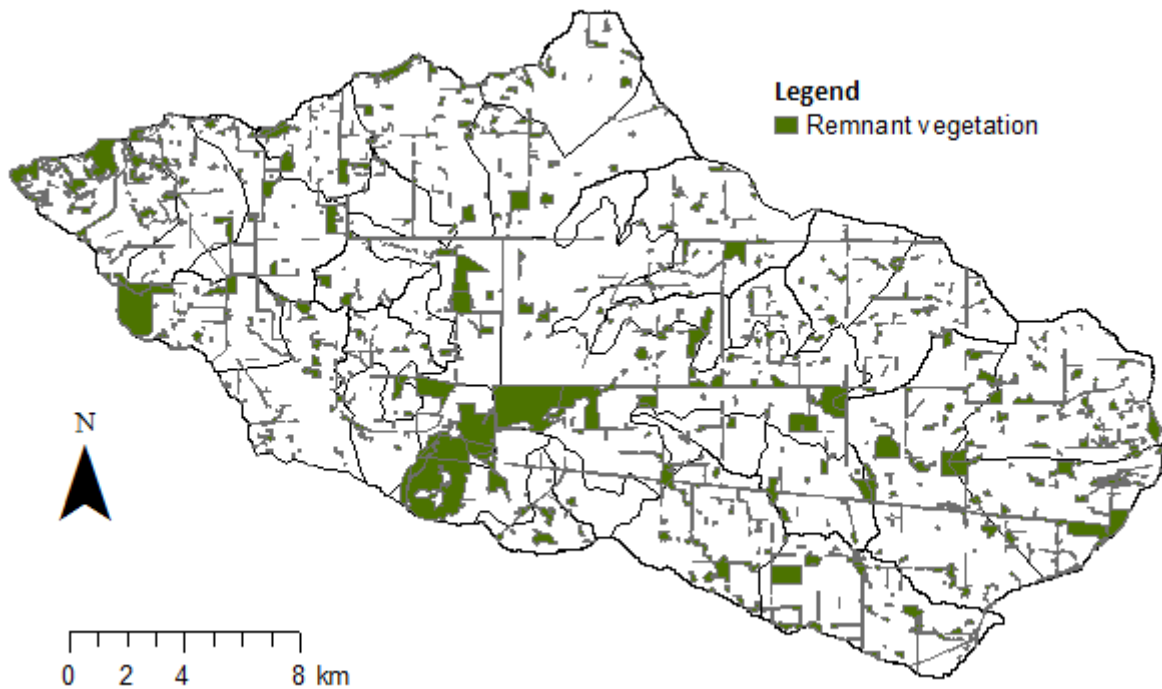


Figure 4: Remnant vegetation coverage in Toolibin Catchment, used as an indicator for deep rooted vegetation.

2.1 The Upland Hydrological Landscape

The upland area has an average topographic slope greater than 1%, which comprises about 65% of the 480 km² catchment. Its soil profile consists of a thick layer of saprolite above bedrock (Figure 5). The saprolite layer is approximately 20 m thick in average and is overlaid by a “wedge” of medium sand that expands its thickness to 3-5 m at the edge of the catchment [Dogramaci *et al.*, 2003]. Little remnant vegetation remains in the upland landscape (<10%).

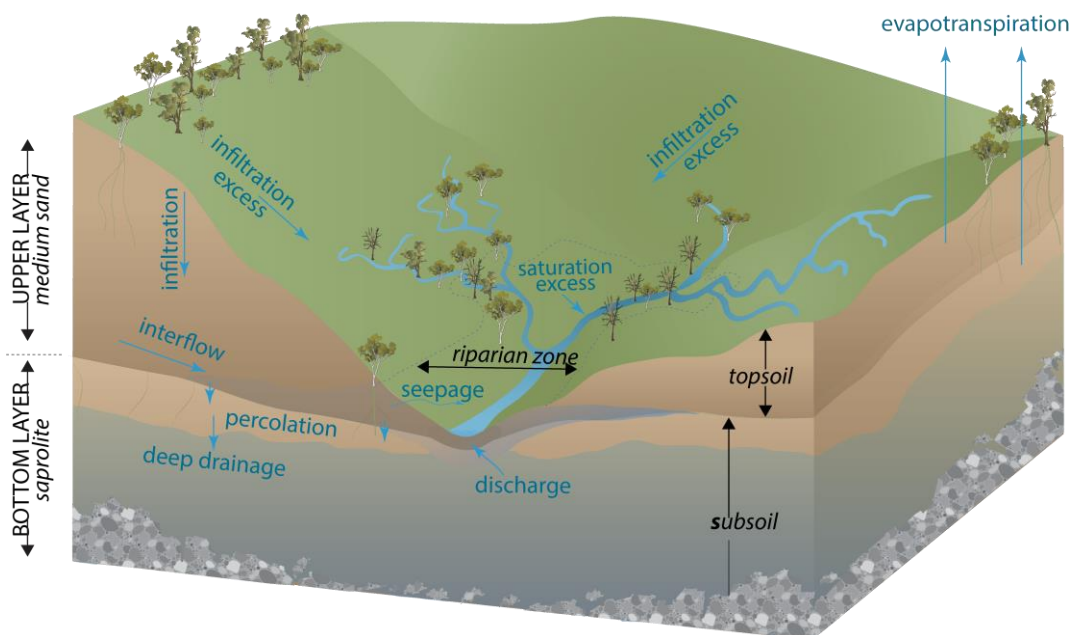


Figure 5: Schematic representation of the hydrological processes typical of the upland hydrological landscape in Toolibin Catchment, indicating the soil layering and relevant hillslope hydrological processes.

Based on the available data (2007-2012), the upland area seems to produce intermittent but relatively frequent, highly variable runoff volumes, as it has reasonable drainage connectivity to convey water downstream. The eastern side produced runoff during winters, after multiple rainfall events, suggesting flows are more characteristic of saturation excess runoff. The western side seems to respond rapidly to individual rainfall events, suggesting an infiltration excess driven runoff regime.

Groundwater level data from bores situated within the upland from 2001-2012 shows an unclear picture of any significant trends over this period. In general, water table levels in many parts of SWWA are increasing due to increased recharge from land-clearing [George *et al.*, 2008b], however there is evidence in some areas of decline due to the marked declining trend in rainfall since the 1970's (Figure 3) [CSIRO, 2007]. Preliminary analysis of data provided by DPaW for Toolibin indicated that very few bores have complete information regarding construction details (depth, their status, length screened interval, etc.) creating some uncertainty, with some of the bores displaying an increasing trend in groundwater level with most showing a stable or decreasing level.

2.2 The Valley Floor Hydrological Landscape

The valley floor of Toolibin Catchment (Figure 6) was formed by an ancient drainage system dominated by deposition of alluvial sands and clays [George and Dogramaci, 2000]. In terms of hydrological function, it is referred to as the "valley flats" [Dogramaci *et al.*, 2003] or "fill" landscapes [Callow, in prep.] and tends to receive water from the upland regions, with some minor internal generation also occurring. Large scale connected flows through this landscape only occur after a prolonged series of rainfall events or during large magnitude or intense rainfall events. This occurs since micro elevation and low topographic gradient create a large amount of surface water detention storage. Man-made structures, such as roads and banks, can also significantly contribute to surface water pooling and affect flow continuity.

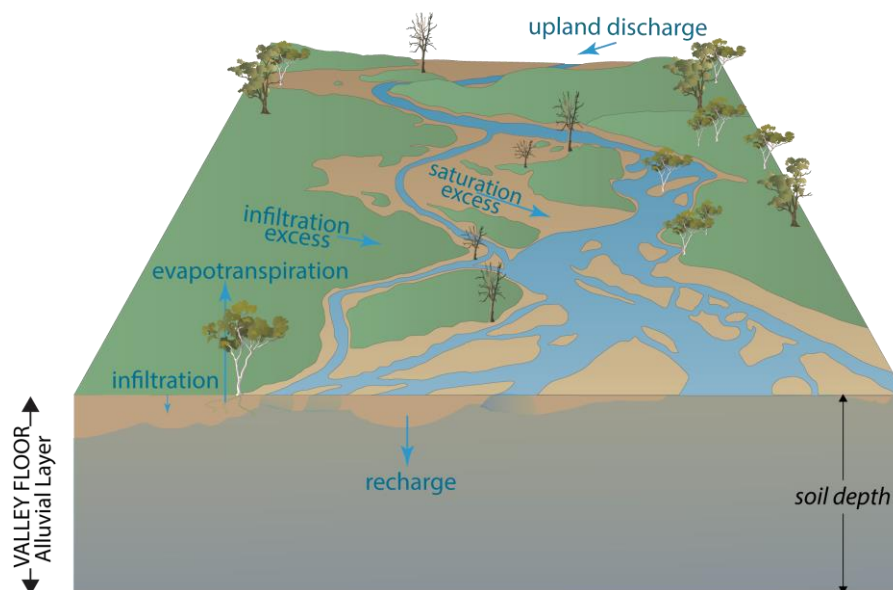


Figure 6: Schematic representation of the landscape and hydrological processes typical of the valley floor.

Over recent decades, Toolibin's valley floor has experienced significant salinisation. Whilst the salinity of groundwater has historically been high, rising groundwater tables bring more salt into the root zone and increase the dissolution of salts stored in the soil profile. The high evapotranspiration rates characteristic of the SWWA climate leads to high salt accumulation and high concentrations in the shallow root zone [George *et al.*, 2008a; Jolly *et al.*, 2008]. Furthermore, changes in the rate of surface runoff has led to an increase in the magnitude and salinity of the surface water flows following rainfall, particularly in the first flows of the season that pick up previously deposited salts. Large surface flows can act to "flush" salts downstream, however, within this "fill" landscape, the dominant low to medium surface water flow events result in significant salt redistribution and further amplify the rate of accumulation in the shallow soil profile within topographic lows such as valley lakes and wetlands and terminal drainage paths. Where the groundwater table is close to the surface then large flood events may also lift saline groundwater to the surface, preventing downward leaching of surface salt. This combination of processes over short and long term timescales has become a particularly damaging phenomenon in the broad valley flats across the wheatbelt where lake systems are a terminal sink for high volume/high salt inflows [Gifford, 1978], and is the case in the Toolibin catchment.

Groundwater level data from 22 bores situated in the valley floor of Toolibin Catchment were available from DPaW, with data going back to 2001. Few bores have complete information regarding construction details (depth, their status, length screened interval, etc.), making conclusive assessments difficult. However, preliminary analysis undertaken identified that several of the bores still have trends of increasing groundwater level, in contrast to the trend in rainfall, while most have a stable or decreasing level. This is similar to what has been observed in the upland catchments, however, in general, the groundwater variation in the valley floor seems to be more responsive to rainfall than what is seen in the upland.

2.3 The Wetland Hydrological Landscape

Toolibin Lake has historically been a fresh to brackish inland wetland located at the terminus of Toolibin Catchment. The wetland is about three kilometres wide and is bounded on the east by aeolian dune deposits, which overlie fluvial sediments. In situ weathered granite occurs to the west [Dogramaci *et al.*, 2003]. The groundwater beneath Toolibin Lake has an average salinity above 30 kg m⁻³ TDS [Drake *et al.*, 2012a]. The lake is the first in a series of nine lakes within the regional playa lake chain, and is the only major lake in the chain that has not become irreversibly saline. The system occurs in what is termed the “flood” landscape in Figure 1 and it receive only periodic inflow pulses when internal storages of the valley floor systems are filled and flow connects throughout the valley floor landscape. As such, the wetland accumulates standing water only infrequently during wet years. In dry years, water inputs are often not sufficient to pond surface water for substantial periods of time (months). The natural inflow of Toolibin Lake occurs in the northeast part of the wetland and the natural outlet occurs on the southern side. Surface water monitoring at the end of the catchment, immediately up gradient of the lake, has occurred since 1977.

In addition to this sporadic catchment runoff (valley floor discharge) into the wetland, other water balance inputs include groundwater and direct rainfall (Figure 7). Groundwater inflow is small relative to the surface water inflow, but it may contribute a significant salt loading by replenishing groundwater beneath the lake. Outflows are dominated by evapotranspiration with some minor losses thought to occur to the regional aquifer [Merz, 2000]. Groundwater seepage can occur into the lateral margins of the lake bed from the unconfined aquifer surrounding the lake and from the confined palaeochannel aquifer which underlies the lake bed. The presence of several dolerite dykes restricts significant groundwater inflow to the lake from the north.

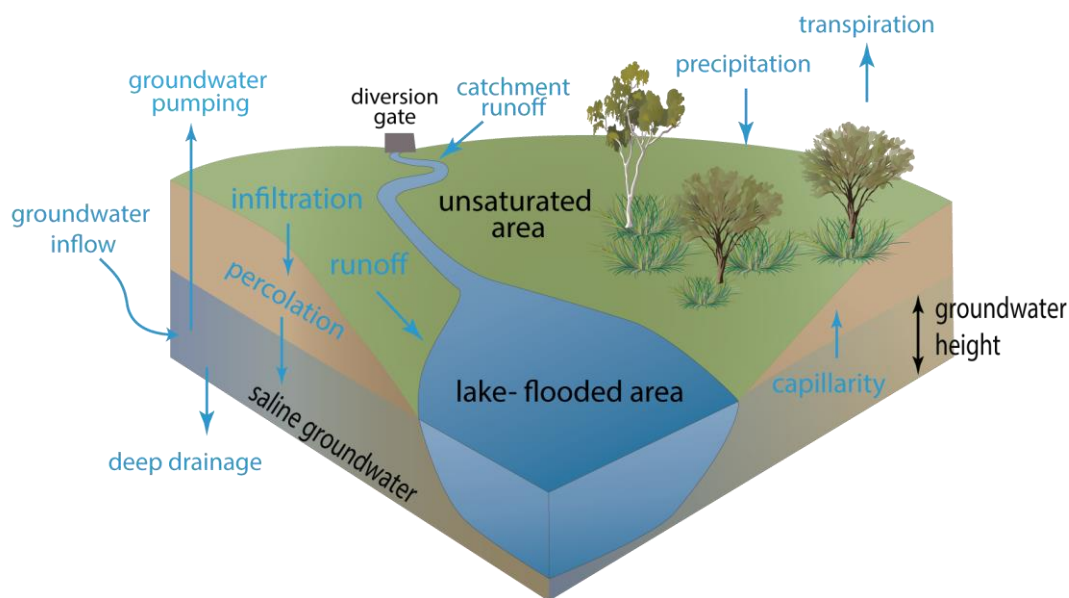


Figure 7: Schematic representation of landscape and hydrological processes typical of the wetland.

Within the lake system, the historical rising water table and salinity has caused the co-dominant plant species *C. obesa* and *M. strobophylla* to be impacted [George *et al.*, 2004]. Surface water diversion and groundwater pumping were implemented in 1996 as management measures to reduce these impacts. By 2004, approximately 4,000 tonnes of salt was diverted from the lake by a surface water diversion gate that selectively lets in flows with a salinity of less than 1000 kg m⁻³ TDS [George *et al.*, 2004]. In parallel, during the 7 years of pumping (from January 1998 to October 2005), it is approximated that more than 590,000 m³ of water per year was extracted (approximately 1,500 m³ per day, on average), which at a concentration of approximately 28 kg m⁻³, has led to the removal of 119,000 t of salt (approximately 5,000 t per year). Low rainfall in 2000-2002 and pumping 660 m³ d⁻¹ were observed to lower piezometric levels beneath the lake by several metres [George *et*

al., 2004]. Pumping continued at near the maximum rate possible from the bore network until 2005 when a series of incidents have caused a prolonged period of intermittent system failure. During this period the groundwater levels have recovered to near the pre pumping levels. Records of pumping volumes after 2005 are also not available.

Previous lake vegetation assessments have been described [Froend et al., 1987]. However, those lake vegetation transect and quadrat data do not have a common pattern and have been collected for the purpose of various botanical investigations, rather than to quantify the average lake biomass. Remotely sensed data has been used to assess overall vegetation changes and a general positive trend in normalized, relative vegetation cover occurs between 1996 and 2009 [Zdunic, 2010]. The best estimate of biomass present on the lake bed comes from a monitoring snapshot of plant diameter at breast height (DBH), performed in 2005 [Ecoscape, 2005]. The survey included all species present in the lake bed, following transects made up of contiguous 20 x 20 m quadrats [Ecoscape, 2005]. *C. obesa* made up around 80% of the total biomass, with *M. strobophylla* and grasses occupying the remaining 20%. This has been converted to biomass using the relationship described in Goel and Behl [2005] for *Casuarina Glauca*, as no DBH to biomass relationship has been published for the target species *C. obesa* and *M. strobophylla*, however this is thought to be a reasonable approximation given other uncertainties associated with the survey data.

Variation across the lake-bed is depicted in Figure 8 based on a nearest neighbour interpolation of the above survey data, with an average biomass over the total area of 6.22 kg m⁻². Considering the relative fractions of species reported, the average value for *C. obesa* was approximately 4.97 kg m⁻², while for *M. strobophylla* it was approximately 1.24 kg m⁻². By assuming that 40% of the total biomass is allocated underground [Running and Coughlan, 1988] and using the relationship between above ground biomass and LAI formulated by Suganuma et al. [2006], it is possible to estimate the average leaf area index (LAI) within the lake bed as being approximately 0.78 m² m⁻².

Together with the vegetation survey, Ecoscape [2005] measured average soil salinity at the root zone in their quadrats (Figure 9). The maximum salt concentration reported was 23.3 kg m⁻³ TDS, which is equivalent to an electrical concentration (EC) of 42.7 dS m⁻¹, assuming that NaCl is the dominant salt in the solution. In the unsaturated zone, soil salinity and water content varies with depth. This is due to not only physical drivers (evaporation and capillarity) but also vegetation water use and subsequent salt exclusion [Drake et al., 2012b]. Between the surface and 1.5 m below ground, where most of the roots of *C. obesa* are accessing water, the soil was found to be, on average, 19% drier than at 3 to 4.5m, the preferential water uptake depth for *M. strobophylla* [Drake et al., 2012a; Vogwill et al., 2010]. With respect to soil salinity, the deeper-rooted *M. strobophylla* experiences, on average, a root zone 10% more saline than *C. obesa* [Taplin, 2010]. The increase in pore water salinity found just above (~ 10 cm) the water table level (DEC field data, unpublished) corroborates with a 1D numerical Richards equation resolved for Toolibin Lake [Bartlett, 2012; Taplin, 2010]. Groundwater salinity was reported as approximately 30 kg m⁻³ TDS [Drake et al., Submitted]. Together, the previous studies of lake hydrology, soil salinity and vegetation surveys allow for the development of an improved conceptual model of lake dynamics, as discussed in the next section.

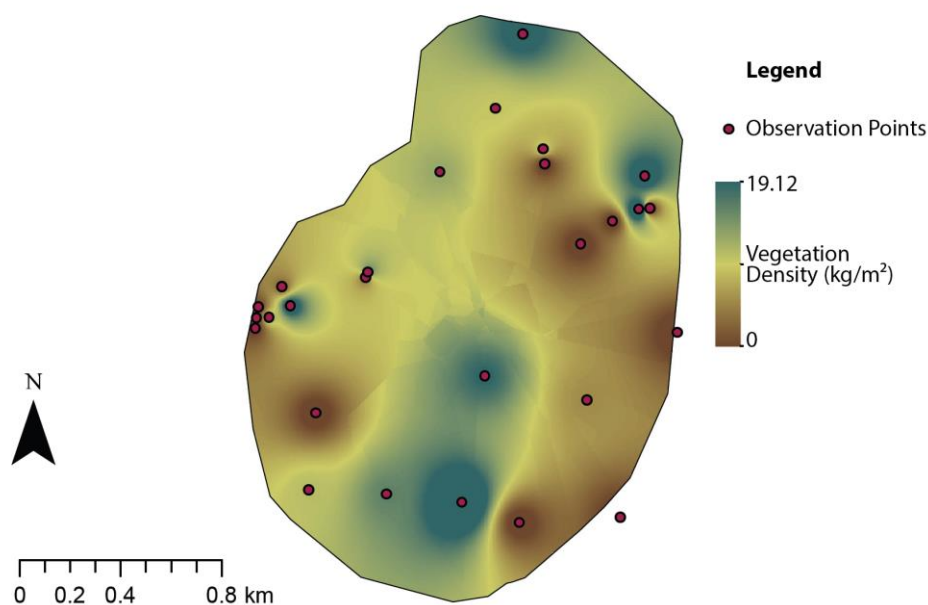


Figure 8: Biomass density map - Toolibin Lake as at January, 2005 [Ecoscape, 2005].

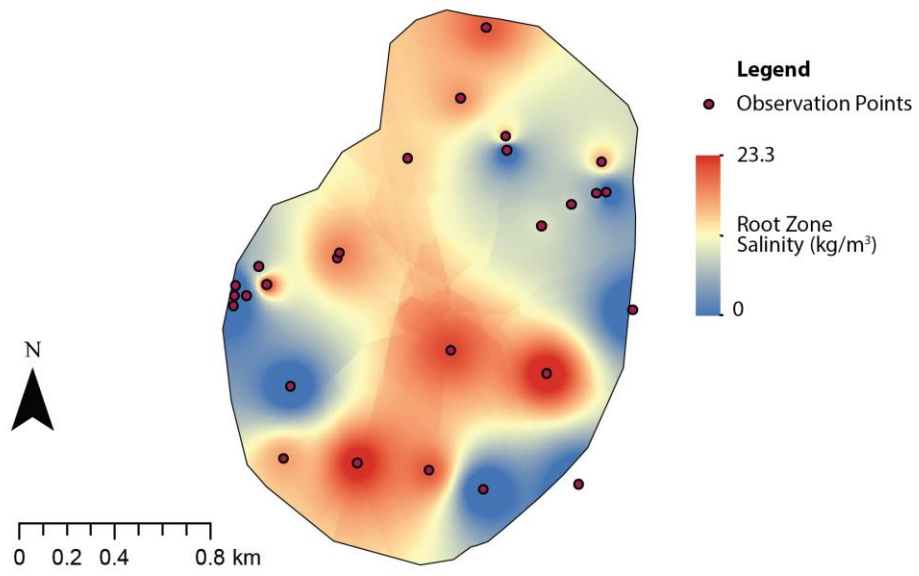


Figure 9: Map of root zone salinity in Toolibin Lake as at January, 2005 [Ecoscape, 2005].

3. Decision Support System Approach

The hydrological conceptualization of Toolibin Catchment and lake-bed outlined above was translated into a modelling framework designed to encompass the range of hydrological landscapes of the catchment, and consistent with the “flow-fill-flood” conceptualisation shown in Figure 1. To overcome the challenges of accounting for hydrological process heterogeneity whilst bearing in mind the patchy and often inadequate data available, we brought together a range of distributed and semi-distributed modelling approaches (Figure 10) designed to suit the hydrological function of different landscape units within the context of the management options under consideration and their required spatial and temporal scales. The adopted modelling methodology is relatively simple in the upper catchment, becoming more complex towards the wetland to accommodate the level of modelling detail in accordance with the calibration and verification data available. The data available for parameterisation and validation of all models, however, was patchy. For instance, detailed spatially explicit datasets of soil and regolith types across the catchment were not available.

To support decision making, a single model “system” would be preferable. Thus, the landscape models chosen have been integrated within a single simulation framework able to address the hydrological questions under consideration in this report (refer to Appendix I for the Operation Summary and the URL where the model is located). The system therefore supports “switches” that may be used to configure engineering interventions (such as surface runoff diversion, for example) and revegetation practices (refer to Appendix J). The framework is particularly suitable for low gradient, low rainfall, dryland catchments with relatively impermeable regolith and designed for investigations over periods of months to decade. Below, we describe the various components of the system and the linking approach.

3.1 Hydrological Regions & Model Domains

The distribution of different landscape hydrological units is depicted in Figure 11. The upland was resolved by a hydrological model that has its physical principles based on LASCAM (LArge Scale Catchment Model) [Sivapalan *et al.*, 2002] but which was adapted for this landscape and modelling framework (described below). This was called LASCAM-S, in reference to the “shedding” function of the upland region. Similarly, to represent the “receiving” hydrological function of the valley floor region, LASCAM-R, whose water storage pools and pathways, was configured to be more appropriate to a low slope landscape. The lake-bed itself was resolved by a wetland ecohydrology model termed WET-0D [Coletti *et al.*, 2013], which was able to resolve the water and salt balance and was further customised to capture the dynamics and competition of the major vegetation species of interest. The original LASCAM sub-routine for water routing between areas by Sivapalan *et al.* [2002], termed LASCAM-Q (for consistency), was responsible for connecting the surface from the upland (LASCAM-S) to the valley floor (LASCAM-R) units, all the way down to the wetland (WET-0D). Table 1 presents a summary of the modelling approach for each landscape, the type of simulation that the model computes and the field data available for calibration and validation.

The water surface routing network between the units was based on data collected by [Callow *et al.*, 2007] and Muirden and Coleman [2014]. Additionally, to connect the groundwater between LASCAM-S and LASCAM-R units (an ability that was not previously resolved in the original LASCAM), and from LASCAM-R to WET-0D, we created functions that estimated groundwater exchange between sub-catchments using Darcy’s law and the average head difference, making the groundwater component resolved in a similar way as earlier FLOWTUBE studies [Argent *et al.*, 2001; Clarke *et al.*, 2001].

Table 1: Summary of the landscape regions and models domains.

Hydrological Region	Model	Type of simulation	Field data available
Upland - “flow”	LASCAM-S	Water and salt balance	GW, surface water and salt export
Valley floor - “fill”	LASCAM-R	Water and salt balance	GW, surface water and salt export
Wetland - “flood”	WET-0D	Water and salt balance and vegetation growth	GW and lake level and sparse vegetation indexes
Upland & valley floor	LASCAM-Q	Surface water routing	Surface water gauges along the way

When coupled the model is therefore semi-distributed and subdivides the upland into 30 LASCAM-S sub-catchments (SC’s), based on topography, soils and drainage, and 4 valley-floor LASCAM-R units. Each SC is represented in the model to have uniform input parameters, but these parameters are able to be unique in

each SC. Since complexity in the valley floor topography and land-use pattern is critical in shaping surface water redistribution, aspects of the hydrological routing model in LASCAM (LASCAM-Q), as required for long-term management assessments, were parameterised from results of previous high-resolution modelling of the valley floor using the 2D flood model, TUFLOW [Coletti et al., 2012]. A detailed description of each of the models is presented in the Appendices A-E.

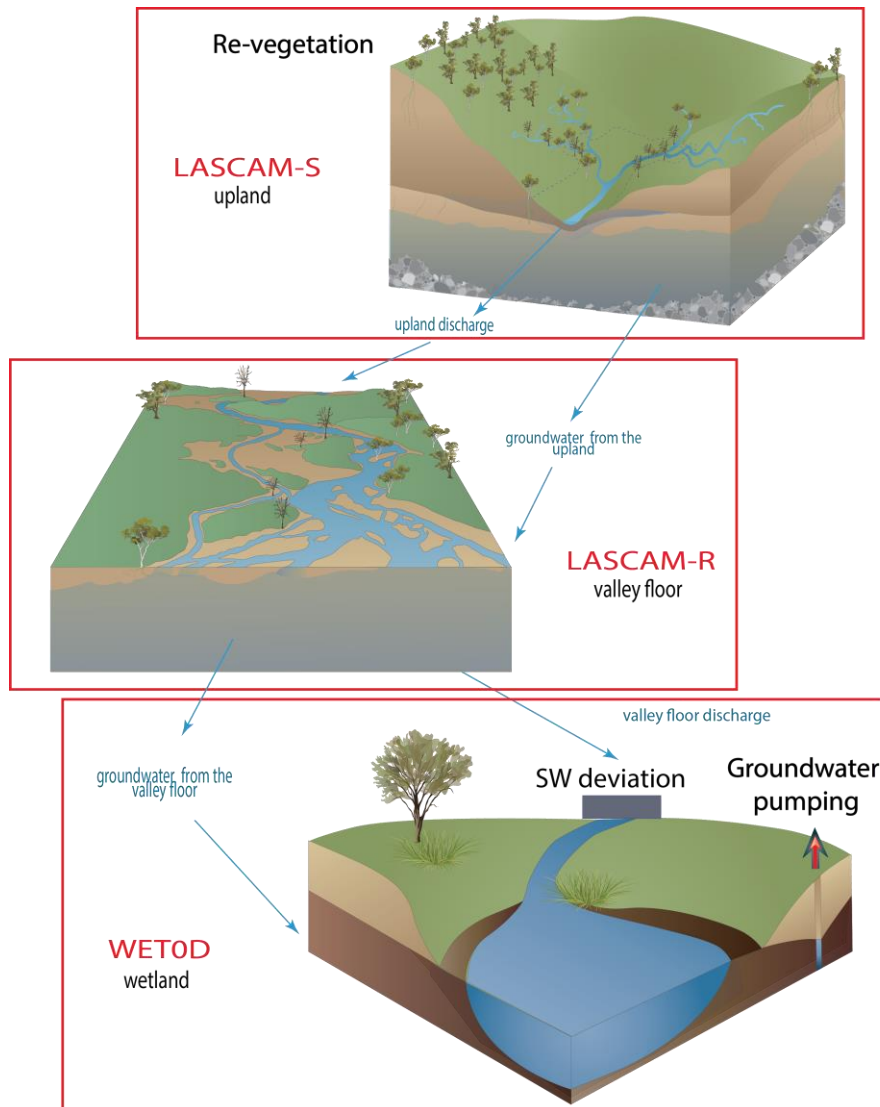


Figure 10: The integrated model system conceptualization showing the landscape partitioned into three major regions of distinct hydrological function resolved by a different modelling approach (red font) and the major engineering interventions tested (black font). Note that flow routing behaviour was also informed by simulations of the high-resolution TUFLOW model.

From a computational point of view, the model system simulates the exchange of groundwater from LASCAM-S into LASCAM-R and from LASCAM-R into WET-0D, and surface water runoff is routed from upstream to downstream catchments via LASCAM-Q, which contains surface water detention thresholds (storages) typical of the micro-topography and low connectivity in the valley floor [Callow, in prep.]. Both the LASCAM and WET-0D model units account for the unsaturated, saturated and surface water environments. Together, the models capture the dominant vertical and horizontal pathways of water and salt. Because the focus of the model was to explore vegetation dynamics within the lake-bed, WET-0D additionally includes a module to predict the growth and mortality of the two co-dominant vegetation species in the wetland in response to changes in hydrology and salinity. WET-0D is a suitable management tool because it quantifies vegetation biomass in response to the level of management intervention while explaining the underlying feedbacks that ultimately determine plant community success or failure.

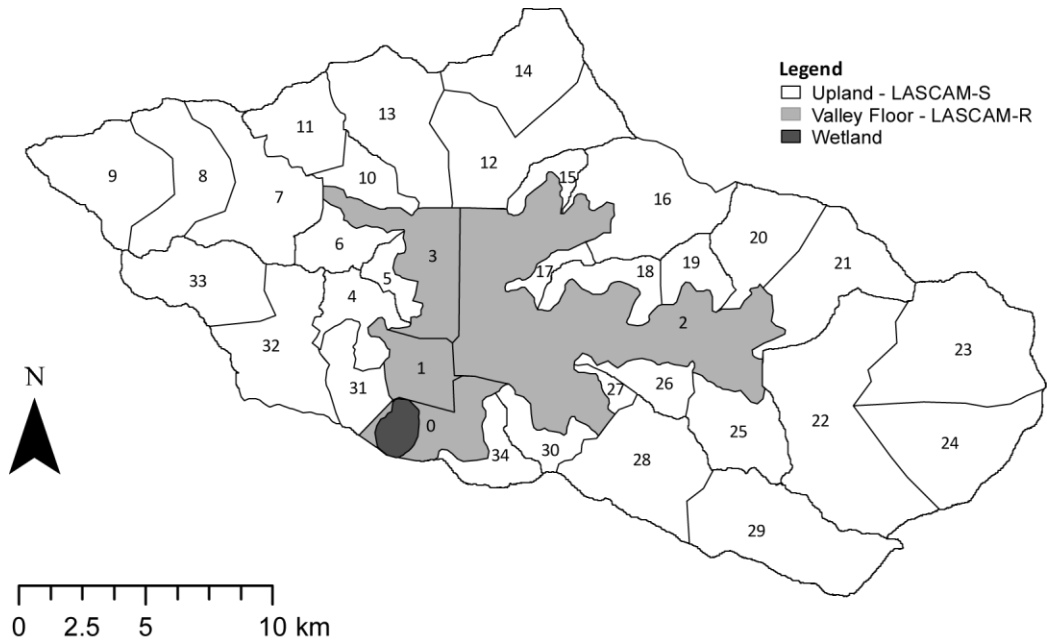


Figure 11: The distribution of the sub-catchments (numbered from 0 to 34) within the Toolibin Catchment map. The domain of each landscape and model is differentiated by colours.

Figure 12 outlines a conceptual flow diagram of how the model system can be used for scenario testing (including management actions and climate change), the model components and the major outputs predicted of relevance to decision-making. Appendix J presents examples of input files used to simulate climate change and re-vegetation scenarios.

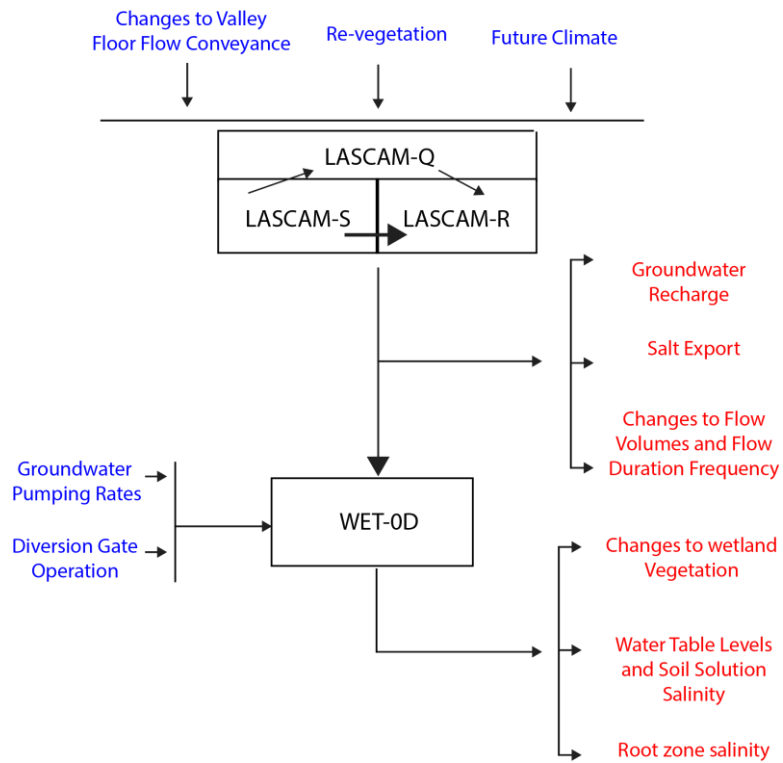


Figure 12: Summary of the decision support system. Possible testing scenarios are depicted in blue, hydrological models are depicted in black and the major outputs are depicted in red.

3.2 Model Parameterization

3.2.1 LASCAM-S

The upland “flow” region was conceptualized as having two soil layers (Figure 13) of different hydraulic conductivity. The upper soil layer is set to have a typical hydraulic conductivity of ~0.15m/day and a total porosity of 35-38%. The lower layer is characterised by fine-grained material with a hydraulic conductivity of 0.01m/day and a total porosity of 40-50% (Table 2). Both layers are further sub-divided into storages based on the degree of saturation as defined below:

- D. The upper soil layer across the upland is typically close to field capacity (except in the very surficial layers in summer), though it may temporarily hold water above field capacity as it drains to the A and F stores. This water is available for transpiration by deep rooted plants and crops.
- A. Nearly saturated areas of the upper soil layer, discharging lower in the landscape of the upland areas. Conceptually, this can be understood as perching/interflow but can also interact with deeper groundwater system and support riparian and lowland woodland vegetation.
- B. The permanent deeper groundwater system, stored within the lower soil layer. In the context of the wheatbelt this is saline groundwater that may discharge to surface water systems and is not subject to substantial use by deep-rooted vegetation due to high salinity.
- F. An intermediate unsaturated infiltration store between the water table and bottom of the top soil horizon. Depending on the water deficit in this storage, it will pull water from the above layer, and will recharge the B storage once it is full.

The LAI for each sub-catchment was derived from analysis of the 1km resolution MODIS LAI product. This accounted for seasonal variations (Figure 14), which were passed into LASCAM-S and LASCAM-R. We assumed that each sub-catchment has a fraction of deep-rooted woodland vegetation (referred as LAI_{gm} in Table 19) based on available mapping of remnant vegetation (Figure 4). This fraction varies from as low as 4% to almost 50% and was assumed as equivalent to the riparian vegetation fraction (referred as LAI_{rip} in Table 19).

Table 2: Summary of typical parameters used in LASCAM-S and their justification. Refer to Appendix A for model equations.

Parameter	Unit	Value	Reference/Remark
A ₀ ; D ₀ ; F ₀ ; B ₀ : Initial water storage	mm	200; 300; 700; 6000	Initial condition based on the depth to the bedrock, depth to the water table and estimated soil water content
Z _{min} : min thickness of top layer	m	0.5 - 1	Parameter used for calibration, based on sub-catchment responsiveness to rainfall
Z _{mean}	m	3 - 5	[Dogramaci <i>et al.</i> , 2003]- Figure 6 and references therein
β _w : slope parameter to account for surface slope on top-soil volume	-	1	Catchments assumed to be having a relatively flat constant grade of 2-5%
Z _{BR} : Depth between bedrock and top of bottom layer soil profile	m	20	[HilleRisLambers <i>et al.</i> , 2001]- Figure 6 and references therein. We acknowledge that in many instances some deeper regolith profiles are described, but from a hydrological point of view, the actual depth of the catchment bears little influence on the near-surface hydrological dynamics
φ _{UL} : Upper Layer (top soil) total porosity	m ³ /m ³	0.35 – 0.38	[Taplin, 2010]
φ _{BL} : Bottom Layer (sub soil) total porosity	m ³ /m ³	0.4 – 0.5	[Dogramaci <i>et al.</i> , 2003]
K _{UL} : Upper Layer (top soil) saturated hydraulic conductivity	m/day	0.15	CSIRO [2008] reported: “perched groundwater flow (throughflow) occurred in the higher permeability (~0.15 m day ⁻¹), near-surface soil materials”
K _{BL} : Bottom Layer (sub soil) saturated hydraulic conductivity	m/day	0.01	CSIRO [2008] reported: “regional groundwater flow occurred in a variably textured, deeply weathered material in which the hydraulic conductivity varied from < 0.001 to 0.14m day ⁻¹ ”
θ _c : Top-soil field capacity	m ³ /m ³	0.1 -0.12	[Taplin, 2010]
γ _A : Parameter governing ET from the riparian zone store.	-	0.9 – 0.95	Adjusted to assure ET equals to approximately 90% of rainfall [CSIRO, 2009; Lambert <i>et al.</i> , 2013]

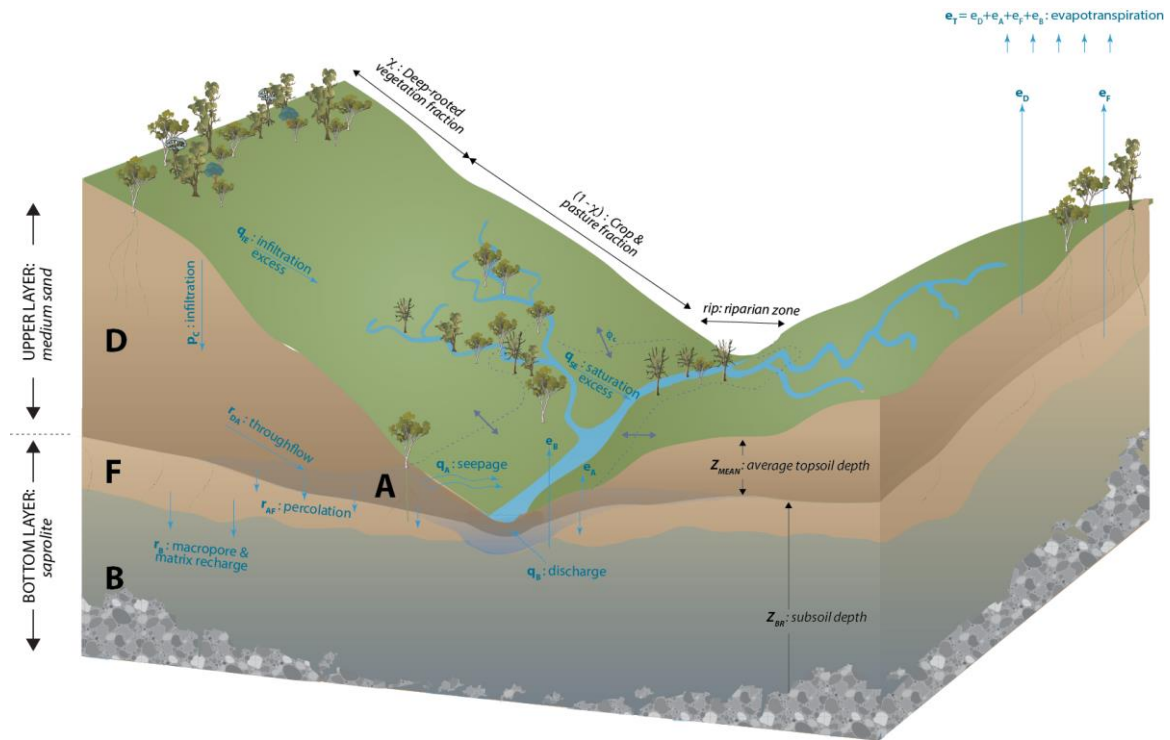


Figure 13: LASCAM-S - Upland hydrological zone model stores and simulated pathways. Refer to Appendix A for model equations.

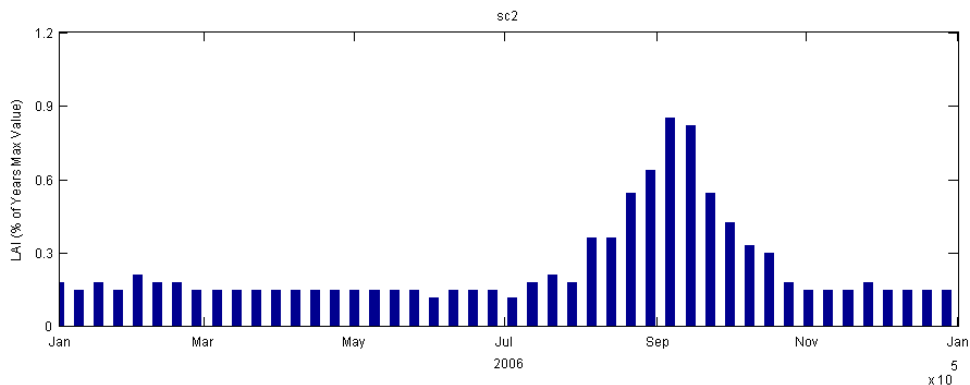


Figure 14: Weekly LAI variation in an example sub-catchment (SC02), as derived from the MODIS LAI products.

3.2.2 LASCAM-R

The valley floor conceptually receives water from the upland and conveys it to the wetland in flood periods, after becoming “filled”. The major water pathways are infiltration, recharge, capillarity rise and evapotranspiration (Figure 15). The end-of-catchment unit is located in the valley floor and is denoted SC1, which corresponds to the drainage area of the Department of Water (DoW) gauging station number 609010. The hydraulic parameters and their sources are summarised in Table 3.

Table 3: Summary of parameters used in LASCAM-R. Refer to Appendix B for model equations.

Parameter	Unit	Value	Reference/Remark
D_0 ; B_0 : Initial water storage	mm	300; 600	Initial condition based on a typical estimated soil water content
ϕ : Soil porosity	m^3/m^3	0.38	[Taplin, 2010]
K_s : Saturated hydraulic conductivity	m/day	0.15	[Taplin, 2010]
θ_{fc} : Top-soil field capacity	m^3/m^3	0.12 -0.1	[Taplin, 2010]
γ_A : Parameter governing ET	-		Adjusted to assure ET equals to approximately 90% of rainfall [CSIRO, 2009; Lambert et al., 2013]

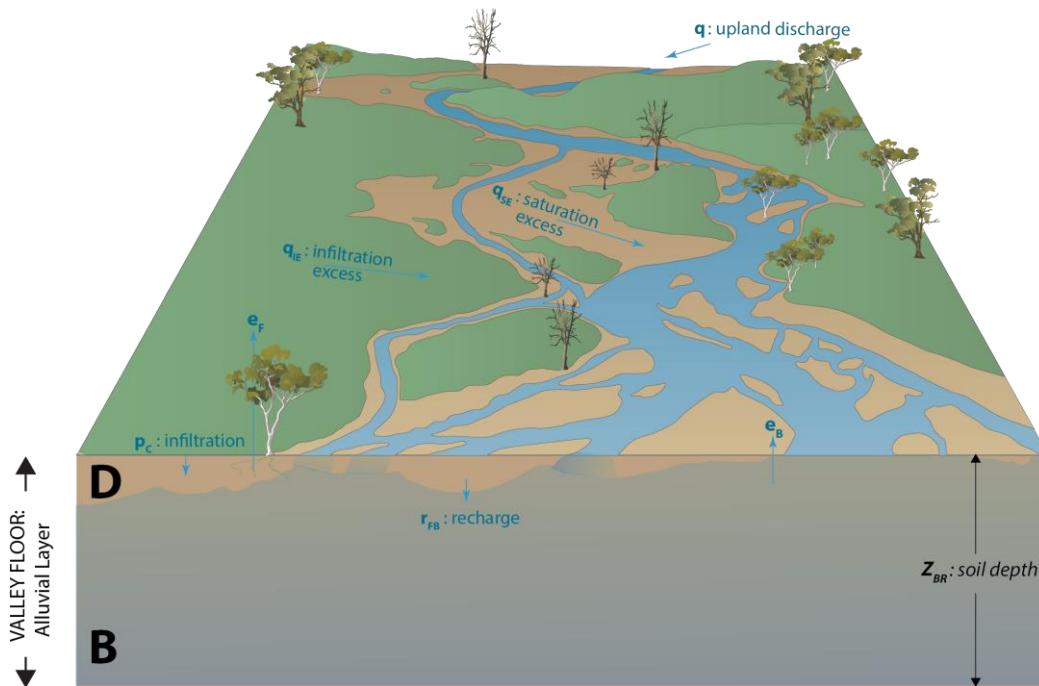


Figure 15: LASCAM-R - Valley floor hydrological stores and pathways. Refer to Appendix B for model equations.

3.2.3 LASCAM-Q

LASCAM-Q is a module of the original LASCAM [Sivapalan *et al.*, 2002], whose function is to convey surface water from consecutive sub-catchments, accounting for the time-lag associated with water originating from different places at different times, and associated losses and detention storage along the way. As is often the case in the SWWA catchments, stream channels are not well defined and water ponding is frequently observed in areas of low-lying relief or disconnections. Once some critical volume is reached in these areas, the flow will proceed downstream and the flow connectivity is reached. To account for this behaviour, LASCAM-Q includes a “lake” function, representing a surface storage, which allows water and salt in the stream network to enter, fill, evaporate and finally overflow. A user-definable “dead” volume must be prescribed, below which no discharge can occur. Note that only a single surface storage can be included within the stream network per sub-catchment, and that the location of the storage is always assumed to be at the sub-catchment outlet.

Flow that does not reach the outlet (does not exceed the dead volume) is accumulated and remains available for routing in the next time-step. Note that, where potential exists for streamflow generated far upstream to enter a dry channel downstream, reinfiltration is assumed to occur (into the A store), before any excess proceeds downstream. When salt is simulated and the stream dries due to excessive transmission losses (i.e. evaporation and reinfiltration), then the salt is retained in a streamside salt store for dissolution in any subsequent flows. Surface storages (“lakes”) are filled by incoming flows, and lose water to downstream discharges and to evaporation. The routing of flow and salt between sub-catchments within LASCAM-Q avoids the use of detailed stream cross-section information and hydraulic routing parameterisation. Instead, it accounts for the flows entering the sub-catchment channel (from the hillslope and upstream sources) and, based on an estimate of the stream velocity and evaporation rate, the amount of water that passes out of the sub-catchment is routed either to the downstream sub-catchment or into the surface storage, if present. Note however, that the parameters used here were guided by the detailed TUFLOW model results which captures the flow redistribution within the valley floor landscape at high resolution, as outlined next.

Table 4: Summary of parameters used in LASCAM-Q, and their justification.

Parameter	unit	Assigned value	Comments and empirical evidence
V_0 : Base stream velocity	m/s	0.1	Callow & Smettem (2007) - stream velocity = 0.1m/s for $Q < 0.1 \text{ m}^3/\text{s}$
dVo: velocity parameter	m^2	50	Callow & Smettem (2007) - stream velocity = 0.5m/s for $Q > 0.5 \text{ m}^3/\text{s}$
L_{max} : Maximum volume of the lake for SC1, SC2 and SC3, respectively.	ML	5, 15, 15	Based on the flow events discussed in Appendix I, as modelled with the 2D distributed TUFLOW model.

3.2.4 TUFLOW

TUFLOW is commercial software package to simulate the shallow water (St Venant) equations and is used for predicting flood inundation. The model uses the provided DEM to simulate water flows, and in each cell requires values for the Manning's roughness parameter (n), and the values used for infiltration (represented by an initial loss, IL, given in mm and a continuing loss, CL, given in mm/h), as are presented on Table 5.

Table 5: Summary of parameters used in TUFLOW.

LAND USE	MANNING'S ROUGHNESS COEFFICIENT – n ($s/m^{1/3}$)	INITIAL LOSS, IL (mm)	CONTINUING LOSS, CL (mm/h)
Channels and roads	0.01	-	-
Grassland	0.03	2	0.03
Remnant Forest	0.05	2	0.04

3.2.5 WET-0D

In the WET-0D domain, the lake is divided into 3 main water stores, including the groundwater, vadose zone and surface lake water. These zones vary in extent each day depending on water balance processes depicted in Figure 15. In addition to the basic hydrological fluxes of water and salt, the model captures the feedbacks between water availability, root zone salinity and vegetation growth such that the vegetation biomass in each zone varies depending on the suitability of that zone at any given time. Multiple vegetation groups exist in each zone and each has unique properties in terms of their water and salt requirements/tolerances, which creates competition between the groups as the water and salt stores change over time.

To parameterise the model, a local DEM was used to produce the relationship between the flooded area, A_L and lake volume, L_V (Figure 16). The phenomenon of clay macro-fissuring that follows dry periods is represented by k_{sd} , the hydraulic conductivity after a drought. It was estimated to be 8 times greater than k_s [Drake *et al.*, 2012b]. In the model, a "drought" is reached when the lake covers less than 10% of the total wetland domain and the water table is deeper than one metre below ground level. In any case, the horizontal hydraulic conductivity, k_h , was assumed as being 10 times greater than k_s [Merz, 2000]. We used the soil porosity, ϕ , and the height of the salinity sensors showing higher salinity content, which were located around 10 cm above water table level [Drake *et al.*, 2012a], to infer the water volume transferred upwards via capillarity, Q_A , which was linearly related to the groundwater height, h_s , via a soil type dependent constant, k_A (Table 6).

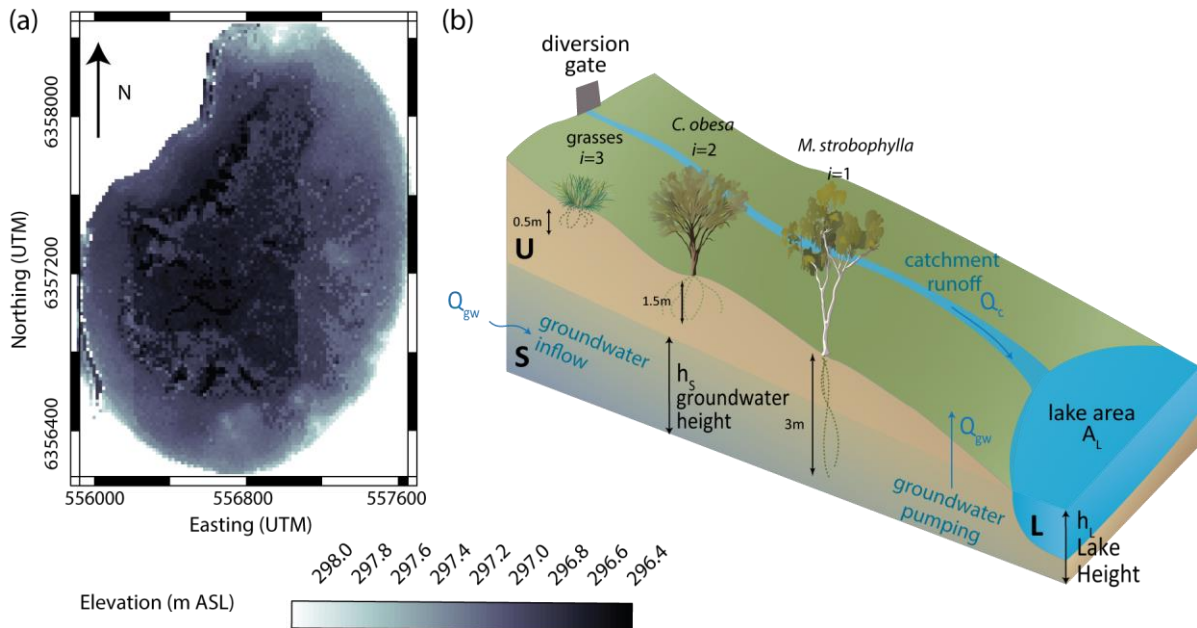


Figure 16: The DEM of Toolibin Lake (a). The wetland hydrological zones represented in WET-0D (U, S and L) and the vegetation species resolved by the model (b). Refer to Appendix D for model equations.

Table 6: Summary of parameters used in WET-0D and their justification. Refer to Appendix D for details of model equations.

Parameter	Unit	Value	Reference/Remarks
k_A : Capillary rise fraction	-	$10^{-6} \times h_s$	DPaW, unpublished data.
ϕ : Soil porosity	$m^3 m^{-3}$	0.38	[Drake et al., 2012b; Taplin, 2010]
θ_c : Soil moisture at field capacity	$m^3 m^{-3}$	0.12	Assumed to represent average condition
k_s : Vertical hydraulic conductivity	$m d^{-1}$	0.33	[Taplin, 2010]
k_{sd} : Vertical hydraulic conductivity after drought	$m d^{-1}$	$8 \times k_s$	[Drake et al., 2012b]
k_h : Horizontal hydraulic conductivity	$m d^{-1}$	$10 \times k_s$	[Merz, 2000]
α_g : Vertical hydraulic conductivity of the deepest layer	$m d^{-1}$	4.4×10^{-4}	This study
a : Albedo	-	0.25	[Ward and Trimble, 2004]
c : Pan-to-lake evaporation factor	-	0.8	[Dogramaci et al., 2003]
h_L : Lake level	m	0.5	Initial condition [George et al., 2004]
h_s : Water table	m	$0.65 \times h_w$	Initial condition [Merz, 2000]
θ : Soil moisture	-	0.15	Initial condition [Barrett-Lennard, 2008]
C_p : Specific heat of water	$kJ kg^{-1} C^{-1}$	0.007	[Ward and Trimble, 2004]
X_U : Ratio litterfall to foliage biomass	$kg C kg C^{-1} y^{-1}$	0.003	[Friend et al., 1997]
X_{Rd} : Ratio root litter to root biomass	$kg C kg C^{-1} d^{-1}$	0.01	[Friend et al., 1997]
CM_{max} : Maximum mesophyll conductance	$m s^{-1}$	0.0008	[Running and Coughlan, 1988]
Φ_0 : Photosynthesis light compensation point	$kJ m^{-2} d^{-1}$	432	[Running and Coughlan, 1988]
$\Phi_{0.5}$: Radiation level to normalize solar radiation	$kJ m^{-2} d^{-1}$	9730	[Running and Coughlan, 1988]
φ : Radiation extinction coefficient (V2, V3 and V1)	-	0.5	[Feikema et al., 2010]
T_{max} , T_{min} : Maximum and minimum photosynthesis temperature	$^{\circ}C$	37 and 0	[Running and Coughlan, 1988]
Φ_p : Photosynthetically active radiation	$kJ m^{-2} d^{-1}$	50% of solar radiation	[Landsberg and Waring, 1997]
CC_{max} : Maximum canopy conductance	$m s^{-1}$	0.0016	[Running and Coughlan, 1988]
LAI_{nmax} : Maximum LAI for n environment ($n = U, S$ and L)	$m^{-2} m^{-2}$	2	Arbitrarily defined
α_G : Recession coefficient for baseflow	-	0.001	[Farmer et al., 2003]
I_{max} : Maximum precipitation interception	m	0.002	Arbitrarily defined

The descriptions given by Bell [1999] and Drake et al. [2012b] about the behaviour of *M. strobophylla* and *C. obesa* were used to generate species-specific physiological parameters (Table 7). Following these reports, *M. strobophylla* represents a species moderately tolerant of inundation, drought and soil salinity. *C. obesa* represents a vegetation type highly tolerant of drought and soil salinity. Terrestrial short-rooted vegetation, referred to as "grasses", seasonally grows in Toolibin Lake. Although in low density and without measurement of their abundance, we estimated its density to be $0.5 kg m^{-2}$ and assumed a root depth of 0.5 m and higher water requirements than *M. strobophylla* and *C. obesa*. Salinity tolerance was set as the same as *M. strobophylla*. In each physiological parameter, sub-indices 1, 2 and 3 indicates *M. strobophylla*, *C. obesa* and grasses, respectively.

Table 7: Vegetation parameters used in WET-0D and their justification.

Parameter	<i>M. strobophylla</i>	<i>C. obesa</i>	grasses *	Reference/Remark	
Total root depth, h_r	3 m	1.5 m	0.5 m	[Drake et al., 2012b]	
Preferential uptake depth observed in the field	10cm above h_s	1 m below ground level	0.5 m	DEC unpublished data	
Soil potential that stops carbon assimilation ($\Psi_{soil} = \Psi_{\theta} + \Psi_{II}$)	-3.7 MPa	-5.1 MPa	-3.29 MPa	[Drake et al., 2012b]	
Wilting point, θ_w (without salinity restriction)	0.1 m ³ m ⁻³	0.07 m ³ m ⁻³	0.11 m ³ m ⁻³	[Drake et al., 2012b]	
Optimum soil moisture for carbon uptake, θ_o	0.45 m ³ m ⁻³	0.45 m ³ m ⁻³	0.55 m ³ m ⁻³	[Drake et al., 2012a]	
Maximum salt concentration acceptable in U, $\zeta_{max U}$	20.7 kg m ⁻³ TDS	36.3 kg m ⁻³ TDS	21.8 kg m ⁻³ TDS	[Drake et al., 2012b]	
Maximum salt concentration acceptable in S, $\zeta_{max S}$	20 dS m ⁻¹	12 dS m ⁻¹	-	These parameters are based on the fact that both <i>M. strobophylla</i> and <i>C. obesa</i> can survive under flooded conditions. However, under high salinity and waterlogged conditions both species decline productivity, especially <i>C. obesa</i> , which experiences a decline in its ability to support water filtration [Carter et al., 2006]	
Maximum salt concentration acceptable in L, $\zeta_{max L}$	3.7 dS m ⁻¹ ++	1.8 dS m ⁻¹ +	-		
Rate of salt uptake in U, $\zeta_{up U}$	0.2 kg m ⁻³	0.2 kg m ⁻³	0.2 kg m ⁻³		
Rate of salt uptake in S, $\zeta_{up S}$	0.2 kg m ⁻³	0.3 kg m ⁻³	0.2 kg m ⁻³		
Carbon uptake efficiency to reach carbon assimilation rate $\eta_{II U}$	1.10 kg C kg CO ₂ ⁻¹	1.05 kg C kg CO ₂ ⁻¹	1.50 kg C kg CO ₂ ⁻¹		
Carbon uptake efficiency to reach carbon assimilation rate $\eta_{II S}$	0.30 kg C kg CO ₂ ⁻¹	0.20 kg C kg CO ₂ ⁻¹	0 kg C kg CO ₂ ⁻¹		
Carbon uptake efficiency to reach carbon assimilation rate $\eta_{II L}$	0.90 kg C kg CO ₂ ⁻¹	0.20 kg C kg CO ₂ ⁻¹	0 kg C kg CO ₂ ⁻¹		
Respiration to biomass parameter, $k_{R U}$	50 m ² d ⁻¹	10 m ² d ⁻¹	37 m ² d ⁻¹		++ Brackish water [Brouwer and Heibloem, 1986]
Respiration to biomass parameter, $k_{R S}$	10 m ² d ⁻¹	10 m ² d ⁻¹	10 m ² d ⁻¹		+ Fresh water [Brouwer and Heibloem, 1986]
Respiration to biomass parameter, $k_{R L}$	20 m ² d ⁻¹	20 m ² d ⁻¹	20 m ² d ⁻¹		

4. Model Verification and Performance Assessment

Hydrological models include numerous parameters that are often calibrated through optimization procedures where a range in model parameters are assessed until the differences between the observed and model simulated data are minimized [Clark *et al.*, 2011]. However, these approaches work well when ample data is available for building statistically significant tests of model parameterisations, but may not be ideal when there are substantial limitations data availability. Hence the process of fully assessing the performance of a model requires a further "subjective" estimate of the accuracy and realism of the simulated behaviour of the model. The common approach to assessing model performance in subjective or behavioural terms is through visual inspection of the simulated and observed hydrographs and other relevant signatures, for example, we formulate subjective assessments of the model behaviour that are generally related to the systematic (e.g., over- or under-prediction) and dynamic (e.g., timing, rising limb, falling limb, and base flow) aspects of simulation output. Objective assessment requires the use of a mathematical estimate of the error between the simulated and observed hydrologic variables – i.e. objective or efficiency criteria [Wainwright *et al.*, 2011]. Both objective and subjective assessment require long term, reliable field data. When good validation data is lacking, computing error statistics can be misleading and model results need to be interpreted more carefully.

The data available to calibrate and assess the model performance in Toolibin Catchment was relatively scarce. Long term (1978 to 2012) surface water gauging is available only from the end of catchment outflow, near Toolibin Lake. Surface water data collection in the upland part of the catchment started in 2007 and finished in 2010. In addition to the limited period of monitoring for these sites, the period also represents a lower-than-average rainfall distribution with limited surface flow events and some with very small peak flow rates, making the calibration process difficult since there were very few substantial events over which to test the model. As such, the confidence in the model's performance was built by combining the traditional assessment of the hydrological predictions against the observed data and also through assessing the model's performance against literature values for the region for key process pathways. For example, long-term estimates of groundwater recharge in the region were used to guide model performance rather than simply calibrating against data from any particular bore. This approach is also a function of the model design (with stores that are spatially averaged on a sub-catchment scale), whereas groundwater hydrographs respond to local scale changes in addition to regional drivers.

Since the main goal of this project was to generate a reliable water and salt balance for the catchment and the consequent flows to the wetland, our approach of comparing literature values with monitoring trends was deemed the most appropriate. As a result, the model is suitable to explore questions related to changes in the catchment water balance on wetland ecohydrology, but its coarse spatial resolution means that impacts of management measures implemented at the scale of individual landholders are unable to be addressed directly. Overall, the model system has been developed to guide decision making associated with identifying the most important approaches or combination of management approaches at the sub-catchment scale in order to restore lake-bed vegetation. As model validation improves with further data collection efforts, model predictability power will increase.

4.1 Comparison Against Literature Values

Firstly, we reviewed and updated the model physical basis to ensure it is consistent with empirical knowledge and secondly, we evaluated the models internal stores, water storage changes and trends, as well as the internal water redistribution pathways, to ensure they reflect our understanding of "typical" wheatbelt hydrology. In particular, we considered the basis for the model setup conceptualization and analysis of model predictions with available evidence for runoff thresholds, recharge rates, groundwater trends, and evapotranspiration rates.

Overall, the model was able to mimic published SWSA wheatbelt values for important hydrological variables. These include: groundwater recharge (3 to 12% of total precipitation); evapotranspiration (70 to 120% of precipitation); and soil water content (60-12% of capacity). In terms of incident rainfall, approximately 30% evaporates from the D store and 70% flows to the B store where some will be lost through "riparian" evapotranspiration, with the rest redistributed to the lower valley floor area, but the proportion of ET to down gradient discharge is highly variable depending on the sub catchment under scrutiny. Appendix G: Summary of Water Storages and Fluxes presents the time series of the major hydrological variables for each gauged sub-catchment in the upland region. A summary of model predictions versus relevant references is presented in Table 8.

Table 8: Summary of the major hydrological processes and average values predicted by the model (based on 1979-2013 simulation) and values reported in the literature for similar sites.

Process	SWWANC-DSS prediction	Literature reports and empirical evidence
ET from the top layer	0.2 – 3 mm	ET from native shrubland is around 1-3mm/day [Sinclair et al., 2011]. Estimates of transpiration from dryland: ~ 1mm/day [Aydin et al., 2005]. Pastures in the wheatbelt: average 1.4 mm/day [Farrington et al., 1992].
ET from the groundwater	0 – 0.4 mm	It is well established that trees tend to source water from the unsaturated zone water supply when high salinity is present in the groundwater [Holland et al., 2006].
Throughflow	Occur in the model when top soil field capacity is exceeded.	CSIRO [2008] highlighted that perched groundwater flow (throughflow) occurred in the higher permeability (~0.15 m day ⁻¹), near-surface soil materials, which is equivalent to the sandy material in the Toolibin Catchment.
Recharge	3-12%	[Hancock et al., 2011] estimated, using a chloride mass balance approach that the additional recharge resulting from clearing of eucalypt forest ranged from 23 to 65 mm/year depending on location and annual rainfall. The recharge was equivalent to 5 to 10% of annual rainfall.” Recharge up to 10% in SWWA [George, 1992]. In the wheatbelt, it was 0.5% is now ~ 4% [Myette et al., 1987]. Net groundwater recharge to the semi-confined and confined systems is usually less than 1 mm yr ⁻¹ [Hatton et al., 2003].
Groundwater trends	Positive relation to the rainfall trends (declining levels)	Mouat et al. [2008] reported that the average recharge rate changes in Toolibin catchment were proportional to changes in annual rainfall.

4.2 Comparison Against Field Data

In this section, we present the daily time-series of observed and predicted values for surface runoff as well as groundwater variations. The specific criteria computed, when applicable, were the Root Mean Square (RMS) error, Mean Absolute Error (MAE), Normalised Root Mean Square (NRMS) error, Nash-Sutcliffe model efficiency coefficient (N-S) and Coefficient of Determination (R²). Those indexes are presented in the plots. The methodologies used for calculating them are given in Appendix F: Model Performance Indices. Note that all metrics were not computed in all cases, based on assessment of the available data sample size, which were available to compare the model to. For example, where a single event was recorded above a background value of 0 (e.g., Figure 17 -18), then it is not appropriate to compute the N-S or other metrics. Similarly, where there was no discernible trend in the data then we were simply seeking to capture the mean rather than compute R² or N-S, for example. In some cases, field data was inconsistent (e.g., runoff when no rain occurred, or physically unrealistic fluctuations in groundwater levels). In these cases we did not deem appropriate to compute exact error metrics, as not to bias readers into assuming model dysfunction when the quality of the forcing data or validation data could not be verified. As such, we relied upon subjective assessment of model performance.

The simulation period spanned from 1979 to 2013, mainly using climate data from the Wickepin BoM Station to force the model. Additional rain gauge data from DAFWA and DPaW were interpolated and used when available, between 2004 and 2012 [Muirden and Coleman, 2014]. These stations did not have a complete record of all climate parameters required. In addition, they were reported as presenting “a potential rain shadow effect from overhanging trees” [Muirden and Coleman, 2014]. From the data available there is a likely variation of incident rainfall across the catchment domain, since the average rainfall across the catchment varies by up to 8 mm per month [Muirden and Coleman, 2014]. As such, some events affecting the catchment would not necessarily be recorded in the Wickepin Station data (and vice-versa) and the overall uncertainty in the model predictions may be attributed to issues associated with this forcing data.

4.2.1 Surface Runoff

The locations of gauging stations with data available for validation are given in Figure 17 and their details in Table 9. Sub-catchments SC7, 10, 12, 22, 28, and 32 (Figure 18 to Figure 23) are located in the upland area and SC3, 2 and 1 are located in the valley floor (Figure 24 to Figure 27). These sites have data from 2007-2010 with the exception of SC1 (the end-of-catchment gauge), which has data from 1979 to 2013. N-S, RMS, MAE and NMRS are provided in the graphs where calculation was deemed appropriate. Appendix H: Monthly Comparison of Surface Flows the Coefficient of Determination (R²) between observed and predicted flow.

Along with hydrographs for SC1, flow duration curves for the model and observed data shows that the model captures the main events but under-predicts overall catchment runoff, but note the extreme distribution of the exceedance probability curve with all events <0.1% AEP (Figure 27). In general, all sub-catchments (both in the

upland and in the valley floor) were well represented (by LASCAM-S and LASCAM-R, respectively) in terms of timing and magnitude of the surface runoff. Some runoff events, which were observed on a sub-catchment scale, have resulted from localised rainfall events that were not recorded in the Wickepin Station, hence the lack of runoff predicted in these cases. In addition, some events were registered in the upstream gauges but not downstream, indicating potentially faulty readings or temporary flow disconnection. Details are provided in Appendix K: Surface Flow (Dis)connection.

Table 9: List of representative surface gauge for each sub-catchment.

Gauge name	Sub-catchment	Modelling domain	Type of data available
DOW609010	SC1	LASCAM-R (Valley Floor)	Runoff and salt load
DUL002	SC2	LASCAM-R (Valley Floor)	Runoff
DOW609038	SC3	LASCAM-R (Valley Floor)	Runoff
10HAL001	SC7	LASCAM-S (Upland)	Runoff and salt load
WDR001	SC10	LASCAM-S (Upland)	Runoff
12EDR001	SC12	LASCAM-S (Upland)	Runoff and salt load
03TIN001	SC22	LASCAM-S (Upland)	Runoff
HAR002	SC28	LASCAM-S (Upland)	Runoff and salt load
HC001	SC32	LASCAM-S (Upland)	Runoff

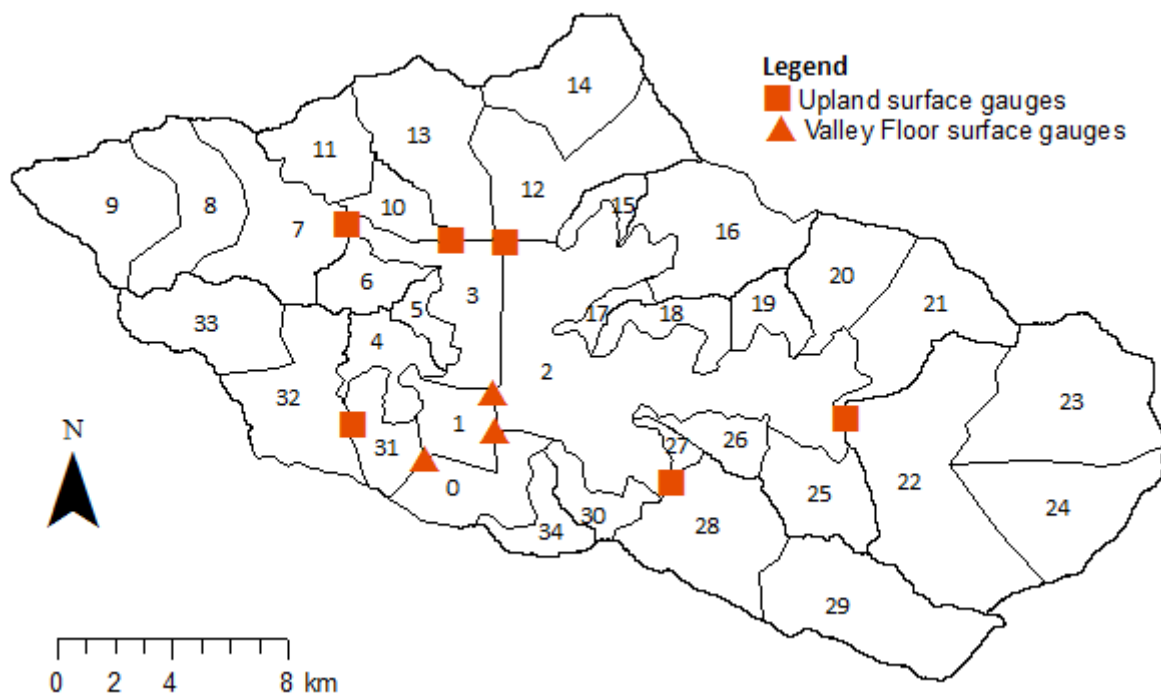


Figure 17: The location of each sub-catchment (SC0 to SC34) and surface gauges in the Upland (squares) and in the Valley Floor (triangles).

Upland

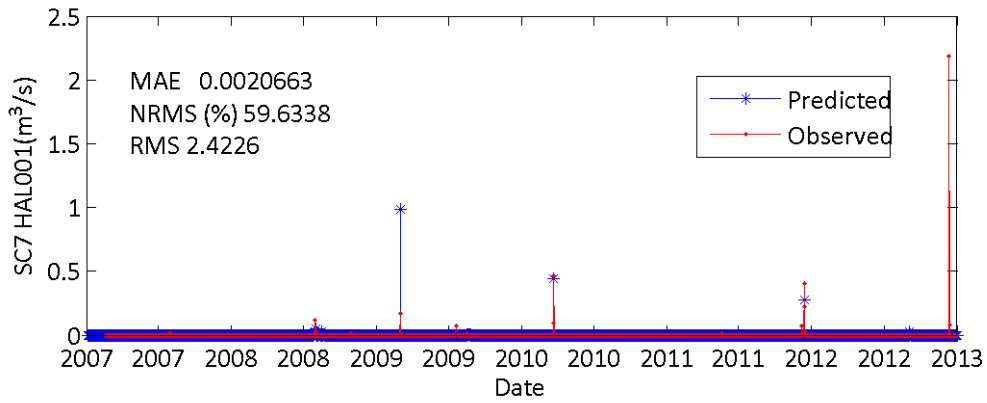


Figure 18: Sub-catchment 7 (SC7) and gauge station HAL001 surface runoff time-series.

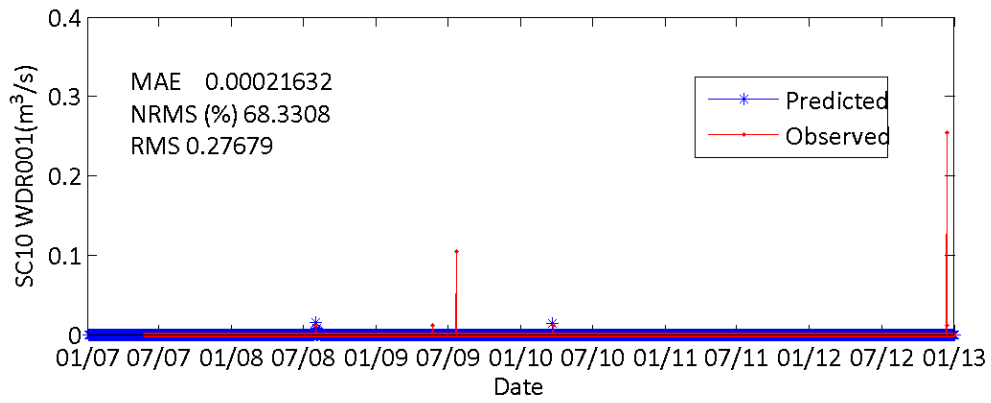


Figure 19: Sub-catchment 10 (SC10) and gauge station WDR001 surface runoff time-series.

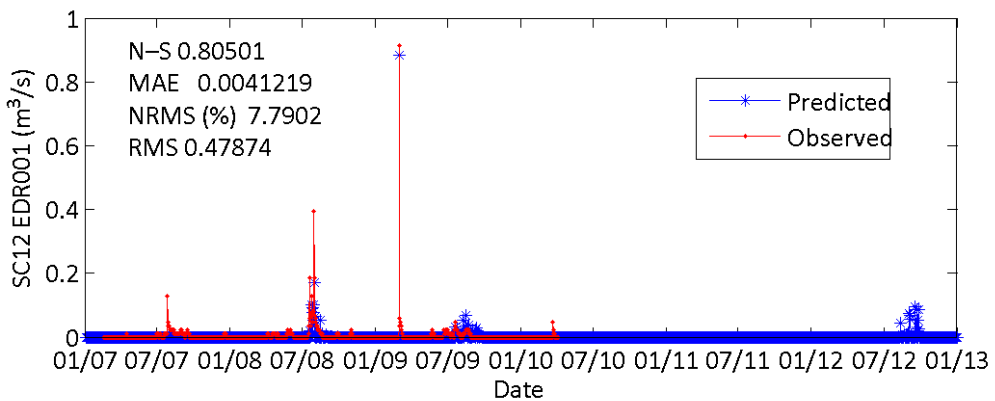


Figure 20: Sub-catchment 12 (SC12) and gauge station EDR001 surface runoff time-series.

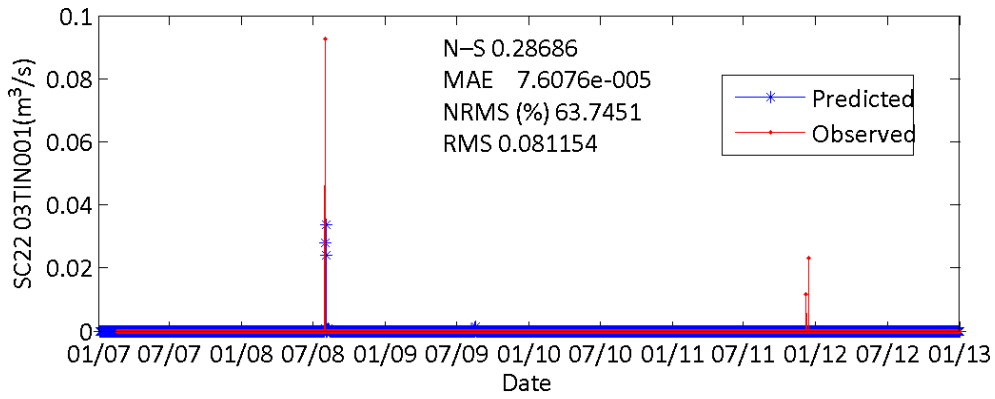


Figure 21: Sub-catchment 22 (SC22) and gauge station 03TIN001 surface runoff time-series.

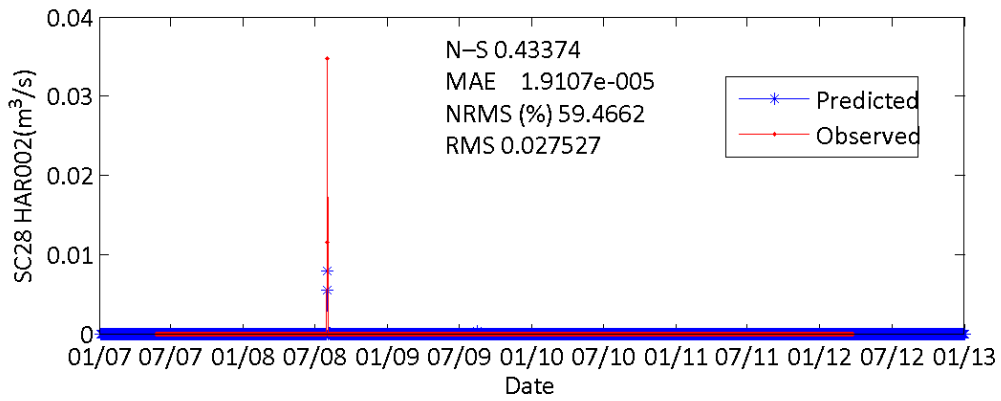


Figure 22: Sub-catchment 28 (SC28) and gauge station HAR002 surface runoff time-series.

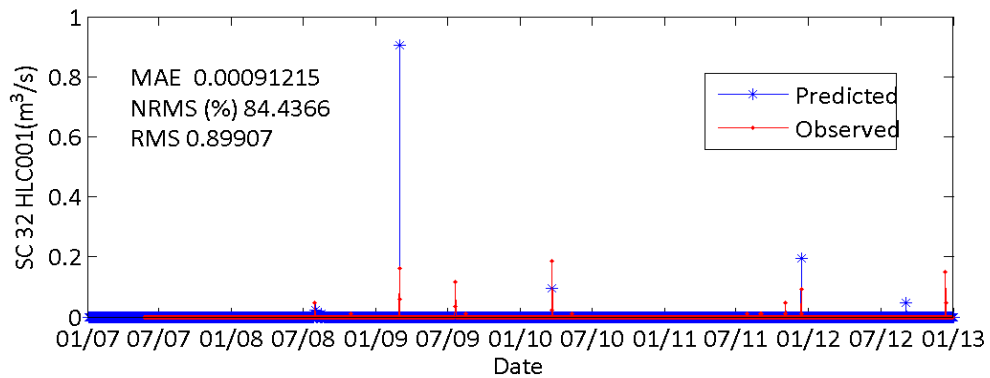


Figure 23: Sub-catchment 32 (SC32) and gauge station HC001 surface runoff time-series.

Valley Floor

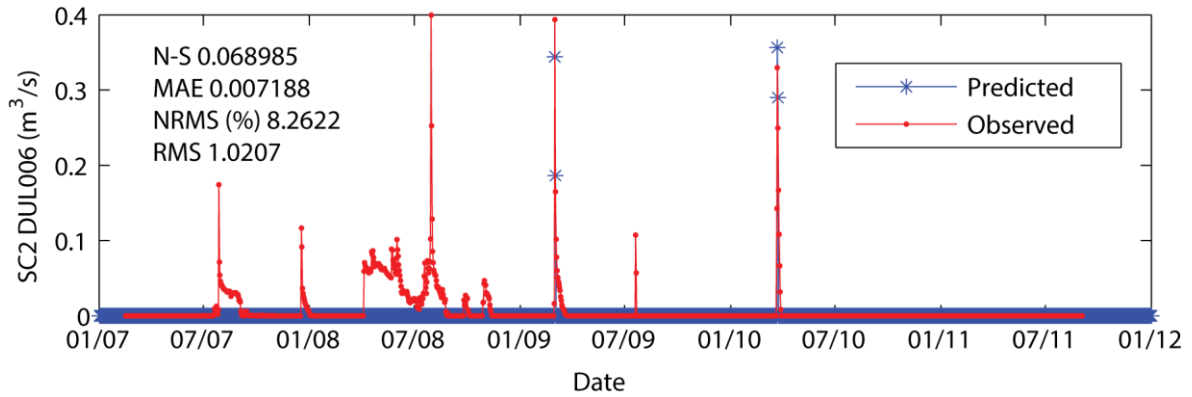


Figure 24: Sub-catchment 2 (SC2) and gauge station DUL006 surface runoff time-series (note the small magnitude of the Y scale).

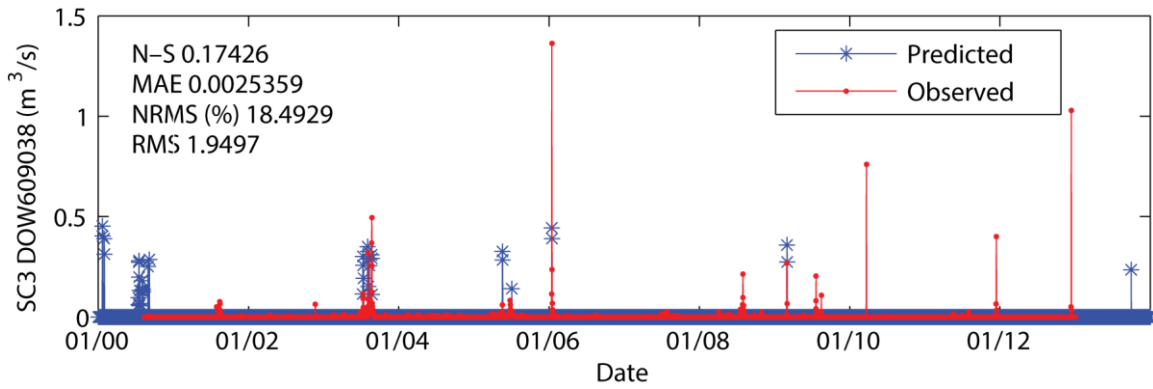


Figure 25: Sub-catchment 3 (SC3) and gauge station DOW609038 surface runoff time-series.

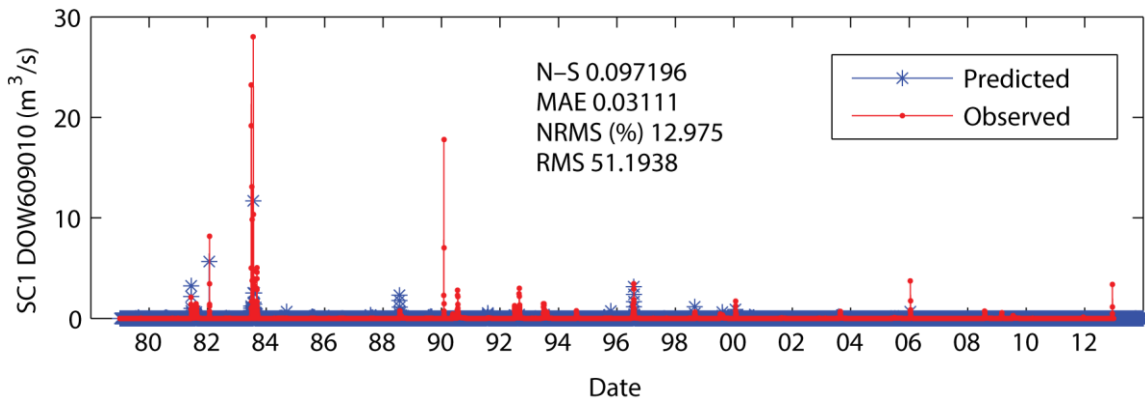


Figure 26: Sub-catchment 1 (SC1 – end-of-catchment) and gauge station DOW609010 surface runoff time-series.

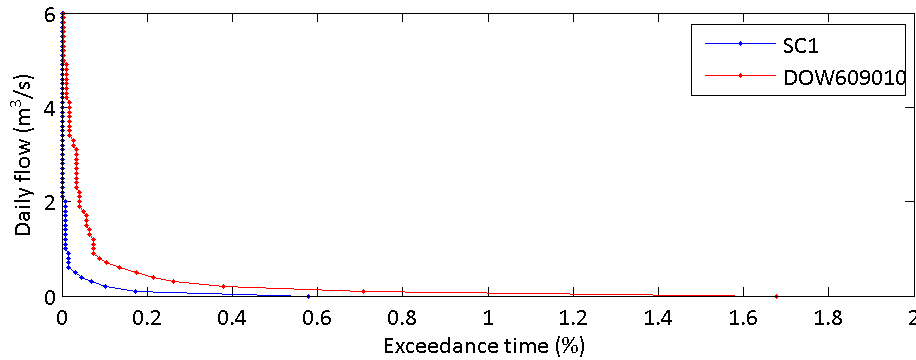


Figure 27: Sub-catchment 1 (SC1) and gauge station DOW609010 flow duration curve (from 1979 to 2013). Note the very small window of exceedance time periods (<2%) on the x-axis.

4.2.2 Salt Load

Daily EC and temperature datasets have been collected from 2007 to 2013 in SC7, SC12 and SC28 [Callow *et al.*, 2007]. Muirden and Coleman [2014] reported in the context of the DoW data that “the conductivity (EC) data was very inconsistent” and is generally deemed poor due to this inconsistency. There were three or four EC checks made at sampling sites during the life of the project, unfortunately these varied wildly to the trace value. Comparison was made more difficult by the lack of record of time of day of the check value and only recording the estimated TDS rather than actual EC.” Muirden and Coleman [2014] suggested that one of the problems could be related to sedimentation and estimate that some gauges can register 2 to 3 times higher salinity than the true value, and recommend the reading of salt load not to be used. Nevertheless, we present the values observed in the gauges for comparison to the ones predicted by the model. Note the general underestimation of the model predictions, which is in accordance to what is expected [Muirden and Coleman, 2014].

From 1988, the DoW collected daily water flows, water temperature and water EC at the gauge DOW609010. These data were obtained from the Water Information Reporting (WIR) section of the DoW website. We corrected the EC measured to a temperature of 25 degree Celsius using the relationship developed by Fofonoff and Millard [1983]. Thirteen days of data had been already converted by the DoW and this is shown as blue dots in Figure 31 b. By assuming NaCl as the dominant salt in solution, we converted the EC into TDS, in kg m^{-3} (Figure 31 b, red line).

The predicted salt concentration have similar values to those observed in gauge DOW609010 (Figure 31b). The discrepancies between measured and predicted salt load (Figure 31 d) occur primarily due to differences between observed and predicted flow (Figure 31 Figure 32 c). Also, some particularly high concentrations, like the ones measured in 1995 and 1996, occur when there was virtually no flow and during summer, when high temperatures (more than 40 °C) were recorded (Figure 31 a). In this case, risk of evapoconcentration cannot be ruled out.

Muirden and Coleman [2014] analysed the long term data (1979 – 2013) from the gauge DOW609010 in an “event-based” form. A strong relationship between inflow and salinity for two distinctive curves was seen, one for summer events, the other for winter events. A comparison between the values predicted by the model and those reported by Muirden and Coleman [2014] is shown in Figure 32, whose insert was extracted from the original report. No runoff event presented salt concentration higher than 4.5 kg m^{-3} (graph is presented in g m^{-3}) in the report. However, the event of 1995, whose concentration exceeded 27 kg m^{-3} , was present in the original data (provided by the authors) and was included in Figure 32. Note that the predicted values in Figure 32 refer to daily flows and not to events.

In general, summer runoff contains much lower salt concentrations, suggesting that the greatest salt contribution to surface water flows occurs when catchment groundwater is discharging to surface water systems, which is more likely in winter. If salt in surface water predominantly originated from surface accumulation of salts, salt concentrations in summer flows would be the same (or higher) than equivalent magnitude winter flows. This corroborates the idea that most salt enters Toolibin Lake from the groundwater rather than surface water.

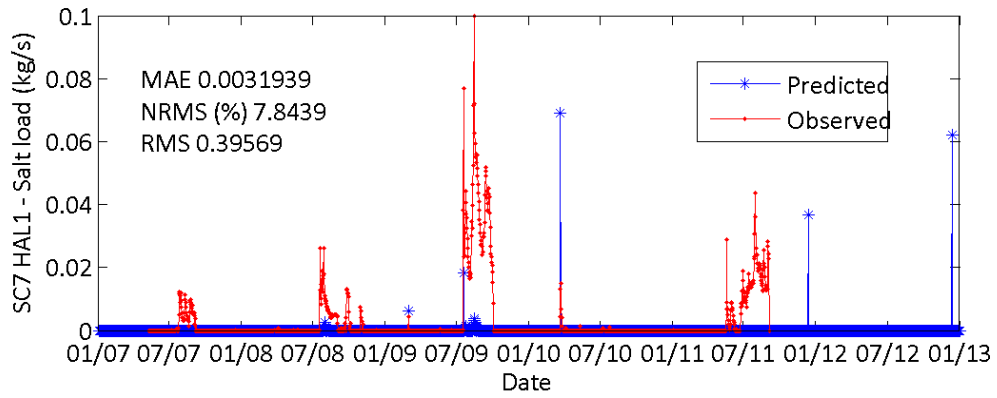


Figure 28: Sub-catchment 7 (SC7) and gauge station HAL001 salt load time-series.

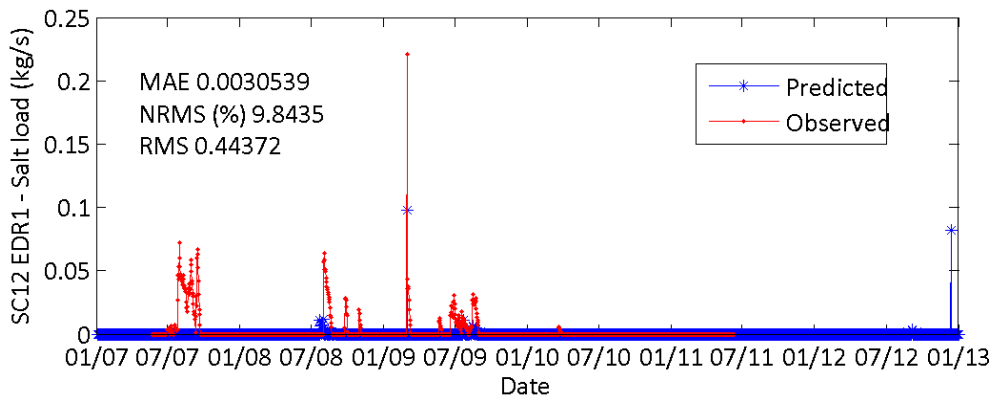


Figure 29: Sub-catchment 12 (SC12) and gauge station EDR001 salt load time-series.

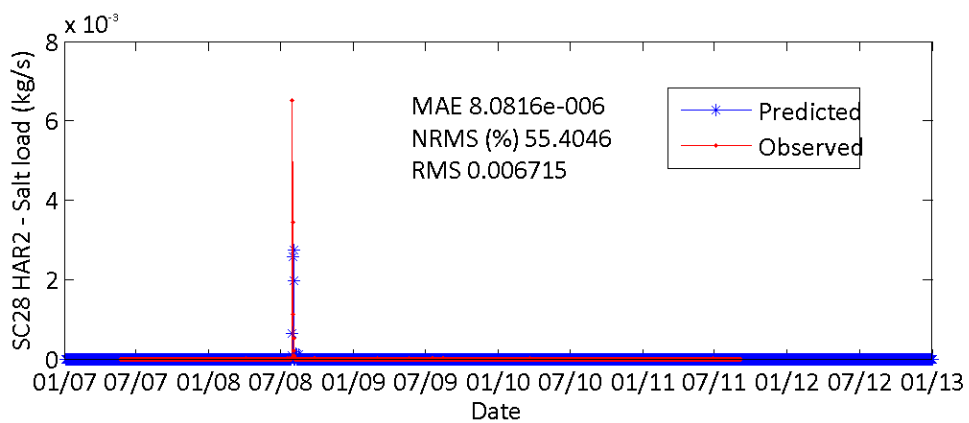


Figure 30: Sub-catchment 28 (SC28) and gauge station HAR002 salt load time-series.

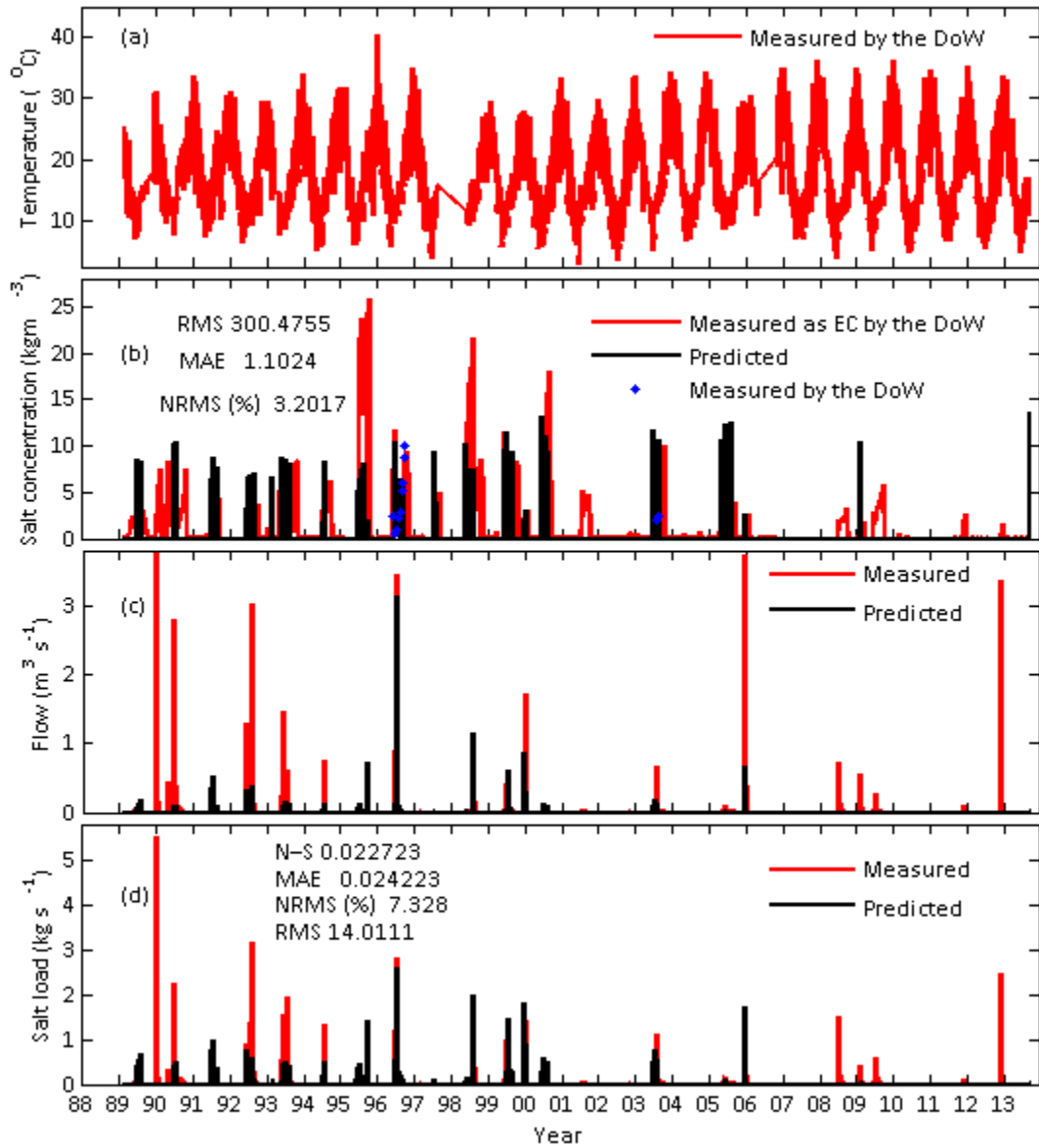


Figure 31: Sub-catchment 1 (SC1) and gauge station DOW609010 water temperature (a), salt concentration (b), flow (c) and salt load (d) time-series from 1989-2013.

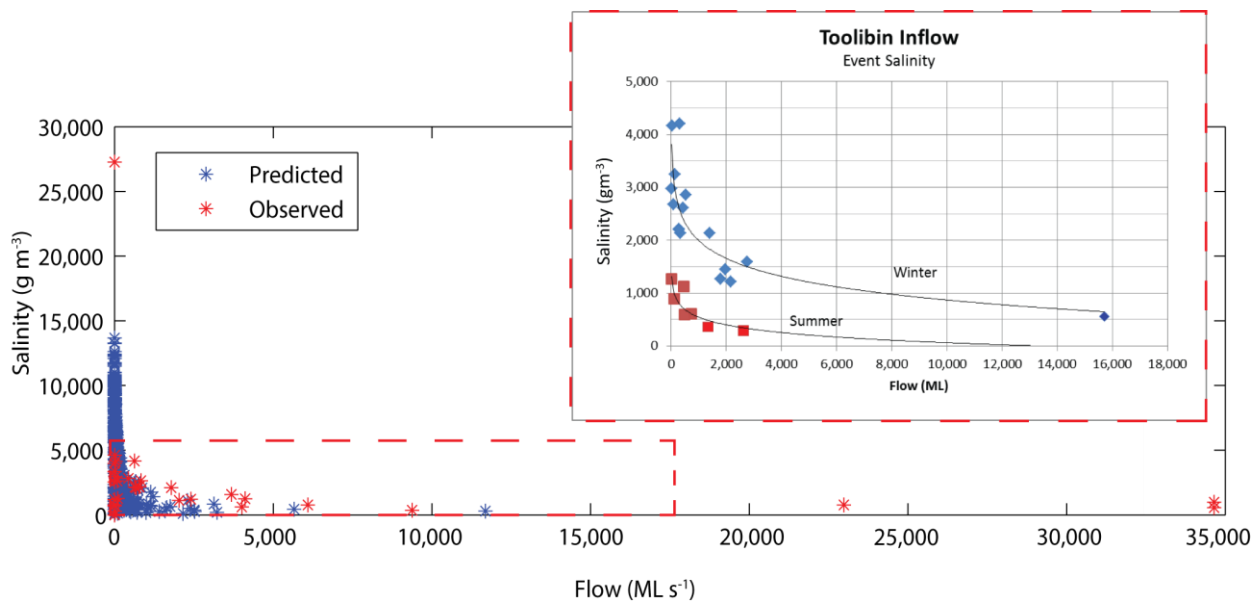


Figure 32: Inflow versus salinity at the gauge DOW609010 predicted by the model (blue stars) and reported (red stars) by [Muirden and Coleman, 2014]. The insert shows the original graph by Muirden and Coleman [2014], where summer (red squares) and winter (blue diamonds) were separated. The dash line shows the extension of the insert.

4.2.2 Groundwater

Upland

For the upland areas, data from 6 bores was provided by DPaW as representative of seasonal variation and trends in groundwater relevant to sub-catchments SC7, SC10, SC12, SC 22, SC 28 and SC 32 (Figure 33, blue triangles). In the valley floor, more bores were available in each sub-catchment so the group of bores lying within the sub-catchment domain was used as a reference for SC1, SC2 and SC3 (Figure 33, red dots). The name of those bores, their location, elevation and their respective sub-catchment are presented in Table 10.

All groundwater predictions by the model across the catchment domain were strongly correlated to the long-term rainfall trend, and reflected the seasonal balance of recharge, evapotranspiration and seepage. As identified in Table 8, net recharge rates of approximately 10% or less are expected, and this reflects the seasonal scale of variability in our B store (e.g., 10% of 300mm = 30mm, which once corrected for porosity is less than a 10cm rise in water table height). It is important to **note that the bore data is not providing a direct measure of the B store** as it is conceptualized in the model, but in fact a composite of B + A depending on the bore location within the landscape. As such the bore data show rapid changes of the order of 40-50cm between monitoring intervals that is not an accurate reflection of the sub-catchment average change to the B store height. For these fluctuations to be maintained across the area of the sub-catchment, then the entire years rainfall would need to recharge the aquifer or substantial lateral flows would need to enter from up-stream catchments. Given the relatively low lateral permeability and the known high evapotranspiration rates, it is therefore difficult to validate the model B store directly against the bore dataset as the individual bores are representative of localized conditions and reflecting a combination of saturated water stored in both the B and A store with in the model (e.g., see Figure 88). Depending on the screening of the bores, net change in water table height may in fact be a product of changes in the A and B store that could easily account for the scale of the variability seen in the field data.

Whilst it is therefore not appropriate to compare the exact values of the B store and bore heights, we are nonetheless able to explore trends. Some groundwater trends matched observed hydrographs well (SC 10, SC12 and SC32), while others do not (SC7, SC22 and SC28). The results for each sub-catchment are presented from the Figure 34 to Figure 42. Since the LASCAM-S resolves the lumped deep groundwater store for the whole extent of each sub-catchment, hydrographs poorly correlated to the long-term rainfall are most likely being driven by local scale hydrology (e.g., farm-scale drainage engineering, farm dams, and/or local clearing/revegetation efforts), that are not adequately represented in the LASCAM-S hillslope model. Therefore, we must turn to subjective measures of model suitability. George *et al.* [2008b] reported that the most common groundwater level trend in the wheatbelt was rising until the 1990's, followed by a gradual decline, and this long-term trend matches the models predictions well. In addition, other groundwater modelling in the Toolibin catchment also verified agreement between the long term rainfall trend and the groundwater predictions [Mouat *et al.*, 2008].

Given that rainfall in the catchment has been decreasing since the 1970's (Figure 3), rising groundwater levels in bores SS97221 (located in SC7), SS9724D (located in SC22) and LTC19 (located in SC28) may be related to small scale site-specific hydrology that is not represented in the current model application.

Table 10: List of representative bore(s) for each sub-catchment.

Bore name	Easting	Northing	Elevation	Sub-catchment
78DINGER	557099	6360702	304.1	SC1
TL03	556558.2	6358617.7	299.24	SC1
85LTC10B	559086.8	6360893	301.26	SC3
85LTC14	559065.2	6361061	302.01	SC3
JC4	559263.3	6361901	302.8	SC3
85LTC9B	559060.2	6361567	302.95	SC3
D11	560104.3	6365831	325.76	SC2
77CM1	561293.7	6361045	300.23	SC2
D113	560784.5	6364453	323.45	SC2
D123	560331.4	6364891	325.09	SC2
D141	560407.1	6364587	323.58	SC2
D175	560038.7	6364066	322.92	SC2
D203	560185	6363842	323.21	SC2
D22	560342.9	6363926	323.71	SC2
D31	560139.7	6365681	327.57	SC2
D42	560225.8	6365348	325.14	SC2
LTC15	566523.2	6360811	306.58	SC2
LTC8	560194.4	6365952	306.82	SC2
RM17	562200	6360995	301.32	SC2
RM22	562632.6	6361200	301.99	SC2
RM3	562406.7	6360857	301.36	SC2
SS97181	562717	6357754	304.14	SC2
SS97221	550945	6366955	325.069	SC7
KM1	556504.4	6365990	312.375	SC10
GM3	560201.8	6366984	309.27	SC12
LTC19	565876.3	565876.3	312.768	SC28
SS9724D	571493	6360212	313.741	SC22
SS97191	552649.8	6360183	312.948	SC32

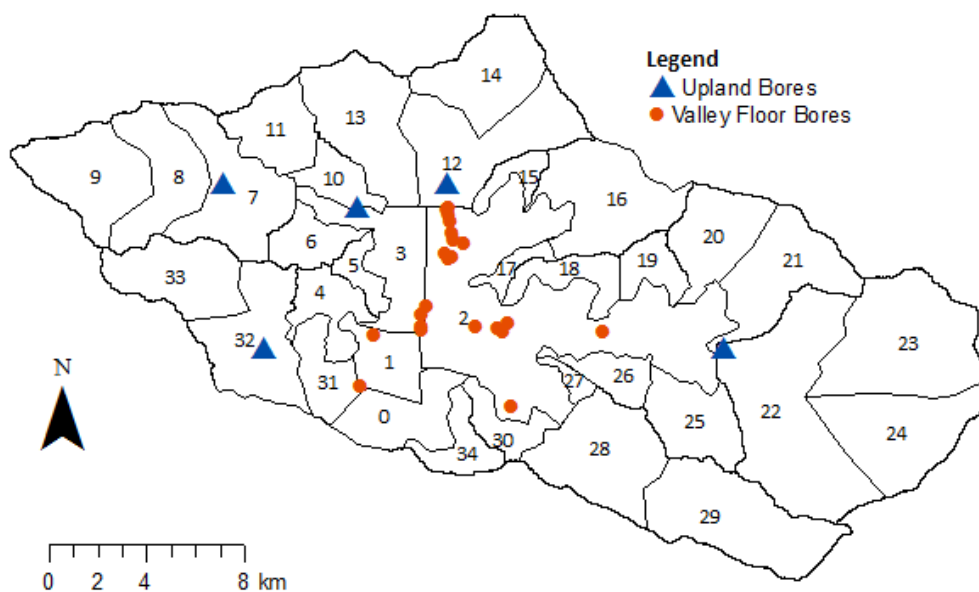


Figure 33: The location of each LASCAM sub-catchment and bores in the upland (blue triangles) and valley floor (red dots).

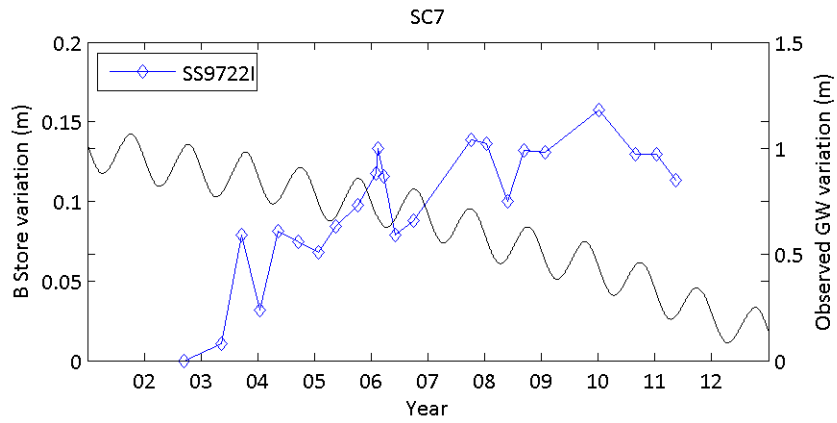


Figure 34: Groundwater variation observed at the reference bore (blue diamond) and predicted by the model at SC7 (black line).

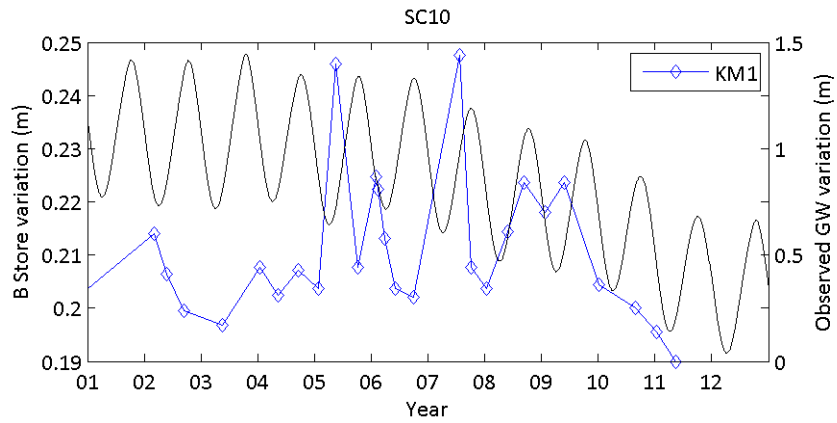


Figure 35: Groundwater variation observed at the reference bore (blue diamond) and predicted by the model at SC10 (black line).

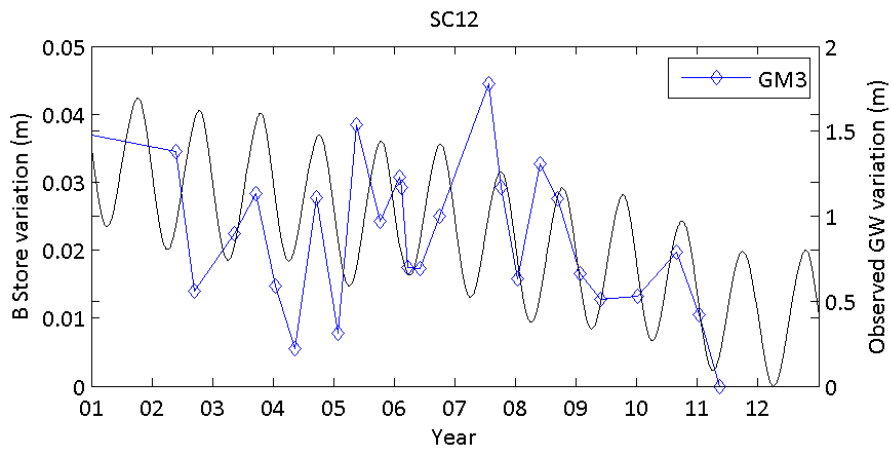


Figure 36: Groundwater variation observed at the reference bore (blue diamond) and predicted by the model at SC12 (black line).

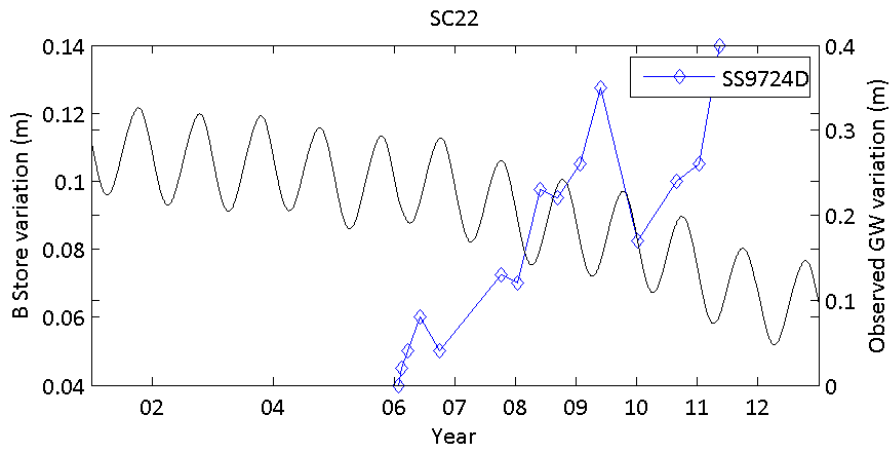


Figure 37: Groundwater variation observed at the reference bore (blue diamond) and predicted by the model at SC22 (black line).

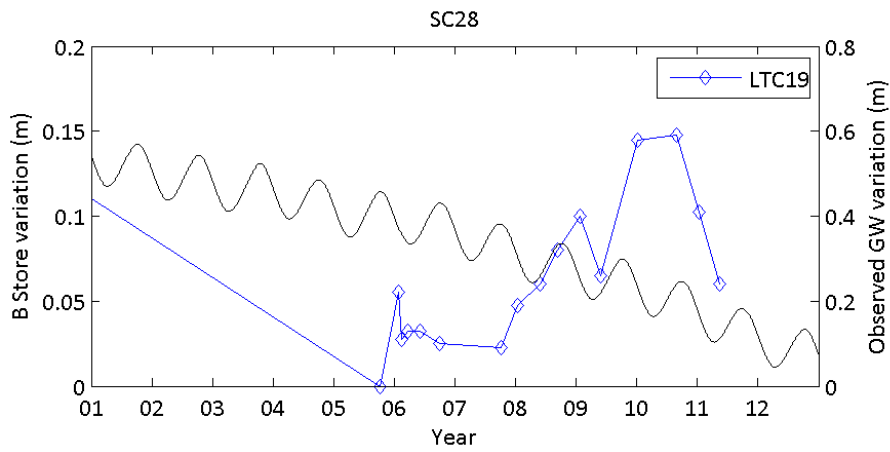


Figure 38: Groundwater variation observed at the reference bore (blue diamond) and predicted by the model at SC28 (black line).

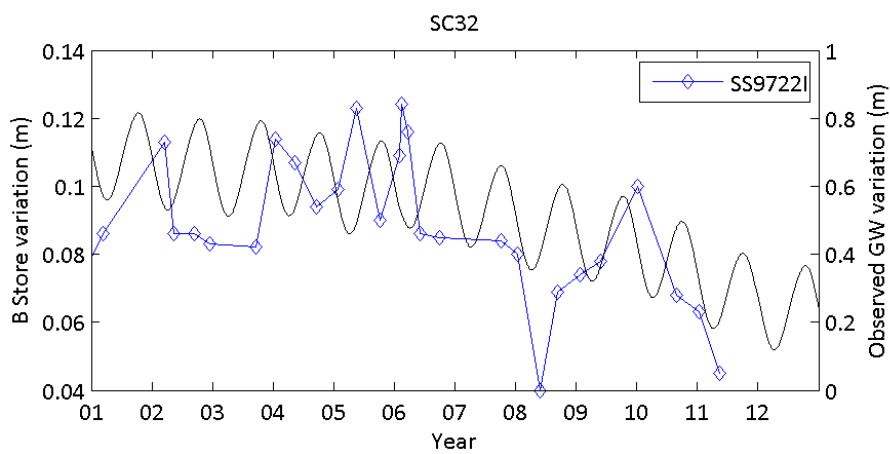


Figure 39: Groundwater variation observed at the reference bore (blue diamond) and predicted by the model at SC32 (black line).

Valley Floor

As identified in Section 2.2 the valley floor bore data shows a range of rising steady and downward trends within a single sub-catchment region. However, since there is a greater number of bores available for model validation in the valley floor (SC1, SC2 and SC3), as compared to the upland region, it allows the spatially averaged trends to be compared. Therefore, to allow comparison between measured data and the single model prediction of groundwater level, bore data within each catchment was normalised and averaged for each quarter, providing a distribution of observed groundwater variability within the region. This then represented as a box-and-whisker plot whereby the central black line represents the median and the size of the box captures the 25th and 75th percentile values of bore data within the simulated SC within that quarter (Figure 40, Figure 41 and Figure 42). Minimum and maximum values are shown by the black ticks and red crosses show outliers.

In general the model matches the level and scale of seasonal variability reasonably well, and the trend is less consistently simulated, potentially again relating to local scale hydrology since some averaging periods contained a limited (or single) sample for the averaging. As previously discussed, climate data distributed across the catchment is not available which would be hampering the model's ability to show the effect of local scale rainfall effects. Local variations in recharge and discharge as well as aquifer storage properties (porosity and specific yield) are also affecting the consistency of groundwater levels and trends in valley floor SC's. Despite that, we consider that the model is fit for purpose in terms of estimating down gradient discharge of water and salt discharge with as much accuracy as is possible given the current limitations of catchment data.

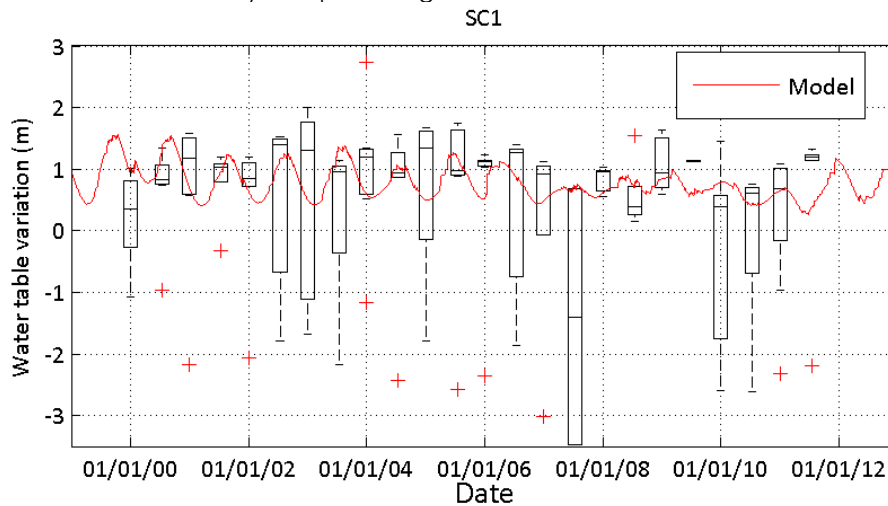


Figure 40: Groundwater variation observed by the reference group of bores (statistical distribution represented by the whisker plot, in black) and predicted by the model at SC1 (red line).

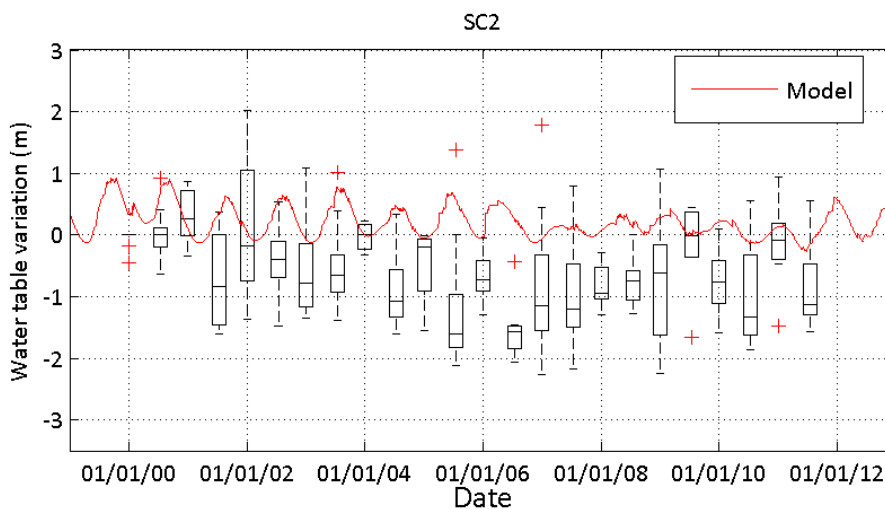


Figure 41: Groundwater variation observed by the reference group of bores (statistical distribution represented by the whisker plot, in black) and predicted by the model at SC2 (red line).

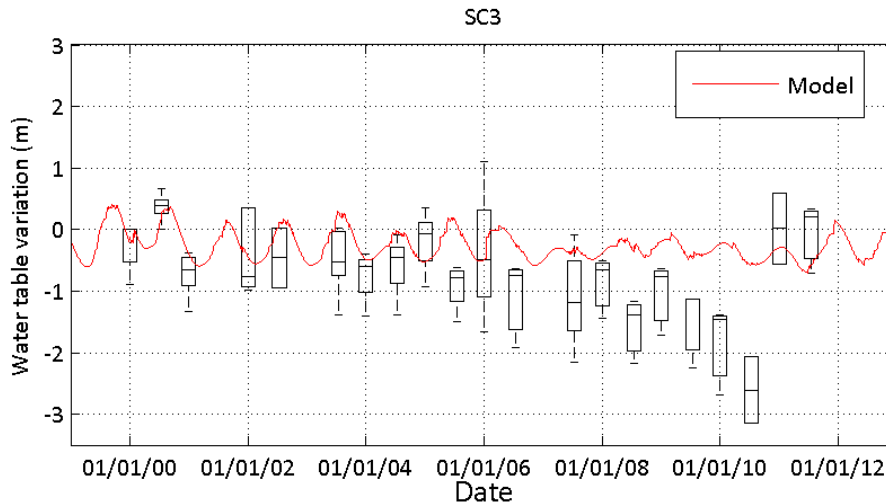


Figure 42: Groundwater variation observed by the reference group of bores (statistical distribution represented by the whisker plot, in black) and predicted by the model at SC3 (red line).

4.3 Wetland Ecohydrology

4.3.1 Groundwater and Surface Water

The locations of monitoring bores used for verification and pumping wells are shown in Figure 43. The model predicted water table depth was compared against the observed data for bores TL23 and TL3/1. Bore TL23 (northern bore) represents the deeper semi confined part of the shallow aquifer and T3/1 (southern bore) represents the water table. These bores were chosen mainly because they are located outside the central paleochannel system, which stretches approximately five kilometres in a north-westerly direction and is 300 metres wide [Dogramaci *et al.*, 2003]. The soil characteristics of the paleochannel are not representative of that found elsewhere in the wetland, so bore data from that area was avoided since it was not considered representative of the average wetland condition.

In general, the model predicted the trend of the hydrograph and magnitude of seasonal fluctuations well (Figure 44), although the model predicted a lower seasonal water table variation than that observed in TL23. This may be due to the effect of the nearby pump (refer to Figure 43) and also the model represents a spatially-averaged water table level over the entire domain, so is not expected to capture the localized drawdown of the water table level near individual pumps, and reflects an averaged water table over the wetland domain.

The multi-annual decline in water table levels over the period of pumping, however, was well predicted relative to the observed data. It was also suggested that groundwater is constrained to move laterally in some areas of the wetland due to soil property heterogeneities [Rutherford *et al.*, 2013]. This would compartmentalise the lake bed hydraulically so division of the wetland into a number of smaller domains would potentially increase the models accuracy and allow local recalibration against all available bore data. For our purposes of defining the average water and salt pathways in the wetland, as well as salt accumulation in the root zone with and without engineering interventions, the water table seasonality produced by the model was considered a good representation relative to the observed data.

Model predictions also matched observed lake level particularly well in both timing and magnitude of inundation (Figure 44). Note that most inflow and wetland inundation events happened before the surface water diversion in 1996. Although the exact date of gate operation was not recorded, we assumed this date as 01/08/1996. This date was inferred from the observed inflow registered in gauge DOW609010 and the water level registered in the lake.

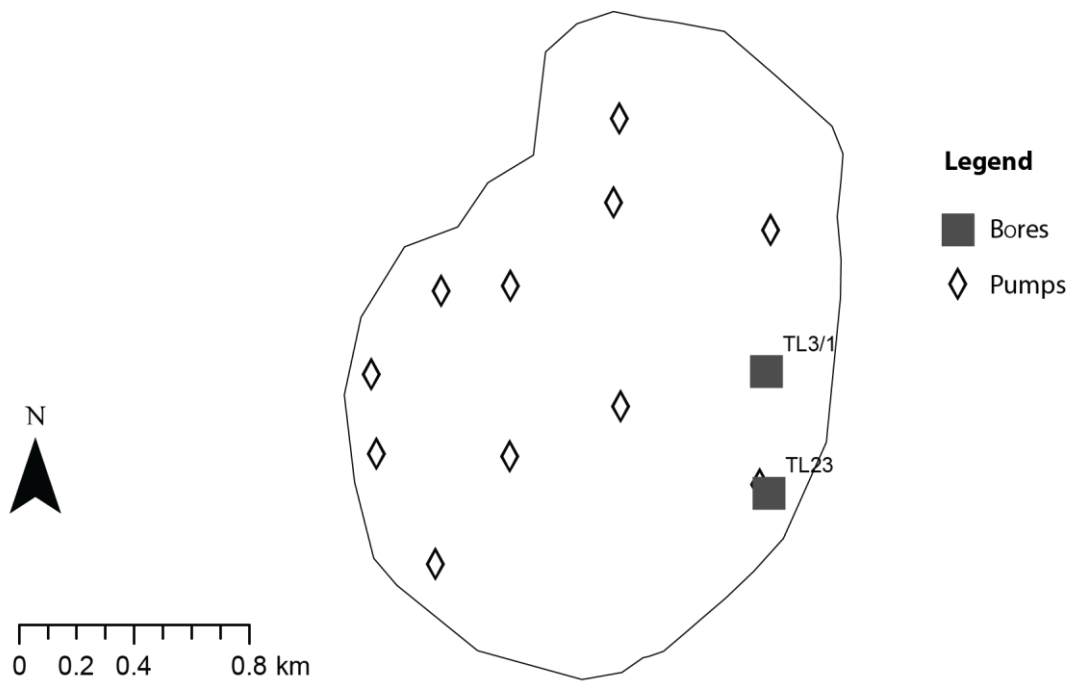


Figure 43: Bores and pumps location within the wetland domain.

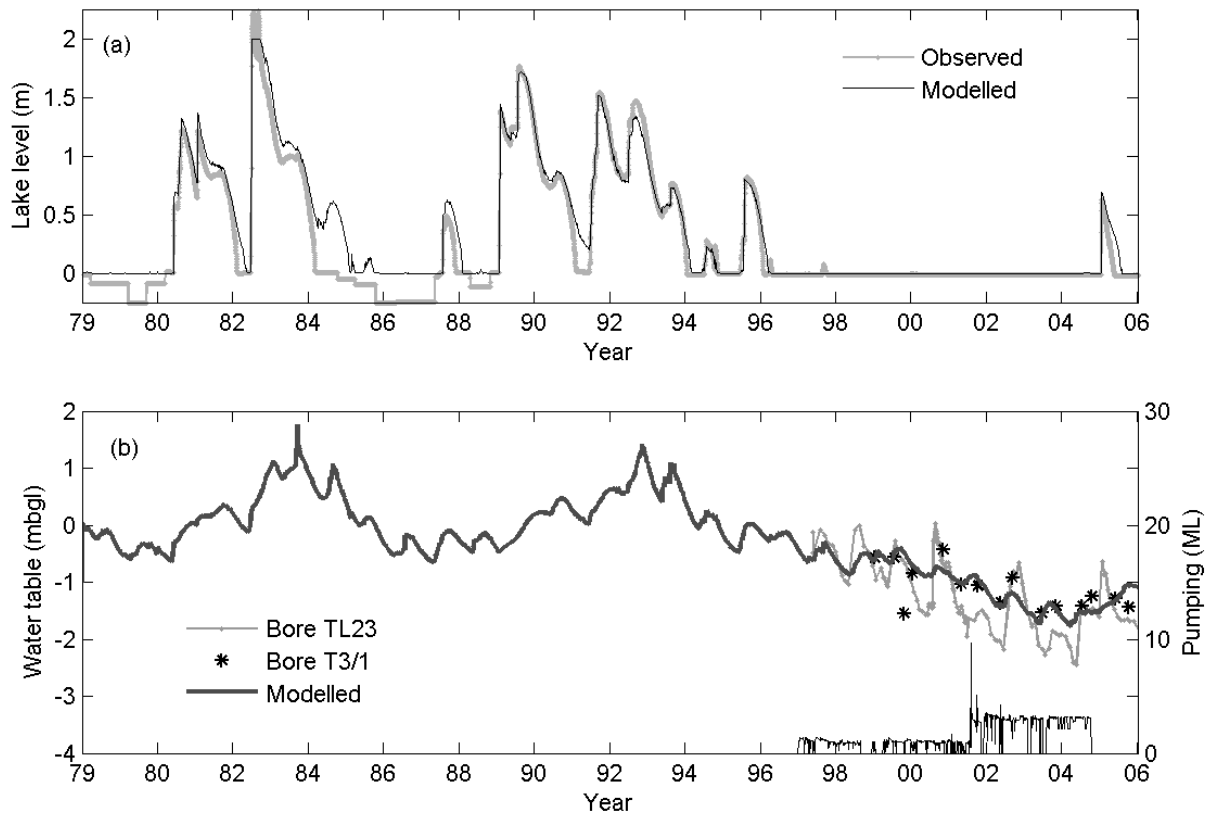


Figure 44: The observed and modelled lake level (a) and water table depth from the surface (b).

4.3.2 Salinity

Predicted and measured groundwater salt concentrations were also compared. Surveyed bores registered an average EC of approximately 46 dS m^{-1} . In Figure 45 c, this value is shown as a red line segment. The porewater EC in the vadose zone was compared to that measured by *Ecoscape* [2005], whose maximum and minimum value are depicted as red lines in Figure 45 b. Note that, although there is variability across the wetland domain in terms of soil type and soil profile [Rutherford *et al.*, 2013], the model is representing a single value, which is the average of the entire domain.

Salt scalds at the soil surface of the wetland have not been detected either by on ground observation nor through remote methods such as satellite imagery or aerial photography. The maximum values predicted by the model, 8 grams of salt per m^2 of surface, would be visually imperceptible and this is therefore consistent. Lake salinity (Figure 45 a) was also within the order of magnitude of values reported by *Halse et al.* [2000], but in general, the model underpredicted the values reported by *Halse et al.* [2000].

During the period of pumping (from January 1998 to October 2005) the salt amount in the wetland domain (to a depth of 12 m) varied from 278,000 t to 306,000 t, remaining on average at 291,000 t. The cumulative contribution from the groundwater during this period was estimated to be 116,000 t, with only 3.56 t from surface inflow. The total salt extracted by pumping during this period was 119,000 t. On average, the salt flux from the groundwater was 15,470 t per year, while from the surface water was 0.47 t per year. Pumping extracted 15,940 t per year, on average. On an annual basis, the groundwater contribute with 5.29% of the total salt amount, while pumping extracted 5.46%. The surface contributed with only less than 0.001%.

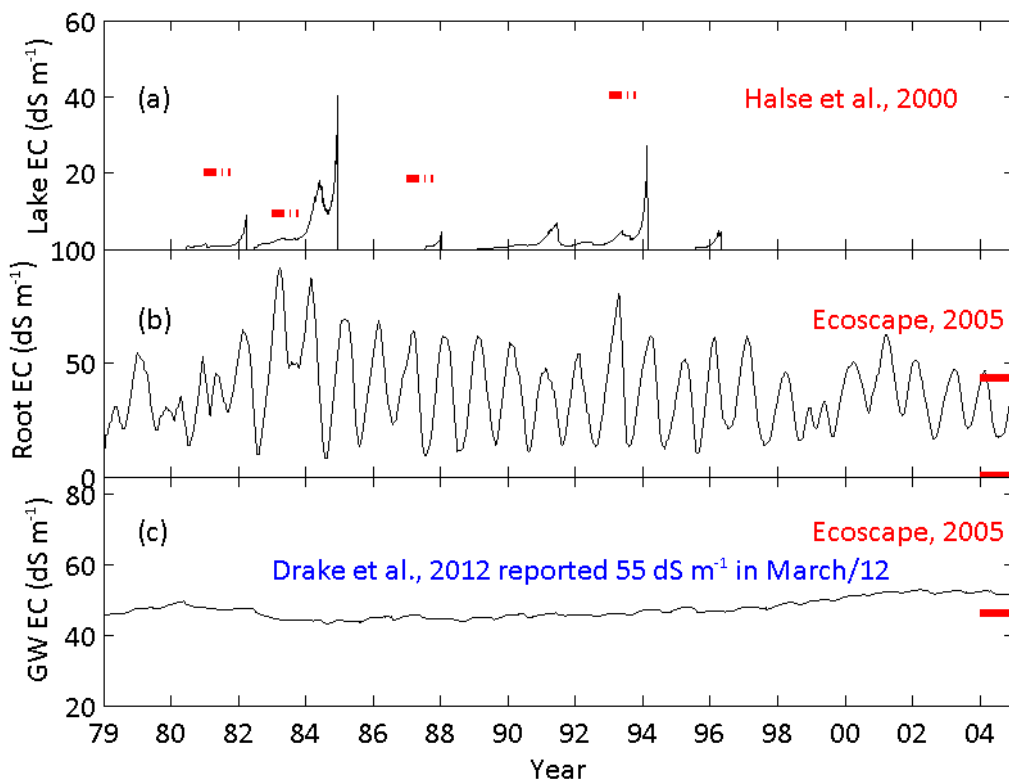


Figure 45: The predicted EC in the lake (a), in the vadose zone (b) and in the groundwater (c), compared to the range observed in the field by various authors (in red and blue).

4.3.3 Vegetation Biomass

The model was able to predict the increase in vegetation density from 1996 to 2000 that was qualitatively observed using satellite imagery [Zdunic, 2010]. The model also predicted the relative amount of *M. strobophylla* and *C. obesa* that was observed in 2005 (**Error! Reference source not found.**). However, the measured data represent a single point estimate. The model indicates that wet years are advantageous for both *M. strobophylla* and *C. obesa*. However, *C. obesa* appears to have a consistency advantage over *M. strobophylla*. It

corroborates anecdotal reports that *M. strobophylla* has been historically more negatively affected than *C. obesa* in the wetland. A better recovery from *C. obesa* relative to *M. strobophylla* was also noticed in the last few years [Vogwill *et al.*, 2010]. The range of vegetation transpiration rates predicted by the model (0 to 11 mm d⁻¹) was also similar to those observed by [Drake *et al.*, 2012b] during March 2012 (2 to 9 mm d⁻¹). We conclude that the model is capable of simulating the general trends, relative assemblage and the annual range of water consumption by the vegetation in the wetland.

4.3.4 Sensitivity Analyses of Vegetation Parameters

Uncertainty remains regarding *M. strobophylla* and *C. obesa* physiological parameters, as studies on their salt and water tolerance are rare. In addition, insufficient data was available to validate biomass prediction by the model. Therefore, a sensitivity analysis was undertaken to explore the variation in model predictions caused by key input parameters, in particular ζ_{\max} and θ_w (Table 11). To stochastically sample those parameters within a wide range of values relative to the prior sample set used in the validation section, we applied a Monte Carlo Markov Chain (MCMC) algorithm [Haario *et al.*, 2001]. The objective function that guided parameter sampling was based on the root mean square error (RMSE) between the observed and predicted lake level, which is the longest data set available.

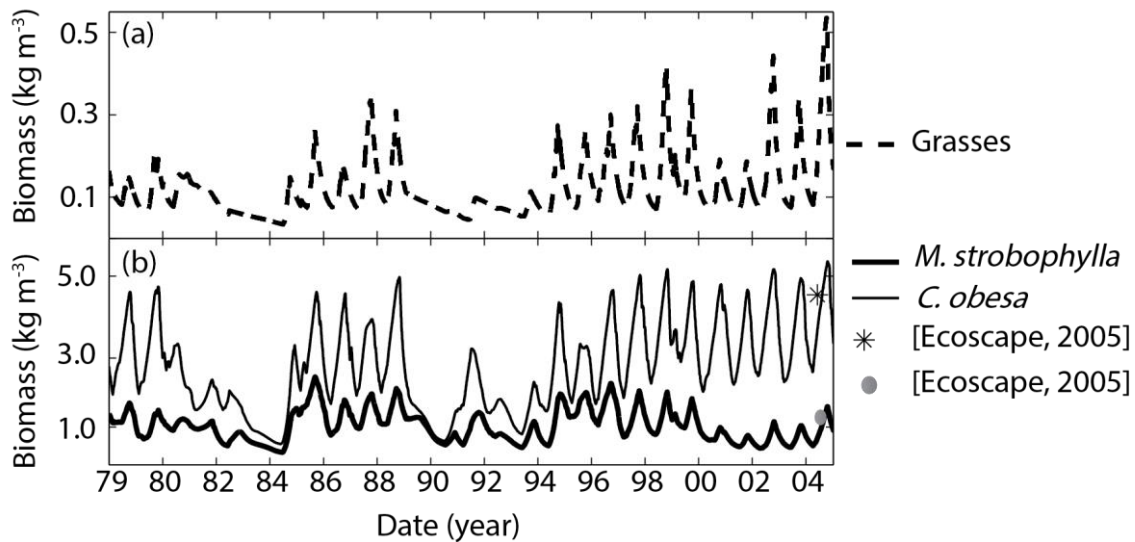


Figure 46: Predicted biomass density (kg m⁻²) for grasses (a) and for *M. strobophylla* and *C. obesa* (b), compared to the values observed by Ecoscape [2005].

Table 11: Target parameters tested to explore their effect on vegetation biomass.

Parameter*	Prior (validation set)	Range tested (%)	Posterior	Standard deviation
$\zeta_{\max 1U}$	20.7 kg m ⁻³	10-210	25.4 kg m ⁻³ (+23 %)	10.92
$\zeta_{\max 2U}$	36.3 kg m ⁻³	10-210	31.9 kg m ⁻³ (-12%)	15.5
$\zeta_{\max 1S}$	10.9 kg m ⁻³	10-210	13.85 kg m ⁻³ (+27%)	5.3
$\zeta_{\max 2S}$	6.5 kg m ⁻³	10-210	8.54 kg m ⁻³ (+30%)	3.3
$\zeta_{\max 1L}$	2.0 kg m ⁻³	10-210	2.05 kg m ⁻³ (+2%)	1.05
$\zeta_{\max 2L}$	1.0 kg m ⁻³	10-210	0.99 kg m ⁻³ (+0.2%)	0.49
θ_{w1}	0.12 m ³ m ⁻³	50-150	0.08 m ³ m ⁻³ (-13%)	0.02
θ_{w2}	0.08 m ³ m ⁻³	50-150	0.082 m ³ m ⁻³ (+3%)	0.02

Figure 47 and Figure 48 present the likelihood distribution (in quartiles) for the biomass of *M. strobophylla* and *C. obesa*, resulting from more than 1043 parameter set combinations. Overall, the prior and posterior predictions were closely related, indicating a high likelihood of the prior set of parameters to be realistic. The biomass of *C. obesa* presented the greatest difference between the prior and the posterior predictions, possibly related to the great difference in $\zeta_{\max 2U}$ (*C. obesa*'s salt tolerance under unsaturated conditions). The model proved to be particularly sensitive to $\zeta_{\max 2U}$ because unsaturated conditions represented more than 75% of simulation time and the biomass of *C. obesa* was greater than 56% of the total vegetation biomass, on average. The lack of a vegetation component in the objective function and the fact that the parameter space explored was extensive

compared to the number of interactions resulted in standard deviation and a weak convergence to most of the parameters (Figure 49).

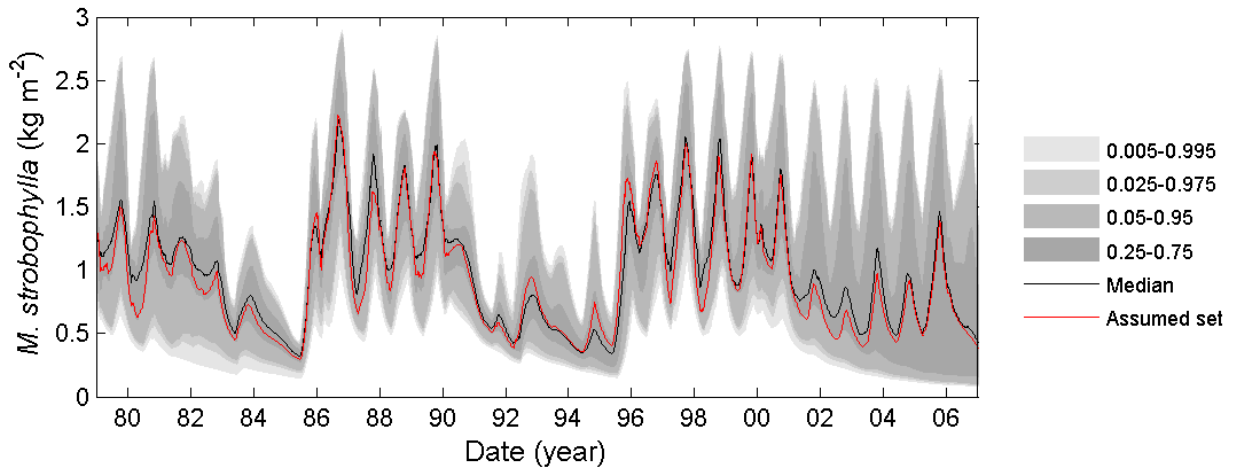


Figure 47: The range of *M. strobophylla* biomass predicted by the parameters distribution tested. The red line prior and the black line represents the median of the posterior.

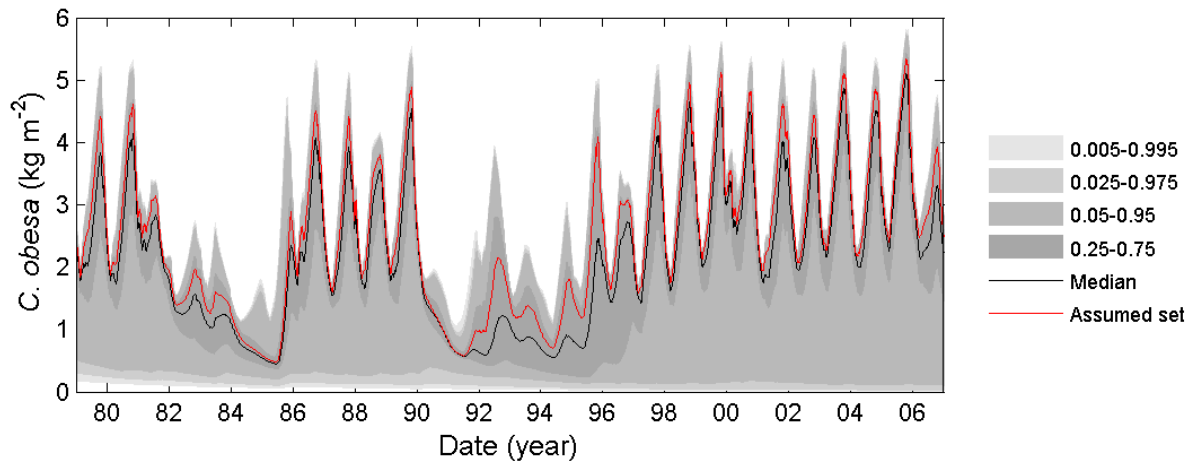


Figure 48: The range of *C. obesa* biomass predicted by the parameters distribution tested. The red line prior and the black line represents the median of the posterior.

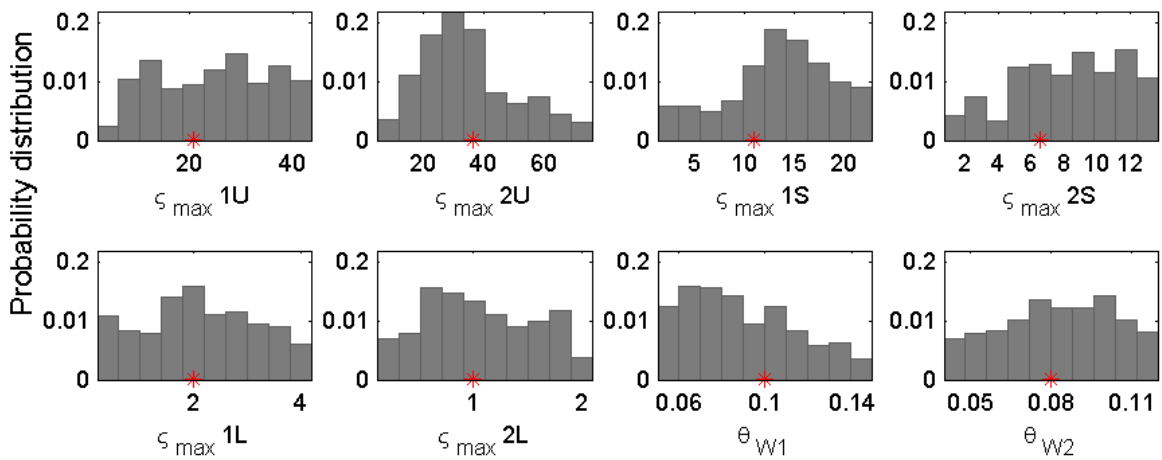


Figure 49: Posterior probability distribution (grey bars) in relation to the prior (red stars).

5. Management Scenarios

To assist DPaW assess the best approaches to manage Toolibin Lake, a number of scenarios have been designed to optimise the benefit of interventions already in place as well as test potential additional management. In the scenarios explored below, we used the integrated model system to test the relative efficiency of partial catchment re-vegetation, groundwater pumping and surface water diversion in terms of flow and salt deliver and vegetation response in the wetland. Those scenarios were formulated following DPaW requests, which in turn were based on DPaW experience of what could be feasible in terms of land purchasing and resources available to carry out the interventions.

5.1 Scenario Settings

All climate data used as a basis for the scenarios described below (Table 12) came from the observed data for the calibration period (Narrogin Station, from 1979 to 2012). The Observed (control) scenario was created by using the observed climate forcing and interventions (namely the groundwater pumping and gate operation) as has occurred from 1997. The climate shift, which occurred in the mid-1970s, with post-1975 rainfalls being 10 to 15 % lower than the long-term mean for the region [CSIRO, 2007], means that earlier data are not likely to represent future climate.

In scenarios where potential changes in rainfall were being evaluated, data from the calibration period (from 1979 to 2012) was used as a base. These historic rainfall data were manipulated to approximate climate scenario with decreasing rainfall consistent with general circulation model's (GCM) predictions [CSIRO, 2007]. All scenarios have been compared to the Observed (control) scenario. As such, when relative statements, such as "decrease" are made, we are referring to a decrease relative to the control scenario. In addition, "null" refers to any result whose predicted change was below 0.0001%.

Vegetation coverage in the Observed (control) scenario was assumed as the same as during the calibration period and based on the remnant vegetation distribution obtained from DPaW. Recent satellite imagery was also used to check that the vegetation coverage was up-to-date. These were converted to % cover in the sub-catchments. To those original values, we applied a factor to increase or decrease vegetation as a means to represent vegetation coverage changes (i.e., re-vegetation or vegetation clearing). In the case of re-vegetation, vegetation distribution was increased incrementally over 10 years, representative of the period where vegetation is growing and not likely to transpire water at the same rate as mature vegetation. The results of Vegetation Change scenarios will be described first followed by engineering.

Table 12: Summary of scenarios as requested by DPaW.

Scenario	Description
Observed (control)	This is the basis for comparison with all other scenarios and it is the same as presented in the validation
D2SC3	2% vegetation clearing in sub-catchment 3
D2SC3R7	2% vegetation clearing & 7.5% rain decrease sub-catchment 3
D2SC3R20	2% vegetation clearing & 20% rain decrease sub-catchment 3
RD4SC2	4% deep-rooted in sub-catchment 2
RD8SC2	8% deep-rooted in sub-catchment 2
RD4S2SC2	4% deep-rooted & 2% saltland pastures in sub-catchment 2
GC9605	Same as "control" scenario with 0.5% of the valley floor re-vegetated
GO9612	0.5% of the valley floor re-vegetated & gate opened at any time
GR9605	0.5% of the valley floor re-vegetated & gate rule from 1996 to 2005
GC7912	0.5% of the valley floor re-vegetated & gate closed at any time
GR7912	0.5% of the valley floor re-vegetated & gate rule at any time
P0	No pumping
P140	140% of the observed pumping
P150	150% of the observed pumping
P160	160% of the observed pumping

5.2 Vegetation Change Scenarios

5.2.1 Rainfall Decrease and Vegetation Clearing in the Valley Floor

There have been concerns that proposed land clearing in the valley floor could negatively impact the catchment's hydrology and consequently Toolibin Lake's vegetation. This possibility was investigated in combination with the effect of a likely decline in rainfall in SWWA. Predictions for the long term average rainfall in the region suggest a decrease in the order of 7.5% over the next 20 years [CSIRO, 2007]. This prediction corresponds to the 50th percentile of several general circulation models (GCM's) used to predict future climatic conditions [CSIRO, 2007]. However, the 10th percentile of all GCM's indicated that there is a chance of 20% decrease in the mean annual rainfall in that area.

We created a total of three scenarios to test the effect of land clearing and rainfall decline on the salinisation processes and vegetation response in the wetland. In the first, we assumed no changes in rainfall but vegetation clearing of 2% in SC3 (Scenario D2SC3). In the second, SC3 vegetation was cleared by 2% and rainfall decreased by 7.5% (Scenario D2SC3R7). In the third, vegetation was clearing by 2% and rainfall was decreased by 20% (Scenario D2SC3R20).

Note that 2% decrease in vegetation cover in SC3 in addition to a predicted climate change was a scenario specifically requested by DPaW. SC3 has around 16% of its total extent covered by remnant vegetation. To represent the decline in vegetation, this area was decreased to around 14%. To represent the decline in rainfall, the precipitation signal was kept the same as observed in terms of event timing, but its total depth (magnitude) was progressively lowered. For every year of simulation, starting in 1979, the daily rainfall data was scaled by a factor. At the end of 20 years period, this factor was equal to 0.925 and 0.8, for the 7.5 and 20% rainfall decrease scenarios, respectively. In all scenarios, surface and groundwater management were in place as in the Observed (control) Scenario. Table 13 presents a summary of results from all scenarios in comparison to the Observed (control) scenario.

The groundwater level in SC3 increased 1.5 mm in Scenario D2SC3 (2% vegetation clearing, same rainfall as observed), decreased 2 cm in Scenario D2SC3R7 (2% vegetation clearing, 7.5% less rainfall) and decreased 6 cm in Scenario D2SC3R20 (2% vegetation clearing, 20% less rainfall). Both D2SC3 and D2SC3R7 scenarios did not have significant (less than 10⁻³ %) impact on runoff from SC3. When the rainfall signal decreased by 20% (Scenario D2SC3R20), runoff was decreased by 50%. This reduction in runoff for the dryer climate scenario was corroborated by other studies carried out in the region [CSIRO, 2009], which found 42% runoff reduction for 20% rainfall decline.

This reduction in runoff is primarily caused by reduced infiltration excess flow due to the smaller magnitude of rainfall peaks. The infiltration excess is an important component of the total runoff in the catchment and changes in the rainfall peaks are particularly important. The rainfall time-series from 1979 to 2012 and the days of runoff in most of the SC's, suggest that an important threshold for runoff generation is daily rainfall above 58 mm, which has an Annual Exceedance Probability (AEP) of 20% or 1 in 5 years.

The reduction in runoff salt concentration in Scenario D2SC3R20 was 0.51%. This small change in salt concentration in the runoff suggests that the lack of leaching in the root zone was balanced out by the decrease in the groundwater level and consequently reduction in saline baseflow. As runoff was reduced by 50%, the total salt load was reduced by 51.5%. Considering a salt export of approximately 1.3 mg m⁻² day⁻¹ (or 6.32 t per year) from SC3, this reduction means a decrease in salt loads of approximately 3 t per year. In Scenario D2SC3R7 the reduction in salt load was 0.22%. The salt load in Scenario D2SC3 did not present significant difference. This exercise showed that vegetation clearing of 2% of the total area is not enough to cause a negative impact in salt exports or surface runoff and that 2% vegetation clearing is at the limit of resolution of the model.

Table 13: Summary of the hydrological changes caused by rainfall decrease and vegetation clearing in the valley floor (SC3) in relation to the Observed (control) scenario.

Scenario	Valley floor GW	Valley floor runoff	Runoff salt concentration	Runoff salt load	Wetland GW	Salt concentration wetland root zone	Wetland biomass
D2SC3 - 2% vegetation clearing	+0.05% (1.5 mm)	null	null	null	+4.1 mm (+0.03%)	+0.06% (14 g m ⁻³)	Null
D2SC3R7 - 2% vegetation clearing & 7.5% rain decrease	-0.84% (2 cm)	null	-0.16%	-0.22%	-15 cm (-1.36%)	-1.63% (343 g m ⁻³)	Melaleuca: +2% Casuarina: +3% Grasses: -0.4%
D2SC3R20 - 2% vegetation clearing & 20% rain decrease	-2.33% (6 cm)	-50%	-0.51%	-50.5%	-40 cm (-3.59%)	-3% (640 g m ⁻³)	Melaleuca: +2.4% Casuarina: +4.2% Grasses: +1.1%

In the wetland, the hydroperiod was significantly altered by the decline in rainfall (Figure 50), with 10% reduction in the days that surface water is present if comparing the Observed (control) scenario with the driest scenario (D2SC3R20). The number of days that surface water is present declined by 4% in Scenario D2SC3R7 and it did not change in Scenario D2SC3. The groundwater increased 4.1 mm in D2SC3, decreased 15 cm in D2SC3R7 and decreased about 40 cm in D2SC3R20. Salinity at the root zone increased 0.06% in D2SC3, and decreased 1.6 and 3% in scenarios D2SC3R7 and D2SC3R20, respectively. Vegetation biomass varied insignificantly (less than 0.005%) in Scenario D2SC3. The effect on vegetation biomass was only important when the rainfall signal were manipulated, i.e., in scenarios D2SC3R7 and D2SC3R20 (Table 13).

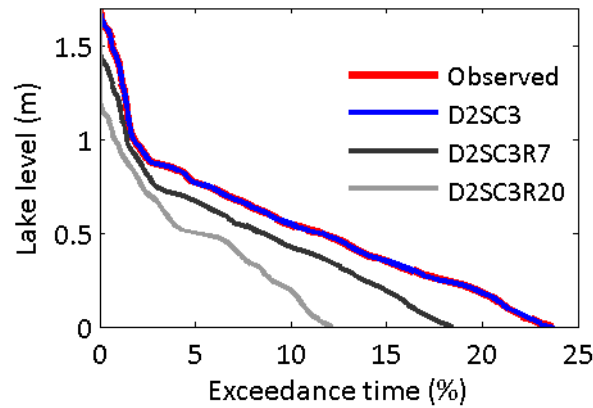


Figure 50: Hydroperiod in Toolibin Lake given vegetation clearing and rainfall decline for the total period of simulation.

The effect of scenarios D2SC3R7 and D2SC3R20 on the wetland ecohydrology was not uniform throughout the entire simulation. The climate used to force the simulations presented two distinctive periods. From Figure 51, where the total annual rainfall is presented, we can distinguish a relatively wetter period for the first 20 years (up to 2000) and a relatively drier period for the remaining years. These periods are separated by a blue line in Figure 51. Progressive scaling factors reaching 0.925 and 0.8 in the end of 20 years were used to build the rainfall for scenarios D2SC3R7 and D2SC3R20, respectively. These factors were kept constant from the 20th year until the end of the simulation. During the drier period the simulation, Scenario D2SC3R20 experienced a total annual rainfall as little as 150 mm, i.e., 20% lower than the Observed (control) scenario (Figure 51).

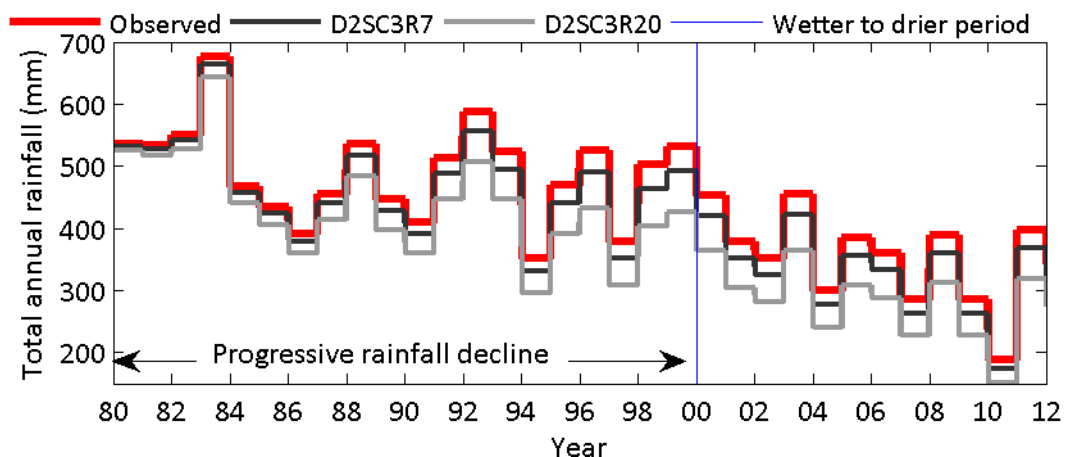


Figure 51: Rainfall forcing for Scenarios D2SC3R7, D2SC3R20 and Observed (control). The blue line marks the starting of the driest period. Coincidentally, the factors for decline rainfall are applied until year 2000.

In general, the rainfall decline experienced in D2SC3R7 and D2SC3R20 showed a positive impact on vegetation during the wetter period and a negative impact during the drier period. In the Observed (control) scenario, vegetation biomass increased during the drier period but decreased during the wetter period (refer to Figure 46). During the wetter period, extensive inundation constrained vegetation growth (particularly Casuarina). When rainfall was reduced in scenarios D2SC3R7 and D2SC3R20, lake hydroperiod decreased (refer to Figure

50). Salt and groundwater conditions (Figure 52 a, b and c) were more favorable and biomass was consequentially higher than the Observed (control) scenario during the wetter period but lower than it during the drier period (Figure 52 d, e and f). In Figure 52, the line marking the wetter and drier period is depicted in red. Note that root zone salinity was highly variable during the wetter period, most likely because the lack of leaching events and the decline of groundwater caused opposite effects.

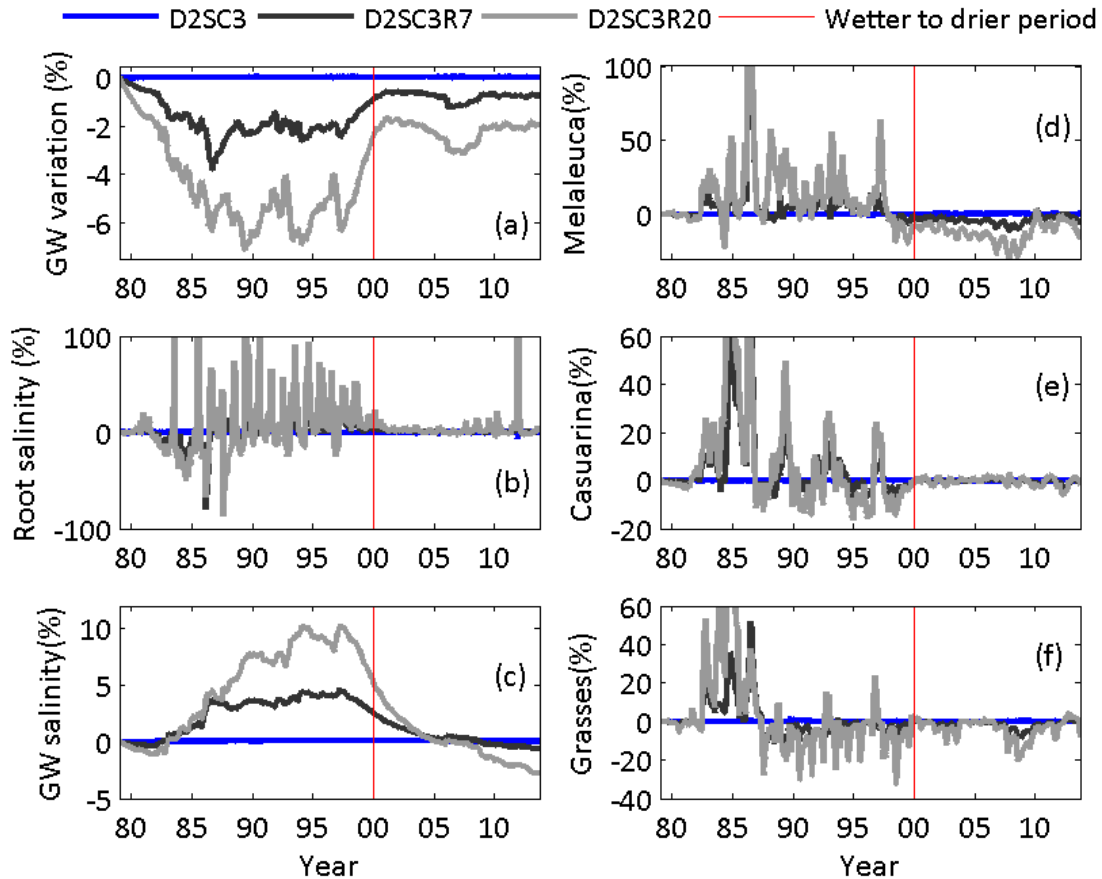


Figure 52: Toolibin Lake's dynamic ecohydrological response to rainfall decline and vegetation clearing in the catchment. All variables are relative to the Observed (control) scenario.

5.2.2 Re-vegetation with Woody Perennials and Saltland Pasture in the Valley Floor

Agroforestry, which combines the cultivation of Saltland Pastures with strips of trees, is an alternative re-vegetation plan that has a considerable appeal for including favorable economic benefit [Ruprecht and Schofield, 1991]. Here, three scenarios were created to compare the hydrological impact of planting Saltland Pastures as opposed to planting deep-rooted vegetation (Woody Perennials) or a combination of the two in SC2. These scenarios were based on DPaW requests, most likely based on its available resources.

In the first scenario, 4% of the area in SC2 was re-vegetated with Woody Perennials (scenario RD4SC2). In the second scenario (RD8S2C2), this area was 8%. In the third scenario, 4% of the area in SC2 was re-vegetated with Woody Perennials and additional 2% of the area was treated with Saltland Pastures (RD4S2SC2). SC2 is located in the valley floor, and has a total area greater than 59 km², 16.97% of which is already covered with remnant vegetation.

Modelling results suggest that the current management possible by DPaW would slightly raise the evaporative losses from the sub-catchment, reducing in situ groundwater level (Table 14) but would have minimal benefits to downstream areas. These management techniques would have to be more widely implanted to have a

significant impact under the climate scenario tested. Under a wetter climate there would likely be more effect due to reduced saturation excess. This hypothesis was not tested here.

Table 14: Summary of the hydrological changes caused by re-vegetation in SC2 in relation to the Observed (control) scenario.

Scenario	Changes in SC GW	Changes in SC runoff	Changes in salt concentration	Changes in salt load
RD4SC2 - 4% deep-rooted	-0.1 % (-3.25 mm)	null	null	null
RD8SC2 - 8% deep-rooted	-0.2 % (-4.8mm)	null	null	null
RD4S2SC2 - 4% deep-rooted & 2% saltland pastures	-0.15 % (-6.5 mm)	null	null	null

5.2.3 Re-vegetation of the Lake Surroundings and Gate Operation

As requested by DPaW, we tested 3 scenarios involving the re-vegetation of an area equivalent to 0.5% of the valley floor (5% of SC0) and the combined operation of the diversion gate. In the first scenario, we tested the influence of the re-vegetation alone, keeping the gate operation exactly as in the Observed (control) scenario, i.e., surface water was diverted from the lake between 1996 and 2005 (Scenario GC9605). In the second scenario, 0.5% of the area of the valley floor was re-vegetated and surface water was allowed into the lake (GO9605). In the third scenario, 0.5% of the valley floor was re-vegetated and the gate was operated by a rule, i.e., surface water was allowed into the lake if its salt concentration was lower than 1,000 gm⁻³ (Scenario GR9605).

The results show that the groundwater level declined as little as 1 cm (0.22%) in SC0, where the re-vegetation was tested. Over the whole period of the simulation, which accounts for the 10 years necessary for the establishment of the vegetation, the evapotranspiration increased by 4.1%. The impact in the surface runoff from SC0 was negligible. We conclude that re-vegetating 5% of SC0 would not bring localized effect on a sub-catchment scale.

In the wetland, the impact of the re-vegetation in SC0 (Scenario GC9605) was also minimum (Table 15). In comparison to the Observed (control) scenario, the re-vegetation of SC0 decreased the groundwater level by 30 mm. The salt concentration in the groundwater decreased by 0.27%. In the root zone, a negligible increase in salinity occur (0.02%). The result for the biomass was a 0.3% decline for all types.

The gate operation had a slightly more noticeable impact on the wetland. When the water was allowed into the lake (Scenario GO9605), despite the re-vegetation in SC0, the groundwater beneath the lake bed increased by 33 mm. The groundwater salinity decreased by 2%. The resultant biomass, however, was 0.6% lower than in the Observed (control) scenario. When the gate was operated following a rule based on runoff salt concentration, the groundwater level decreased by 20 mm. The groundwater salinity decreased by 0.6%. The resultant biomass was 0.5% lower than in the Observed (control) scenario.

Table 15: Summary of the ecohydrological changes in the wetland caused by re-vegetation in the lake surroundings and gate operation in relation to the Observed (control) scenario.

Scenario	Wetland GW	Salt concentration in the wetland GW	Salt concentration in the wetland root zone	Wetland biomass	Wetland total biomass
GC9605 - 0.5% of the valley floor re-vegetated – gate operation as in the Observed (control) scenario	-0.29% (30 mm)	-0.27%	+0.02%	Melaleuca: -1% Casuarina: -0.15% Grasses: -0.3%	-0.3%
GO9605 - 0.5% of the valley floor re-vegetated & surface water allowed in the lake	+0.32% (33 mm)	-2%	-0.49%	Melaleuca: +0.44% Casuarina: -0.38% Grasses: -1.2%	-0.6%
GR9605 - 0.5% of the valley floor re-vegetated & gate ruled by concentration	-0.19% (20 mm)	-0.6%	-0.22%	Melaleuca: -0.88% Casuarina: -0.35% Grasses: +0.07%	-0.5%

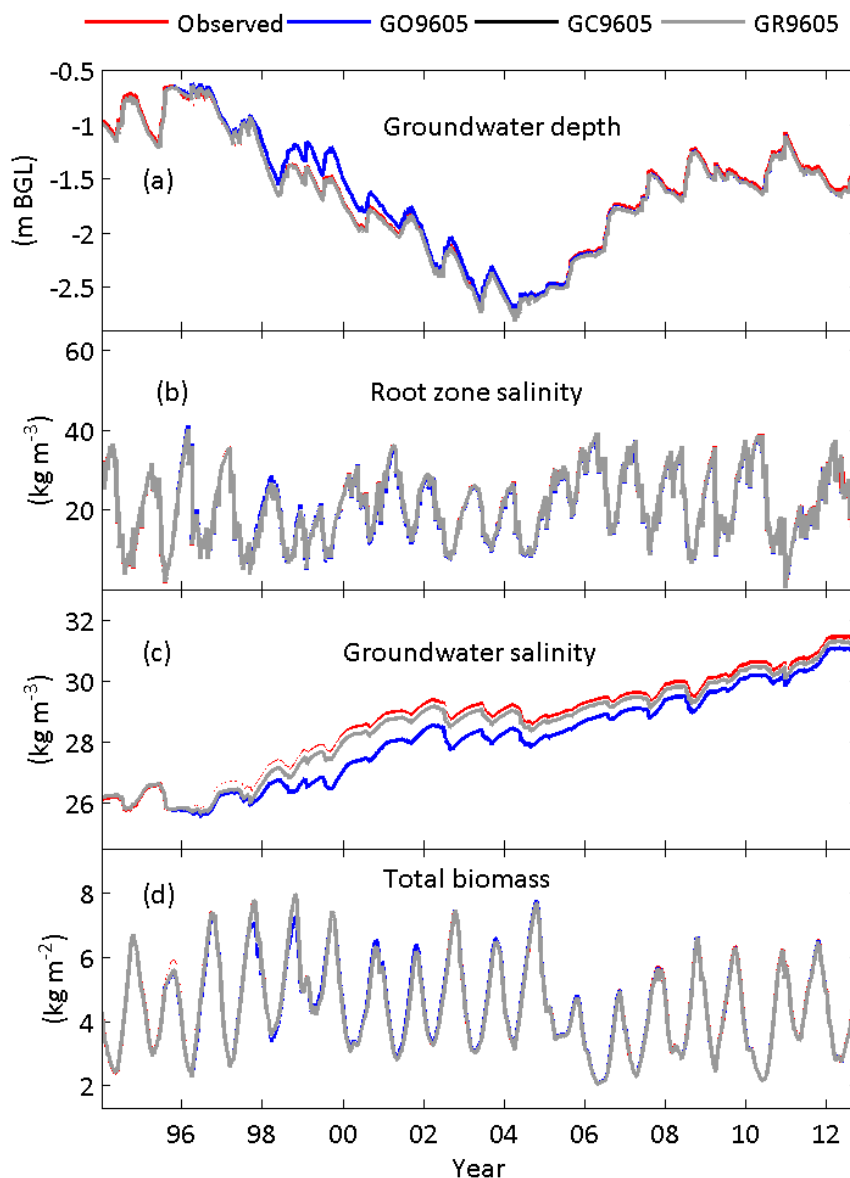


Figure 53: The effect of re-vegetation and surface water diversion on ground water level (a), salinity at the root zone (b), groundwater salinity (c) and total biomass (d) in the wetland.

In all scenarios tested, gate operation also appears to have little effect on vegetation biomass and on salinisation processes. However, from 1996 onwards, where the gate was in operation, a particularly dry period occurred, and almost no surface water flow was recorded. As a result, the effect of gate operation in controlling flooding events and groundwater level could not be evaluated (Figure 53). To draw a clearer conclusion on how the gate should be operated to minimise wetland salinisation and maximize vegetation biomass, a series of additional scenarios were designed. Those scenarios were not requested by DPaW and are presented in the Engineering Scenarios section.

5.2.4 Vegetation Clearing in the Upland and Priority Catchments for Re-vegetation

To test how vegetation clearing in the upland affects water and salt delivery to the wetland, DPaW requested a scenario where the vegetation cover of SC22 was decreased by 4%. SC22 is located in the eastern side of the catchment and comprises an area of approximately 35 km², which represents 7% of the total catchment. Results show that after vegetation clearing, groundwater level rose about 0.19%, which represents as little as 8 cm. The flow rate increase after vegetation clearing is estimated at 9%, as an average for the entire simulation. This higher sensitivity to the surface runoff in the upland (SC22) compared to the valley floor (see SC3) was due to the lack of detentions in the upland, consistent with the flow, fill, flood theory [Callow, in prep.]. The salt load

increased was estimated in about 0.09% (from 4.3 to 4.7 mg m⁻² day⁻¹), which represents about 5.11 t of salts per year.

SC22 does not produce the highest yields in the catchment (Figure 54). Runoff is generally higher on the western side of the catchment, where it shows characteristics of infiltration excess, as it responds quickly to rainfall events higher than 58 mm in 24 hours (AEP of 20%). Runoff produced on the eastern side of the catchment has characteristics compatible to saturation excess. It occurs in late winter and generally during lower rainfall intensity than in the western side (see discussion in the Validation section). Figure 54 is an indicative map that shows the areas of higher runoff generation in lighter colours, where we recommend the re-vegetation efforts should be focus on to maximize results. We point out, however, that the period between 2007 and 2010 was particularly dry, and may not represent the general behaviour of the catchment during wet periods.

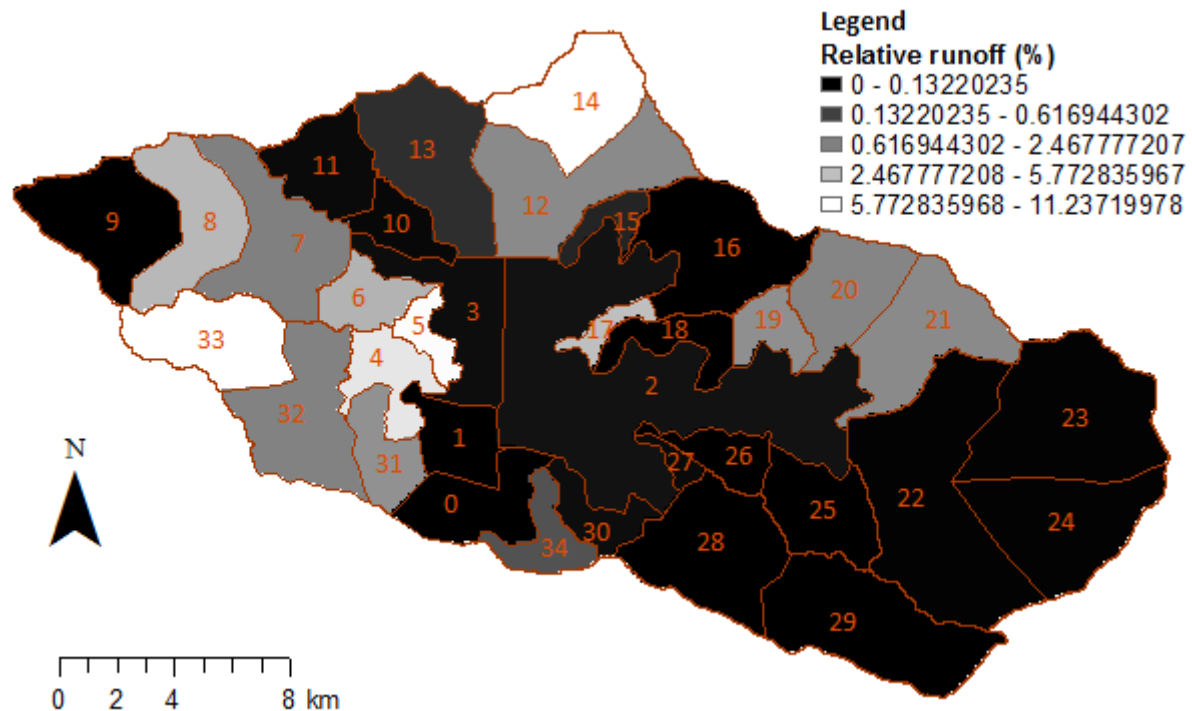


Figure 54: Map of the relative runoff generation between 2007 and 2010. Values represent percentage of the total flow for the period. Brighter areas represent higher runoff. In general, the western side presents infiltration excess runoff and the eastern side presents saturation excess runoff.

5.3 Engineering Scenarios

5.3.1 Groundwater Pumping

Groundwater pumping has been regarded as an important intervention for recovering vegetation biomass in Toolibin Lake [Vogwill *et al.*, 2010], and it is suggested that the cessation of this practice threatens vegetation survival [Drake *et al.*, 2012a]. Here, we used the model to test how important this intervention has been, not only in terms of groundwater level control but also in terms of salt balance and vegetation response. We created 4 scenarios for the period between 02/01/1998 and 07/10/2005, when the pumping system was operative. In all of them, we created the daily time-series of groundwater extraction by scaling the observed daily pumping volumes. The scaling factors used were 0, 1.4, 1.5 and 1.6, for the scenarios P0, P140, P150 and P160, respectively.

The results showed that had the groundwater pumping never taken place (Scenario P0), the groundwater level at the end of the simulation would be 1.4 meters higher than it was in the Observed (control) scenario (Figure 55 c). Root and groundwater salinity would be 13 and 0.2% higher, respectively. The total biomass would be 7.5% lower and the soil moisture 2% higher. It is important to note that regardless of the pumping, the water table in Toolibin Lake would have decreased during the 2000's, if compared to the 1980's and 1990's. This decline would be solely due to the decrease in precipitation showed in Figure 3. Our results suggest that this rainfall and subsequent groundwater decline has been beneficial to the vegetation in the lake.

The progressive increase in pumping by 40, 50 and 60% (scenarios P140, 150 and 160, respectively) declined the water table by 64, 80.9 and 97.8 cm, respectively. The total biomass benefited accordingly, increasing its biomass by 1.8, 2.36 and 2.98% (Figure 55). The interaction between water, salt and the two dominant vegetation species is complex and nonlinear. Although pumping was always beneficial to the total vegetation biomass, this was not the case for *M. strobophylla*, which presented an opposite trend than the total biomass in response to groundwater pumping (Figure 56a). When pumping was not present (Scenario P0), *M. strobophylla* increased its biomass by 0.9%. When pumping increased (scenarios P140, P150 and P160), it decreased its biomass by 5.2, 5.9 and 6.4%, respectively. Soil moisture deficits seems to have played a major role in the species competition, with *M. strobophylla* declining at the expense of *Casuarina*. This exercise showed the importance of modelling different species with distinct physiological characteristics.

The period of observed pumping (between 02/01/1998 and 07/10/2005) was not long enough to reach hydrological equilibrium and was also particularly dry. In addition, all surface water was diverted from the lake via gate operation. The importance of pumping and gate diversion, therefore, could be obscured by the lack of flooding events and by the already low groundwater levels. To overcome the lack of runoff events, we created additional scenarios involving both gate and pumping operation. They enable us to draw a clearer conclusion on how the gate should be operated to minimise wetland salinisation and maximize vegetation biomass.

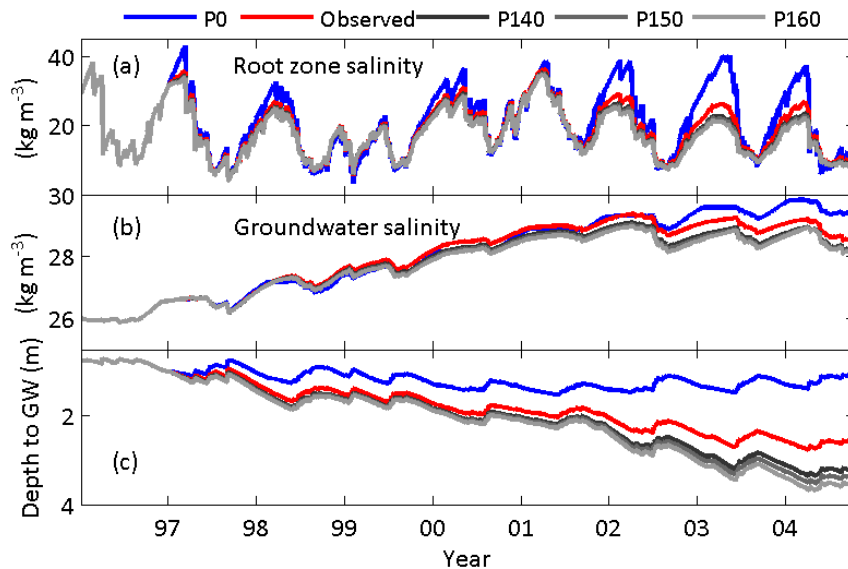


Figure 55: Root zone (a), groundwater salinity (b) and groundwater depth (c) in Toolibin Lake as a result of different volumes of water extracted by pumping.

Table 16: Summary of the ecohydrological changes during pumping in relation to the Observed (control) scenario.

Scenario	Lake bed GW	Salt concentration in the root zone	Salt concentration in the GW	Total biomass	Biomass in the lake bed (%)	Soil moisture
P0 - No pumping	2.3% (+1.4m)	+13% (21.23 kg m^{-3})	+0.2% (28.3 kg m^{-3})	-7.5%	Melaleuca: +0.9 Casuarina: -10.6 Grasses: -14.5	+2%
P140 - 140% of the observed pumping	-0.96% (-64cm)	-5.17% (17.82 kg m^{-3})	-0.67% (28.2 kg m^{-3})	+1.8%	Melaleuca: -5.2 Casuarina: +4.34 Grasses: +8.8	-0.7%
P150 - 150% of the observed pumping	-1.22% (-80.9cm)	-6.46% (17.57 kg m^{-3})	-0.83% (28.0 kg m^{-3})	+2.36%	Melaleuca: -5.9 Casuarina: +5.37 Grasses: +10.6	-0.88%
P160 - 160% of the observed pumping	-1.5% (-97.8cm)	-7.67% (17.34 kg m^{-3})	-1% (27.9 kg m^{-3})	+2.98%	Melaleuca: -6.4 Casuarina: +6.4 Grasses: +12.8	-1.04%

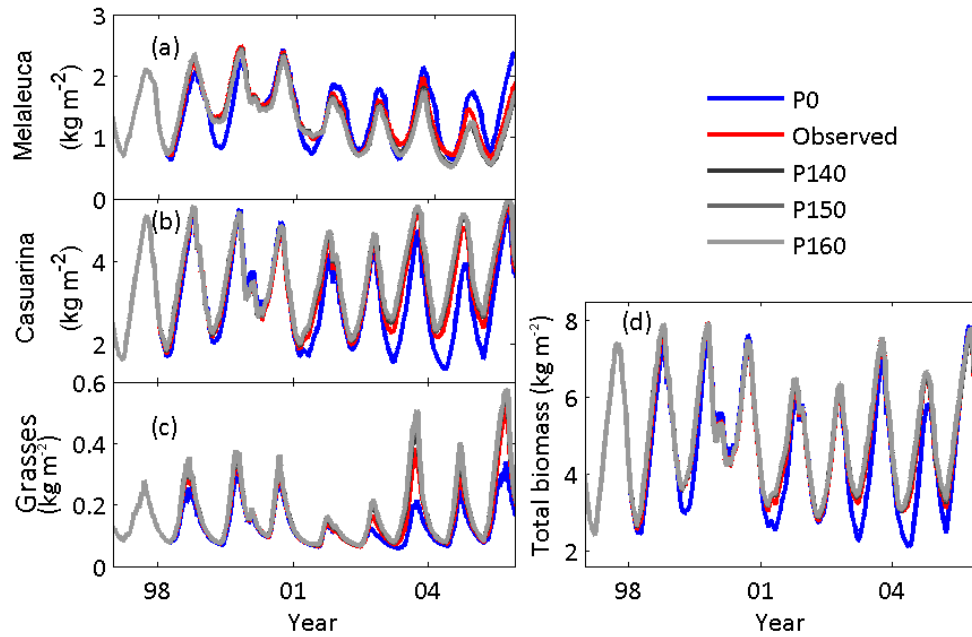


Figure 56: Vegetation biomass in response to pumping operation.

5.3.2 Combined Effect of Pumping and Surface Water Diversion- Recommendation for Future Management

The surface water diversion structure (gate) was constructed to carry surface water around Toolibin Lake into the diversion channel. The idea was to use this structure to divert saline, low volume flows from the lake, while allowing fresher flows to be directed into it. The rule imposed to control the gate is that surface water is allowed into the lake if its salt concentration is lower than $1,000 \text{ gm}^{-3}$. The greatest flow that the gate can control is $1 \text{ m}^3\text{s}^{-1}$, which is likely to present a low salt concentration [Muirden and Coleman, 2014].

To investigate the optimal way to manage the surface water diversion and the pumping regime, we created 10 additional scenarios, based on distinct pumping schedules and diversion operation. They encompass 400, 600, 800, 1000 and 1200 m^3 of water extraction per day via groundwater pumping, with and without water diversion (Table 17). The maximum groundwater extraction ever registered in Toolibin Lake was 2500 m^3 in one day, with all pumps in operation. It is unlikely that the pumps could yield this water volume in perpetuity, so values above $1200 \text{ m}^3 \text{ d}^{-1}$ were not tested here. The simulations were forced by climate data from 1979 to 2014.

Table 17: Summary of additional groundwater pumping scenarios.

Scenario name	Daily groundwater extraction (m^3)	Surface water diversion	Scenario name	Daily groundwater extraction (m^3)	Surface water diversion
P400Gc	400	Yes	P400Go	400	No
P600Gc	600	Yes	P600Go	600	No
P800Gc	800	Yes	P800Go	800	No
P1000Gc	1000	Yes	P1000Go	1000	No
P1200Gc	1200	Yes	P1200Go	1200	No

The results of the simulations presented in Table 17 are shown in Figure 57 to Figure 61. Long term groundwater pumping at the rate of $800 \text{ m}^3\text{d}^{-1}$ (which was the average rate actually observed during 1998 and 2005) kept the groundwater level 4 m below ground level, which is the depth to the groundwater recommended by Vogwill *et al.* [2010]. When the volume extracted increased to $1200 \text{ m}^3\text{d}^{-1}$, the groundwater was kept at 6 m below ground level even if the surface water was allowed into the lake. The groundwater reached dynamic equilibrium after approximately 10 years of pumping when all surface water was diverted. It took 24 years for dynamic equilibrium to be reached when the surface water was allowed into the lake. This fact suggests that wetter periods may require pumping rates higher than $800 \text{ m}^3\text{d}^{-1}$ to maintain the groundwater level at 4 meters below ground. The volume of water extracted by pumping reduced the days of flooding considerably (Figure 61). For the total period of 35 years, increasing pumping from 400 to $1200 \text{ m}^3\text{d}^{-1}$ decreased the days under flooded conditions to 700, which represents a reduction of approximately 5%.

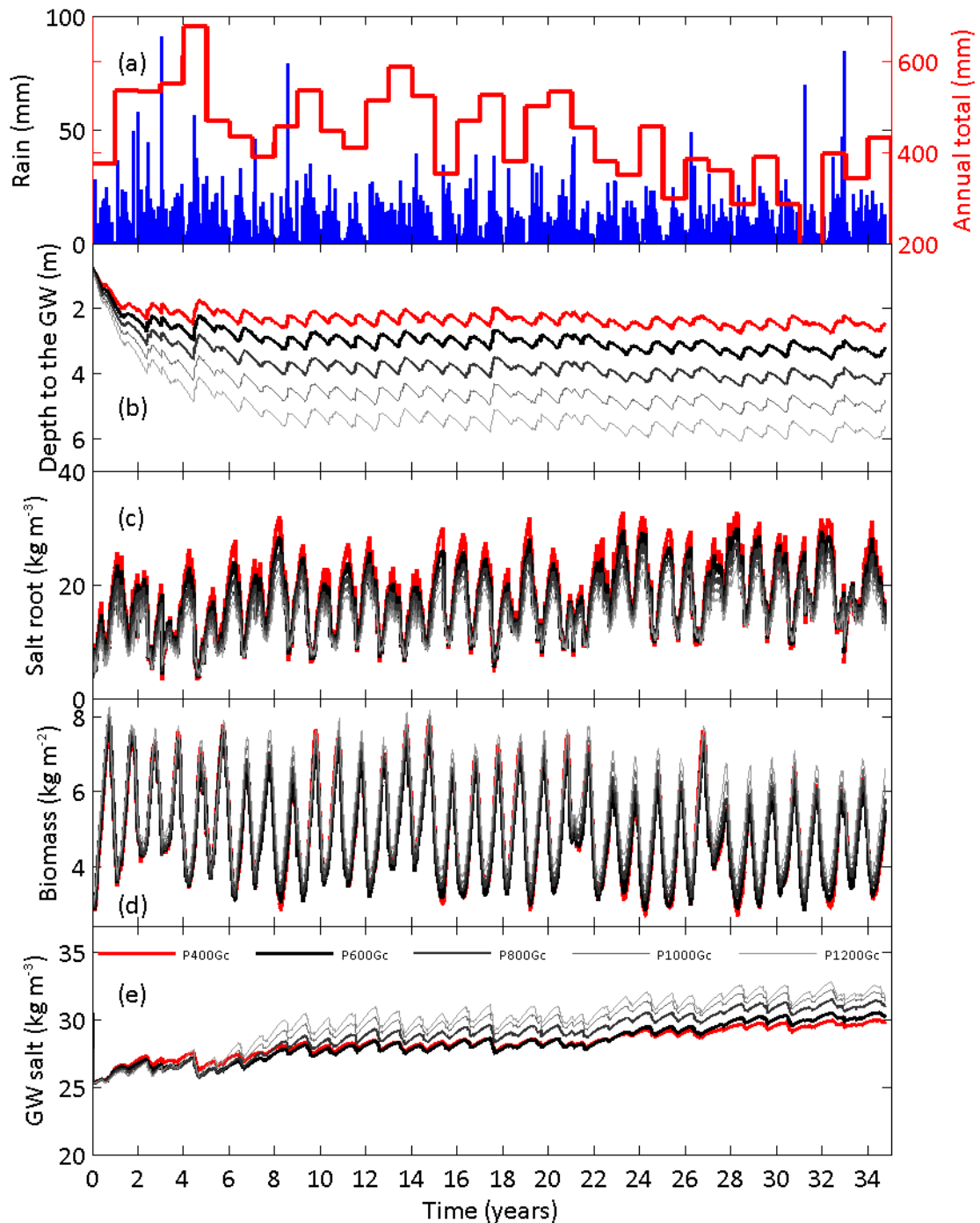


Figure 57: Hydrological response to different pumping schedule (from 400 to 1200 m³ d⁻¹) and no contribution of surface runoff from the catchment.

Groundwater salinity in scenarios where surface water was diverted from the lake was approximately 8% higher if compared to those where surface water was allowed into it (Figure 59 b). Surface water inflows increased recharge and diluted the salts in groundwater. This is best observed in the 6th year of the simulation (Figure 57 and Figure 58 e), where a series of large rainfall events caused inundation, groundwater dilution and groundwater elevation. During this period, groundwater salinity was up to 13% lower.

Salinity at the root zone had a similar response in both set of scenarios (with and without diversion), with values 4% higher when the water was diverted from the lake (Figure 59 a). The results suggest that the “flushing” of soil by infiltration was buffered by the higher groundwater levels and capillary export. Root zone salinity depends on groundwater salt concentration but also on groundwater level. Our simulations indicate that the threshold at which the groundwater levels are controlling root zone salinity is around 2.5 m (Figure 60). If groundwater is below 2.5 meters from ground level, the groundwater salinity is less important in determining root zone salinity. Thus, we recommend this threshold to be a trigger to initiate groundwater salinity monitoring.

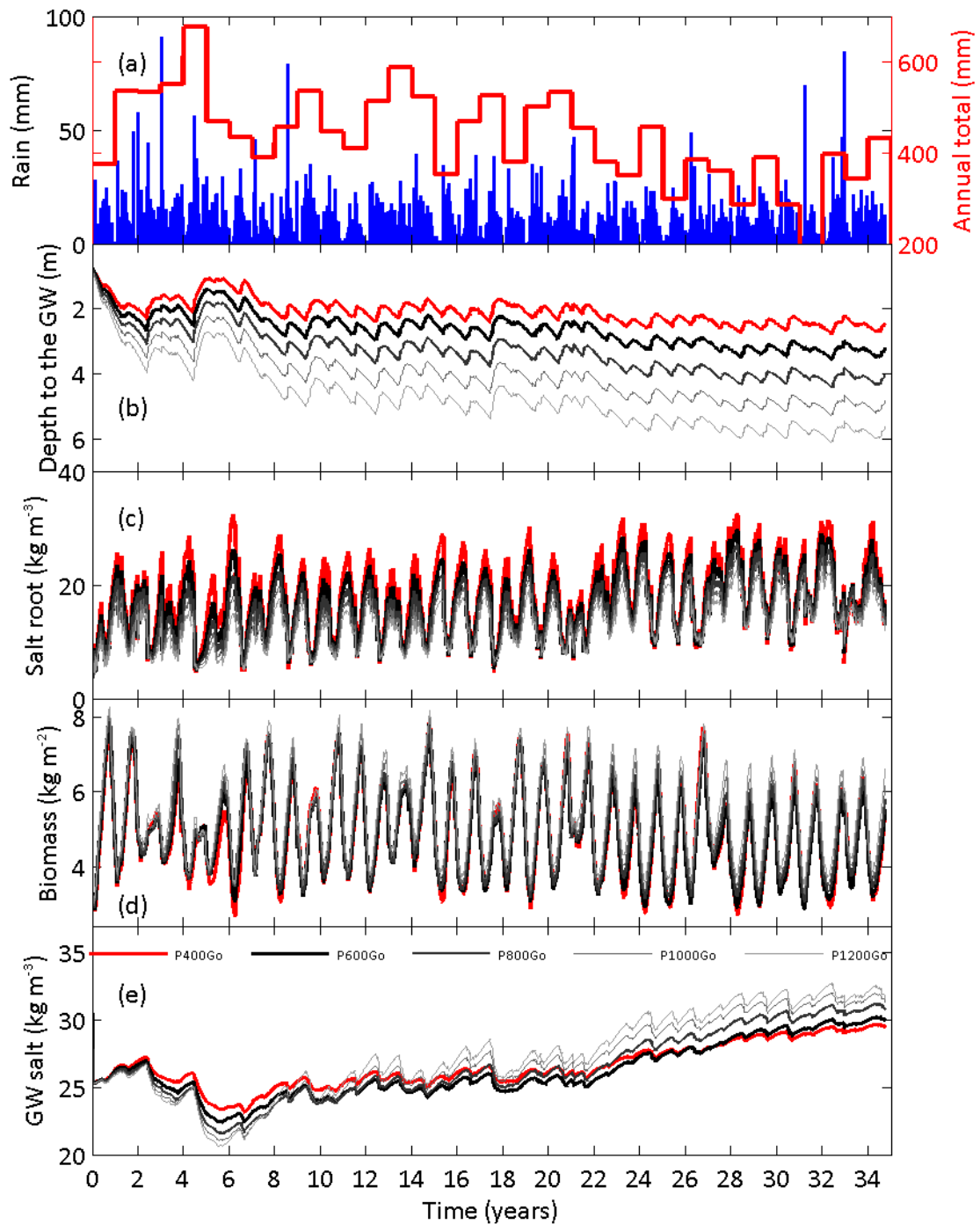


Figure 58: Hydrological response to different pumping schedule (from 400 to 1200 m³ d⁻¹). Surface water was allowed in the lake.

Soil moisture in scenarios where surface water was allowed into the lake was on average 8% higher than in the scenarios where surface water was diverted from it. Higher soil moisture did not compensate, in some cases, for the vegetation mortality caused by sustained inundation. Thus, higher biomass occurred when surface water was diverted. When assessed over the 35 years simulations, the greatest impact on total biomass was the volume extracted by pumping, with higher daily volumes enabling higher total biomass (Figure 55 c). Individually, *C. obesa* and *M. strobophylla* also presented higher biomass as pumping volume increased. However, *M. strobophylla* biomass decreased when daily pumping volume was 600 m³ d⁻¹, compared to the scenario where a lower volume was extracted (Figure 55e). This is probably due to the competition between the two species for water in the root zone, as *C. obesa* biomass (and subsequent water use) was lower when pumping was 400m³d⁻¹ (Figure 59 e).

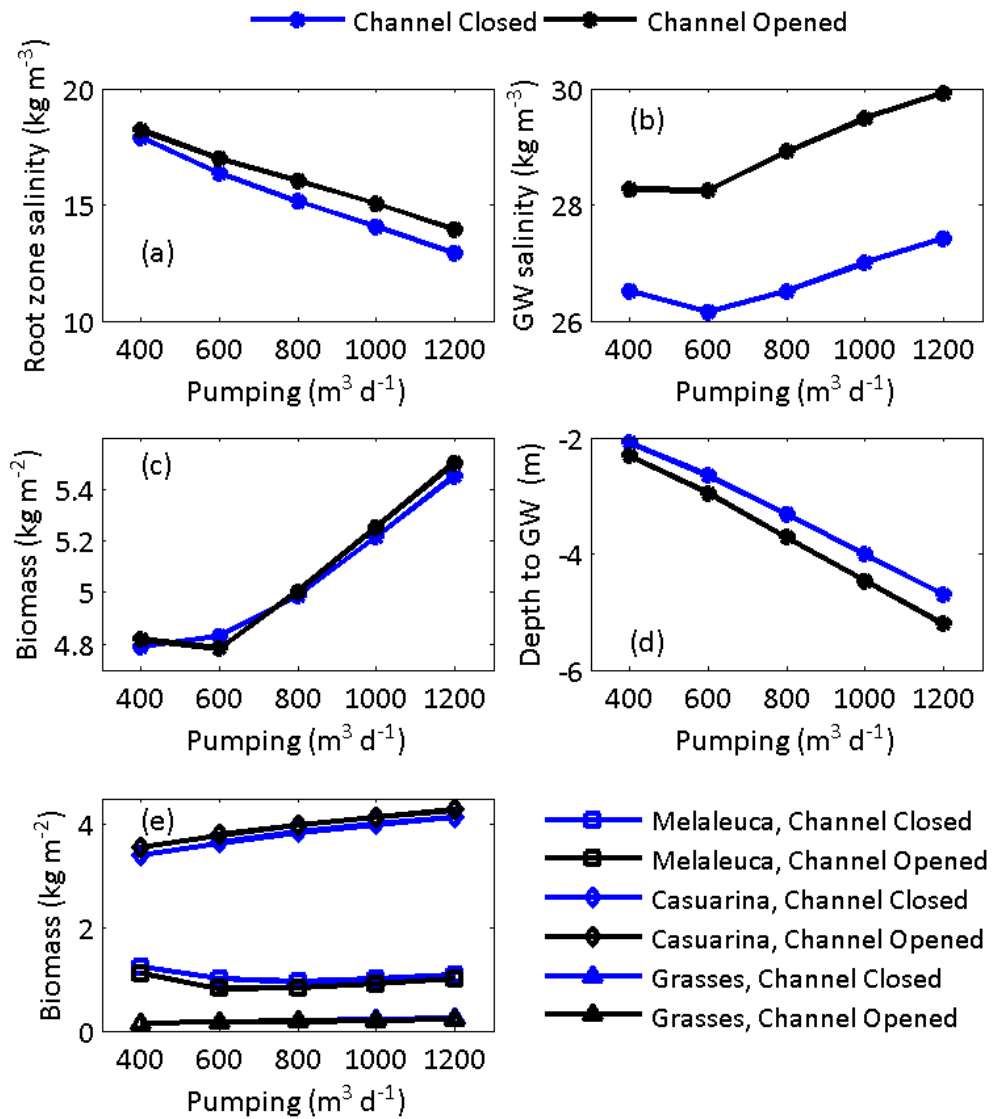


Figure 59: Summary of the ecohydrological response to pumping schedule with the diversion channel closed (in blue) and with the diversion channel opened (in black). In panel (c), diamonds represent *C. obesa*, squares represent *M. strobophylla* and triangles represent grasses. Panel (d) represents the total biomass.

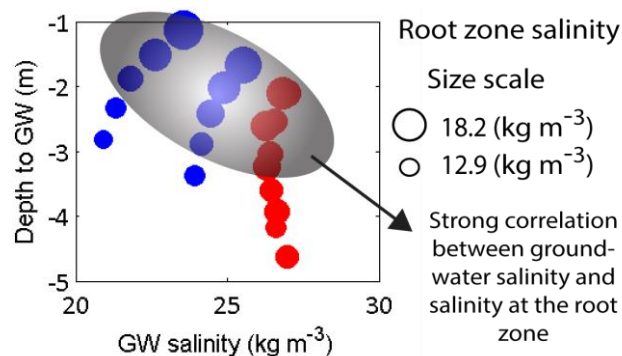


Figure 60: Salinity at the root zone (dots) as a function of depth to the groundwater and salinity in the groundwater. Channel opened scenarios are depicted in red, channel closed scenarios are depicted in blue.

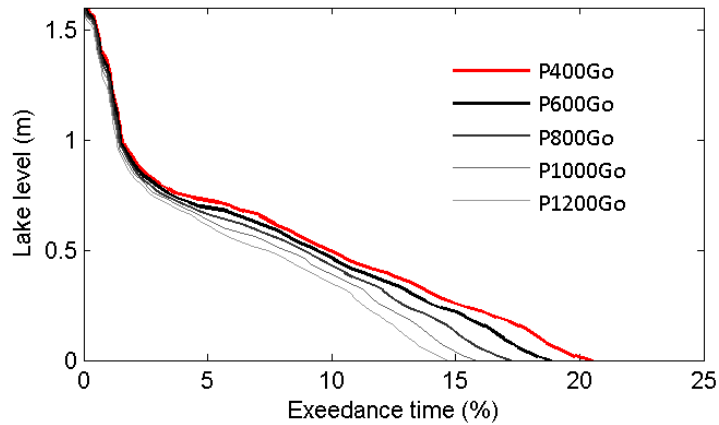


Figure 61: Influence of pumping schedule (from 400 to 1200 m³ d⁻¹) on hydroperiod.

5.3.3 Lake Bed Re-vegetation

In this simulation, the model was forced with an increment of 3% in the biomass of each specie after 10 years of the beginning of the simulation, which started in 1979. As the simulation proceeded (after the biomass increment in 1989), the vegetation responded to the forcing climate and returned to the dynamic equilibrium that was predicted by the Observed (control) scenario after approximately 3 years (Figure 62). This simulation shows that without controlling the hydrological forcing on the wetland or without changes in the climate, it is more likely that the system will not accommodate more vegetation than it currently does. As such, re-vegetation needs to be followed by hydrological intervention, such as groundwater pumping.

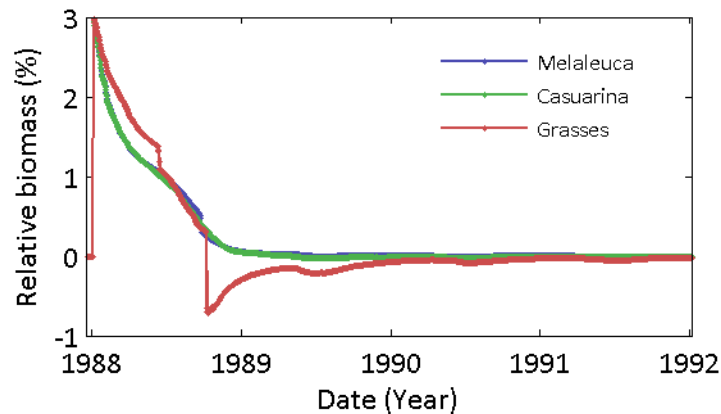


Figure 62: Vegetation response in relation to the Observed (control) scenario after attempt to re-vegetate the lake bed without hydrological intervention.

5.3.4 Implementation of Dulbinning Channel

To investigate the benefit of surface water engineering in the catchment, short term individual flow events were run in TUFLOW. The first scenario evaluated implementations on Dulbinning Channel, a major surface water conveyance located in the valley floor. The channel was constructed in 2008 to protect the vegetation from long periods of flooding, which could lead to salinization and vegetation mortality. To test the efficiency of the channel, we ran the previously calibrated set up for TUFLOW during a particularly intense rainfall event, which reached 106 mm on the 29/01/1990 (Figure 63). We used the LASCAM-S predicted values as inflow boundary conditions for TUFLOW.

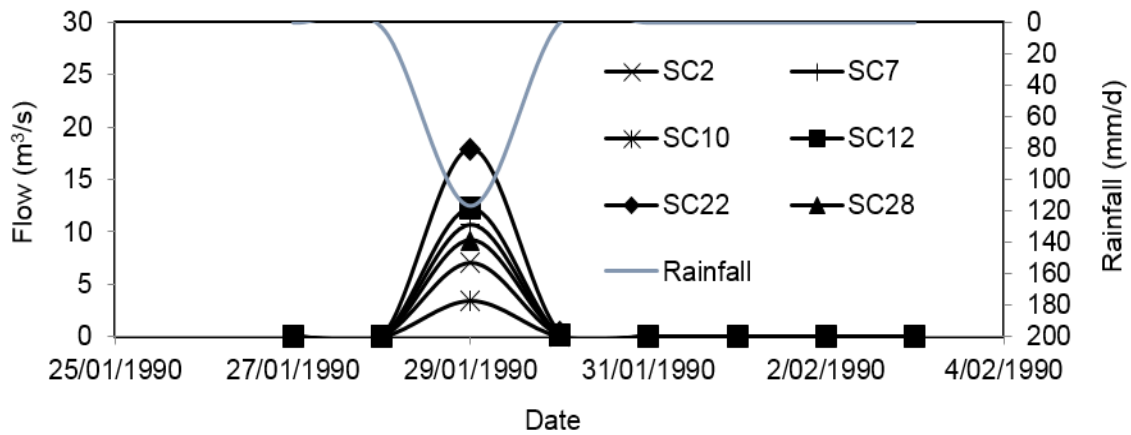


Figure 63: The rainfall event observed in January 1990 and the gauges response predicted by LASCAM.

Figure 64 shows the flooded area if the channel was not constructed and Figure 65 show the flooded area if it was implemented. These figures represent snapshots of ponded water location and depth on the third day of the simulation at the flood peak. Note the considerable decline of inundated area and water level in the latter scenario (with the channel). Besides decreasing the inundation area, the hydrograph at the catchment's outlet also changed significantly (Figure 66). The water arrived at the outlet (location given on Figure 67) half a day earlier and a greater volume was drained, decreasing risk of evapoconcentration of salts and groundwater recharge in the Dulbinning Reserve.

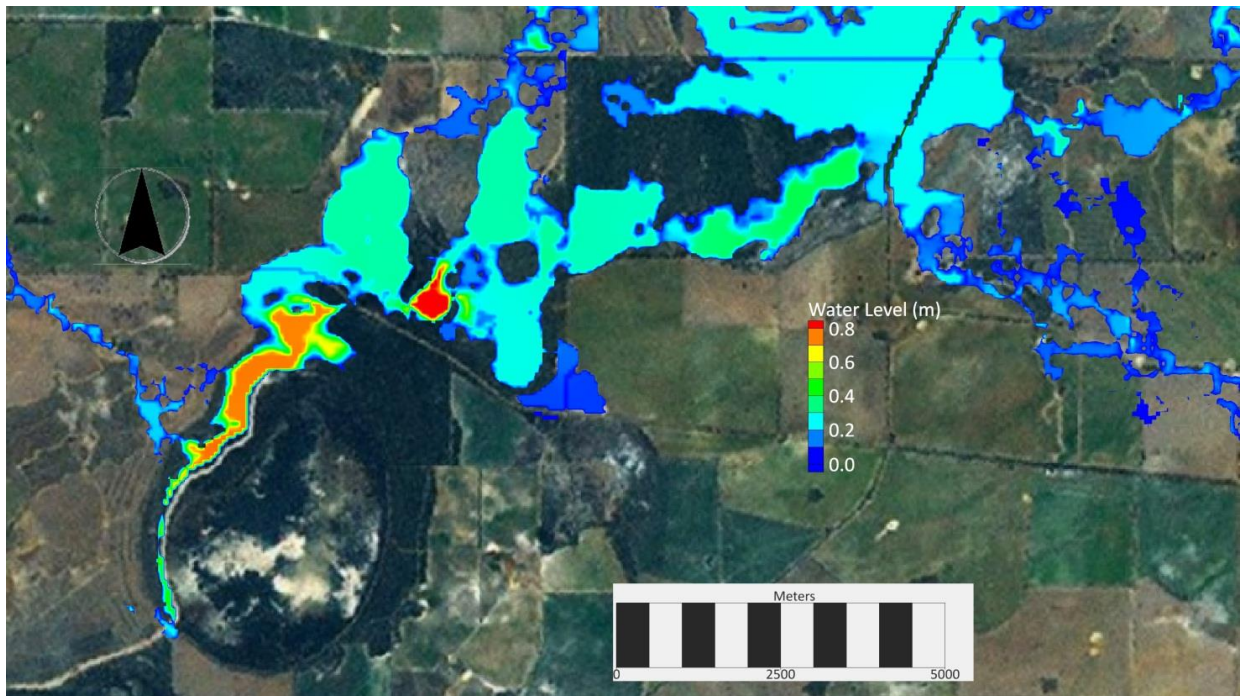


Figure 64: The flood extension on 29/01/1990, 3 days after the beginning of the simulation, for a scenario without channel in the Dulbinning Reserve.

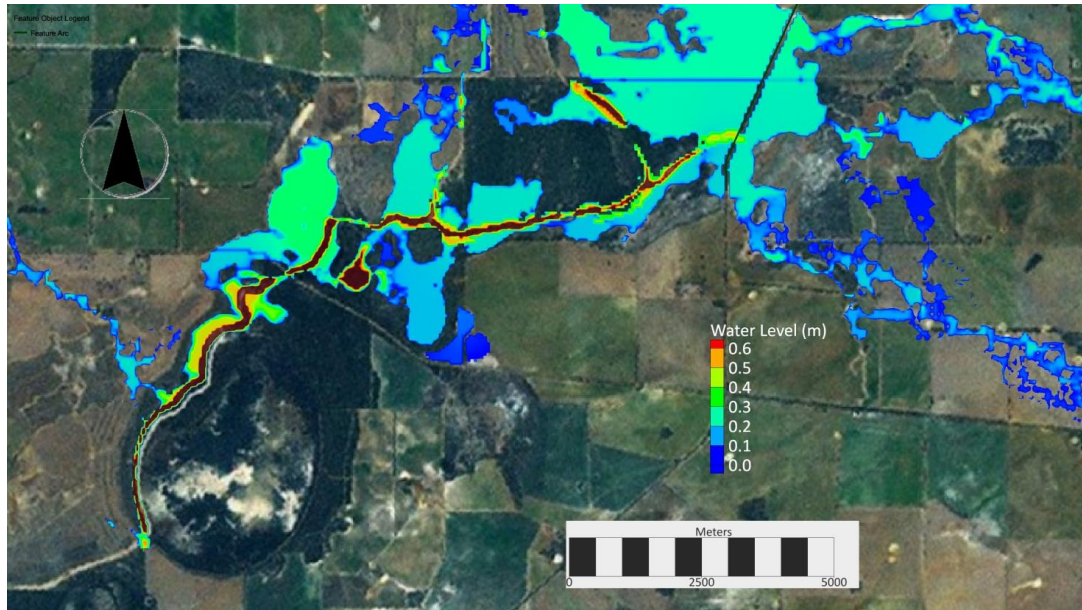


Figure 65: The flood extension on 29/01/1990, 3 days after the beginning of the simulation, for a scenario where the channel in the Dulbinning Reserve was built.

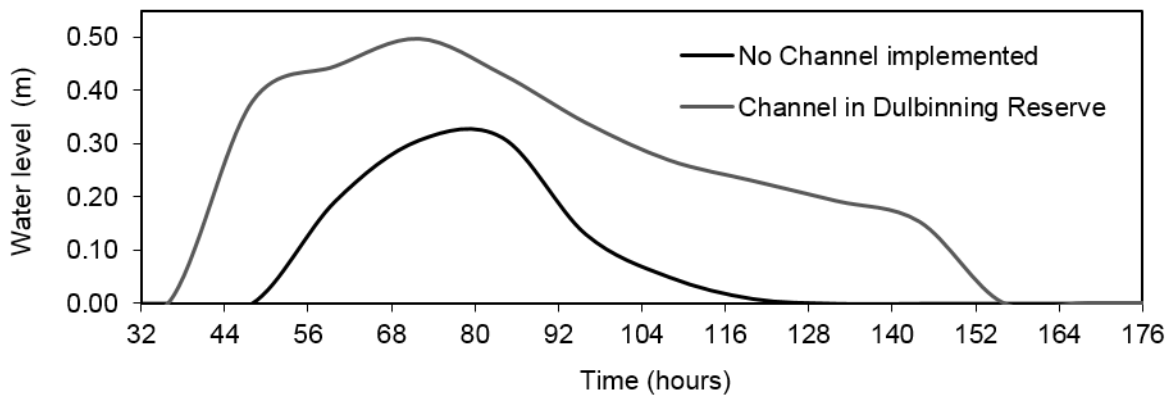


Figure 66: The changes in the hydrograph at the catchment outlet with and without the Dulbinning Channel implementation.



Figure 67: Location of the observation point at the catchment outlet.

5.3.5 Channel Implementation at Canal Road

Canal road was identified by DPaW as an area where surface water management was required due to excessive surface water ponding observed and subsequent salinisation. To test the drainage efficiency gained by the implementation of a channel along the road, we ran TUFLOW during the same intense rainfall event as used above, from January 1990. Two scenarios were tested. In the first, the topography was unaltered. In the second, a north-south 0.4 meters deep excavated channel was created along Canal Rd. This surface water conveyance steps to the east-south-east half way to Brown Rd. Figure 68 presents the resultant flooded area and water level for the second day of simulation without a channel. Figure 69 presents the results from a simulation with the channel in place. The simulations showed little change in flooded area. However, a greater depth of water was predicted (Figure 70) at the observation point (Figure 71, indicating a better drainage from the uplands after the channel). A substantial portion of the ponded water was located at the beginning of the channel, at the intersection of Canal Rd and Wogoling Rd South. There is a major depression in the terrain, south-easterly oriented. Soil bunds could potentially prevent overflow to the east and improve the effectiveness of the conveyance.

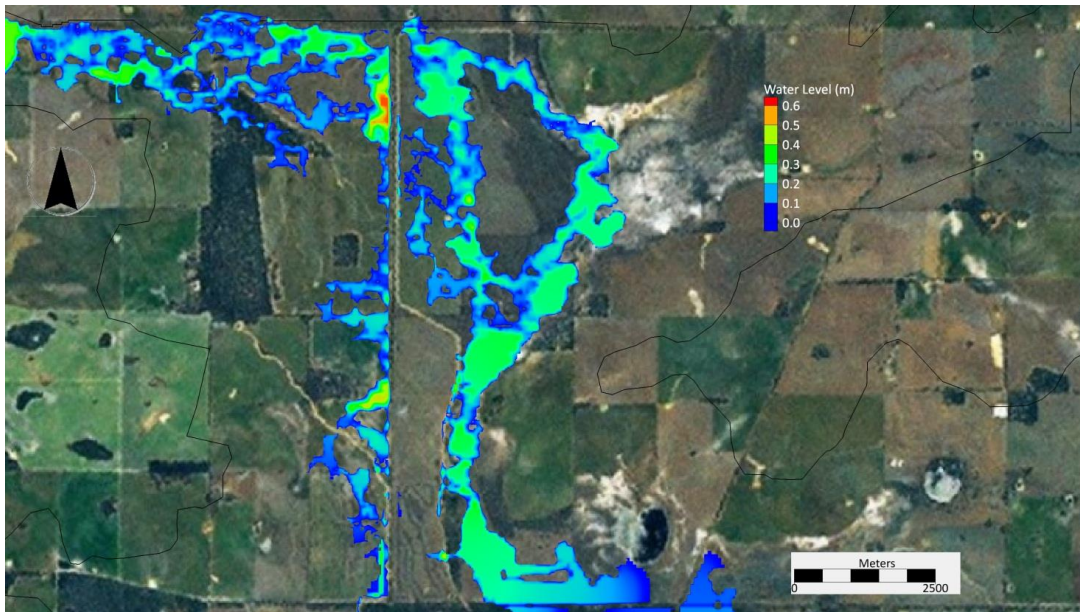


Figure 68: Flood extension after 2 days of simulation, no channel implemented along Canal Rd.

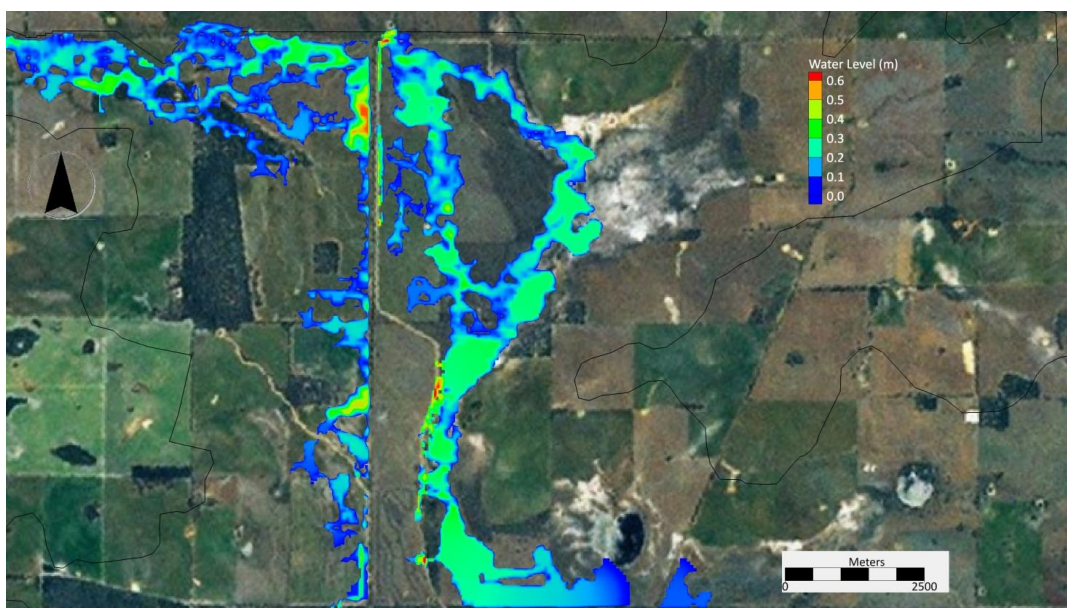


Figure 69: Flood extension after 2 days of simulation, a 0.4m deep channel is implemented along Canal Rd in this simulation.

To assess if a deeper structure would improve flow conveyance, we ran a simulation with a total depth of 0.6 m (Figure 72). For the January 1990 event the channel was successful in conveying the total volume of water to

the Dulbinning Reserve area. However, January 1990 is a rainfall event whose Annual Recurrence Interval (ARI) is approximately 1 in 10 years. Other simulations of higher magnitude events, with longer ARI's, should be tested to verify the efficiency of the channel in more intense events.

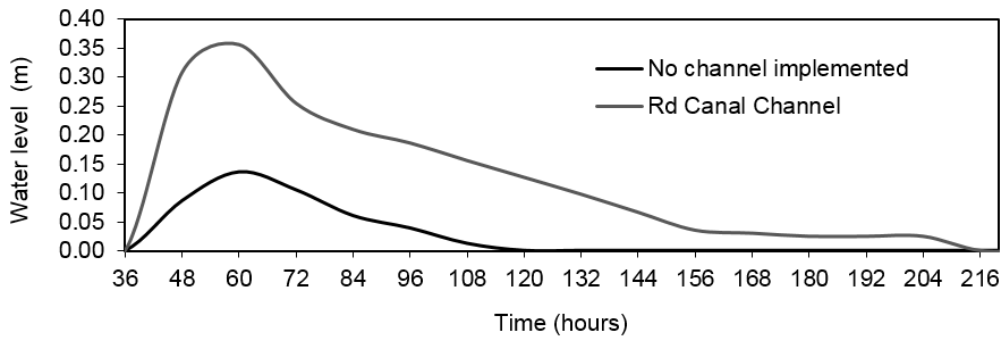


Figure 70: The changes in the hydrograph that the implementation of a 0.4 m deep channel along Canal Rd generated.



Figure 71: Location of the observation point.

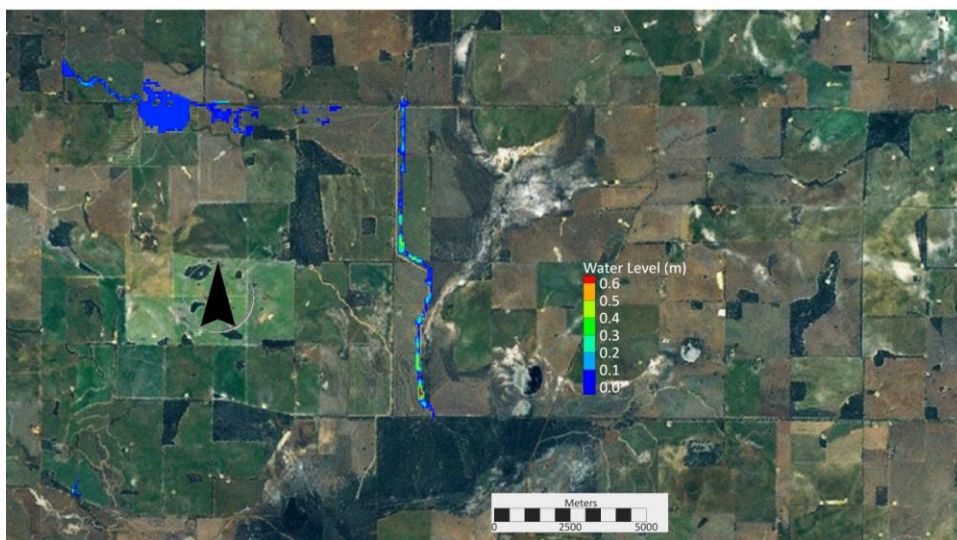


Figure 72: Simulation with a further 0.2m excavation in the channel along the Canal Rd.

5.3.6 Mallee Plantation in the Valley Floor

Mallee plantation is reported to increase the infiltration rate by means of increasing the surface roughness and consequently the time window for infiltration [Mendham *et al.*, 2012]. To test the effect of Mallee plantations on surface water event timing and magnitude, we implemented a Mallee plantation in TUFLOW. Mallee treatment areas were placed downstream to the main inflows to the valley floor (Figure 73). In these areas, we placed a Mallee row every 100m, each row being perpendicular to the topography.

We adjusted model parameters in the Mallee areas to increase infiltration (initial loss=4mm and continuing loss 2 mm/h) and surface roughness ($n= 0.05$). We also represented the subtle topographic effect of Mallee plantations due to litter and sediment mounding from planting earthworks and growth by creating a 5 cm elevation at each row. The event used to force the model was the one from January 1990. Figure 74 presents the flooded area after 2 days of simulation for a scenario without the Mallee plantation. Figure 75 is a snapshot of the inundated area and water level after 2 days from the beginning of the simulation for a scenario where the Mallee plantation is included.

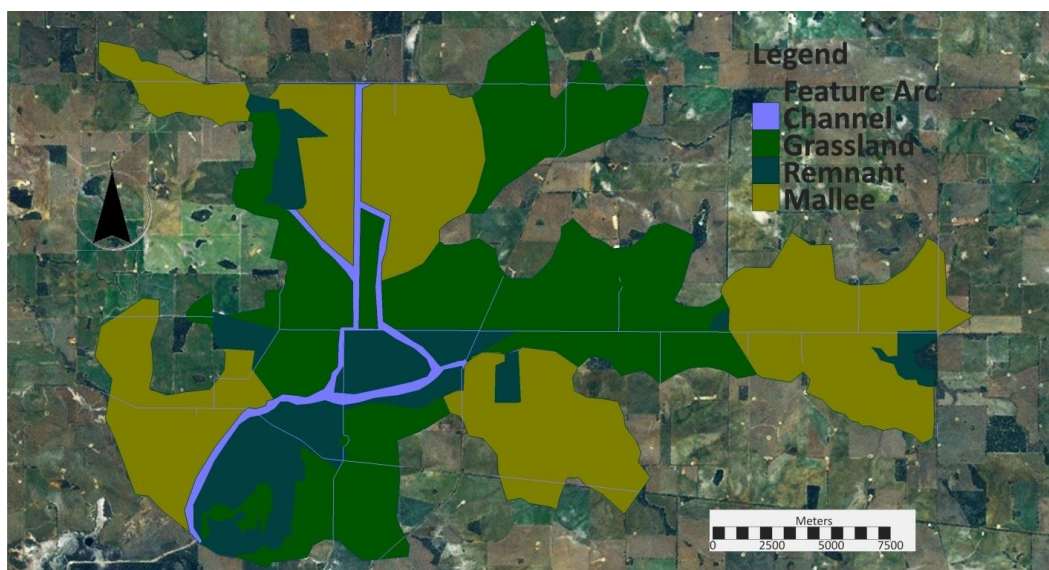


Figure 73: Land coverage map defining the spatial distribution of the hypothetical Mallee plantation.

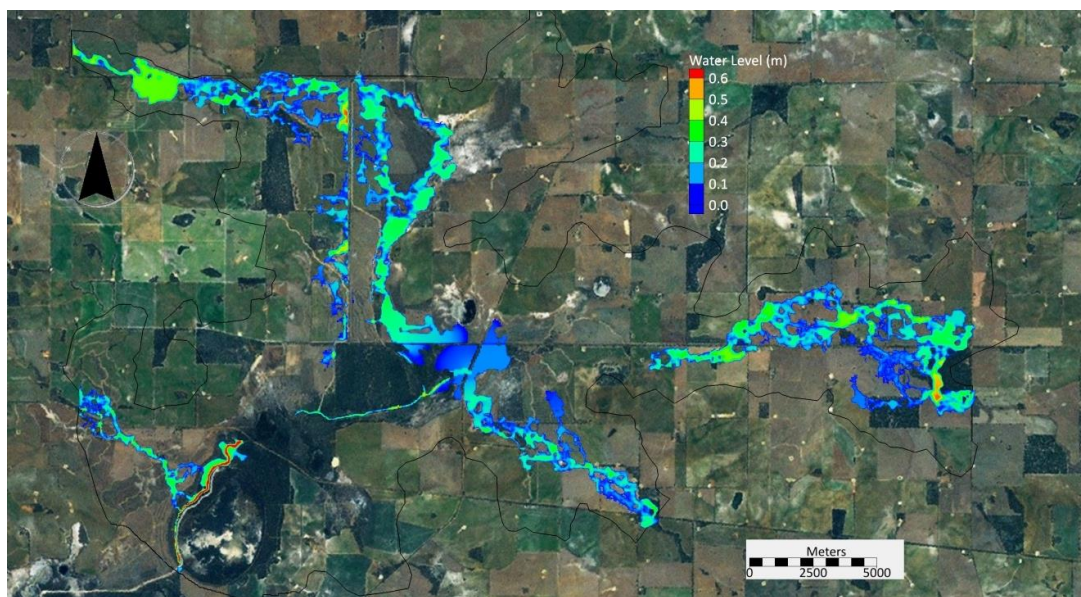


Figure 74: The extension of flooding after 2 days of simulation for a scenario without Mallee plantation.

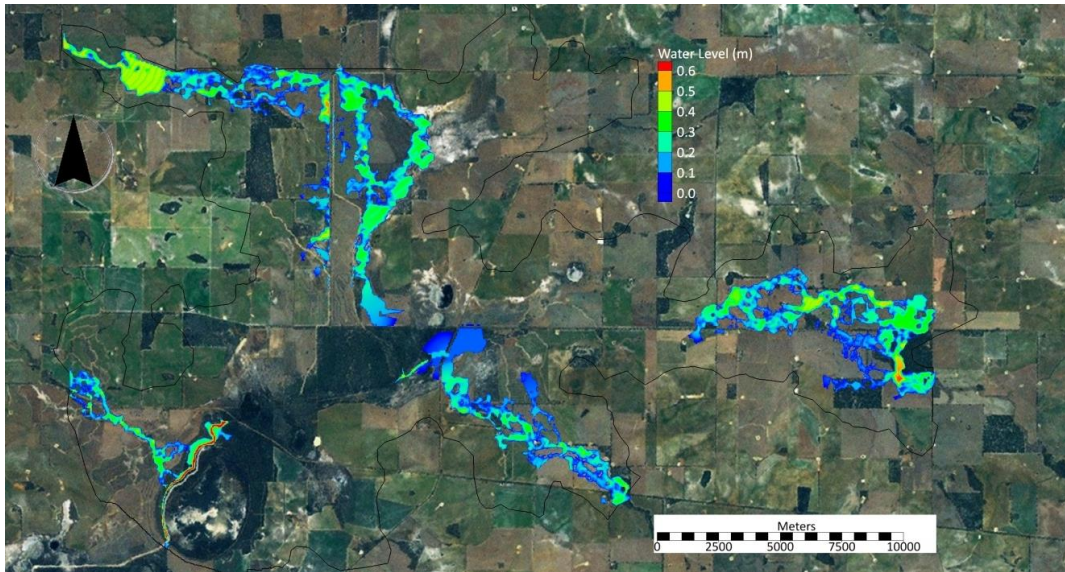


Figure 75: The extension of flooding after 2 days of simulation for a scenario with Mallee plantation.

The hydrograph (Figure 76) at the start of the Dulbinning channel (location shown in Figure 78) reveals a 12-hour delay for the initiation of runoff. Although there is no difference in the event timing at the catchment outlet, the water depth predicted had a modest reduction (Figure 77). The greater infiltration caused by the Mallee plantation accelerated the drainage of ponded areas (Figure 79) if compared to a scenario without the Mallee plantation (Figure 80).

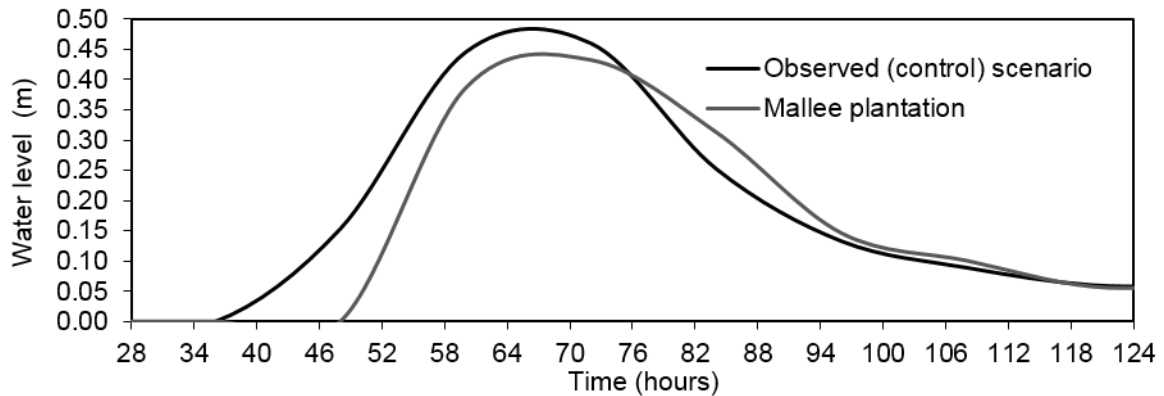


Figure 76: The hydrograph at the beginning of the Dulbinning Channel for a scenario without Mallee plantation (Observed scenario) and a scenario with the Mallee plantation.

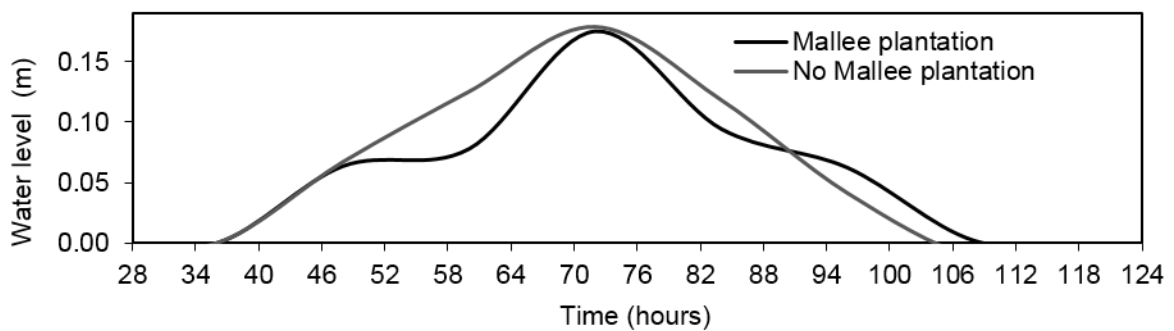


Figure 77: The hydrograph at the catchment outlet for scenarios with and without the Mallee plantation.



Figure 78: Observation point at the beginning of Dulbinning Channel.

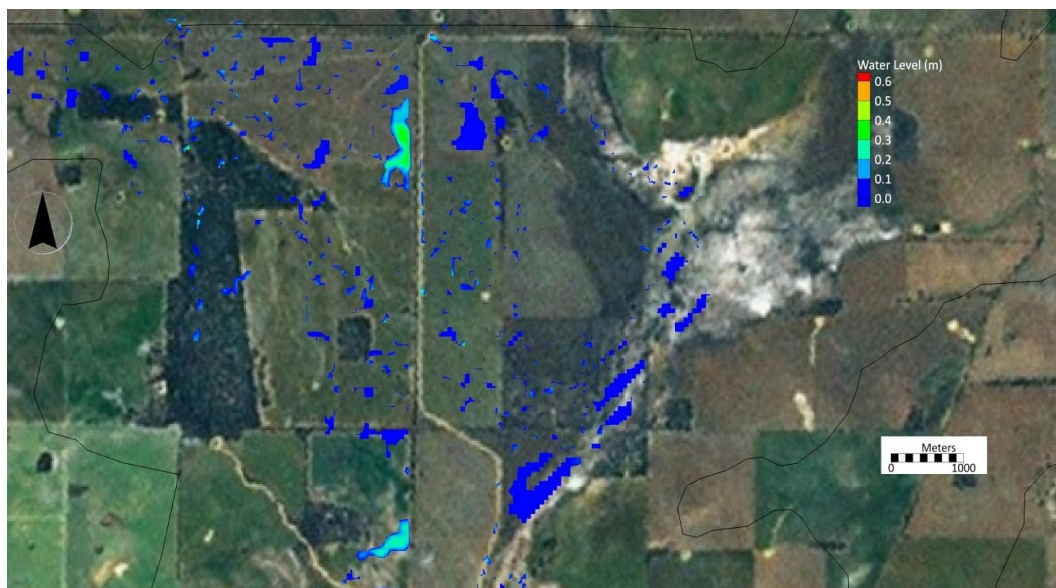


Figure 79: Reduced scattered ponding areas 5 and a half days after the beginning of the simulation for a scenario with the Mallee plantation.

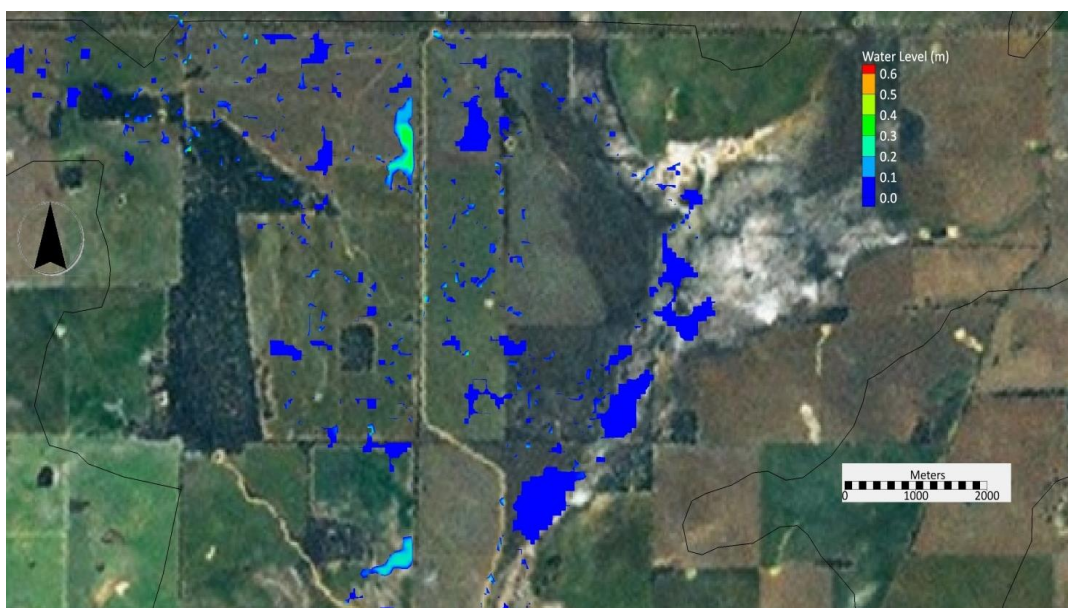


Figure 80: Remaining scattered ponding areas 5 and a half after the beginning of the simulation for a scenario without the Mallee plantation.

5.3.7 Culverts Implementation along Brown Rd and Toolibin Rd North

An extensive area of ponding was observed north of Brown Rd, at the junction of Toolibin Rd North in all TUFLOW simulations. We tested if the implementation of a culvert in Brown Rd and another in Toolibin Rd North (location in Figure 82) could effectively decrease the inundation time in that area. Figure 81 shows the flood extension without the culverts, and Figure 82 shows the flooded area if the culverts were in place, both representing 3 days into the flow event. The water elevation north of Brown Rd is higher by approximately 0.15 m for the simulation without culverts. The hydrograph at the outlet of the catchment (Figure 83) shows a greater water volume leaving the catchment after the installation of the culverts.

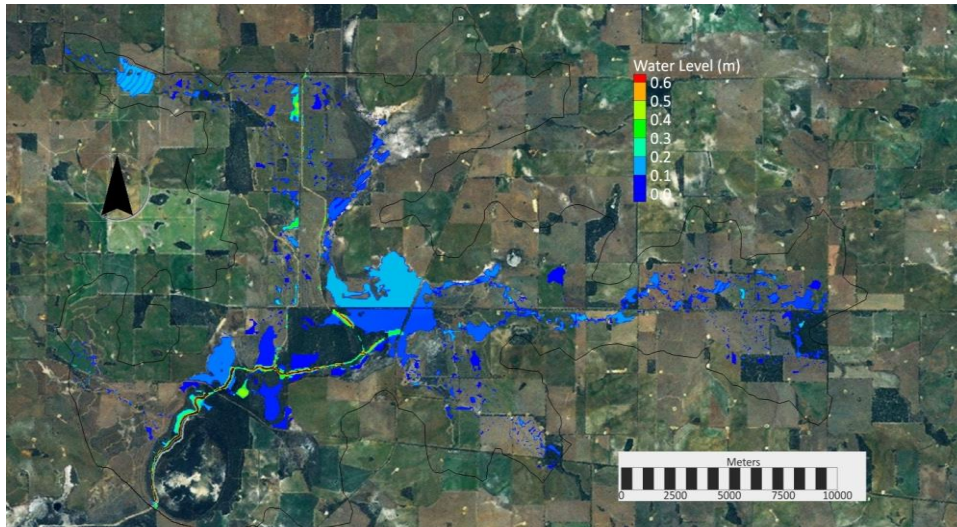


Figure 81: The extensive area of ponding waters at the corner of Brown Rd and Toolibin Rd North.

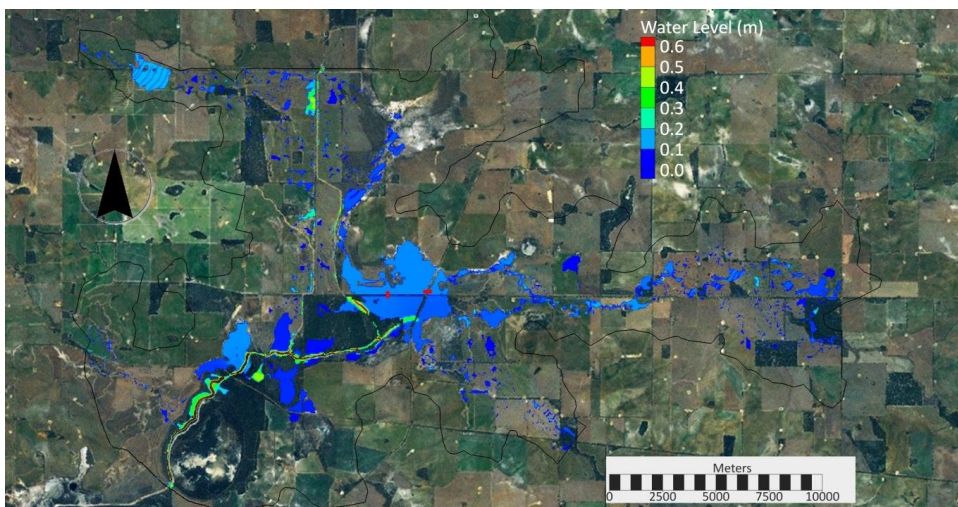


Figure 82: The position of the two extra culverts, under Brown Rd and under Toolibin Rd North (red dots).

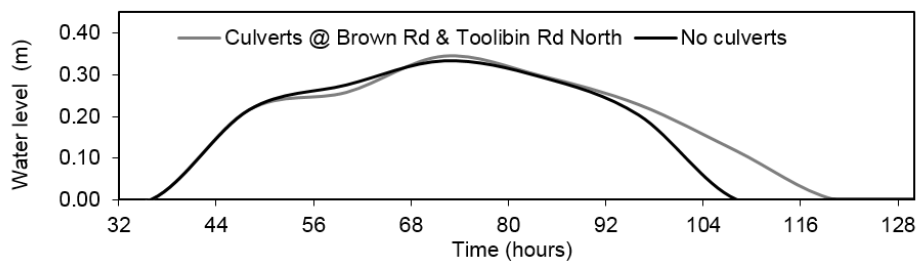


Figure 83: The hydrograph at the outlet of the catchment before and after the implementation of the culverts at Brown Rd and Toolibin Rd North.

5.4 The Combined Effect of Groundwater Pumping and Surface Water Diversion

For the last 15 years, the management policy for Toolibin Lake has recommended groundwater pumping to keep the water table level four meters below the ground. Modelling simulations have estimated that a rate of approximately $800 \text{ m}^3 \text{ d}^{-1}$ is necessary to achieve this goal. The current policy also enforces the catchment water diversion from the wetland when its salt concentration is greater than 1 kg m^{-3} . In this analysis, 10 different groundwater (GW) and 11 different surface water (SW) intervention levels were tested (Table 18). The aim was to assess how the combined SW and GW interventions could affect vegetation niche availability and consequently their biomass and relative abundance.

The management interventions tested are variations of the pumping rate and of the trigger threshold for surface water diversion. For GW interventions, we tested pumping rates ranging from 0 to $1000 \text{ m}^3 \text{ d}^{-1}$, with each intermediate level of GW intervention being an increment of $100 \text{ m}^3 \text{ d}^{-1}$. For SW interventions, 11 different diversion threshold levels were tested, all based on the salt concentration (in kg m^{-3}) in the catchment runoff. This ranged from zero (i.e., all surface runoff is diverted) to 20 kg m^{-3} TDS (i.e., all surface runoff was allowed into the lake). Values above 20 kg m^{-3} TDS were not registered for the simulation period, between 1979 and 2013.

Combining all SW and GW interventions, 220 scenarios were tested. They represent the average for each SW/GW combination during the years 1979 and 2013. The simulation, however, started in 1969, so that the initial condition would not bias the result. Notionally, we ranked the SW and GW interventions as “high” when the threshold for salt concentration was low and when the pumping rate was high. Using this arbitrary and notional rank, the current policy in Toolibin Lake was deemed highly interventional, sitting at level 8/8 for SW/GW (marked in grey in Table 18).

The results showed that the current policy put in practice in Toolibin Lake would be able to keep the average groundwater around the recommended four meters below ground level. Groundwater pumping was more important in controlling the groundwater level than diversion of the surface water. Management of the surface water without pumping would keep the groundwater level between one to two metres deep (Figure 84a). In general, the total biomass showed a positive and strong correlation ($R=0.884$) to the groundwater depth. The level of intervention currently practiced in Toolibin Lake was able to increase the vegetation biomass by up to 17% (Figure 84b), if compared to a scenario without intervention (i.e., sitting at the 0/0 level), which corroborates with observations that management interventions improved vegetation health [Vogwill *et al.*, 2010]. Increasing the level of intervention to 10/10 would increase the biomass to up to 25% compared to the 0/0 level.

The results corroborated with the observation [Vogwill *et al.*, 2010] that *C. obesa*, but not *M. strobophylla*, has been positively affected by the current policy. In addition, they revealed that *M. strobophylla* would reach a higher total biomass if no intervention was taken place (Figure 85). It is explained partially by the reduction in soil moisture and increase in groundwater salinity as the level of SW intervention increased (Figure 86). *M. strobophylla*'s biomass presented a positive correlation ($R=0.26$) to soil moisture. Contrary to anticipated, however, *M. strobophylla*'s biomass related negatively ($R=-0.87$) to groundwater depth and positively ($R=0.56$) to groundwater salinity. It also related positively to salinity at the root zone up to a concentration equals to 13 kg m^{-3} TDS. After this threshold, any increase in salinity deeply decreased *M. strobophylla*'s biomass.

The results suggests that competition with *C. obesa*, the dominant species in Toolibin Lake, has been an important control on *M. strobophylla*'s biomass. In fact, the correlation between *C. obesa* and *M. strobophylla*'s biomass was negative and greater than 88.9%, representing the singular more important control on *M. strobophylla*'s biomass. The narrow window that allowed *M. strobophylla* to reach its maximum abundance (Figure 87) sited between the peak of *C. obesa*'s biomass and an intolerable environment to *M. strobophylla*, which was determined by the combined effect of high groundwater salinity and low soil moisture. Management intervention also gave benefit to the colonization of terrestrial grasses, but they only represented a low percentage of the total vegetation biomass (around 4%, on average).

To test how *M. strobophylla*'s biomass would respond to the management interventions if *C. obesa* was not present, we tested scenarios where all parameters and boundary conditions were kept the same, except that *C. obesa*'s biomass was forced to zero. In those scenarios, *M. strobophylla* responded differently to the level of intervention, reaching a maximum biomass at the level 6/2 (Figure 88a). Without *C. obesa* competition, *M. strobophylla*'s biomass was controlled by the groundwater level and root zone salinity (Figure 88b). Invasive grasses, which had a peak biomass that was well related to groundwater depth ($R=0.96$), also presented a limitation to the biomass of *M. strobophylla* ($R=-0.33$).

Table 18: Notional level of intervention for SW and GW.

Level of SW and GW intervention	Runoff concentration (kg m^{-3})	Volume extracted ($\text{m}^3 \text{d}^{-1}$)
10	0	1000
	0.25	
9	0.5	900
	0.75	
8	1	800
	1.25	
7	1.5	700
	1.75	
6	2	600
	2.5	
5	3	500
4	4	400
	5	
3	6	300
	7	
2	8	200
	9	
1	10	100
	15	
0	20	0

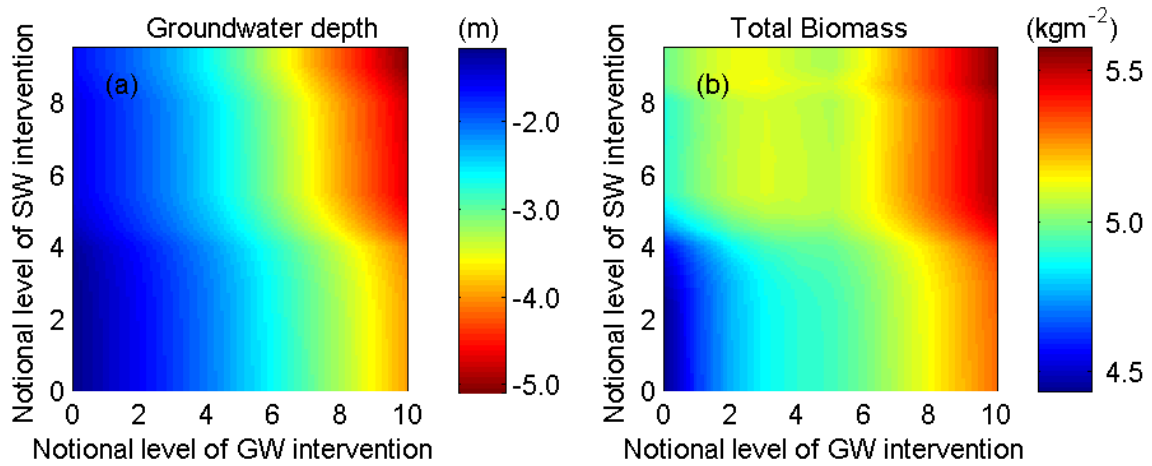


Figure 84: Groundwater level (a) and total vegetation biomass (b) as determined by the level of SW and GW interventions.

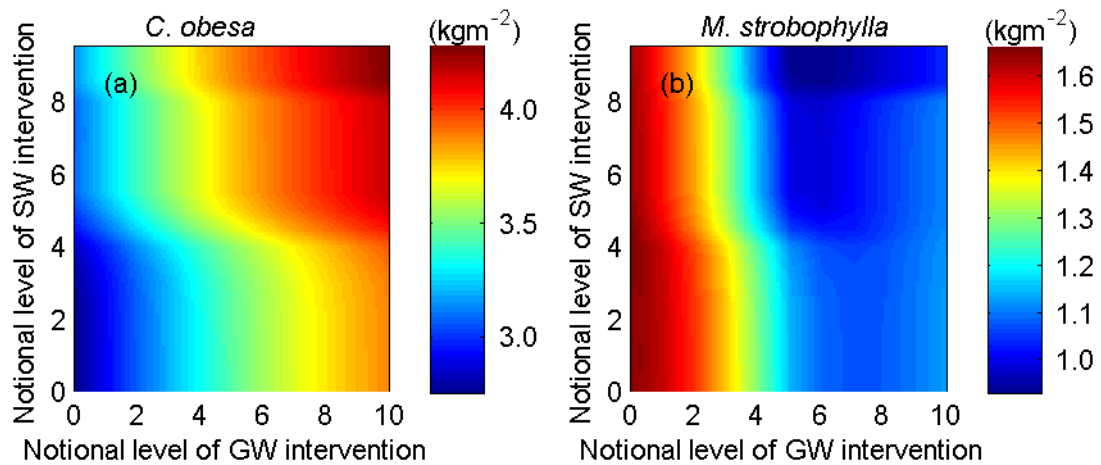


Figure 85: *C. obesa*'s (a) and *M. strobophylla*'s (b) biomass as determined by the level of SW and GW interventions.

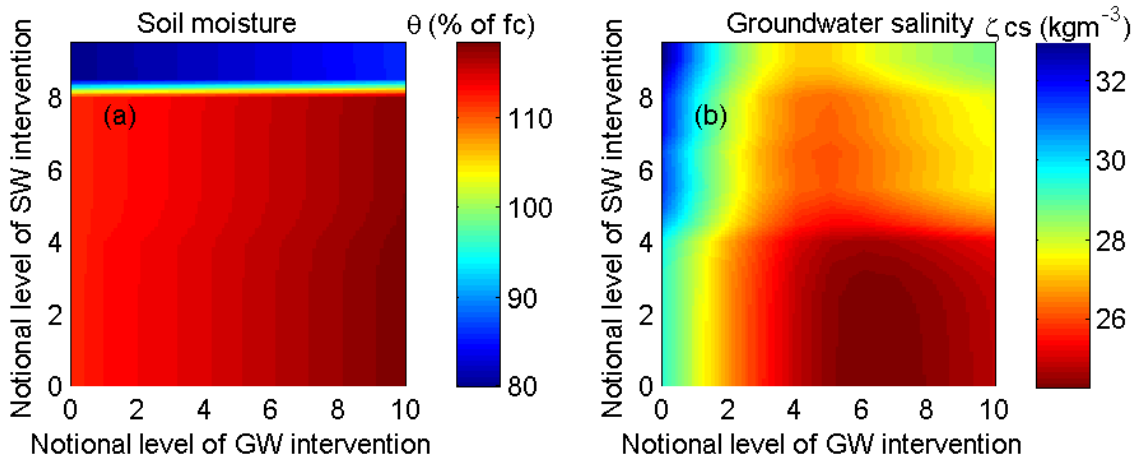


Figure 86: Root zone (a) and groundwater salinity (b) as a function of SW and GW interventions.

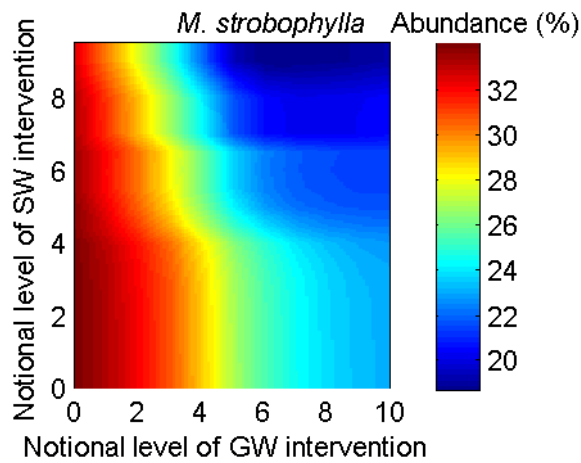


Figure 87: The relative abundance of *M. strobophylla* as a function of SW and GW interventions.

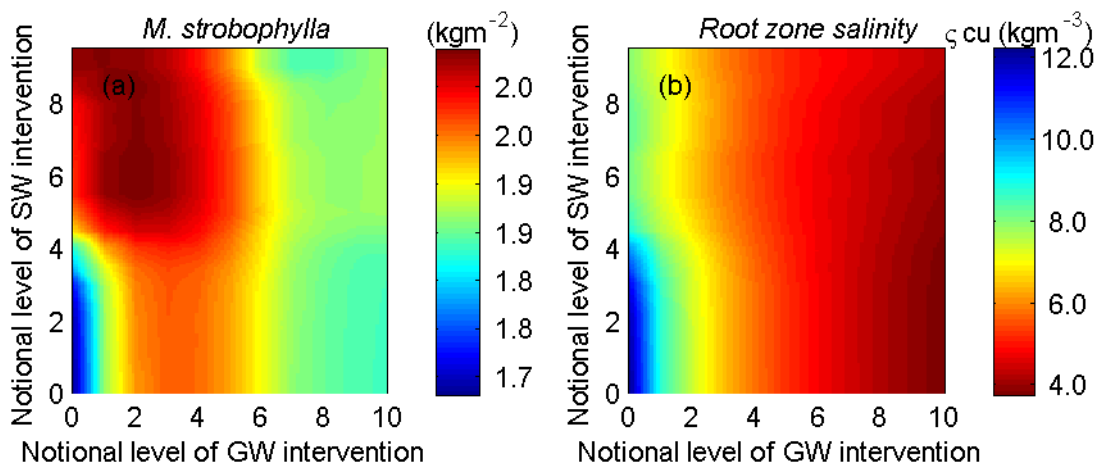


Figure 88: *M. strobophylla*'s biomass (a) and root zone salinity (b) in response to SW and GW interventions if *C. obesa* was not present.

6. Conclusions and Recommendations

As a means of recovering the health of vegetation in the Toolibin Catchment, multiple concurrent management interventions have been implemented over recent decades. The interventions have ranged from re-vegetating the surrounding landscapes and within the wetland domain, pumping the lake's saline groundwater, construction of surface water conveyances and diverting catchment runoff away from the lake. To date, the efficiency of these interventions in controlling water table level and salinity in the wetland, including the response of the vegetation, has been difficult to assess/quantify, particularly in the context of a drying climate. In addition, the impact of hydrological pulses on the lake's flora and fauna has been discussed mainly in an empirical, anecdotal way, with exception of scattered data "snapshots" on the condition of Toolibin Lake's biodiversity assets [Froend *et al.*, 1987]. Here, for the first time, we have attempted to connect important variables such as climate forcing, hydrology, salinity status and vegetation biomass in the wetland, over time-scales from days to decades. The decision support system created is an integration of several models that operate as a tool where management options can be tested (individually or in combination) and their impact on the wetland ecosystem quantified and optimised. In particular, we tested the effect of management actions on growth potential of *M. strobophylla* and *C. obesa*, the co-dominant plant species in Toolibin Lake.

6.1 Model Validation, Limitations and Suitability

Within the wetland system itself, the lake and groundwater levels and salinity variation showed a good agreement between the observed and modelled values. Validation of vegetation dynamics is never straightforward when scarce data is available. Nevertheless, biomass dynamics and growth trends were predicted within the range described by the literature and available field data. In the upland and valley floor, the model predictions were assessed against available flow gauging, surface water salinities and sub-catchment scale average groundwater levels. The lack of long-term data made traditional model calibration procedures not possible (e.g., in some gauges only one flow event was recorded in 5 years). The localized nature of rainfall events in this landscape were not captured in sufficient detail in available climate data, which made model validation difficult. However, the magnitude and behavior of surface runoff and salt export were predicted in accordance with the field measurements. To overcome the lack of data availability, a further hydrological 'process validation' was undertaken by comparing predicted water fluxes with those described in the literature as typical of the WA wheatbelt. This collateral validation built confidence in the model predictions as values for the major water pathways, such as recharge and evapotranspiration, were in agreement with the literature.

Model limitations in describing the ecohydrology of Toolibin Lake and the surrounding catchment were also identified:

- The main model system resolves catchment dynamics at the scale of individual hydrological units (referred as sub-catchments) and is not suited to assess small-scale management questions. The surface water dynamics may be able to be resolved at high-resolution for individual events and the effect of increased flow conveyance on ponding and travel time using the model TUFLOW as we have demonstrated here. However the role of individual drains, contour banks, etc. on the long-term evolution of groundwater are not directly resolved in the water balance model and are captured through generic increases to infiltration losses or decreased recharge rates at the sub-catchment scale, for example. Similarly, the pumps installed in the lake-bed are well distributed over the wetland domain, but can cause localized water table drawdown to an unknown extent. The model does not account for heterogeneities in pumping related drawdown, the underlying aquifer or the unsaturated zone, so the modelled drawdown represents the average over the entire lake-bed. The model cannot make predictions of the response of specific areas of the lake bed to management intervention, it is focused on predicting an ecohydrological trajectory for the wetland as a whole. Spatial heterogeneity in the model appears to be a result of multiple vegetation-salt-water interaction, as the main goal was to provide long-term vegetation response to hydrological changes. Local differences from the mean based on point-scale data and anecdotal knowledge of specific bores should be factored in when interpreting the results from the model.
- The diversion of water into or away from the lake-bed is controlled by simple gate rules in WET-0D, where water is assumed to either enter or be diverted. It does not assess whether the current inlet/outlet structures give sufficient control over the salinity of water and salt load entering the lake.
- Some uncertainty related to the predictions of the ability of the vegetation to cope with salinity and inundation exists, since the model parameter values were based on limited (albeit local) tree physiological data. More experiments considering prolonged flooding and the subsequent plant photosynthesis rates would improve our degree of confidence in the model parameterization.

6.2 Future Studies

Based on the current model suitability and some of concerns that may be sustained regarding the management of Toolibin Lake and Toolibin Catchment, we suggest the following:

- For more detailed assessments of aquifer response to configuration of the pumping network, a fully distributed groundwater modelling study using numerical codes such as MODFLOW or FEFLOW is recommended. We highlight, however, that such a model study would not be able to resolve the dynamic feedbacks that occur between the root zone hydrology, soil solution salinity and vegetation productivity. Such a model would also be very difficult to be run at the temporal resolution required (i.e. length of model run and daily time step). Therefore, further research and model development effort on coupling the spatially distributed flow modelling with an ecohydrology model able to capture species-specific plant physiological dynamics is recommended if vegetation response is the management concern.
- For assessment of whether the current inlet/outlet structures give sufficient control over the salinity of water and salt load entering the lake, and to suggest alternatives to the current configuration, a further dedicated study of the hydraulics of the gate and lake entrance region may be undertaken. TUFLOW model simulations could be designed to undertake this task. However, further configuration of the TUFLOW setup presented herein is required to resolve this level of detail. Outcomes from such a study can be used to provide an improved set of rules for the WETOD model such that the combination of models can be used to see the long-term salinity reduction goal.
- Data available from hydrological monitoring of the upland and valley floor was patchy and in many cases of limited duration. Most available data was obtained during a particularly dry period and the long-term catchment outlet gauge data has some significant errors in it, particularly in the early data covering the wet period. Further monitoring of hydrological responses to significant rainfall events should be carried out as a priority to collect further data to enable improved model calibration.

6.3 Application of the Model System to Management Scenario Assessment

A series of modelling scenarios were undertaken to demonstrate the ability of the model system to address targeted hydrological questions related to lake-bed and catchment-wide management strategies (refer to the Objectives section). Other scenarios were implemented that focused on assessing the impact of re-vegetation or vegetation clearing in small areas of sub-catchments where DPaW had particular interests, however we highlight that the overall level of re-vegetation in these instances was relatively low. Assessments of the combined effect of groundwater and surface interventions, across different degrees of intervention, were also undertaken to demonstrate the uncertainty of management decisions on wetland ecohydrological response.

6.3.1 Lake-Bed Interventions

From the point of view of current management practices being undertaken, the most efficient action to control groundwater level within the lake-bed was the extraction of saline groundwater by the network of pumping bores. Increasing the daily groundwater extraction from 400 to 1200 m³ d⁻¹ reduced the number of days under flood conditions by 5%, over a 35 year simulation. The depth to the groundwater in this region also showed a positive relationship when combined with surface water exclusion from the wetland, but we note that under the recent dry climate there have been almost no potential inflow events. Under a prolonged wet climate, or considerably drier climate results would likely be different. Our results show that the decline in rainfall observed in the last 15 years caused a decline of the water table level in the wetland of up to 0.9 m. Regardless of groundwater pumping, vegetation has benefited from this precipitation decline, and this has resulted in a shorter wetland hydroperiod and increased biomass relative to that predicted during the rainfall conditions of the mid 80's to early 90's. Although climate is not a manageable variable, changes in rainfall have been attributed to a significant degree of the observed reduction in groundwater level in the lake-bed and management plans need to therefore factor in climate forecasts. In particular, future dry periods will require different management than wet periods, and under these conditions, it is more appropriate to allow surface water into the lake, whereas under extended wet periods total surface water diversion would result in a benefit to the vegetation.

Optimal conditions for both vegetation health and waterbird populations are feasible, if the surface water hydroperiod does not surpass approximately 60% of the year, which is a similar period as waterbird breeding cycles. Model simulations that presented standing water for periods extending greater than 60% of the year resulted in substantial loss of vegetation biomass. During periods of lake inundation, groundwater pumping must be maintained, with sump pumping also implemented to improve lake drainage. Draining the lake will obviously

be influenced by the presence of waterbirds breeding and it was outside the scope of this report to optimize that relationship, which is a dedicated study in its own right.

Previous studies suggested that groundwater level should be kept at greater than 4 meters below ground level and we agree with that criterion. We recommend the volume extracted by pumping to be 800 m³ per day as a long term (20 years +) management target. A flow of 800 m³ per day can maintain the average groundwater level at around 4 meters below ground, if rainfall remains similar to that observed in the last 15 years. If the climate is wetter (similar to the late 1980's to 90's) then it is unlikely that even an increased (150%) pumping rate will hold groundwater levels. If the climate remains relatively dry and antecedent groundwater levels can be maintained below 4 mBGL, surface water should be allowed into the lake but drained as quickly as possible. The benefit of salt flushing and increased moisture content in the unsaturated zone occurs quickly and once soils are saturated, upward salt diffusion occurs potentially reversing the benefit of inflow. According to the model there are no indications that the salt load coming from runoff is the main cause of lake salinisation. The most detrimental effect that surface runoff appears to have on vegetation biomass is prolonged inundation and the rise of the saline groundwater. Under such circumstances, pumping should be maintained and higher pumping rates would be beneficial if possible. Under no circumstances surface water runoff should be forced into the lake if groundwater is less than 2.5 m from the lowest point of the wetland. At depths to groundwater less than 2.5 mBGL, root zone salinity is driven by groundwater salinity. During periods of surface water inundation, it will be critical to frequently monitor shallow groundwater level and salinity to guide pumping rates.

6.3.2 Flow Management in the Valley Floor

Based on the hydrological data, we identified an important threshold for runoff generation to be around the Annual Exceedance Probability (AEP) of 20% (58 mm in 24 hours). Our model suggests that this is a significant rainfall event that generates runoff to the catchment outlet, connecting the upland to the valley floor and wetland. Depending on the status of the water table level in the wetland, this significant rainfall event (AEP of 20%) may or may not trigger operation of the gate. In the context of a rainfall event greater than 58 mm per day, the groundwater level should be used as the criteria for gate operation and to guide sump pumping rate, not just surface water inflow salinity. At surface water salinities of greater than 1,000mg/l (up to a maximum of 4,500 mg/l) substantial beneficial flushing of the soil zone will occur.

By evaluating the benefit of the Dulbinning channel with the model, we noticed a considerable decline in inundated area, period of inundation and water level in the Dulbinning Reserve with the channel in place. The channel also increased the speed of water delivery at the catchment outlet by half a day and increased the volume of delivered surface water, decreasing the risk of water logging and evapoconcentration of salts in the Reserve. The major effect caused by the Mallee plantation (without integrated surface water management) and Salt Land Pastures, as predicted by the model simulations, was the delay of the surface runoff, rather than effectively decreasing it. Only large rainfall events generate catchment scale flows and under these conditions the marginal increase in infiltration from revegetation has little effect on end of catchment flows. However, the greater infiltration potential and water use did accelerate the drainage of scattered ponding areas that would have otherwise remained as prolonged inundation. This highlights an important improvement since prolonged flooding promotes expansion of areas of localized salinization. The benefit of catchment scale Mallee plantations (agro forestry) coupled to surface water management (contour banks) has not been tested due to some uncertainty about the ability of this scale of treatment to be implemented. This could be done in future studies using the DSS.

The level of intervention currently practiced in Toolibin Lake, which diverts surface water when salt concentration exceeds 1 kg m⁻³ TDS, and pumps groundwater at 800 m³ d⁻¹ rate, was able to increase the vegetation biomass by up to 17% relative to a scenario without intervention. Note this is in the context of the recent dry climate. *M. strobophylla* correlated negatively to the water table depth and positively to groundwater salinity. These counterintuitive relationships were explained by vegetation competition. The current water management in Toolibin Lake has decreased the groundwater level and the hydroperiod, without considerably decreasing groundwater salinity. Under these conditions, the groundwater became unavailable to *M. strobophylla*. The co-dominant species moved their competition to the root zone, where *C. obesa* has physiological advantages. In addition to a lower wilting point, *C. obesa* possesses a shorter, more broadly distributed root system, which allows it to access sporadic rainfall events before *M. strobophylla*. Thus, water management enhanced the vegetation competition in the wetland by restricting the niche of *M. strobophylla*. The relative abundance of the co-dominant species were found in the opposite ends of the water management levels, with *M. strobophylla* reaching its maximum biomass when the level was intervention was kept to a minimum. In SWWA, where evapotranspiration can reach more than 4 times the precipitation, the lack of groundwater availability due to salinization, proved to be a threat for *M. strobophylla*, which was always outcompeted by *C. obesa* in the dry vadose zone. If *C. obesa* was not present, *M. strobophylla* would respond more positively to the current level of

management intervention. Its biomass would be then controlled by root zone salinity and by competition with invasive terrestrial grasses.

6.3.3 Re-vegetation Effort

Re-vegetation of the upland and valley floor has the potential to decrease the local groundwater level, surface runoff and salt exports to the wetland. However, the re-vegetation area has to be in excess of 8% of a sub-catchment to achieve any significant impact. Interpreting the field data and the modelling results, we noticed that the western side of the catchment and the near saturated parts of the valley floor, generates the majority of the runoff. This result corroborates with similar studies carried out in the wheatbelt, which have suggested that replanting 25% of the catchment would be necessary to reduce groundwater discharge to an acceptable level, consequently reversing the salinisation process [Salama *et al.*, 1993]. Upland areas generated runoff via infiltration excess under the current dry climate. As such, re-vegetation efforts will yield the greatest benefit in the valley floor and the western part of the upland areas, under current climatic conditions. Direct efforts re-vegetating within the wetland area have been considered. Our results suggested that without also controlling hydrological pulses as part of an integrated strategy to increase plant available water while preventing rising groundwater or prolonged inundation, it is unlikely that the system can accommodate more vegetation than will naturally co-evolve under the altered hydrological regime.

As outlined in the previous section, re-vegetation of small areas, such as many of the areas requested by DPaW, are not well resolved in the spatially lumped model. We urge caution with respect to using the model developed here where a precise local-scale assessment of impacts is required. A local scale model would be a more appropriate tool to precisely assess the benefit of these small-scale interventions, although our predictions are indicative of the order of magnitude of the response.

7. References

- Allison, H. E., and R. J. Hobbs (2004), Resilience, adaptive capacity, and the "Lock-in trap" of the Western Australian agricultural region, *Ecol Soc*, 9(1).
- Argent, R. M., R. J. George, and W. Dawes (2001), Flowube: A Groundwater Calculator for Salinity Estimation, in *International Congress on Modelling and Simulation*, edited by MSSANZ, Canberra.
- Aydin, M., S. L. Yang, N. Kurt, and T. Yano (2005), Test of a simple model for estimating evaporation from bare soils in different environments, *Ecological Modelling*, 182(1), 91-105.
- Barrett-Lennard, A. (2008), Surface Water Ponding on Low-Lying Valley Floors in South-West Western Australia: Interactions with Groundwater and its Role in Secondary Dryland Salinity, Dissertation thesis, 83 pp, The University of Western Australia, Crawley, Australia.
- Bartlett, M. (2012), Water and Salt Dynamics in Arid Zone soils Using HYDRUS-1D, 34 pp, The University of Western Australia, Perth, Australia.
- Bell, D. T. (1999), Australian trees for the rehabilitation of waterlogged and salinity-damaged landscapes, *Aust J Bot*, 47(5), 697-716.
- Brouwer, C., and M. Heibloem (1986), *Irrigation Water Management: Irrigation Water Needs*, 102 pp., Food and Agriculture Organization of the United Nations, Rome, Italy.
- Callow, N. (in prep.), Flow-Fill-Flood: Topography and Rainfall Variability Control Surface Water Connectivity and Valley Floor Salinity in Low-Gradient Drylands.
- Callow, N., T. Pope, and N. Coles (2007), Surface water flow redistribution processes: Toolibin Lake biodiversity recovery catchment Rep. CER 07/01 – SESE129, Report by the ARWA – Centre for Ecohydrology for the Department of Environment and Conservation. Perth, Western Australia.
- Carter, J. L., T. D. Colmer, and E. J. Veneklaas (2006), Variable tolerance of wetland tree species to combined salinity and waterlogging is related to regulation of ion uptake and production of organic solutes, *New Phytologist*, 169(1), 123-133.
- Cattlin, T. (2006), The impact of redistributed surface water and spatially distributed recharge on water quality decline in the Toolibin Lake catchment: a modelled approach to process management, MSc thesis, University of Technology, Sydney.
- Cattlin, T., and D. Farmer (2004), Surface Water Assessment for the Toolibin Lake Recovery Catchment Rep., Department of Agriculture Western Australia, Perth, Australia.
- Choudhury, B. J., and B. J. Blanchard (1983), Simulating Soil-Water Recession Coefficients for Agricultural Watersheds, *Water Resour Bull*, 19(2), 241-247.
- Clark, M. P., H. K. McMillan, D. B. G. Collins, D. Kavetski, and R. A. Woods (2011), Hydrological field data from a modeller's perspective: Part 2: process-based evaluation of model hypotheses, *Hydrol Process*, 25(4), 523-543.
- Clarke, C. J., R. J. George, R. Bell, and R. J. Hobbs (1998), Major faults and the development of dryland salinity in the western wheatbelt of Western Australia, *Hydrol Earth Syst Sc*, 2(1), 77-91.
- Clarke, C. J., R. Bell, R. J. George, R. M. Argent, and T. J. Hatton (2001), A simple groundwater computer program for dryland salinity management in Australia, *New Approaches Characterizing Groundwater Flow, Vols 1 and 2*, 279-282.
- Coletti, J., C. Hinz, R. Vogwill, and M. R. Hipsey (2013), Hydrological controls on carbon metabolism in wetlands, *Ecological Modelling*, 249(0), 3-18.
- Coletti, J., G. Gunaratne, M. R. Hipsey, B. Bush, N. Callow, and R. Vogwill (2012), BioRisk – Model assessment of wheat-belt biodiversity asset response to ecohydrological dynamics Rep., 91 pp, The University of Western Australia & WA Department of Environment and Conservation, Perth, Australia.
- Crites, R. W., E. J. Middlebrooks, and S. C. Reed (2010), *Natural Wastewater Treatment Systems*, Taylor & Francis.
- Crosbie, R. S., K. L. McEwan, I. D. Jolly, K. L. Holland, S. Lamontagne, K. G. Moe, and C. T. Simmons (2009), Salinization risk in semi-arid floodplain wetlands subjected to engineered wetting and drying cycles, *Hydrol Process*, 23(24), 3440-3452.
- CSIRO (2007), *Climate Change in Australia Rep.*, CSIRO, Australia.
- CSIRO (2008), *SWIM v2*, edited, CSIRO Australia.
- CSIRO (2009), *Water yields and demands in south-west Western Australia Rep.*, CSIRO, Australia.

- Dall'O', M., W. Kluge, and F. Bartels (2001), FEUWAnet: a multi-box water level and lateral exchange model for riparian wetland, *J Hydrol*, 250(1-4), 40-62.
- Davis, J. A., M. McGuire, S. A. Halse, D. Hamilton, P. Horwitz, A. J. McComb, R. H. Froend, M. Lyons, and L. Sim (2003), What happens when you add salt: predicting impacts of secondary salinisation on shallow aquatic ecosystems by using an alternative-states model, *Aust J Bot*, 51(6), 715-724.
- Dogramaci, S., R. J. George, G. Mauger, and J. Ruprecht (2003), Water balance and salinity trend, Toolibin catchment, Western Australia Rep., 60 pp, Narrogin.
- Drake, P., B. Coleman, and R. Taplin (2012a), Optimising conditions of the root zone to restore wetland vegetation, paper presented at Society for Ecological Restoration Australasia Conference, Perth, Australia.
- Drake, P., B. Coleman, and R. Vogwill (2012b), The response of semi-arid ephemeral wetland plants to flooding: linking water use to hydrological processes, *Ecohydrology*, n/a-n/a.
- Drake, P., B. Coleman, and R. Vogwill (Submitted), The response of semi-arid ephemeral wetland plants to flooding: linking water use and growth traits, edited.
- Ecoscope (2005), Vegetation Monitoring of Toolibin Lake and Reserves Rep., 126 pp, North Fremantle, Australia.
- Eeman, S., A. Leijnse, P. A. C. Raats, and S. E. A. T. M. van der Zee (2011), Analysis of the thickness of a fresh water lens and of the transition zone between this lens and upwelling saline water, *Adv Water Resour*, 34(2), 291-302.
- Farmer, D., M. Sivapalan, and C. Jothityangkoon (2003), Climate, soil, and vegetation controls upon the variability of water balance in temperate and semiarid landscapes: Downward approach to water balance analysis, *Water Resour Res*, 39(2).
- Farrington, P., R. B. Salama, G. D. Watson, and G. A. Bartle (1992), Water use of agricultural and native plants in a Western Australian wheatbelt catchment, *Agr Water Manage*, 22(4), 357-367.
- Feddes, R. A., P. Kowalik, K. Kolinskamalinka, and H. Zaradny (1976), Simulation of Field Water-Uptake by Plants Using a Soil-Water Dependent Root Extraction Function, *J Hydrol*, 31(1-2), 13-26.
- Feikema, P., J. Morris, C. Beverly, P. Lane, and T. Baker (2010), Using 3PG+ to simulate long term growth and transpiration in Eucalyptus regnans forests, in *International Congress on Environmental Modelling and Software Modelling for Environment's Sake*, edited by W. Y. David A. Swayne, A. A. Voinov, A. Rizzoli, T. Filatova, p. 8, International Environmental Modelling and Software Society, Ottawa, Canada.
- Fofonoff, P., and R. C. Millard (1983), Algorithms for computation of fundamental properties of seawater Rep., 53 pp, Unesco.
- Friedl, M. A., J. Michaelsen, F. W. Davis, H. Walker, and D. S. Schimel (1994), Estimating Grassland Biomass and Leaf-Area Index Using Ground and Satellite Data, *Int J Remote Sens*, 15(7), 1401-1420.
- Friend, A. D., A. K. Stevens, R. G. Knox, and M. G. R. Cannell (1997), A process-based, terrestrial biosphere model of ecosystem dynamics (Hybrid v3.0), *Ecological Modelling*, 95(2-3), 249-287.
- Froend, R. H., E. Heddle, D. Bell, and A. J. McComb (1987), Effects of salinity and waterlogging on the vegetation of Lake Toolibin, Western Australia, *Aust J Ecol*, 12(3), 281-298.
- George, R. J. (1992), Groundwater Processes, Sandplain Seeps and Interactions with Regional Aquifer Systems in South-Western Australia, *J Hydrol*, 134(1-4), 247-271.
- George, R. J., and A. J. Conacher (1993), Mechanisms responsible for streamflow generation on a small, salt-affected and deeply weathered hillslope., *Earth Surf Processes*, 18(4), 291-309.
- George, R. J., and S. Dogramaci (2000), Toolibin—A life and death struggle for the last freshwater Wheatbelt lake, in *3rd International Hydrology and Water Resources Symposium*, edited by E. Australia, pp. 733-738, Perth, Australia.
- George, R. J., S. Dogramaci, and J. Wyland (2004), Can Groundwater Pumps and Surface Water Engineering Protect Lake Toolibin? Rep., [123]-[128] pp, Engineers Australia, Barton, A.C.T.
- George, R. J., J. Clarke, and P. English (2008a), Modern and palaeogeographic trends in the salinisation of the Western Australian wheatbelt: a review, *Aust J Soil Res*, 46(8), 751-767.
- George, R. J., R. J. Speed, J. A. Simons, R. H. Smith, R. Ferdowsian, G. P. Raper, and D. Bennett (2008b), Long-term groundwater trends and their impact on the future extent of dryland salinity in Western Australia in a variable climate., paper presented at 2nd International Salinity Forum: Salinity, water and society-global issues, local action, Adelaide, Australia.

- Gifford, G. F. (1978), Rangeland hydrology in Australia - A brief review, *Australian Rangeland Journal*, 1(2), 150-166.
- Goel, V. L., and H. M. Behl (2005), Growth and productivity assessment of *Casuarina glauca* Sieb. ex Spreng on sodic soil sites, *Bioresource Technol*, 96(12), 1399-1404.
- Guswa, A. J. (2005), Soil-moisture limits on plant uptake: An upscaled relationship for water-limited ecosystems, *Adv Water Resour*, 28(6), 543-552.
- Haario, H., E. Saksman, and J. Tamminen (2001), An adaptive Metropolis algorithm, *Bernoulli Society for Mathematical Statistics and Probability*, 223-242.
- Halse, S. A. (2004), Impacts of drainage disposal on biodiversity in wetlands of the Western Australian wheatbelt, in *1st National Salinity Engineering Conference*, edited by S. W. Dogramaci, Alex p. 562 Engineers Australia, Perth, Western Australia.
- Halse, S. A., and T. Massenbauer (2005), Incorporating research results into wetland management: lessons from recovery catchments in saline landscapes, *Hydrobiologia*, 552, 33-44.
- Halse, S. A., G. B. Pearson, J. M. McRae, and R. J. Shiel (2000), Monitoring aquatic invertebrates and waterbirds at Toolibin and Walbyring Lakes in the Western Australian wheatbelt, *Journal of the Royal Society of Western Australia*, 83, 9.
- Hancock, G. R., T. J. Coulthard, C. Martinez, and J. D. Kalma (2011), An evaluation of landscape evolution models to simulate decadal and centennial scale soil erosion in grassland catchments, *J Hydrol*, 398(3-4), 171-183.
- Hatton, T. J., J. Ruprecht, and R. J. George (2003), Preclearing hydrology of the Western Australia wheatbelt: Target for the future?, *Plant Soil*, 257(2), 341-356.
- HilleRisLambers, R., M. Rietkerk, F. van den Bosch, H. H. T. Prins, and H. de Kroon (2001), VEGETATION PATTERN FORMATION IN SEMI-ARID GRAZING SYSTEMS, *Ecology*, 82(1), 50-61.
- Holland, K. L., S. D. Tyerman, L. J. Mensforth, and G. R. Walker (2006), Tree water sources over shallow, saline groundwater in the lower River Murray, south-eastern Australia: implications for groundwater recharge mechanisms, *Aust J Bot*, 54(2), 193-205.
- Humphries, M. S., A. Kindness, W. N. Ellery, J. C. Hughes, J. K. Bond, and K. B. Barnes (2011), Vegetation influences on groundwater salinity and chemical heterogeneity in a freshwater, recharge floodplain wetland, South Africa, *J Hydrol*, 411(1-2), 130-139.
- Jolly, I. D., K. McEwan, and K. Holland (2008), Groundwater - surface water interactions in arid/semi-arid wetlands and the consequences of salinity for wetland ecology., *Ecohydrology*, 1(1).
- Kasten, F., and G. Czeplak (1980), Solar and Terrestrial-Radiation Dependent on the Amount and Type of Cloud, *Sol Energy*, 24(2), 177-189.
- Lambert, T., R. Silberstein, C. Macfarlane, J. Byrne, C. Johnstone, and N. Smart (2013), Water and Carbon Balances in a Groundwater Recharge Area, Gingin, WA Rep., TERN - CSIRO.
- Landsberg, J. J., and R. H. Waring (1997), A generalised model of forest productivity using simplified concepts of radiation-use efficiency, carbon balance and partitioning, *Forest Ecol Manag*, 95(3), 209-228.
- Laurance, W. F., et al. (2011), The 10 Australian ecosystems most vulnerable to tipping points, *Biol Conserv*, 144(5), 1472-1480.
- Lohammar, T., S. Larsson, S. Linder, and S. O. Falk (1980), FAST: Simulation Models of Gaseous Exchange in Scots Pine, *Ecological Bulletins*(32), 505-523.
- Ludwig, J. A., D. J. Tongway, D. O. Freudenberger, J. C. Noble, and K. C. Hodgkinson (1997), *Landscape ecology, function and management: principles from Australia's rangelands*, CSIRO Publishing, Melbourne, Australia.
- McGrath, G. S., K. Paik, and C. Hinz (2012), Microtopography alters self-organized vegetation patterns in water-limited ecosystems, *Journal of Geophysical Research: Biogeosciences*, 117(G3), G03021.
- Mendham, D., J. Bartle, A. J. Peck, R. Bennett, G. Ogden, G. S. McGrath, A. Abadi, R. Vogwill, D. Huxtable, and P. Turnbull (2012), Management of Mallee Belts for Profitable and Sustained Production Rep., Australia.
- Merz, S. K. (2000), Lake Toolibin Numerical Groundwater Model Rep., Conservation and Land Management WA, Armadale, Australia.
- Mouat, N. C., R. J. George, K. Smettem, and R. J. Gilkes (2008), Identifying dominant catchment properties for predicting dryland salinity development in the Western Australian wheat belt, paper presented at 2nd International Salinity Forum: Salinity, water and society-global issues, local action, Adelaide, Australia.

- Muirden, P., and S. Coleman (2014), Review of Surface Water Monitoring Rep. *NRB-HR-2013_010*, Department of Parks and Wildlife, Kensington, Australia.
- Muneepeerakul, C. P., F. Miralles-Wilhelm, S. Tamea, A. Rinaldo, and I. Rodriguez-Iturbe (2008), Coupled hydrologic and vegetation dynamics in wetland ecosystems, *Water Resour Res*, 44(7).
- Myers, N., R. A. Mittermeier, C. G. Mittermeier, G. A. B. da Fonseca, and J. Kent (2000), Biodiversity hotspots for conservation priorities, *Nature*, 403(6772), 853-858.
- Myette, C. F., D. G. Johnson, and J. C. Olimpio (1987), Area of influence and zone of contribution to superfund site wells Rep., Geological Survey, Massachusetts, U.S.
- Nemani, R. R., and S. W. Running (1989), Testing a Theoretical Climate Soil Leaf-Area Hydrologic Equilibrium of Forests Using Satellite Data and Ecosystem Simulation, *Agr Forest Meteorol*, 44(3-4), 245-260.
- Petrone, K. C., J. D. Hughes, T. G. Van Niel, and R. P. Silberstein (2010), Streamflow decline in southwestern Australia, 1950-2008, *Geophys Res Lett*, 37.
- Pracilio, G., G. J. Street, P. Nallan Chakravartula, J. R. Angeloni, D. Sattel, M. Owers, and R. Lane (1998), Airborne geophysical surveys to assist planning for salinity control. 3. Lake Toolibin saltmap survey : interpretation report Rep., National Airborne Geophysics Project, World Geoscience Corporation, Perth, WA.
- Ridolfi, L., P. D'Odorico, and F. Laio (2006), Effect of vegetation-water table feedbacks on the stability and resilience of plant ecosystems, *Water Resour Res*, 42(1).
- Running, S. W., and J. C. Coughlan (1988), A General-Model of Forest Ecosystem Processes for Regional Applications .1. Hydrologic Balance, Canopy Gas-Exchange and Primary Production Processes, *Ecological Modelling*, 42(2), 125-154.
- Running, S. W., and S. T. Gower (1991), Forest-Bgc, a General-Model of Forest Ecosystem Processes for Regional Applications .2. Dynamic Carbon Allocation and Nitrogen Budgets, *Tree Physiol*, 9(1-2), 147-160.
- Ruprecht, J. K., and N. J. Schofield (1991), Effects of partial deforestation on hydrology and salinity in high salt storage landscapes. I. Extensive block clearing, *J Hydrol*, 129, 19-38.
- Rutherford, J., A. Viezzoli, E. Grunewald, R. Vogwill, T. Munday, B. Coleman, and P. Drake (2013), Integrating borehole NMR and temporal EM data -developing a new conceptual hydrogeological model to manage Toolibin Lake SW Australia, in *23rd international Geophysical Conference*, edited, Melbourne, Australia.
- Salama, R. B., D. Laslett, and P. Farrington (1993), Predictive modelling of management options for the control of dryland salinity in a first-order catchment in the wheatbelt of Western Australia, *J Hydrol*, 145(1-2), 19-40.
- Semeniuk, C. A., and V. Semeniuk (1995), A Geomorphic Approach to Global Classification for Inland Wetlands, *Vegetatio*, 118(1-2), 103-124.
- Sinclair, K. E., S. J. Marshall, and T. A. Moran (2011), A Lagrangian approach to modelling stable isotopes in precipitation over mountainous terrain, *Hydrol Process*, 25(16), 2481-2491.
- Singh, V., and D. Frevert (2002), Mathematical models of large watershed hydrology, edited, Water Resources Publications.
- Sivapalan, M., N. R. Viney, and C. Zammit (2002), LASCAM: Large Scale Catchment Model, in *Mathematical models of large watershed hydrology*, edited, Water Resources Publications, Colorado, USA.
- Skaggs, T. H., M. T. van Genuchten, P. J. Shouse, and J. A. Poss (2006), Macroscopic approaches to root water uptake as a function of water and salinity stress, *Agr Water Manage*, 86(1-2), 140-149.
- Street, G. J., G. Pracilio, and A. M. Anderson-Mayes (2002), Interpretation of geophysical data for salt hazard identification and catchment management in southwest Western Australia, *Explor Geophys*, 33(2), 65-72.
- Suganuma, H., Y. Abe, M. Taniguchi, H. Tanouchi, H. Utsugi, T. Kojima, and K. Yamada (2006), Stand biomass estimation method by canopy coverage for application to remote sensing in an area of Western Australia, *Forest Ecol Manag*, 222(1-3), 75-87.
- Taplin, R. (2010), Time scales of a wetland regime: impacts of climate and management on Lake Toolibin, WA, Dissertation thesis, 76 pp, The University of Western Australia, Perth, Australia.
- Tooth, S., and T. S. McCarthy (2007), Wetlands in drylands: geomorphological and sedimentological characteristics, with emphasis on examples from southern Africa, *Prog Phys Geog*, 31(1), 3-41.

- van der Kamp, G., and H. M. (1998), The Groundwater Recharge Function of Small Wetlands in the Semi-Arid Northern Prairies, *Great Plains Research*, 8(1), 39 - 56.
- Viney, N. R., R. Ali, and S. K. Aryal (2007), Modelling the Hydrological Impacts of Artificial Drainage in The Western Australian Wheatbelt, in *MODSIM - International Congress on Modelling and Simulation*, edited by L. Oxley and D. Kulasiri, pp. 2506 - 2512, Modelling and Simulation Society of Australia and New Zealand.
- Vogwill, R., P. Drake, B. Coleman, and S. Noorduijn (2010), Toolibin Lake 2010, combining hydrogeology, remote sensing and plant ecophysiology to explain the response to management interventions, paper presented at National Groundwater Conference - Grounwater 2010 The challenge of sustainable management, IAH Geological Society of Australia, Canberra, Australia.
- Wainwright, J., L. Turnbull, T. G. Ibrahim, I. Lexartzza-Artza, S. F. Thornton, and R. E. Brazier (2011), Linking environmental régimes, space and time: Interpretations of structural and functional connectivity, *Geomorphology*, 126(3-4), 387-404.
- Ward, A., and S. Trimble (2004), *Enviromental Hydrology*, Lewis Publ.
- Wetlands, T. R. C. o. (2013), *The Annotated Ramsar List*, edited, Gland, Switzerland.
- Zammit, C., N. R. Viney, and M. Sivapalan (2002), LASCAM: The Large Scale Catchment Model - User Manual -Version 3, edited by C.-. UWA, p. 106.
- Zdunic, K. (2010), *Lake Toolibin Vegetation and Landsat TM AnalysisRep.*, 6 pp, DEC, Perth, Australia.

Appendix A: Model Overview - LASCAM-S

Similarly to the original LASCAM [Sivapalan *et al.*, 2002], LASCAM-S is a conceptual hydrological model that disaggregates the catchment of interest into numerous sub-catchments. The smallest spatial scale the model can therefore resolve is the sub-catchment (termed SC) unit. Therefore, within the context of this model, management activities conducted at a local scale (e.g. farm-scale, drainage works or re-vegetation) are resolved within such a unit domain and their impact is “averaged” over this domain (SC). Each of those sub-catchments forms the basis of the water and salt balances. All the water storages and rates are given in millimetres (mm) and the salt content in grams (g). The time-step is one day (d). At each model time-step, infiltration, percolation, recharge, evaporation and runoff are calculated according to a hillslope idealization, which assumes each unit (SC) further subdivided into 4 water and salt storages described as:

- A. The near-stream perched aquifer;
- B. The permanent deeper groundwater system;
- D. The vadose zone;
- F. The unsaturated store below the perched aquifer.

Once the rainfall (P) enters a SC domain (Figure 89), it is partitioned into “throughfall” (pg) and canopy interception (pi) (Equation 3). In the pg equation, the rain is further split, based on the magnitude and type of vegetation cover, parameterized based on leaf area index (LAI), which is able to vary across sub-catchments and seasonally. The LAI in the model is notionally converted into a fraction of vegetated area. As such, pg is divided into the fraction retained by forest and the fraction intercepted by crops (see Equation 1 in Table 19) and those fractions are user-defined. The fraction of throughfall that failed in infiltrating the soil becomes infiltration excess (qie).

Infiltration excess (qie) (Equation 5) depends on the infiltration capacity (fs) (Equation 11), the fraction of land that is under saturated condition (ϕ_c) and the magnitude of the sub-catchment that is impervious (imp). The infiltration capacity (fs) depends on the notional parameter $fs1$ and $fs2$, which encompass the vegetation status of the area, so that densely vegetated sub-catchments are expected to have higher values. Besides, the capacity for infiltration depends on the soil water content (represented by D/D_{max}). The partitioning of $fs1$ and $fs2$ define how sensitive to soil water content the infiltration capacity is. ϕ_c is defined by the ratio of waterlogged land (based on A) and imp represents the impervious fraction, so that roads and bedrock outcrops can be accounted for.

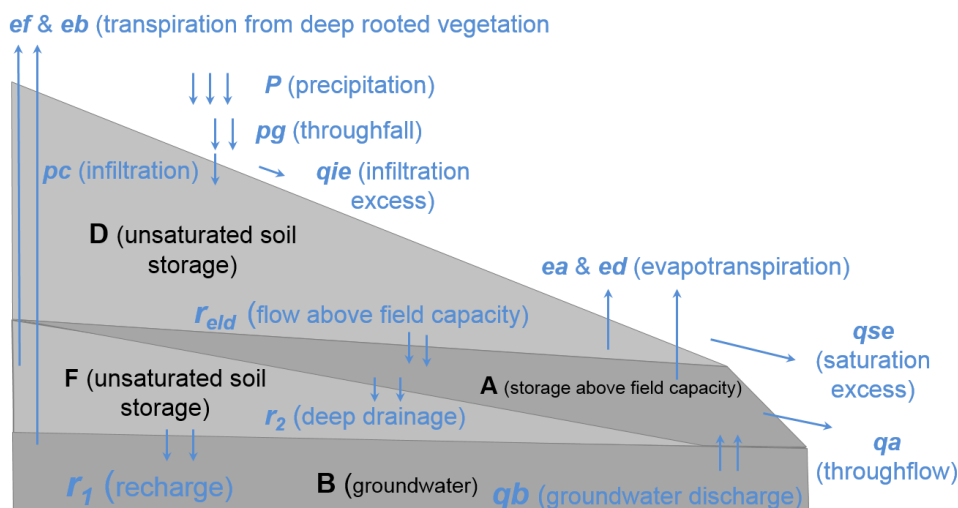


Figure 89: Conceptual water fluxes (in blue) and water storages (in black) resolved by LASCAM-S.

Surface runoff (qt) is the sum of infiltration excess (qie), saturation excess (qse) and throughflow (qa) processes. Throughflow (qa) is calculated as a function of the A storage, whose minimum value (A_{min}) represents a threshold to flow initiation and is particular of each SC.

The percolation from the unsaturated zone (D) to the perched aquifer (A) is governed by the soil moisture at field capacity, which is converted into a water depth (D_{min}). All the water present in storage D that is greater than this value (after evapotranspiration is taken place), accumulates as A storage (Equation 13). Part of the A storage that is not lost through the surface (qa) can eventually reach the deeper unsaturated soil storage (F).

This vertical flow ($r2$) depends on the lower layer infiltration rate, fss (Equation 7) but is also regulated by the sub-surface saturation area, which is calculated based on a redistribution of the A store value (A/A_{max}).

Recharge of the permanent groundwater ($r1$) (Equation 8) is generated by percolation from the F store and is calculated using both matrix ($rmat$) (Equation 9) and macropore ($rpor$) (Equation 10) recharge expressions. If the groundwater (B store) is great enough to reach a user-define threshold ($Bmin$), it is assumed that B discharges water slowly (governed by αb) to the A store. The discharge rate also depends on the volume of the lower layer total water capacity ($FBmax$), which is the sum of the maximum F and maximum B storage depth (multiplied by the deep soil porosity, θd). Once the groundwater discharge enters the A store, it is available for discharge into the stream.

Non-linear functions relate the actual evaporation rate to the potential evaporation rate based on the amount of water available in each soil storage and the (estimated) LAI. Evapotranspiration for the upper soil water stores, A and D, accounts for bare-soil and plant transpiration, whereas losses from the B and F stores are solely governed by the action of deep-rooted vegetation. Within a SC, separate vegetation cover fractions are prescribed for the riparian (which effectively can consume water from the A store) and non-riparian regions. Those fractions are user-defined and are based on the surface water.

Table 19: List of the major equations of LASCAM-S.

Description	Equation	
Throughfall (P after interception)	$pg = \max(\min(LAI_{av} * P^{1.21} + (1 - LAI_{av})\beta g * P, P), 0)$	1
Infiltration rate	$pc = \max(pg - qie - qse, 0)$	2
Canopy interception	$pi = \max(P - pg, 0)$	3
Throughflow	$qa = ka1 ((A - Amin)/(Amax - Amin))^{ka2}$	4
Infiltration excess	$qie = (pg - fs) (1 - \phi c) (1 - imp)$	5
Groundwater discharge	$qb = \max(0., (\alpha b((B - Bmin)/(FBmax - Bmin))^2))$	6
Deep drainage	$r2 = \delta b (A/Amax) fss$	7
Recharge	$r1 = rmat + rpor$	8
Matrix recharge	$rmat = Ksb (F/Fmax)^{\delta F}$	9
Macropore recharge	$rpor = \beta mcr (F/FBmax)$	10
Infiltration capacity	$fs = fs1 + fs2 * (D/Dmax)$	11
Soil moisture	$\theta = \max(\min(D/u_{cap}, 1), 0)$	12
Percolation	$reld = (D + pc - ed) - Dmin$	13
Transpiration from D	$ed = ep LAI_{grn} (D/WT_{max})^{\delta ed}$	14
Transpiration from A	$ea = \min(ep LAI_{rip}, ep - ed)$	15
Transpiration from F	$ef = \min(ep LAI_{grn}, ep - ed - ea)$	16
Transpiration from B	$eb = \min(ep LAI_{grn} (B/Bmax)^{\delta eb}, ep - ed - ea - ef)$	17
D storage	$dD/dt = pc - reld - ed + qb$	18
B storage	$dB/dt = reld - eb - qb$	19

Table 20: List of variables in LASCAM-S.

Name	Description
P	Precipitation (mm)
ea	Evapotranspiration from A (mm)
ed	Evapotranspiration from D (mm)
eb	Transpiration from deep rooted vegetation that reaches B (mm)
ef	Transpiration from deep rooted vegetation from F (mm)
et	Total evapotranspiration (mm)
r1	Groundwater recharge (mm)
r2	Drainage from A to F storage (mm)
reld	Release from water above filed capacity from the vadose zone (mm)
qb	Capillarity (mm)
u_{cap}	Soil water capacity in the vadose zone (mm)
ep	Evapotranspiration potential (mm)

The salt-balance model within LASCAM-S is implemented similarly to the water balance, such that each soil store also includes a salt store and, except for evapotranspiration, every water flux has a companion salt flux.

However, in order to capture the dynamics of the large salt mass stored in the soil profile just above the water table, a typical phenomenon in SWWA, the salt balance includes an additional *P* store [McGrath *et al.*, 2012]. This salt store is not considered dissolved, and is only mobilized through either:

1. recharge of the F store to the B store, but only when it is so large that matrix flow and the usual macropore flow is operational. Under these conditions, the matrix flow will leach the relevant amount of P store into the B store or ;
2. rising of the B store into the part of the profile occupied by the P store, which will dissolve the relevant amount of salt accumulated there.

Appendix B: Model Overview - LASCAM-R

Due to difficulties representing the flat broad valley floor catchments in traditional LASCAM, which has a hillslope conceptual model, LASCAM-R was developed as part of the integrated model system. Figure 90 shows the major water pathways resolved by LASCAM-R. Note that salt load (not shown on the Figure) follows the same pathways as water flow. LASCAM-R catchments receive inflow from rainfall, surface water from the upstream catchments and groundwater from neighbouring sub-catchments. Rainfall and surface water interact with the unsaturated zone (D store) where evapotranspiration is the main outflow term. As a result of the sub catchment scale water and solute balance, some of the surface water and rainfall inflow infiltrate into the deep groundwater and part is discharged to the down gradient sub-catchments of LASCAM-R and WET-0D. In contrast to LASCAM-S, LASCAM-R does not simulate lateral sub-surface flow in the unsaturated zone (interflow). In LASCAM-R, groundwater fluctuations result from the daily balance of inflows and outflows of the B store and from a function that simulates the groundwater forcing from the upstream catchments at the boundaries based on the previous 2 years data. The most important variables and equations that describe the water flow in LASCAM-R are described below (Table 21).

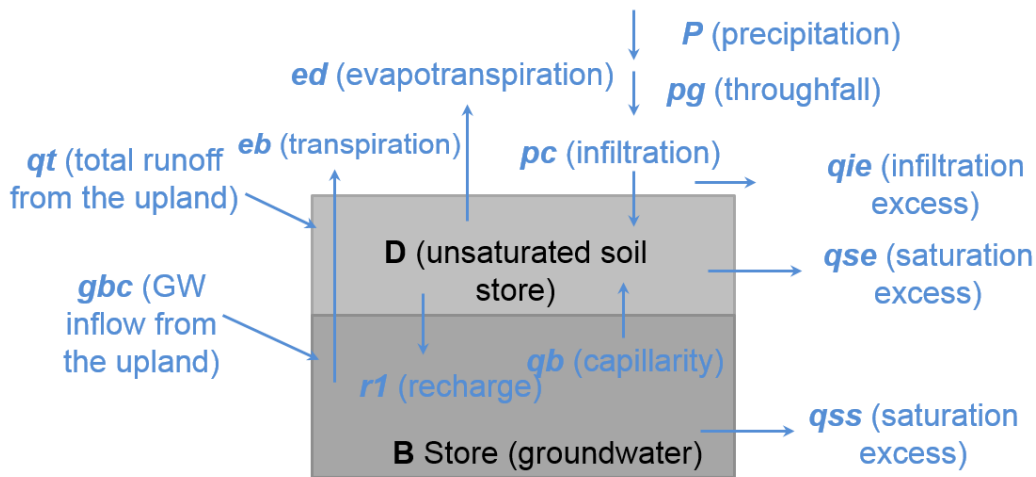


Figure 90: Conceptual diagram of LASCAM-R showing the use of two stores and relevant processes.

Table 21: List of the major equations of LASCAM-R.

Description	Equation	
Infiltration rate	$pc = ks e^{-\theta}$	20
Capillarity	$qb = alphas * B$	21
Soil moisture	$\theta = \max(\min(D/u_{cap}, 1), 0)$	22
Infiltration	$pc = ks e^{-\theta}$	23
Percolation	$reld = D + pc - ed - u_{cap}\theta_{fc}$	24
Saturation excess	$qse = qseu + qseb$	25
Saturation excess from the vadose zone	$qseu = \max(D - u_{cap}, 0)$	26
Saturation excess from the saturated zone	$qseb = \max(B - WT_{max}, 0)$	27
Transpiration from D	$ed = ep(D/WT_{max})^{\delta_{ed}}$	28
Transpiration from B	$eb = (ep - ed)^{\delta_{eb}}$	29
D storage	$dD/dt = pc - reld - ed + qb$	30
B storage	$dB/dt = reld - eb - qb$	31

Appendix C: Model Overview - LASCAM-Q

LASCAM-Q is a module of the original LASCAM [Sivapalan *et al.*, 2002], whose function is to convey surface water from consecutive sub-catchments. The ordering of each of the sub-catchments is important and determined by the nature of the stream network and flow paths, which is user-defined. Each sub-catchment is able to receive runoff at the upslope stream boundary, generate new runoff as outlined above, and then discharge the combined runoff at the sub-catchment outlet. Sub-catchment sizes and the density of the stream network need to be determined by assessing the length scale of the catchment heterogeneities, such as land-use, soil and rainfall [McGrath *et al.*, 2012].

As is often the case in the SWWA catchments, stream channels are not well defined and it is frequently observed water ponding in areas of low-lying relief or disconnections. Once some critical volume is reached in these areas, the flow will proceed downstream. To account for this behaviour, LASCAM-Q includes a "lake" function, representing a surface storage, which allows water and salt in the stream network to enter, fill, evaporate (accumulating salts) and finally overflow. A user-definable "dead" volume must be prescribed, below which no discharge can occur. Note that only a single surface storage can be included within the stream network per sub-catchment, and that the location of the storage is always assumed to be at the sub-catchment outlet.

Flow that does not reach the outlet (does not reach the dead volume) is accumulated and remains available for routing in the next time-step. Note that, where potential exists for streamflow generated far upstream to enter a dry channel downstream, re-infiltration is assumed to occur (into the A store), before any excess proceeds downstream. When salt is simulated and the stream dries, the salt is retained in a streamside salt store for dissolution in any subsequent flows. Surface storages ("lakes") are filled by incoming flows, and lose water to downstream discharges and to evaporation. The routing of flow and salt between sub-catchments within LASCAM-Q avoids the use of detailed stream cross-section information and hydraulic routing parameterisation. Instead, it accounts for the flows entering the sub-catchment channel (from the hillslope and upstream sources) and, based on an estimate of the stream velocity and evaporation rate, the amount of water that passes out of the sub-catchment is routed either to the downstream sub-catchment or into the surface storage, if that is the case of that particular sub-catchment. The equations governing the storage and release of the water in LASCAM-Q are presented in Table 22 and the major variables in Table 23 as defined by [Zammit *et al.*, 2002].

Table 22: List of the major equations of LASCAM-Q.

Description	Equation	
Stream velocity (ms^{-1})	$v = v_0 + v_1 \ln(l + q_l)$	32
Stream flow evaporation (mm^3)	$es = EP w l (q/v\Delta t)^{1/2}$	33
Lake storage evaporation (mm^3)	$el = EP l_{max} (L/L_{max})^\theta$	34
Lake discharge (mm^3)	$q_l = \begin{cases} 0, & \text{if } L \leq L_{dead} \\ l_{qmax}(L - L_{dead}/L_{max} - L_{dead})^{\theta_{q_l}}, & \text{if } L > L_{dead} \end{cases}$	35

Table 23: List of parameters required for LASCAM-Q.

Name	Description
v_0, v_1	Stream velocity parameters
EP	Evapotranspiration potential (mm)
l	Length of the river (length of the sub-catchment) (mm)
w	Width of the river (width of the sub-catchment) (mm)
L_{max}	Maximum volume of the lake (mm^3)
l_{max}	Maximum length of the lake (mm)
l_{qmax}	Maximum flow from the lake (mm^3)

Appendix D: Model Overview - WET-0D

WET-0D dynamically resolves the partitioning of hydrological environments that generate niches for several different vegetation functional groups. The wetland domain is schematically represented as a linked cell model (Figure 91). Water table level (h_s) and lake level (h_L) are used to divide the wetland into discrete hydrological cells or “environments” of uniform salinity concentration and water content. Each cell n (n =unsaturated soil, saturated soil and lake, represented by U, S and L, respectively) is treated as a well-mixed pool that exchanges water and salt with neighbouring cells. Inputs and outputs of water and salt from outside the system, including inflow, outflow, and evaporation from bare soil and plant transpiration are applied to each cell, and calculated as a function of vegetation biomass, water availability and salinity found at each time step in each cell.

Each defined vegetation group most optimally obtains water and increase biomass within areas suited to their water uptake strategies. The amount of water that each vegetation group transpires depends on the hydrological environment and the salinity of the cell in which they are situated at any given time and also on its own characteristics. The approach is therefore a quasi-spatially explicit analysis. As a result, over short timescales, the vegetation may be considered to be fixed in space and may experience changes in the nature of its hydrological environment (i.e. trees situated in terrestrial fringe may be exposed to standing water following a flood, leading to a temporary change of growth efficiency). Over longer timescales, the persistence of non-suitable conditions will lead to an inability for a certain plant type to survive and compete with other groups, and ultimately this will drive a shift in the composition of the vegetation assemblage within the discrete environment.

The model is driven by daily climate forcing represented by relative humidity, precipitation, temperature, solar radiation and wind speed. Plant functional groups respond differently to solar radiation, relative humidity, air temperature, water availability and soil salinity, which are dynamically calculated in each one of the hydrological cells. As a result, if the system reaches a steady state, each i plant ($i=1,2$ or 3) will reach a biomass at a particular cell n , given the water and salt content in n , which is strongly influenced by the climate but also by the plants themselves. This close dependency between plants and hydrology enables the model to assess long term evolution of wetland states and function.

As the length of the simulations is much longer than the time-step, a simple 1st order explicit finite difference method was used as a suitable approximation to the final solution, and the model was implemented in MATLAB (Mathworks Inc.) at a daily time step.

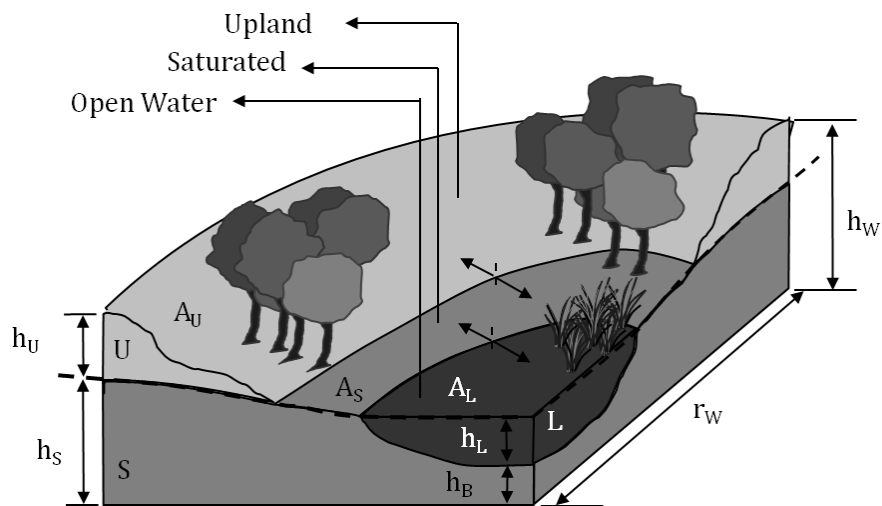


Figure 91: The three storage cells or environments with distinct hydrological function (U, S and L) and their correspondent surface areas (A_U , A_S and A_L).

Water budget

The climate forcing that drives the water balance is precipitation and potential evapotranspiration, E_0 . Effective precipitation, P , is distributed over the simulated area and is subject to interception losses, such that $P = P_t - I_{max} (LAI_n/LAI_{nmax})$, where P_t is the above-canopy precipitation rate, I_{max} is the maximum precipitation interception, LAI_n is the Leaf Area Index of the n^{th} wetland sub-environment and LAI_{nmax} is the maximum LAI expected within any environment. The potential evapotranspiration, E_0 , is calculated from the relative humidity,

solar radiation, wind speed and air temperature, according to the Penman-Monteith equation. As an approximation for solar radiation, clear-sky solar radiation as described by *Ward and Trimble* [2004] is used and reduced according to the observed cloud cover fraction [*Kasten and Czeplak*, 1980].

The major hydrological fluxes that redistribute water within the wetland domain dynamically change the volume of the three conceptual water storages (cells), namely the open water/lake (L) and the unsaturated (U) and saturated (S) soil storages (Figure 92). Based on the morphology, the surface area of each hydrological environment (cell), changes accordingly. Water fluxes in the model are defined as length of water per time ($m\ d^{-1}$) and multiplied by the relevant areas to be converted into flow ($m^3\ d^{-1}$). The volume of water entering the surface and the groundwater of the wetland at every time-step is converted into flooded and saturated area following the DEM (Figure 16 a) of the terrain. Those areas are read back into the model to define the hydrological environments in an iterative process.

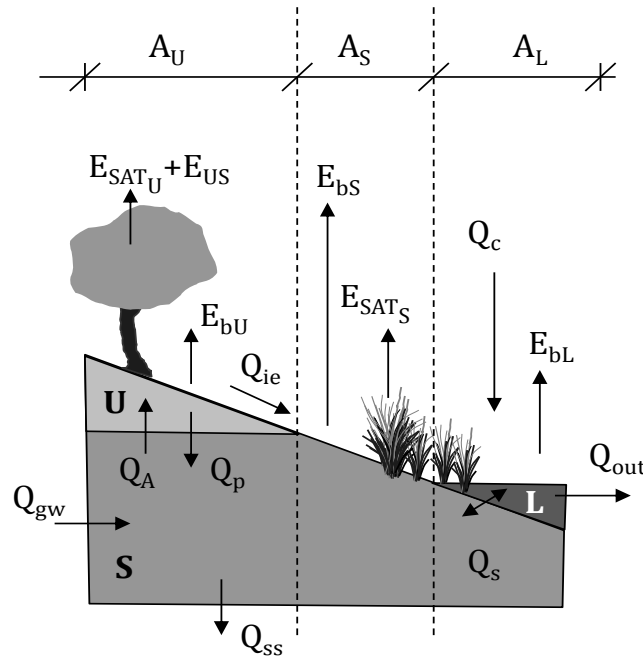


Figure 92: Water fluxes through the three storage cells and their relative areas.

If the water table level, h_s , is higher than the lake level h_L , the terrestrial area is further divided into an unsaturated (A_U) and a saturated portion (A_S), with the latter being conceptualized as the wetland seepage face. When the water table is at its maximum level, $h_s = h_{smax} = h_w$. The water table slope is assumed as equal to zero. As such, A_S and h_s are defined by the DEM and the volume of water contained in the cell S, S_{sat} , which needs to be multiplied by the soil porosity, ϕ , to represent the volume occupied by the cell S and h_s . The total area of the wetland, A_w , is constant and equals to the sum of all surface areas, so that $A_w = A_S + A_U + A_L$.

As a result, lake and water table levels define the partitioning of the n^{th} environment within the wetland: the open water/lake zone and the saturated and unsaturated soils (denoted by L, S, and U subscripts throughout the text, respectively). The volumes of the L, S and U pools, and consequently A_L , A_S and A_U , vary as a function of time in response to changes in the wetland water balance and are updated daily. The time-varying balance and redistribution of water into the wetland stores are described next.

Standing Water Storage

The variation of lake volume, dL_V/dt ($m^3\ d^{-1}$), is calculated as:

$$\frac{dL_V}{dt} = P_L + Q_c + Q_w - Q_s - E_{bL} - Q_{out} \quad 36$$

where P_L ($m^3\ d^{-1}$) is the volume of precipitation that enters the lake, calculated as $P_L = P A_L$ ($m^3\ d^{-1}$), and similarly for evaporative loss, $E_{bL} = c E_0 A_L$ ($m^3\ d^{-1}$), where c is the pan-to-lake evaporation correction factor. Q_c is the inflow ($m^3\ d^{-1}$) from the catchment area outside the wetland domain, and can be prescribed based on field data or the output from a hydrological model. Q_s is the seepage that flows through the area of lake base, and the free saturated area, A_S . Q_s is defined as being proportional to the hydraulic gradient between the water

level in the lake, $h_L + h_B$, and the surrounding water table, h_S , based on an assumed hydraulic conductivity k_S . The horizontal length scale used for the seepage calculation is assumed to be half of the wetland radius, r_W . Seepage volume is positive when flowing from the lake to the groundwater according to:

$$Q_S = 2k_S(h_L + h_B - h_S) \frac{(A_{SL} + A_S)}{r_W} \quad 37$$

where the area of the lake base, A_{SL} , is defined as the surface of a paraboloid:

$$A_{SL} = \frac{\pi r_L}{6h_L} + (r_L^2 + 4h_L^2)^{\frac{3}{2}} - r_L^2 \quad 38$$

r_L is the average distance between the wetland rim and its centre (m).

Q_{out} is the flux of water exiting the wetland system, defined as the amount of water that exceeds the maximum lake capacity, L_{max} , at any timestep according to:

$$Q_{out} = Q_{in} - (L_{max} - (L_v - E_L)) \quad 39$$

Flow to the area of standing water from the surrounding terrestrial component within the wetland domain, Q_w , is generated through infiltration (Q_{ie}) and saturation excess (Q_{se}) mechanisms:

$$Q_w = Q_{se} + Q_{ie} \quad 40$$

Saturation excess, Q_{se} , only happens when the infiltration, I ($m^3 d^{-1}$), exceeds the soil capacity, U_c , such that $Q_{se} = I - U_c$. Infiltration (defined below) occurs only in the unsaturated area of soil, and therefore all precipitation reaching A_S is converted to runoff. Q_{ie} ($m^3 d^{-1}$) is the amount of effective precipitation that is greater than the capacity of the soil to infiltrate, I , and is defined as:

$$Q_{ie} = (P A_U - I) + P A_S \quad 41$$

Soil Water Storage

The maximum soil storage, S_{max} , is the difference between the maximum volume of the wetland, W_{max} , and the maximum lake volume, L_{max} , multiplied by soil porosity, ϕ . S_t is the total effective volume present in the soil. It depends on the infiltration, I , the seepage from/to the lake, Q_S , the volume lost as baseflow, Q_{SS} , the groundwater inflow from the catchment, Q_{gw} , and the total evapotranspiration from the ground, E_{soil} :

$$\frac{dS_t}{dt} = I \pm Q_S - Q_{SS} + Q_{gw} - E_{soil} \quad 42$$

In the above equation, E_{soil} is the sum of transpiration (E) and bare-soil evaporation (E_b) from both unsaturated and saturated environments, such that $E_{soil} = E_{bu} + E_{bs}$

+ $E_u + E_s$ (terms defined further below). The groundwater inflow from the catchment, Q_{gw} , depends on the hydraulic conductivity perpendicular to the flow direction, k_h ($m d^{-1}$) as it can be described by Darcy's Law [Crites et al., 2010; van der Kamp and M., 1998]. The pressure head gradient is the difference between the regional groundwater level (h_{BC}) and the local (wetland) water table level (h_S). If assuming a circumferential domain:

$$Q_{gw} = k_h(h_{BC} - h_S) \frac{(2\pi r_w h_w)}{r_w} \quad 43$$

As such, according to the hydrogeomorphic classification introduced by Semeniuk and Semeniuk [1995], "dampland" wetlands are characterized by a groundwater level at the boundary condition (regional) that is higher than in its domain. A "trough" wetland has its boundary conditions forcing the groundwater flow across its domain. Schematically, a "trough" wetland has part of its domain (defined by A_f , with $A_f < 1$) with lower water table level than the regional groundwater level and part of its domain ($1 - A_f$) with higher water table level than the local groundwater level. In that case, Q_{gw} is defined as:

$$Q_{gw} = k_h \left[(h_{BCU} - h_S) \frac{A_f(2\pi r_w h_w)}{r_w} - (h_{BCD} - h_S) \frac{(1-A_f)(2\pi r_w h_w)}{r_w} \right] \quad 44$$

In the above equation, h_{BCU} represents the upstream regional groundwater level and h_{BCD} the downstream level. Assuming those simplifications, the model is suitable to simulate a great range of landforms/hydrogeomorphic

contexts. Finally, the volume lost as baseflow, Q_{ss} , depends is linearly related to h_s by an arbitrary parameter, α_G , and is defined as:

$$Q_{ss} = (\alpha_G h_s) A_W \quad 45$$

The maximum net capacity of water storage in the unsaturated zone, U_c , is the difference $S_{max} - S_{sat}$, where S_{sat} is the volume of water (m^3) that is stored in the saturated pool below the water table level, h_s , such that $S_{sat} = S \phi$. When the soil is totally saturated, $S_t = S_{sat} = S_{max}$ and $S_{us} = U_c = 0$, where S_{us} is the effective volume of water (m^3) present in the U zone. Under such a condition, the infiltration rate, I , is equal to zero. For all other times, the total water store is a combination of the saturated and unsaturated region, such that:

$$S_t = S_{sat} + S_{us} \quad 46$$

The water balance of sub-region U and S is respectively defined as:

$$\frac{dS_{us}}{dt} = I - E_U - E_{bU} + Q_A - Q_p, \quad 47$$

and

$$\frac{dS_{sat}}{dt} = Q_p + Q_{gw} - Q_s - E_s - E_{bs} - Q_A \pm Q_{ss}, \quad 48$$

Q_A ($m^3 d^{-1}$) represents the volume transferred from S to U via capillarity. It is inversely related to the soil moisture via a constant based on the soil type, k_A .

The infiltration rate depends on the unsaturated zone soil moisture content prior to rainfall [Choudhury and Blanchard, 1983; Dall'O' et al., 2001], θ (-), defined as S_{us}/U_c . Soil type affects the infiltration rate through the saturated hydraulic conductivity, k_s ($m d^{-1}$), and the dimensionless recession coefficient for infiltration, k_i . Besides, the density of vegetation biomass in A_U , D_U ($kg m^{-2}$), creates a positive feedback loop with infiltration, as roots facilitate the water flow into the soil. On the contrary, salinity (or more specifically the salt crust on top of the soil, A_{Uc} , defined later) acts to halt infiltration:

$$I = \min \left(-k_s (\theta - 1)^{k_i} A_U \left(\frac{D_U + I_{bare}}{D_{max}} \right) \left(\frac{I_{fr}}{A_{Uc} + I_{fr}} \right), P A_U, U_c \right) \quad 49$$

In the above equation, I_{bare} and I_{fr} (given in grams of salt, for consistency) are notional parameters adjusted to limit the effect that biomass and salinity have on infiltration.

The evaporation from bare soil, E_b ($m^3 d^{-1}$), is calculated based on the potential evaporation, E_0 . If the soil is not saturated, the ratio of θ to water content at field capacity, θ_{fc} , is also considered as a scaling factor [Aydin et al., 2005]. Further, evaporation from bare soil is adjusted based on total LAI (sum of all vegetation types) to reflect the cover that vegetation causes due to shading of the exposed soil surface. Therefore, the evaporative rate applied over the relevant areas, A_s and A_u , respectively, are:

$$E_{bs} = E_0 \left(1 - 0.9 \frac{LAI_s}{LAI_{max}} \right) A_s \quad 50$$

and

$$E_{bU} = E_0 \left(1 - 0.9 \frac{LAI_U}{LAI_{max}} \right) \left(\frac{\theta}{\theta_{fc}} \right) A_U \quad 51$$

Transpiration, E , is modelled as a function of the plant water uptake rate, W ($m d^{-1}$), integrated over the relevant environment, n , such that:

$$E_n = W_n A_n \quad 52$$

where W is a function of the normalized potential water uptake, Ψ (-) and potential evapotranspiration [Skaggs et al., 2006]. Ψ depends on the plant functional type, i , and their associated water uptake strategy, and normalized depending on the wetland zone maximum LAI_{nmax} , ($n = L, U, S$), and associated soil moisture conditions experienced by the roots at a given time. As a result, the total water uptake rate is the sum of all vegetation groups, i , coexisting in a particular environment, n , such that:

$$W_{i,n} = \sum_i \Psi_{i,n} E_0 \frac{LAI_{i,n}}{LAI_{max,n}} \quad 53$$

For mass balance purposes, all the water that is obtained by plants from below the water table level is added to E_s , independently if the plants are standing over the saturated or unsaturated area. Note that the ability of vegetation to regulate their water storage is not taken into account, meaning that there is no change in water use efficiency of the vegetation. Thus, vegetation water usage is linearly proportional to LAI_n (m^2 leaf m^{-2} land). Further, the vertical root profile is assumed as constant in time and aside from competition for water and light, no other specific competition factors are considered.

Percolation of water from the vadose to the saturated zone, Q_p ($m^3 d^{-1}$), takes place when the volume of water in the unsaturated zone at the end of time-step surpasses the volume that can be held at field capacity, $U_c \theta fc$. Since the water table is shallow the distance the water needs to percolate is short, so we assumed the soil can reach field capacity within one day. The percolation is calculated following losses from evapotranspiration and surface runoff are computed, such that:

$$S_{US}^* = S_{US}^{t-1} + I - E_{US} - E_{bU} \quad 54$$

and

$$Q_p = \begin{cases} S_{US}^* - U_c \theta fc & \text{if } S_{US}^* > U_c \theta fc \\ 0 & \text{if } S_{US}^* \leq U_c \theta fc \end{cases} \quad 55$$

Note that from a computational point of view, the infiltration rate is calculated based on the soil moisture from the previous day, which means that at the first day the water table level reaches ground level, infiltration can be different from zero. In this case, the exceeding volume is diverted to the lake by adding to Q_{se} .

A common feature of clay rich soils is the formation of fissures after a drought period. At the end of a dry period, this fissured clay creates macropores that significantly raises the velocity of water and infiltration rate in the vadose zone. The model accounts for this phenomenon by simply increasing the hydraulic conductivity, ks . Schematically, ks is multiplied by a constant, ks_M , when the area of the unsaturated zone, A_U , is above a defined threshold, k_{AU} . k_{AU} is a fraction of the total wetland domain, A_w , and represents a proxy for dry conditions.

Biomass Budget

The total carbon amount accumulated as vegetation biomass, B ($kg C$), is governed by the rate of carbon uptake via photosynthesis, Π_A ($kg C d^{-1} m^{-2}$), and losses due to litterfall, (L_i), root death (R_d) and respiration (R), with all the loss terms given in $kg C d^{-1} m^{-2}$. Although the biomass of any particular plant type i , B_i , changes in time, it is spatially stationary and equally distributed within any distinct hydrological environment, n . As the spatial extent of each area with distinct hydrological function (U , S and L) changes, the amount of any vegetation type present in each environment changes accordingly. Therefore, the balance equation for any vegetation type is defined as:

$$\frac{dB_{i,n}}{dt} = \begin{cases} (\Pi_{A_{i,n}} - L_{i,n} - R_{i,n} - R_{d,i,n}) A_n + D_{i,n-1} \frac{dA_n}{dt} & \text{if } \frac{dA_n}{dt} > 0 \\ (\Pi_{A_{i,n}} - L_{i,n} - R_{i,n} - R_{d,i,n}) A_n + D_{i,n} \frac{dA_n}{dt} & \text{if } \frac{dA_n}{dt} \leq 0 \end{cases} \quad 56$$

where A_n is the area of the n^{th} wetland zone (m^2), and D is the carbon density per unit area ($= B/A$). Vegetation biomass is constrained by D_{max} , the maximum carrying capacity that the system can hold given a soil water-holding capacity and climate, when in hydrological equilibrium [Nemani and Running, 1989]. Mass conservation is assured if a portion of biomass previously belonging to another area, B_{n-1} , is incorporated into A_n when $dA_n/dt > 0$ (i.e., A_n expanding) such that:

$$D_{i,n-1} = \frac{B_{i,n-1}}{A_{i,n-1}} \quad 57$$

Conversely, when A_n is shrinking ($dA_n/dt < 0$), the following mass is removed:

$$D_{i,n} = \frac{B_{i,n}}{A_{i,n}} \quad 58$$

Here it is assumed that B_i is linearly related to LAI_i , as indicated by *Suganuma et al.* [2006] in their study of Western Australian vegetation. Parameters for conversion of LAI into biomass for trees (X_1) and grasses and aquatic vegetation (X_2) are available in the studies of *Suganuma et al.* [2006] and *Friedl et al.* [1994], respectively.

Litterfall (L_i) and root turnover (R_d) are linearly related to biomass according X_{Li} and X_{Rd} , respectively [Friend et al., 1997]. Plant respiration is configured as a function of temperature, such that:

$$R = k_R e^{\mu T} (K_R B_r + K_L B_l) B, \quad 59$$

where k_R ($m^2 d^{-1}$) adjusts the respiration to the hydrological environment such that it is lowest when vegetation is exposed to its preferred hydrological conditions. K_R , K_L and μT are scaling factors, whose values are given by *Running and Coughlan* [1988]. B_{ri} and B_{li} are the fraction of the biomass that is allocated to roots and leaf respectively [Running and Gower, 1991]. Respiration from plant stems is neglected.

The gross assimilation of carbon, Π_A ($kg\ C\ m^{-2}\ d^{-1}$), is a function of the uptake efficiency η_{Π} ($kg\ C\ kg\ CO_2^{-1}$), the potential uptake rate, Π_0 ($m\ d^{-1}$), ΔCO_2 , the carbon dioxide air – leaf diffusion gradient ($kg\ CO_2\ m^{-3}$) [Lohammar et al., 1980] and LAI:

$$\Pi_A = \eta_{\Pi} \Pi_0 \Delta CO_2 LAI \quad 60$$

The potential photosynthesis rate is a function of the canopy and mesophyll conductance, CC and CM ($m\ s^{-1}$) respectively, integrated over the day length, dl ($s\ d^{-1}$) [Running and Coughlan, 1988]:

$$\Pi_{0i} = \frac{CC\ CM}{CC + CM} dl \quad 61$$

CM is based on a maximum mesophyll conductance ($m\ s^{-1}$) [Running and Coughlan, 1988], modified by normalizations that account for temperature and solar radiation dependencies, summarized as:

$$CM = CM_{max} CM_{\Phi} CM_t \quad 62$$

where:

$$CM_{\Phi} = \frac{\Phi_c - \Phi_0}{\Phi_c + \Phi_{0.5}} \quad 63$$

and

$$CM_t = \frac{T_{max} - T}{T - T_{min}} \quad 64$$

Φ_0 and $\Phi_{0.5}$ are the photosynthesis light compensation point and the radiation level that causes CM_{Φ} to be equal to 50% of its maximum. T_{min} and T_{max} are the minimum and maximum temperature for photosynthesis and T is the air temperature and Φ_c is the solar radiation at the understory or overstorey canopy level (denoted by sub-index u or o , respectively).

The canopy intercepts the incident radiation in a non-linear proportion to its LAI as given by the radiation extinction coefficient, φ , which is set for each vegetation level, u or o . Overstorey vegetation is comprised of trees and understory vegetation comprises grasses and aquatic plants. The absorbed photosynthetic radiation by the overstorey vegetation is [Feikema et al., 2010]:

$$\Phi_{Co} = \Phi_p (1 - e^{(\varphi_o LAI_o)}) \quad 65$$

where Φ_p is the photosynthetically active radiation, assumed to be 50% of the incoming solar radiation [Landsberg and Waring, 1997]. The solar radiation at the understory level is that which is left after interception by the overstorey vegetation. Therefore:

$$\Phi_{Cu} = (\Phi_p - \Phi_{Co}) (1 - e^{(\varphi_u LAI_u)}) \quad 66$$

Similar to CM , CC is based on a maximum conductance CC_{max} , modified by the normalized potential water uptake, Ψ such that:

$$CC = \Psi CC_{max} \quad 67$$

where Ψ is a function of the normalized water availability for plant uptake, α and the root length in contact with the water table, β [Skaggs et al., 2006]. Water availability for plant uptake depends on the soil water content and the water table depth, and follows the principles introduced by *Ridolfi et al.* [2006] and *Muneepeerakul et al.* [2008], whereby different plant functional groups can uptake water from either above the vadose zone,

below the water table level, or from both. Any compensation in root water uptake by enhanced water uptake from more moist regions of the soil profile is neglected. Thus:

$$\Psi = c_o \alpha_U (1 - \beta) + c_a \alpha_S \beta \quad 68$$

Water availability under saturated conditions, α_S , is always equal to 1 since there is no water limitation. Conversely, in the vadose zone, water availability for plant uptake, α_U , depends on soil moisture (θ) and also on plant characteristics such as the soil moisture at wilting point (θ_w) and optimal soil moisture for plant uptake (θ_0):

$$\alpha_U = \begin{cases} \left(\frac{\theta - \theta_w}{\theta_0 - \theta_w} \right) + 1, & \text{if } \theta < \theta_0 \\ 1, & \text{if } \theta_0 \leq \theta < 1 \\ 0, & \text{if } \theta = 1 \text{ \& \text{ if } } \theta < \theta_w \end{cases} \quad 69$$

This approach follows that of [Feddes *et al.*, 1976], using soil moisture instead of pressure head as thresholds, with example values for θ_0 and θ_w available from Guswa [2005], who studied plant transpiration under water-limited environments.

Whether plants effectively take water from below or above the phreatic surface (or from both regions) depends on the uptake strategy of the relevant functional group. For each it is conceptually defined by the parameters c_o and c_a , which represent the plant compatibility to take water from saturated or unsaturated conditions, respectively (Table 24). As a result, each plant group can only obtain water from the wetland environment that matches its hydrological requirements. The model is able to simulate as many plant types as required. By default, three plants, whose type is defined by parameters, are set-up. An example of three vegetation types and their compatibility parameters are described below:

Aquatic vegetation: plants require standing water conditions.

Facultative vegetation: plants can take water from the unsaturated and saturated zones.

Mesophyte vegetation: the water uptake occurs just in the unsaturated portion of soil.

Table 24: Example of values for the water uptake strategy compatibility parameter.

Vegetation type	Plant requirement	Compatibility parameter		
		U	S	L
Aquatic	standing water	$c_o=0; c_a=0.$	$c_o=0; c_a=0.$	$c_o=0; c_a=1.$
Facultative	saturated or unsaturated soil	$c_o=1; c_a=1.$	$c_o=0; c_a=1.$	$c_o=0; c_a=0.$
Mesophyte	unsaturated soil	$c_o=1; c_a=0.$	$c_o=0; c_a=0.$	$c_o=0; c_a=0.$

Salinity Budget

In the salinity module, salt concentration at the soil surface, within the vadose zone and below water table as part of the saturated zone is evaluated based on a simple mass balance. Schematically, the model adopts a similar approach as described by Singh and Frevert [2002], whereby precipitation introduces a small amount of salt, and a salt pool overlays the soil surface (salt "crust"). This pool responds to dilution by precipitation and concentration through bare-soil evaporation. The non-evaporated surface water is subject to runoff and infiltration with proportional transfers of salt mass and a limited fraction of this pool is considered to remain adsorbed by the soil. Changes in water table level redistribute salt content between the saturated and the unsaturated zones.

Salt in the Soil Surface

The major salt pathways are depicted in Figure 93. Salt mass (g) is deposited in the top soil, which can create salt stains (crusts) at the surface. This salt crust, A_c , is primarily left behind by evaporation and carried away by runoff and infiltration. The salt balance in the top soil of the unsaturated and saturated area is given respectively by:

$$\frac{dA_{Uc}}{dt} = P_{Uc} + E_{bUc} - I_c - Q_{wUc} - T_{ULc} \mp T_{USc} \quad 70$$

$$\frac{dA_{Sc}}{dt} = P_{Sc} + E_{bSc} - Q_{wSc} - T_{SLc} \mp T_{USc} \quad 71$$

The precipitation, P (m), is multiplied by a constant salt concentration (in g m^{-3}) and by the respective areas (A_s and A_u) to generate the salt load to the saturated and to the unsaturated areas, P_{Sc} and P_{Uc} (g d^{-1}), respectively. I_c represents the salt load that enters the vadose zone driven by infiltration, I . No decrease in infiltration rate is

associated with the increase in the top soil salt deposit. $E_{bn\zeta}$ represents the salt load ($g\ d^{-1}$) that is left behind by bare soil evaporation, which is proportional to the evaporation from the bare soil, E_{bn} , and the salt concentration in the soil pore water, denoted as ζ_{cn} ($g\ m^{-3}$):

$$E_{bn\zeta} = E_{bn} \zeta_{cn} \quad 72$$

The salt load that reaches the lake through runoff, $Q_{wn\zeta}$, is proportional to the surface runoff, Q_w (m^3d^{-1}), which comprises infiltration and saturation excess (Q_{ie} and Q_{se} , respectively). The concentration at which the runoff carries the top soil salt is assumed as being the same as the salt density ($1065\ gm^{-3}$). Similarly, the infiltration that occurs to the vadose zone also carries a salt load that is proportional to the infiltration flow, I (m^3d^{-1}), and has the concentration of the salt bulk density.

$T_{US\zeta}$ ($g\ d^{-1}$) is the top soil salt redistribution that occurs between the saturated and unsaturated areas when the water table fluctuates. If the water table decreases, part of the top soil salt (crust) that belonged to the saturated zone, A_s , is passed on to the unsaturated area, A_U . The opposite occurs when the water table rises. Thus:

$$T_{US\zeta} = \begin{cases} A_{U\zeta} \frac{(A_U^t - A_U^{t-1})}{A_S^{t-1}} & \text{if } A_U^t > A_U^{t-1} \\ A_{S\zeta} \frac{(A_S^t - A_S^{t-1})}{A_U^{t-1}} & \text{if } A_S^t > A_S^{t-1} \end{cases} \quad 73$$

$T_{UL\zeta}$ and $T_{SL\zeta}$ ($g\ d^{-1}$), is the fraction of the top soil salt deposit that is transferred to the lake when its level rises. By definition, the top soil salt that is transferred to the lake is added to the lake water and becomes soluble, eventually passing on to the groundwater via seepage. When the lake recedes, no salt is left on the top soil/sediments. Therefore:

$$T_{SL\zeta} = \begin{cases} 0 & \text{if } A_L^t < A_L^{t-1} \\ A_{S\zeta} \frac{|A_S^t - A_S^{t-1}|}{A_S^{t-1}} & \text{if } A_L^t > A_L^{t-1} \end{cases} \quad 74$$

$$T_{UL\zeta} = \begin{cases} 0 & \text{if } A_L^t - A_L^{t-1} < A_S^{t-1} \\ A_{U\zeta} \frac{|A_U^t - A_U^{t-1}|}{A_U^{t-1}} & \text{if } A_L^t - A_L^{t-1} > A_S^{t-1} \end{cases} \quad 75$$

Salt in the Vadose Zone

The salinity in the vadose zone is affected by the salt from the top soil that is carried with the infiltration, I_ζ ; the salt that percolates into the saturated zone, $Q_{p\zeta}$; the amount assimilated by the vegetation, whose roots are sitting in the unsaturated portion of the soil, $E_{\zeta iU}$, ($i=V1$ or $V2$); the salt that conceptually moved from the vadose zone through evaporation and is left in the top soil, $E_{b\zeta U}$; the salt that is exchanged with the saturated zone when the water table moves, $T_{wt\zeta}$, and the salt that is brought up from the groundwater via capillarity rise, $Q_{A\zeta}$, such that:

$$\frac{dU_\zeta}{dt} = I_\zeta - E_{b\zeta U} - E_{\zeta 1U} - E_{\zeta 2U} - Q_{p\zeta} \mp T_{wt\zeta} + Q_{A\zeta} \quad 76$$

$Q_{A\zeta}$ is linearly related to Q_A , the capillarity rise. $k_{A\zeta}$ represents the salt concentration at ascension, which can be lower than the salt concentration found in the groundwater, given stratification. The salt amount assimilated by the vegetation, E_ζ ($g\ d^{-1}$), depends on the plant transpiration, $E_{i,n}$, and the salt concentration that any vegetation type i can tolerate at a certain environment n , $\zeta_{up\ i,n}$.

Conceptually, the model simulates two ways which vegetation deals with salinity, termed case 1 and case 2. In case 1, the vegetation has the ability to tolerate salt by "filtering" the water, the assimilation concentration, ζ_{up} , remains constant and depends only on the vegetation type and environment. Nevertheless, the actual transpiration is constrained by the salinity level by a normalized function, which reaches zero if a maximum concentration, at which water is no longer available for plant uptake, $\zeta_{max\ i,n}$, is reached.

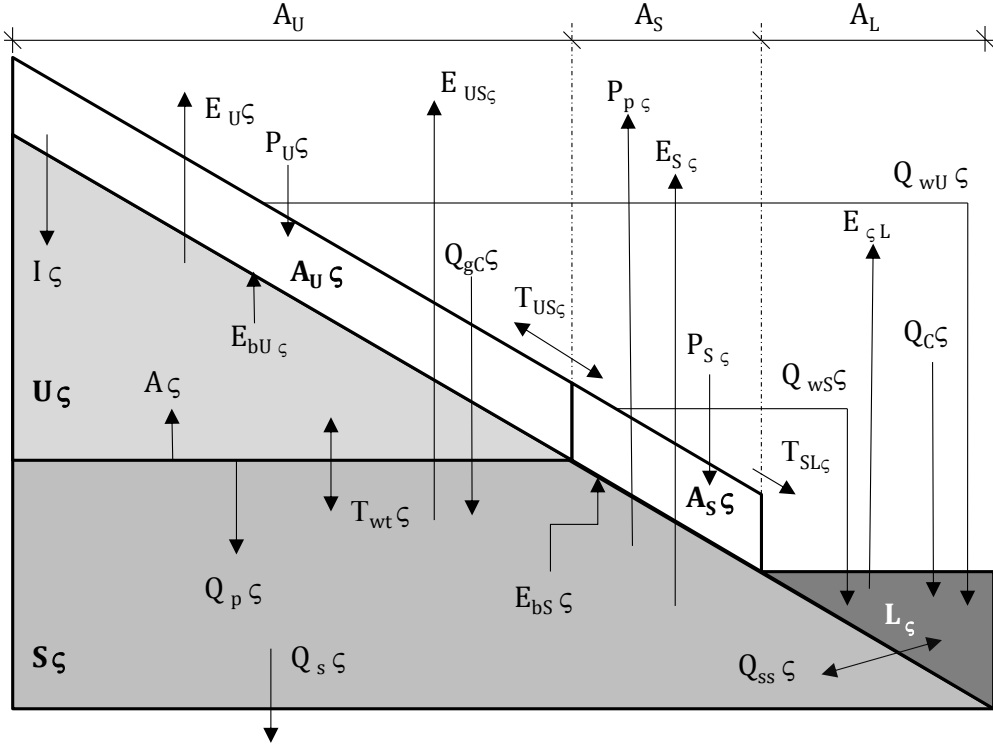


Figure 93: The main salt pathways within the wetland domain.

In case 2, the vegetation has no ability for excluding salts from the water, the salt assimilation is equals to the concentration found at the moment ($c_{c,n}$) and the water uptake stops when the concentration in the pore water reaches the maximum tolerated by the plant, c_{up} . In this case, the normalized function is directly proportional to the salt concentration at the soil, reaching zero at the maximum tolerated concentration. In general terms, the salt assimilated by plants is described as:

$$E_{\zeta i,n} = \begin{cases} c_{sup i,n} E_{i,n} & \text{case 1} \\ c_{c,n} E_{i,n} & \text{case 2} \end{cases} \quad 77$$

The normalized function that represents the vegetation stress caused by salinity (Γ) and define the concentration at which water is no longer available for plants is described as:

$$\Gamma_{n,i} = \begin{cases} -\left(\frac{n c_{\zeta}}{c_{max i,n}}\right)^{k\Gamma} + 1 & \text{case 1} \\ -\left(\frac{n c_{\zeta}}{c_{sup i,n}}\right)^{k\Gamma} + 1 & \text{case 2} \end{cases} \quad 78$$

Salt tolerance in plants is generally expressed as the osmotic potential, Ψ_{π} (MPa). The osmotic potential is a fraction of the total soil potential, Ψ_{soil} (MPa), which represents a combination (by addition) of the osmotic and matric, Ψ_{θ} (MPa), potentials. The matric potential is soil type specific and related to the soil moisture at any time. In practice, the combined effect of salinity and water restrictions represents a pressure that the plants need to overcome to obtain the water. Above certain soil potential, water uptake by vegetation stops as the plant can no longer overcome the pressure.

Following the approach presented by [Skaggs *et al.* [2006]], we normalized the individual effect of water and salinity restrictions and schematically represented their combined effect acting over vegetation in a multiplicative way. As such, we normalized Ψ_{θ} (MPa) and interpreted it as the water availability for plant uptake given soil moisture, α (dimensionless). In the same way, Γ (dimensionless), represents the normalized water availability for plant uptake given salinity. If, for instance, the soil moisture is below wilting point, even though salinity is not present, ($\Gamma=1$), vegetation stops carbon assimilation. To incorporate the restrictions imposed by the water salt concentration, Γ , the dimensionless normalized potential water uptake, Ψ , regulates carbon uptake by plants according to:

$$\Psi_{i,n} = c_{i,n} \alpha_{i,n} \beta_{i,n} \Gamma_{i,n} \quad 79$$

where c is the compatibility parameters between the plant and environment to which it is subjected at any time t ; β is root density in contact with the saturated zone ($\beta_u=1-\beta_s$) and α is the plant water uptake restrictions given soil moisture. Therefore, the combined effect of salinity and water deficit also alters the actual plant transpiration, $E_{i,n}$ (m^3d^{-1}):

$$E_{i,n} = E_0 \alpha_{i,n} \Gamma_{i,n} \beta_{i,n} \left(\frac{LAI_{i,n}}{LAI_{max,i,n}} \right) A_n \quad 80$$

In the above equation, LAI is the leaf area index (m^2m^{-2}); LAI_{max} is the maximum LAI expected from a certain vegetation type i at a certain environment n and A is the area of the n environment to be considered.

The salt load that is lost via percolation, $Q_{p\zeta}$ ($g d^{-1}$), depends on a normalized linear function for salt leaching efficiency, ζ_{le} (dimensionless). ζ_{le} enforces that only after the salt concentration in the unsaturated zone reaches a threshold ($\zeta_{cu,max}$), $Q_{p\zeta}$ is directly proportional to the concentration of salt in the pore water of the vadose zone, ζ_{cu} ($g m^{-3}$), and to the percolation rate, Q_p ($m^3 d^{-1}$). Thus, the salt leaching efficiency and the percolated salt load are defined respectively as following:

$$\zeta_{le} = \begin{cases} \frac{\zeta_{cu}}{\zeta_{cu,max}} & \text{if } \zeta_{cu} \leq \zeta_{cu,max} \\ 1 & \text{if } \zeta_{cu} = \zeta_{cu,max} \end{cases} \quad 81$$

$$Q_{p\zeta} = Q_p \zeta_{cu} \zeta_{le} \quad 82$$

The salt concentration is defined as the total salt amount (g) present in the total water volume of a cell n (m^3). As such, the salt concentration in the unsaturated zone is:

$$uc\zeta = \frac{U_\zeta}{S_{us}} \quad 83$$

Salt in the Groundwater

The salt pool in the S cell, S_ζ (g), is given by:

$$\frac{dS_\zeta}{dt} = Q_{p\zeta} + Q_{ss\zeta} - E_{b\zeta S} - E_{\zeta i S} \mp T_{wt\zeta} - A_\zeta - Q_{s\zeta} \quad 84$$

In the above equation, $E_{\zeta i S}$ is the salt amount assimilated by the i^{th} vegetation group. $Q_{ss\zeta}$ is the salt load lost to or gained from the lake via seepage, positive when occurring from the lake to the groundwater. As such, $Q_{ss\zeta}$ is defined as:

$$Q_{ss\zeta} = \begin{cases} Q_{ss} lc\zeta & \text{if } Q_{ss} < 0 \\ Q_{ss} sc\zeta & \text{if } Q_{ss} \geq 0 \end{cases} \quad 85$$

$lc\zeta$ and $sc\zeta$ are the salt concentration in the lake and in the groundwater ($g m^{-3}$), the latter being defined as:

$$sc\zeta = \frac{S_\zeta}{S_{sat}} \quad 86$$

In zones with saline groundwater, fresh groundwater lenses may form due to infiltration of rain water [Eeman et al., 2011]. To account for this fact, the groundwater is divided into two layers of different concentration. By definition, it occurs only when the salt concentration in the root zone is lower than the concentration in the groundwater. In this case, a fresher water layer remains over the groundwater until the concentration of the root zone is higher than the concentration in the groundwater. The thickness of this layer, h_f (m), is calculated as:

$$h_f = \begin{cases} 0 & \text{if } sc\zeta < uc\zeta \\ \log(sc\zeta - uc\zeta + 1) & \text{if } sc\zeta \geq uc\zeta \end{cases} \quad 87$$

If the condition for fresh groundwater lens exists, the salt concentration in the lens, $fc\zeta$, and the salt concentration at the bottom of the groundwater, $bc\zeta$, are defined respectively as:

$$fc\zeta = sc\zeta \left(\frac{h_f}{h_s} \right) \quad 88$$

$$bc\zeta = sc\zeta \left(1 + \frac{h_f}{h_s} \right) \quad 89$$

Plants can benefit from this lower salinity water lenses, provided that h_f is greater than an arbitrary $h_{f \min}$ (m). As such, the following equation is applied to the groundwater according to:

$$\Gamma_{S,i} = \begin{cases} -\left(\frac{sc\zeta}{\zeta_{\max i,S}}\right)^{k\Gamma} + 1 & \text{if } hf < h_f \min \quad \text{case 1} \\ -\left(\frac{fc\zeta}{\zeta_{\max i,S}}\right)^{k\Gamma} + 1 & \text{if } hf \geq h_f \min \quad \text{case 1} \\ -\left(\frac{s\zeta c}{\zeta_{\sup i,S}}\right)^{k\Gamma} + 1 & \text{if } hf < h_f \min \quad \text{case 2} \\ -\left(\frac{f\zeta c}{\zeta_{\sup i,S}}\right)^{k\Gamma} + 1 & \text{if } hf \geq h_f \min \quad \text{case 2} \end{cases} \quad 90$$

Salt in the Lake

The variation of the salt load, dL_ζ/dt ($g \text{ d}^{-1}$), and the salt concentration, lc_ζ ($g \text{ m}^{-3}$), in the lake are calculated respectively as:

$$\frac{dL_\zeta}{dt} = Q_{c\zeta} + Q_{w\zeta} + T_{SL\zeta} + T_{UL\zeta} - Q_{ss\zeta} \quad 91$$

$$lc_\zeta = \frac{L_\zeta}{L_v} \quad 92$$

$Q_{c\zeta}$ ($g \text{ d}^{-1}$) is the salt load from the catchment runoff, calculated as Q_c (m^3d^{-1}) multiplied by ζ_{cc} ($g \text{ m}^{-3}$), the salt concentration in the catchment inflow. $Q_{w\zeta}$ is the runoff from the unsaturated and saturated zone and comprises the infiltration and saturation excess multiplied by the salt concentration at the top soil of A_u and A_s , assumed as the salt bulk density.

Appendix E: Model Overview - TUFLOW

TUFLOW is a computer program for simulating depth-averaged, two and one-dimensional free-surface flows such as occurs from floods and tides. TUFLOW was originally developed for modelling two-dimensional (2D) flows, and stands for Two-dimensional Unsteady FLOW. However, it incorporates the full functionality of the ESTRY 1D network or quasi-2D modelling system based on the full one-dimensional (1D) free-surface St Venant flow equations.

The 2D solution algorithm solves the full two-dimensional, depth averaged, momentum and continuity equations for free-surface flow. The scheme includes the viscosity or sub-grid-scale turbulence term that other mainstream software omit. TUFLOW is specifically orientated towards establishing flow and inundation patterns in coastal waters, estuaries, rivers, floodplains and urban areas where the flow behaviour is essentially 2D in nature and cannot or would be awkward to represent using a 1D model. TUFLOW solves the depth averaged 2D shallow water equations (SWE). The SWE are the equations of fluid motion used for modelling long waves such as floods, ocean tides and storm surges. They are derived using the hypotheses of vertically uniform horizontal velocity and negligible vertical acceleration (i.e., a hydrostatic pressure distribution). These assumptions are valid where the wave length is much greater than the depth of water. In the case of the ocean tide the SWE are applicable everywhere. The 2D SWE in the horizontal plane are described by partial differential equations of mass continuity and momentum conservation in the X and Y directions for an in-plan Cartesian coordinate frame of reference. The solution has been enhanced and improved to provide much more robust wetting and drying of elements, upstream controlled flow regimes (e.g. supercritical flow and upstream controlled weir flow), modifications to cells to model structure obverts (e.g. bridge decks) and additional energy losses due to fine-scale features such as bridge piers.

TUFLOW was used to answer hydraulic questions that could not be answered by the hydrological models developed in this project. For instance, what would be the flooded area if changes were made in the Dulbinning channel or in the channel of the Canal Rd. Also, how plantation of Mallee rows would affect the water ponding in the valley floor (spatiotemporally) and how culverts implementation could speed up the drainage in the valley floor.

Model setup simply requires an accurate DEM, rainfall and evaporation rates, and estimates of land-surface roughness and infiltration capacity. The below section outlines work undertaken on model validation for an event in 2008, however, this was only a very small flow, with limited depth of water at the gauge locations. The model setup should be further tested against new gauge data as it comes in for more significant flow events as ultimately the level of model predictions will be heavily influenced by DEM and parameter errors at very low flows, making it an unreliable test.

Validation

The water level observed at the gauge ASWTLB13DUL006 (Figure 94) during the greatest flow event observed between 15/07/2008 and 20/08/2008 was used to calibrate the hydrodynamic model TUFLOW. The model was forced by the inflows from six gauges (in blue in Figure 95) and by the rainfall (Figure 96).

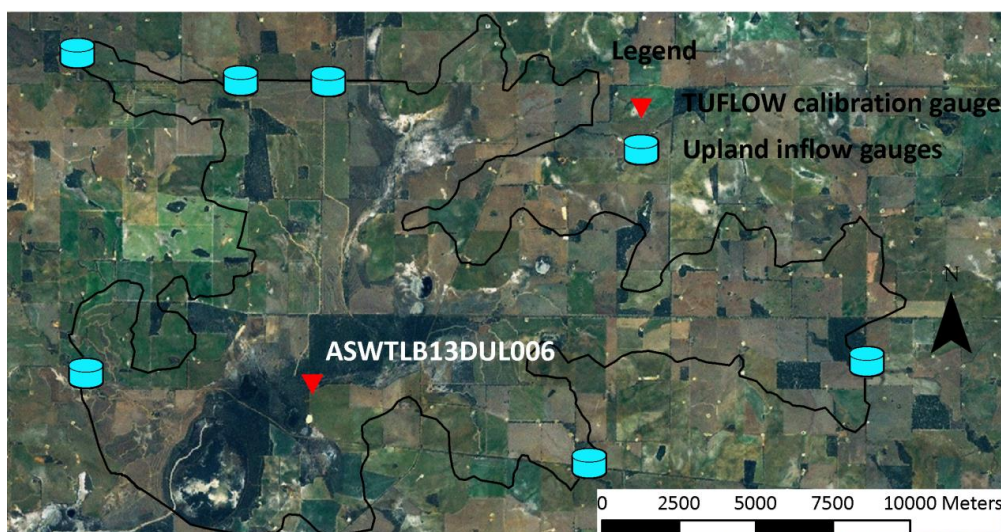


Figure 94: TUFLOW domain. The red dot indicates the observation point (Gauge ASWTLB13DUL006) used in the model assessment. Blue dots indicate the inflow gauges from the upland area used to drive the model.

A map of the land use for the area (Figure 94) and the roads and culvert location map (Figure 98) were also used to assist the parameterisation. We also considered the existence of other engineered flow modifications such as the channel along the Canal Rd, the drain built along the western side of the Canal Rd, the diversion channel built along western side of the lake and the diversion gate, northwest of the lake. In addition, we consulted previous reports describing the flow drainage implementations (e. g. Toolibin Lake technical notes, Callow et al., [2008]) and satellite imagery/photography (Figure 99) to further represent the land use and modifications at Toolibin catchment that could represent changes in its hydrological characteristic.

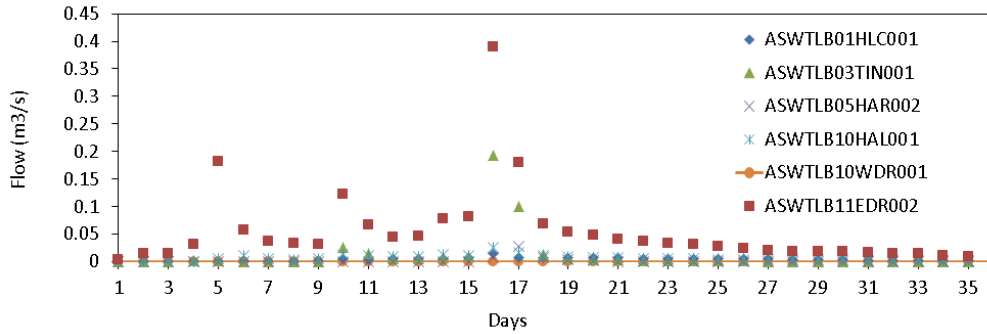


Figure 95: Observed water flow between 15/07/2008 and 20/08/2008 at the 6 monitoring gauge stations that intercept the main water pathways of the catchment.

The land coverage was divided in four materials with distinct Manning's roughness coefficient, n : sparse trees (remnant vegetation), grasses, channels and roads. Their values were: 0.05, 0.03, 0.01 and 0.01 $s\ m^{-1/3}$, respectively. Roads elevation was based on pictures observations and Callow et al. (2008) report. For Canal Rd the elevation was of 0.4 m. Roads like Wogolin Rd South and Brown Rd were assumed as having 0.1 m of elevation and to vicinal roads 0.05 m of elevation was attributed. TUFLOW incorporates in its simulations the land use through both n and infiltration values. Roads are represented via changes in the grid elevation. Also, given the dimension, slope, elevation and n , culverts are also resolved in TUFLOW. The culvert simulated consisted of two cement pipes (circular culvert) of 0.45 m of diameter and $n = 0.001$.

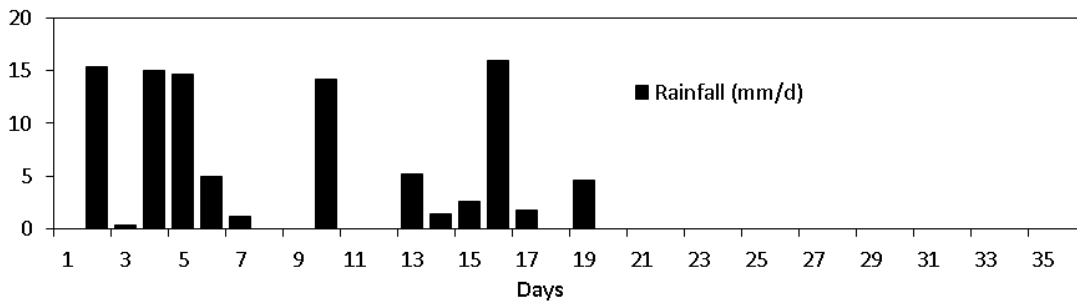


Figure 96: Observed rainfall between 15/07/2008 and 20/08/2008 at the BoM Station # 10654.

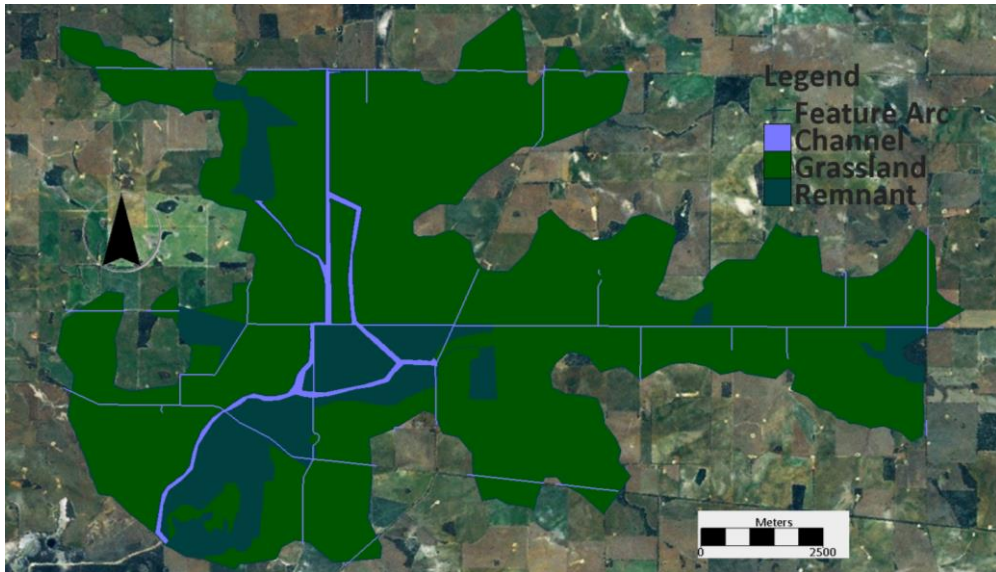


Figure 97: Land coverage map defining the spatial distribution of two Manning's Roughness Coefficients.

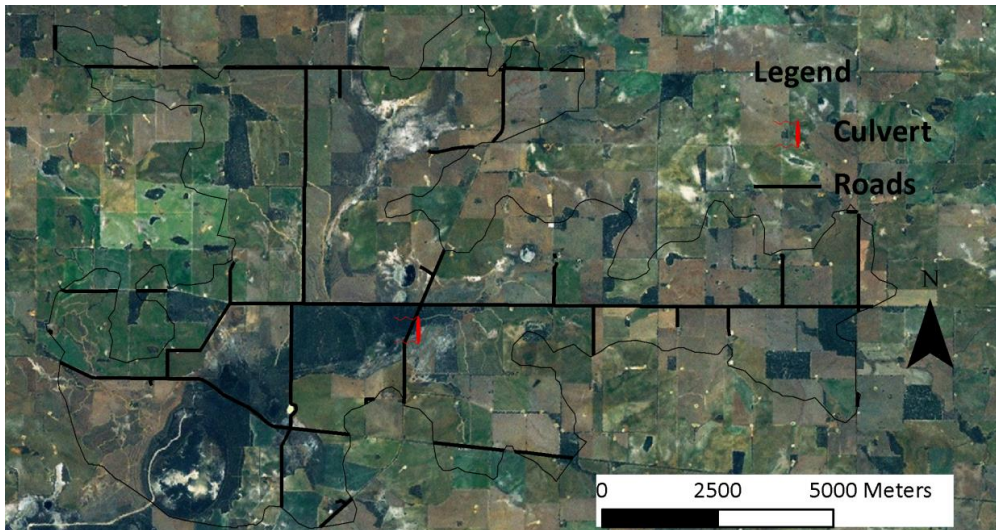


Figure 98: Roads and culvert location.



Figure 99: Drainage built from Rd Canal at the point that crosses Brown Rd (Google Maps, 2008)

Station ASWTLB13DUL006 was chosen to calibrate the model because it does not suffer influence from the gate operation schedule. The hydrograph observed at the ASWTLB13DUL006 station and the water level predicted by the model at that location is presented on Figure 100.

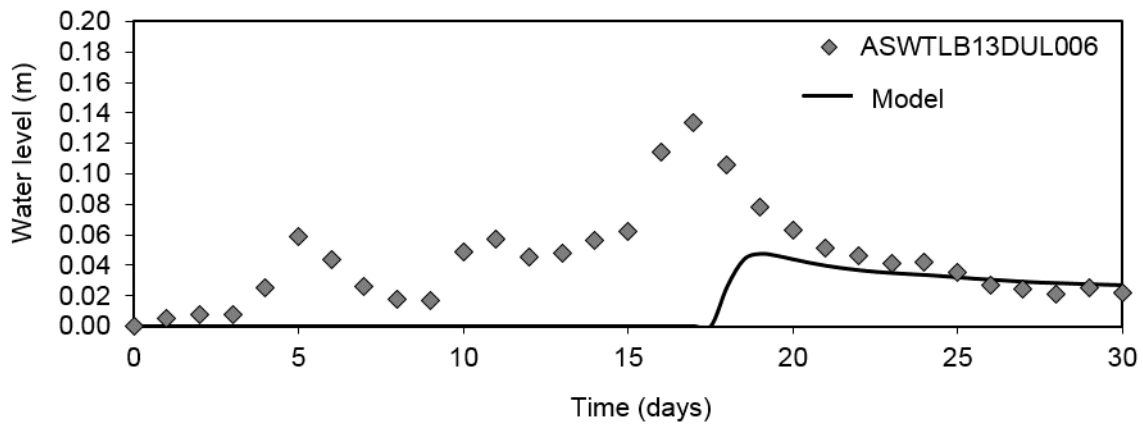


Figure 100: The water level observed in the gauge ASWTLB13DUL006 and the level predicted by TUFLOW at that location. Note the small range on the y-axis indicating flows during the initial rain period <5cm deep.

During TUFLOW's calibration, we found that better results of calibration were obtained when using zero initial infiltration (Initial Loss, in terms of TUFLOW) and zero continuous infiltration (Continuing Loss, in TUFLOW terms), but we rejected those parameters. We concluded that the gauge was responding to the precipitation. As the previous event was more than 30 days apart, we assumed that a rainfall around 15 mm/day would not be sufficient to generate any flow. On the other hand, as the simulated event runs, we expected that the soil would be closer to saturation and a rainfall of around 15 mm/day could generate readings in the gauge, as the model predicted. Thus, we used the infiltration and Manning's roughness values given by the literature (e.g. Ward and Trimble, 2003) and presented in Table 5. Ultimately, however, the magnitude of this event is not significant enough to undertake a serious calibration of the model since at these very low flow depths the model predictions would be heavily influenced by errors associated with the DEM and grid generation.

Appendix F: Model Performance Indices

- 1) The Root Mean Square (RMS) error, which represents the amount of physical error in the prediction, in the units of flow (m³/s or mm) or salt load (kg/s). The RMS of a model prediction with respect to the estimated variable X_{model} is defined as the square root of the mean squared error:

$$RMSE = \sqrt{\frac{\sum_{i=1}^n (X_{obs,i} - X_{model,i})^2}{n}}$$

where X_{obs} is observed values and X_{model} is modelled values at time i .

- 2) The Mean Absolute Error (MAE), which is the absolute error divided by the number of observations:

$$MAE = \sqrt{\sum_{i=1}^n (X_{obs,i} - X_{model,i})^2}$$

where X_{obs} is observed values and X_{model} is modelled values at time i .

- 3) The Normalised Root mean Square (NRMS) error (given in %), which is the normalized RMS to the range of the observed data, defined as:

$$NRMS = \frac{RMS}{X_{obs,max} - X_{obs,min}} \cdot 100$$

- 4) The Nash-Sutcliffe model efficiency coefficient (N-S), defined as:

$$N - S = 1 - \frac{\sum_{i=1}^n (X_{obs,i} - X_{model})^2}{\sum_{i=1}^n (X_{obs,i} - \overline{X_{obs}})^2}$$

where X_{obs} is observed values and X_{model} is modelled values at time/place i .

An efficiency of 0 indicates that the model predictions are as accurate as the mean of the observed data, whereas an efficiency less than zero ($-\infty < E < 0$) occurs when the observed mean is a better predictor than the model, in which case, it was not presented in the plots.

- 5) The Coefficient of Determination (denoted as R^2), which represents how well the relation between model and prediction fits a linear relation.

Appendix G: Summary of Water Storages and Fluxes

Sub-catchment 7 (SC7)

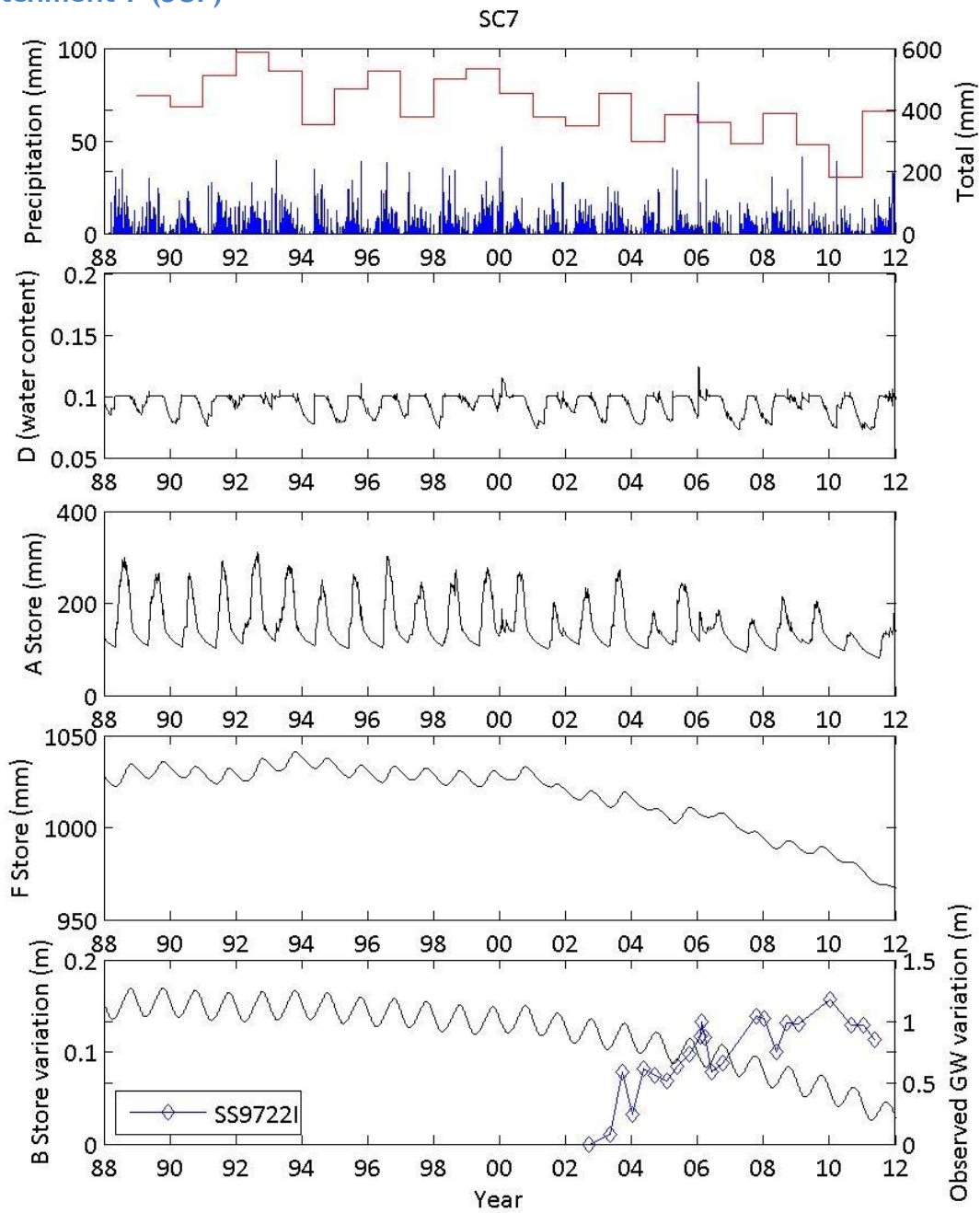


Figure 101: Long term trend groundwater and soil water content - SC7. Note the rising trend in the observed bore height data during the drying period from 2004-2011, in contrast to the model predictions.

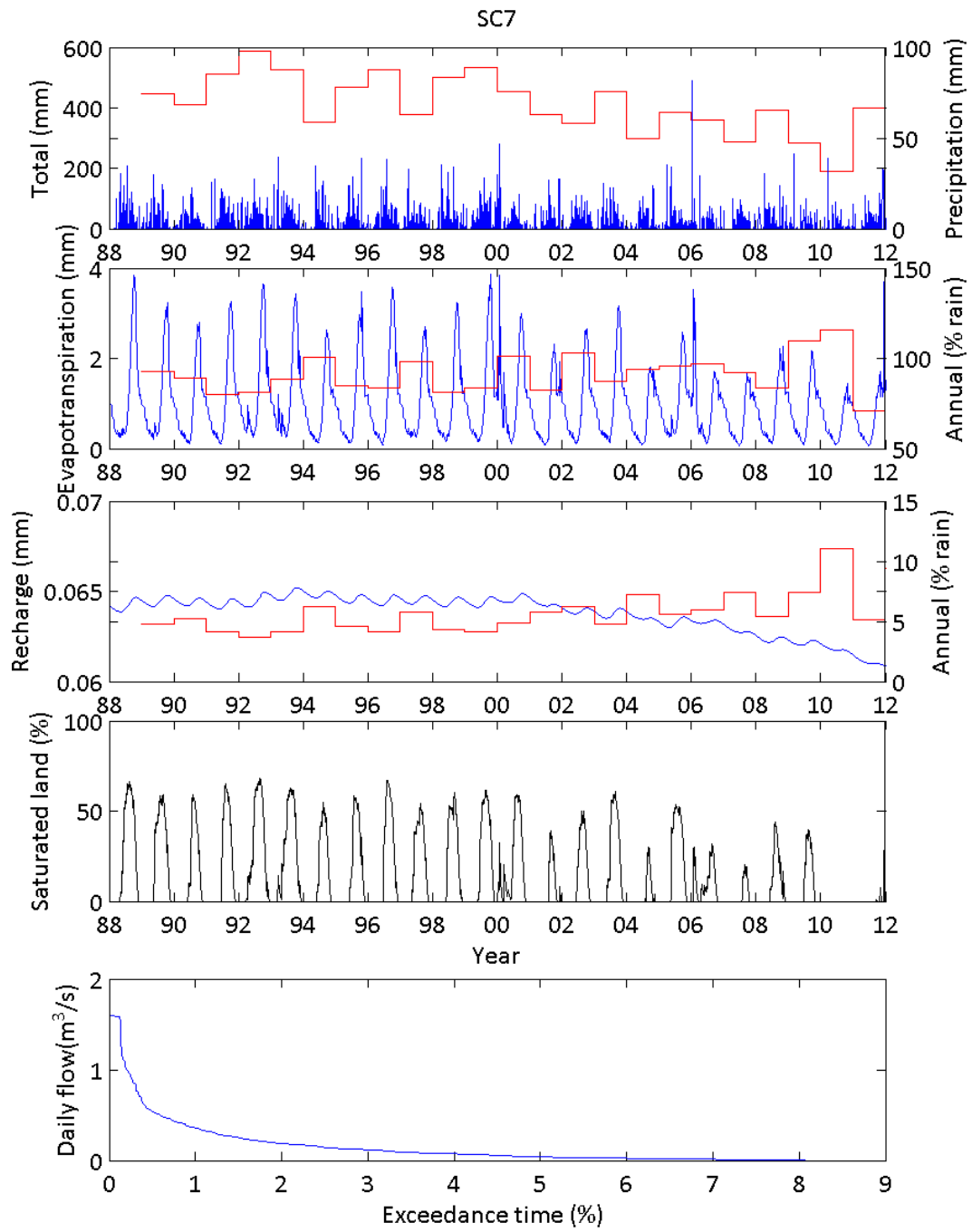


Figure 102: Long term trend surface water, recharge and evapotranspiration - SC7.

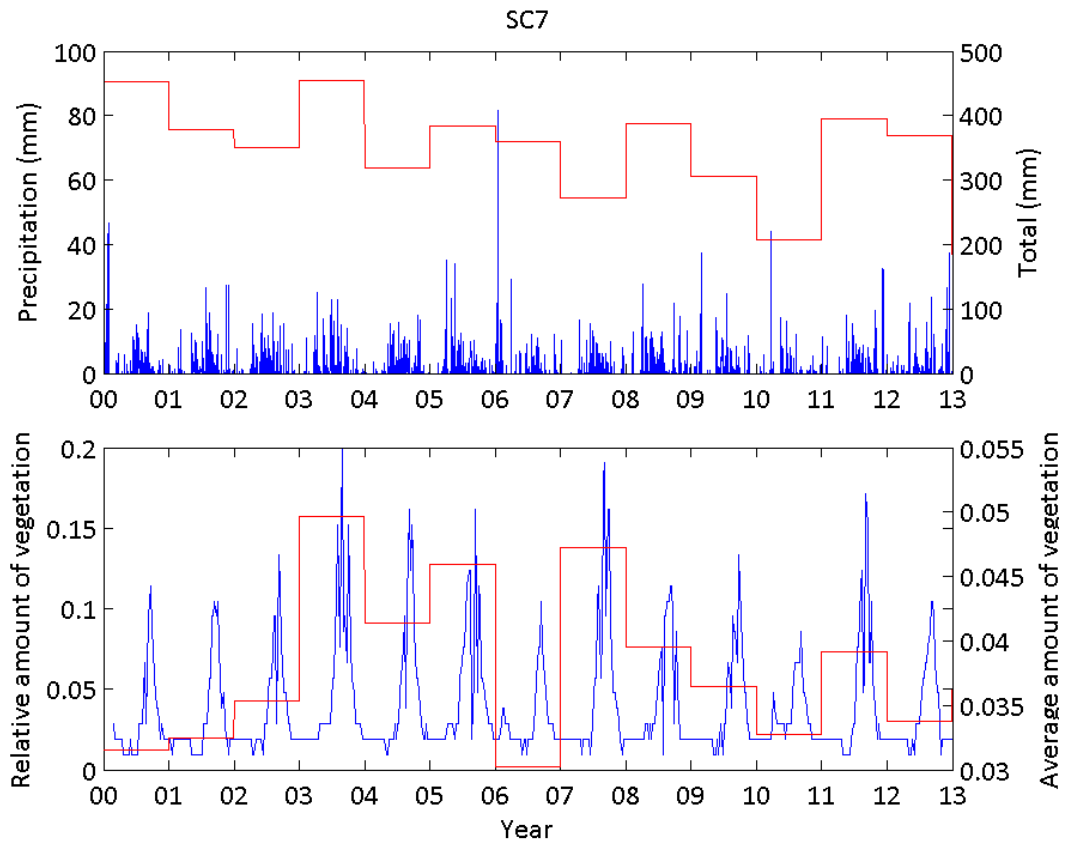


Figure 103: Long term trend vegetation - SC7.

Sub-catchment 10 (SC10)

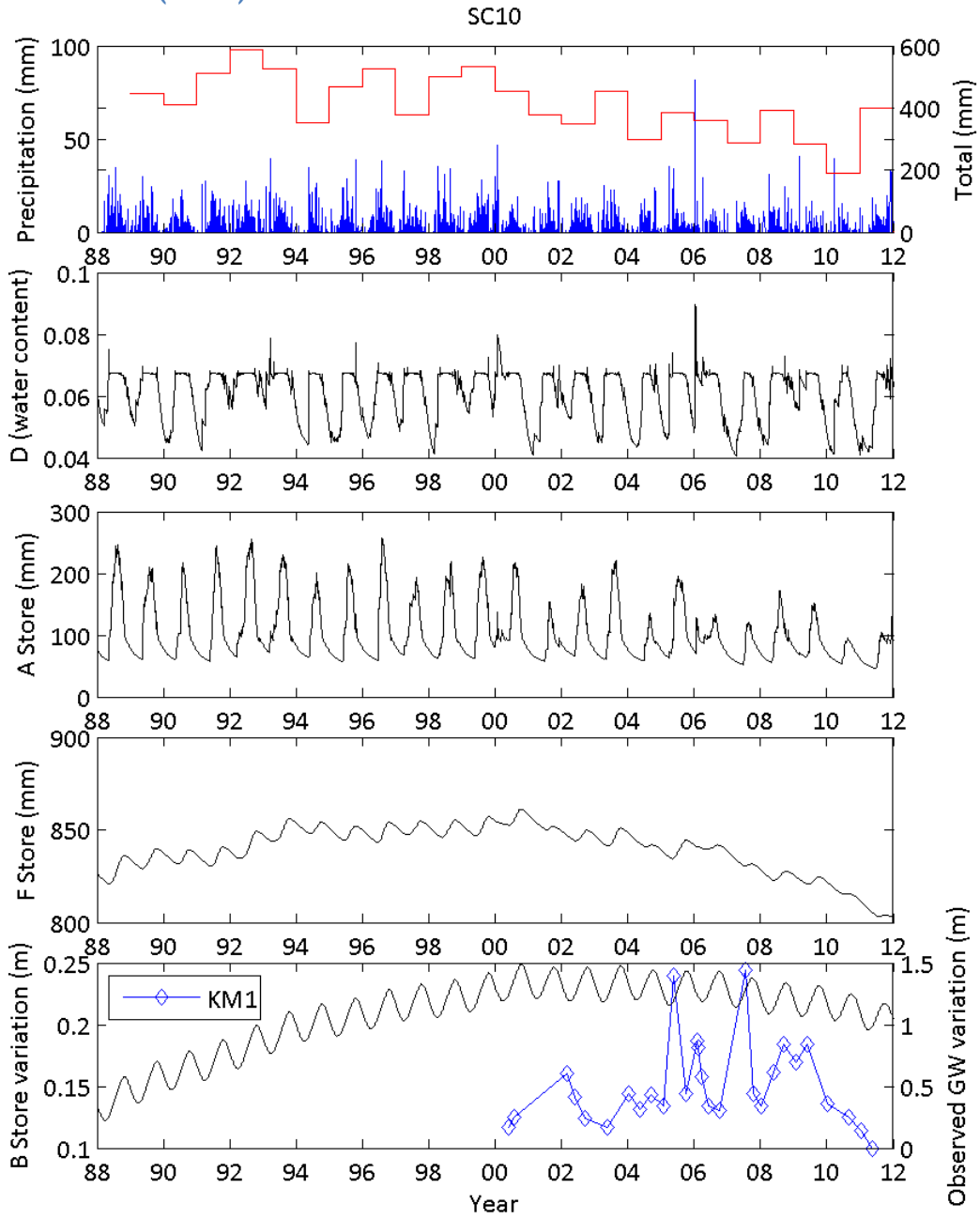


Figure 104: Long term trend groundwater and soil water content – SC10.

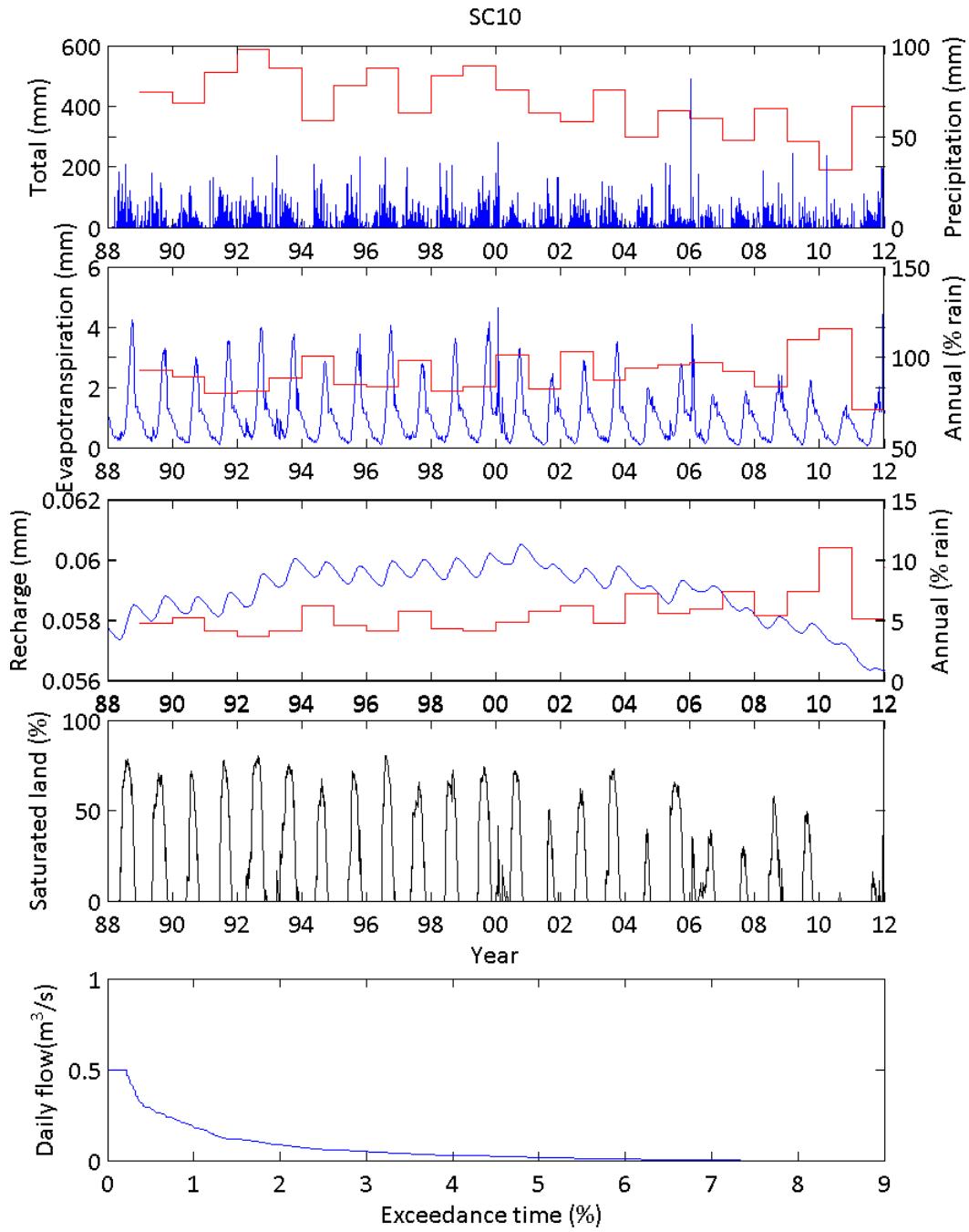


Figure 105: Long term trend surface water, recharge and evapotranspiration – SC10.

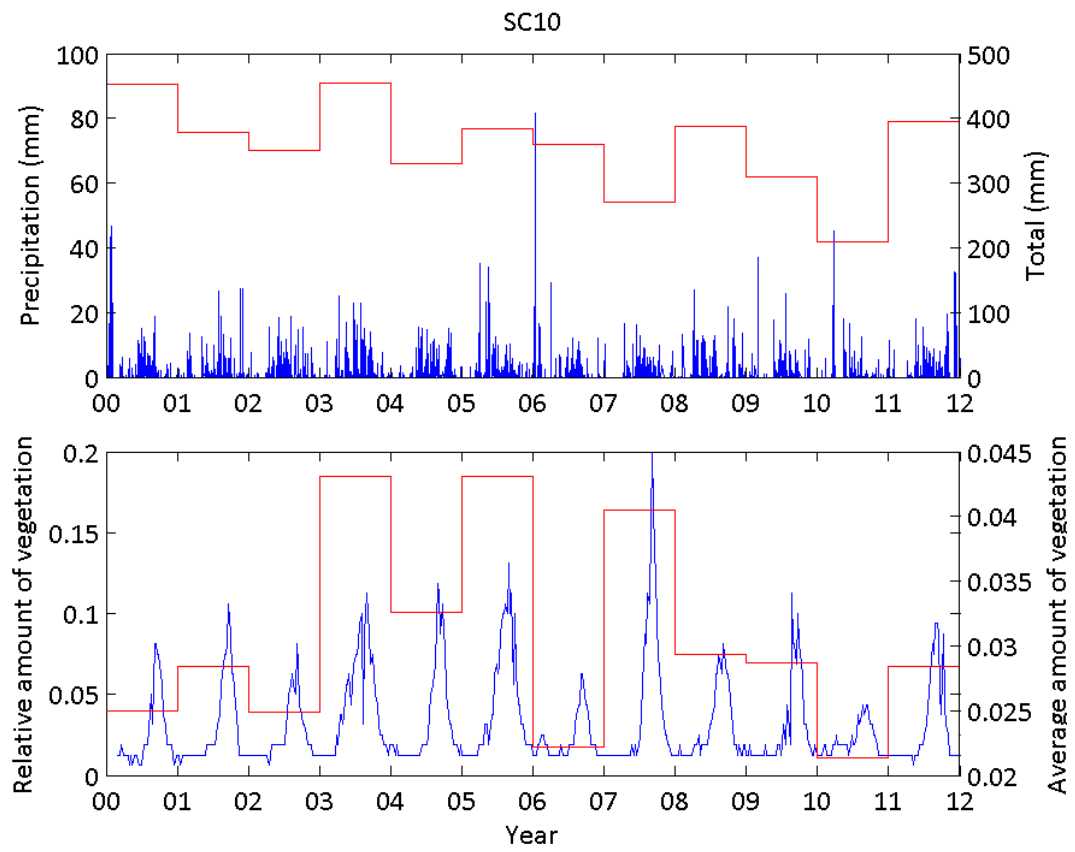


Figure 106: Long term trend vegetation – SC10.

Sub-catchment 12 (SC12)

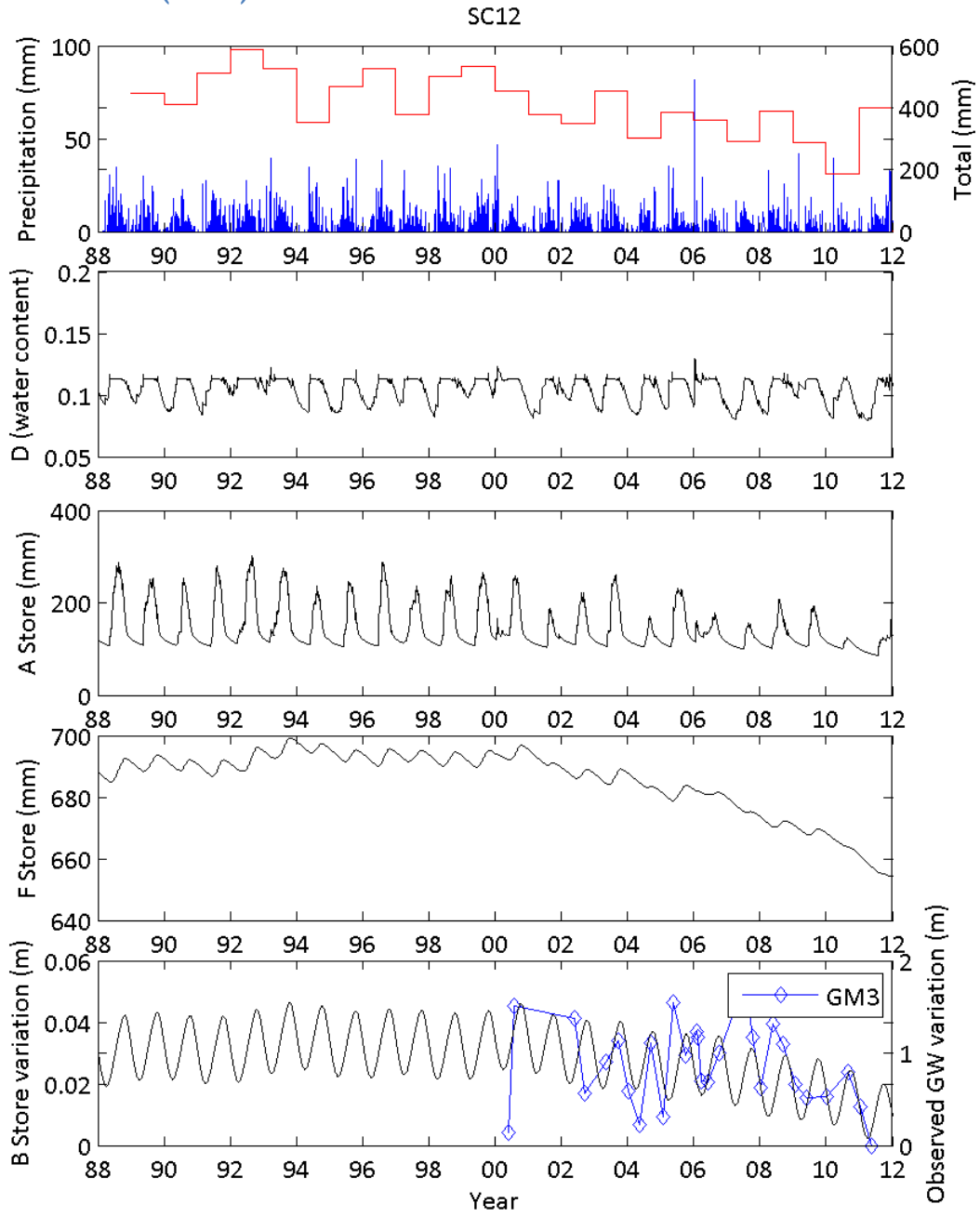


Figure 107: Long term trend groundwater and soil water content – SC12.

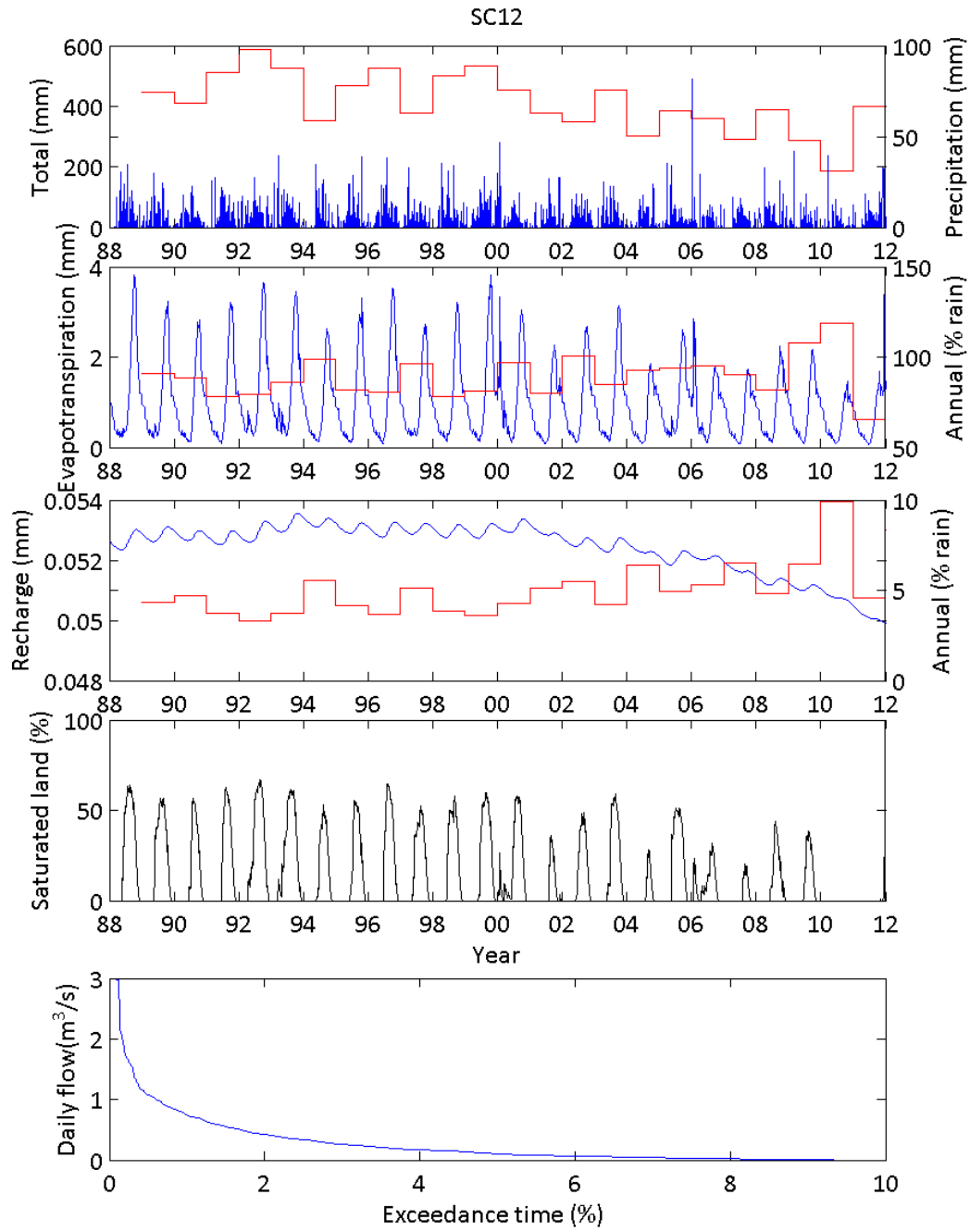


Figure 108: Long term trend surface water, recharge and evapotranspiration – S12.

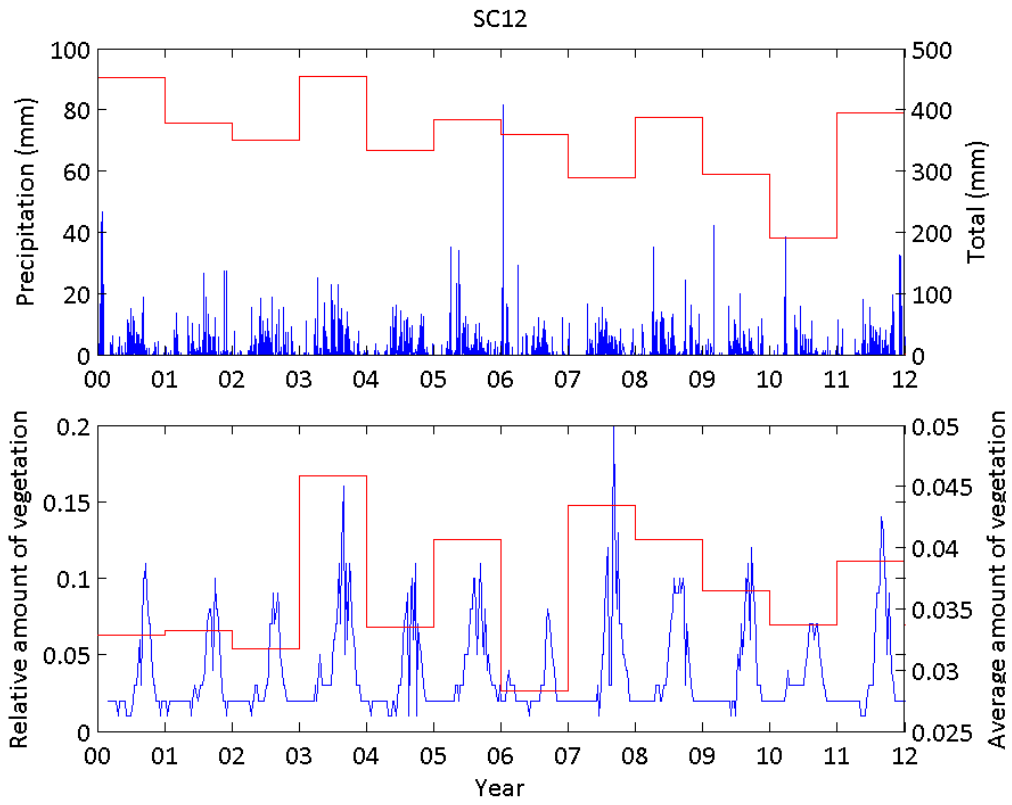


Figure 109: Long term trend vegetation – SC12.

Sub-catchment 22 (SC22)

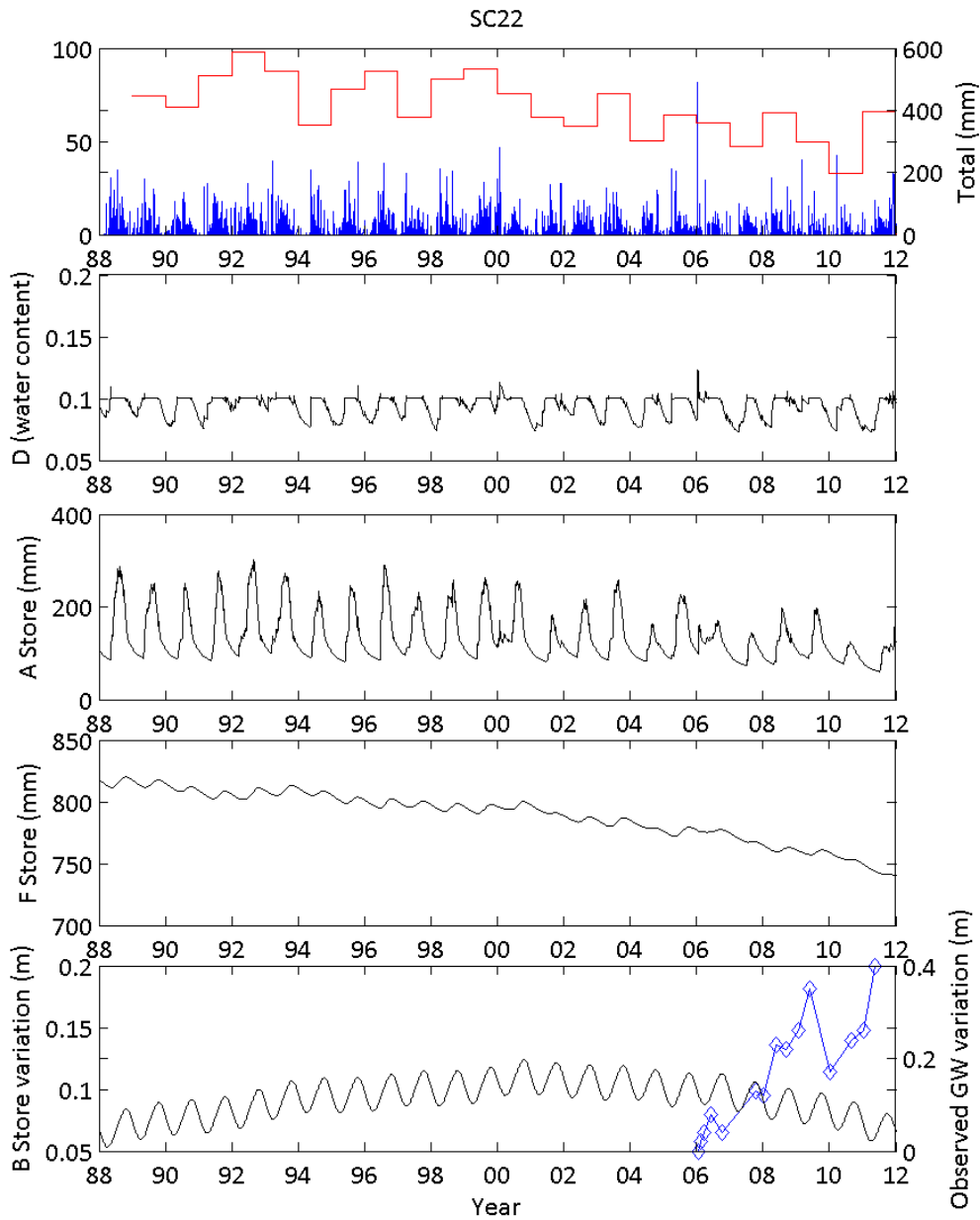


Figure 110: Long term trend groundwater and soil water content – SC22.

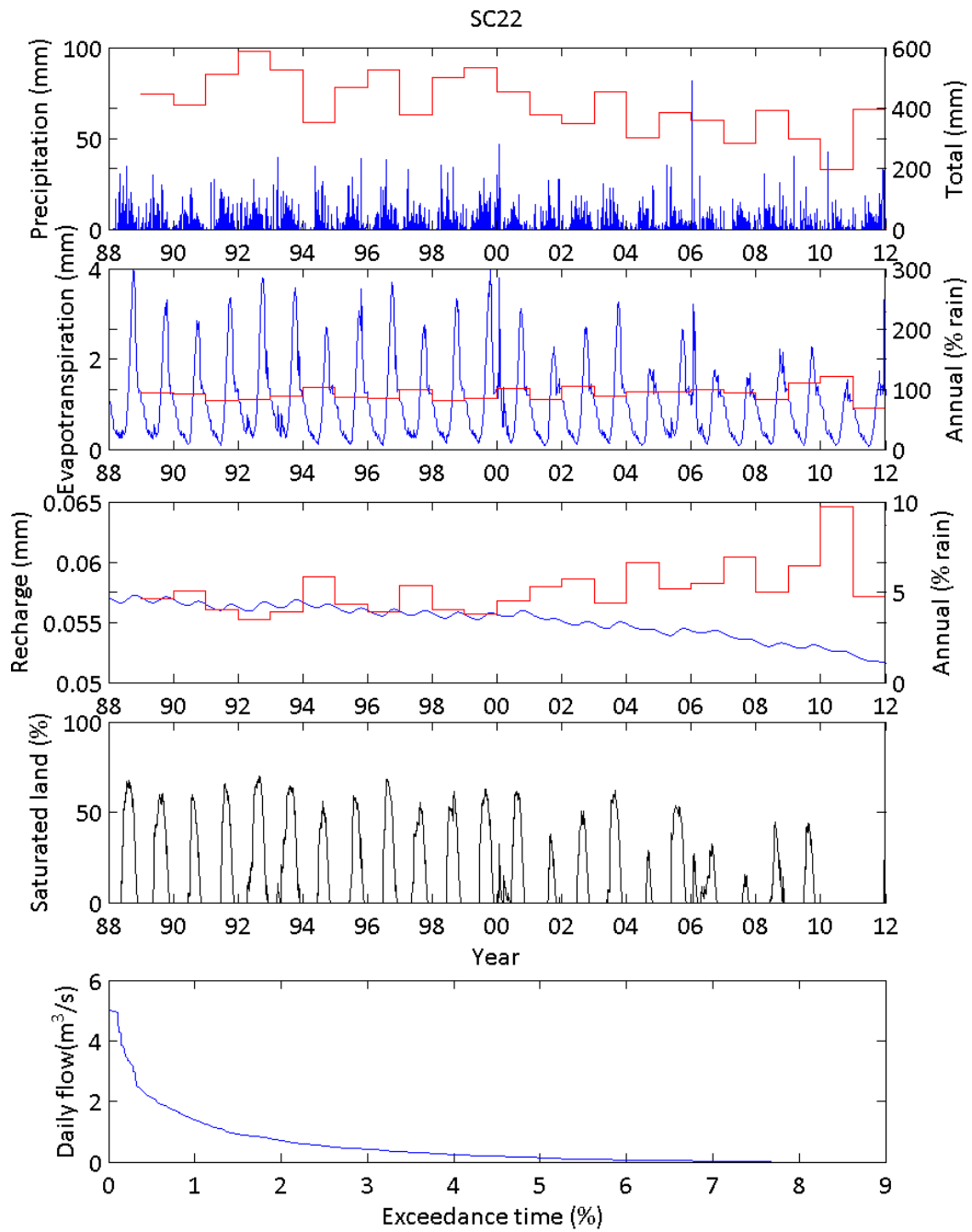


Figure 111: Long term trend surface water, recharge and evapotranspiration – SC22.

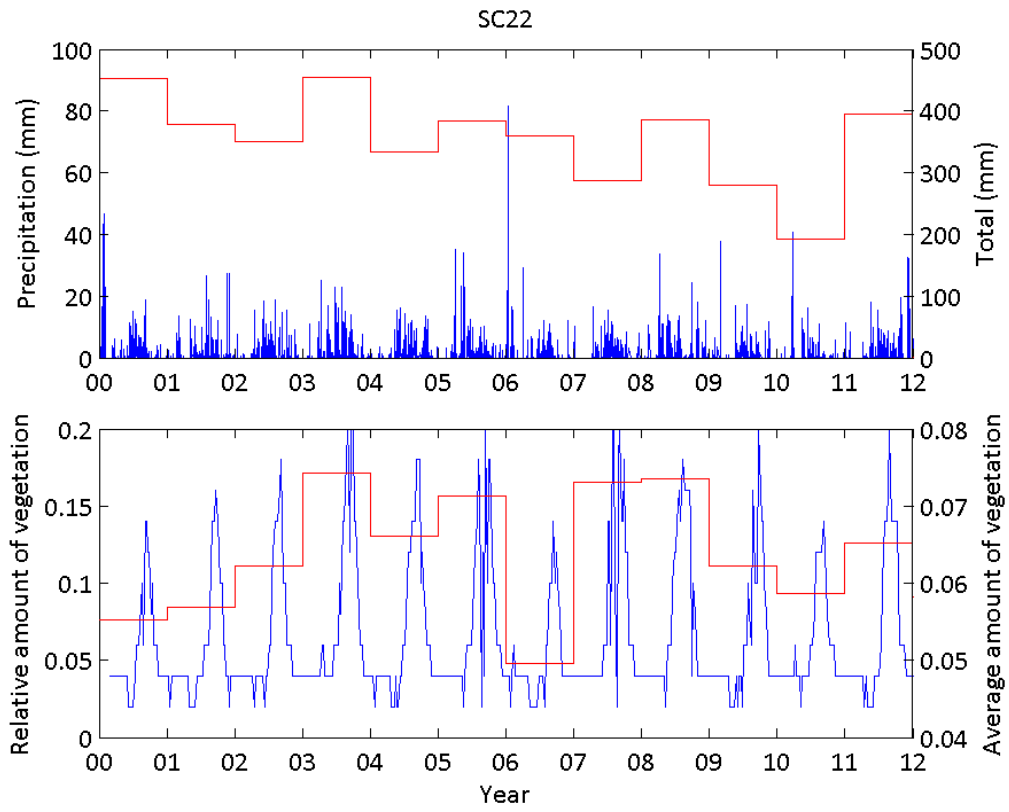


Figure 112: Long term trend vegetation – SC22.

Sub-catchment 28 (SC28)

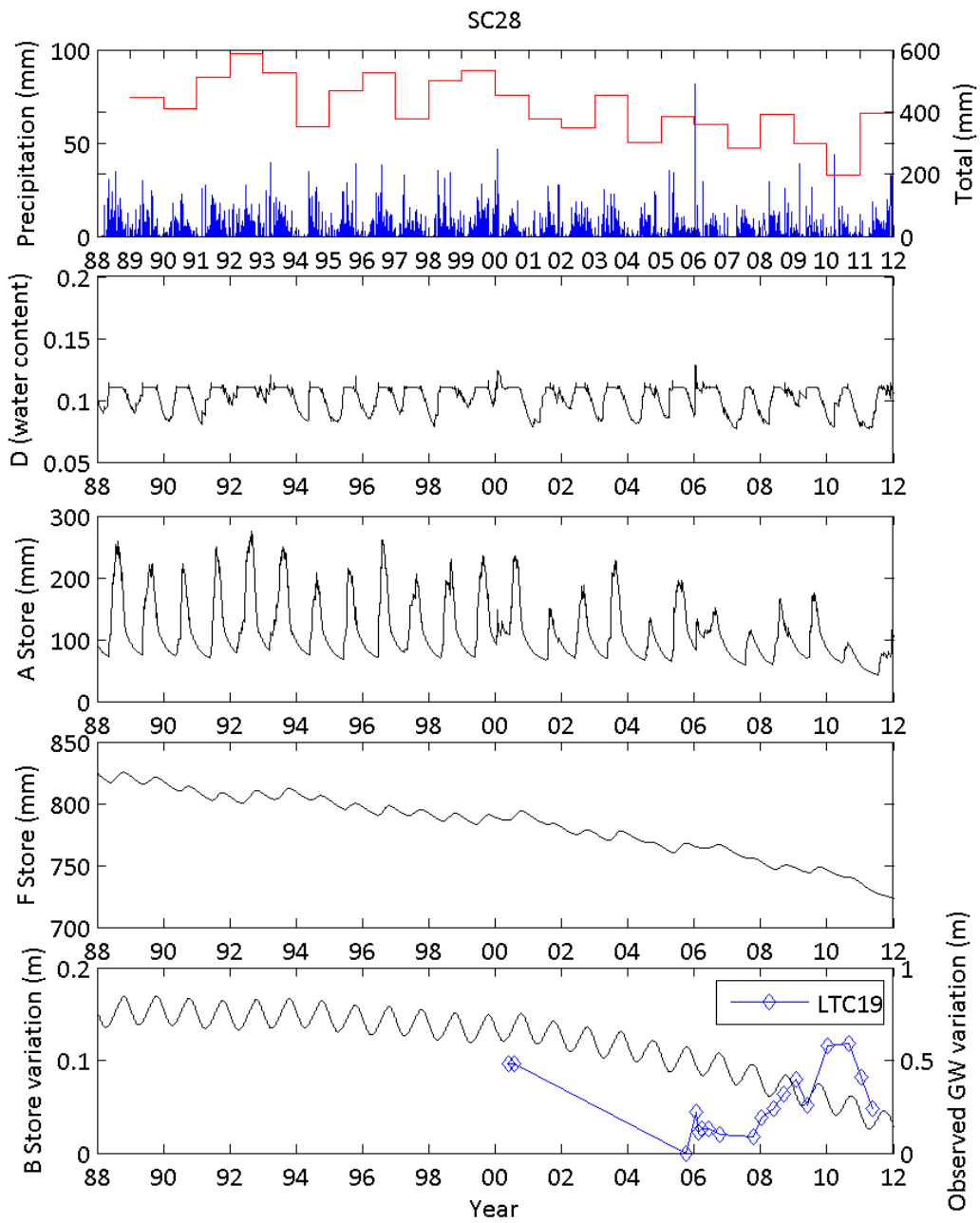


Figure 113: Long term trend groundwater and soil water content – S28. Note the observed groundwater levels increase during the driest year of the simulation period, in contrast to the models predicted drying of the stores.

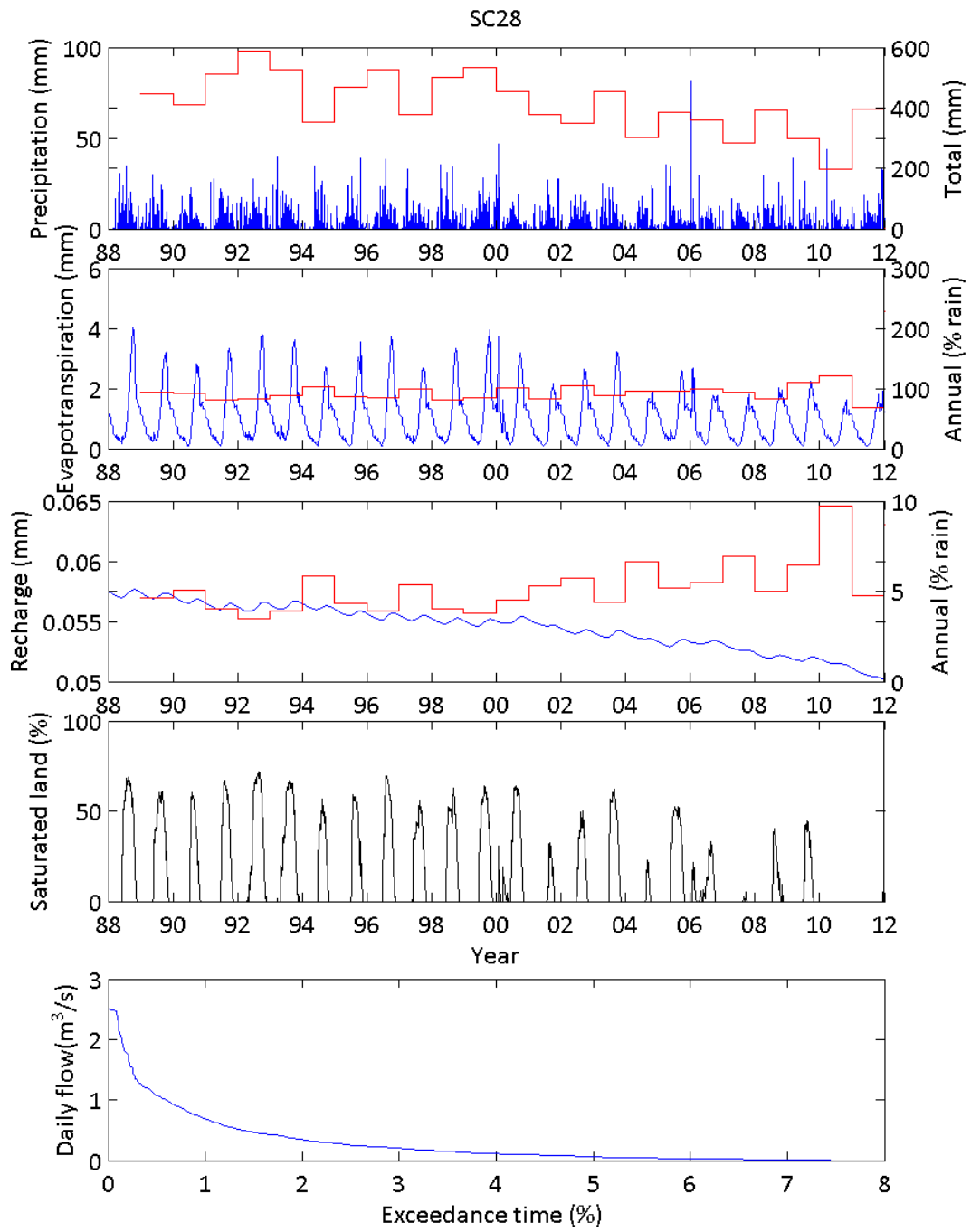


Figure 114: Long term trend surface water, recharge and evapotranspiration – SC28.

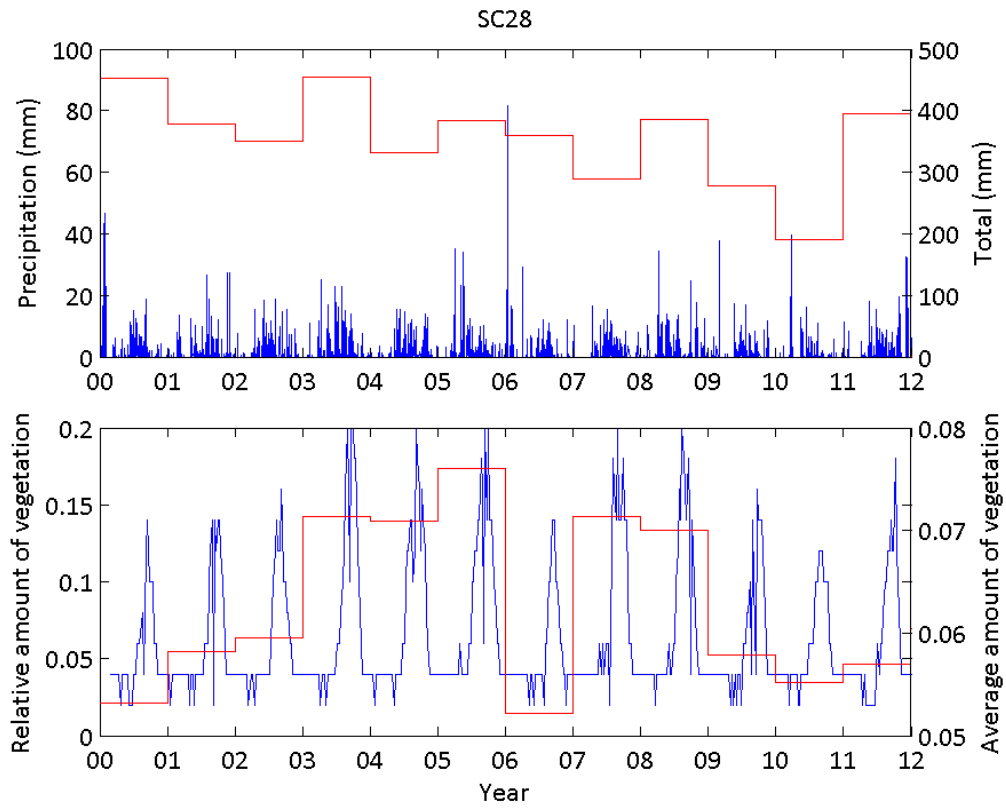


Figure 115: Long term trend vegetation – SC28.

Sub-catchment 32 (SC32)

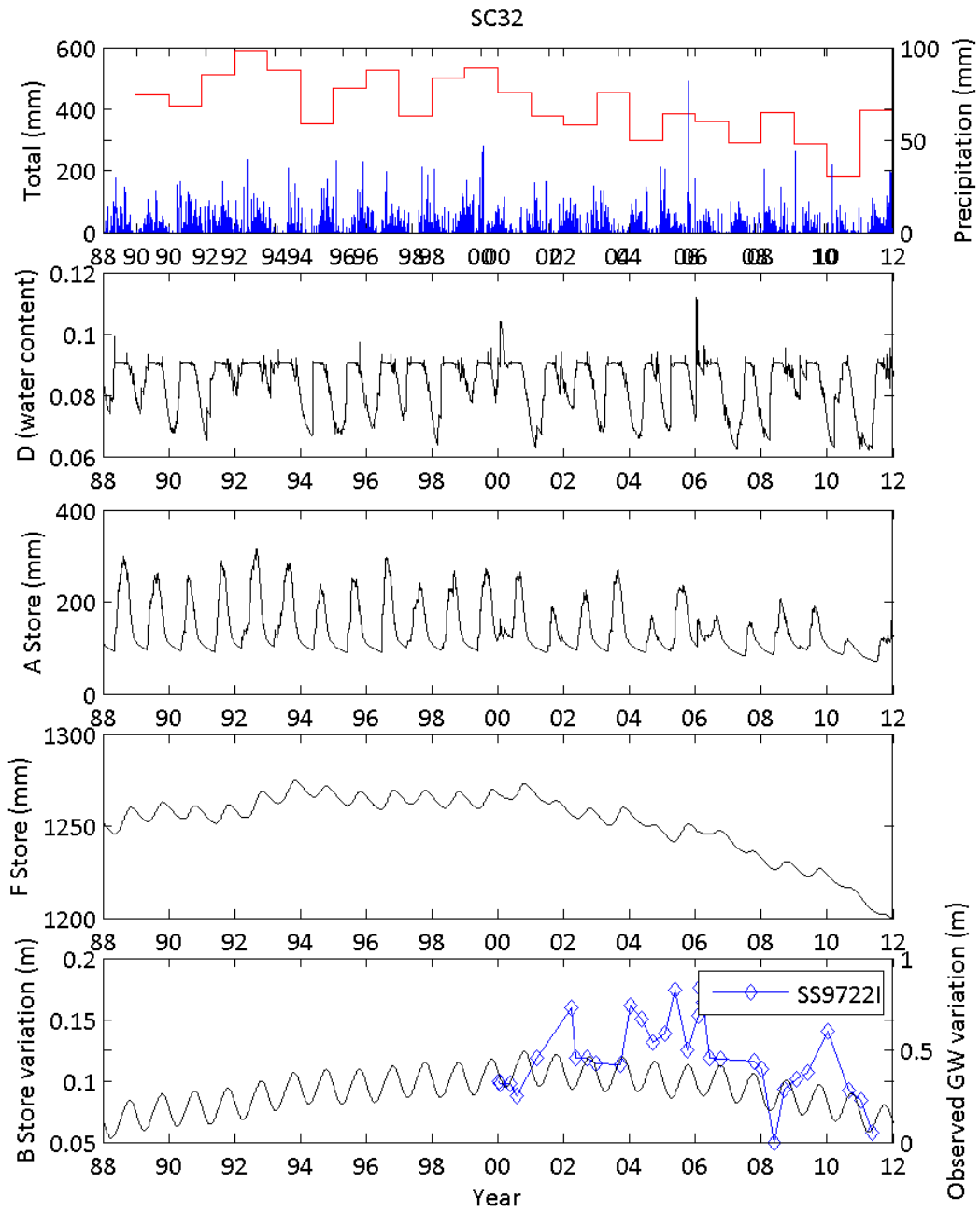


Figure 116: Long term trend groundwater and soil water content – SC32.

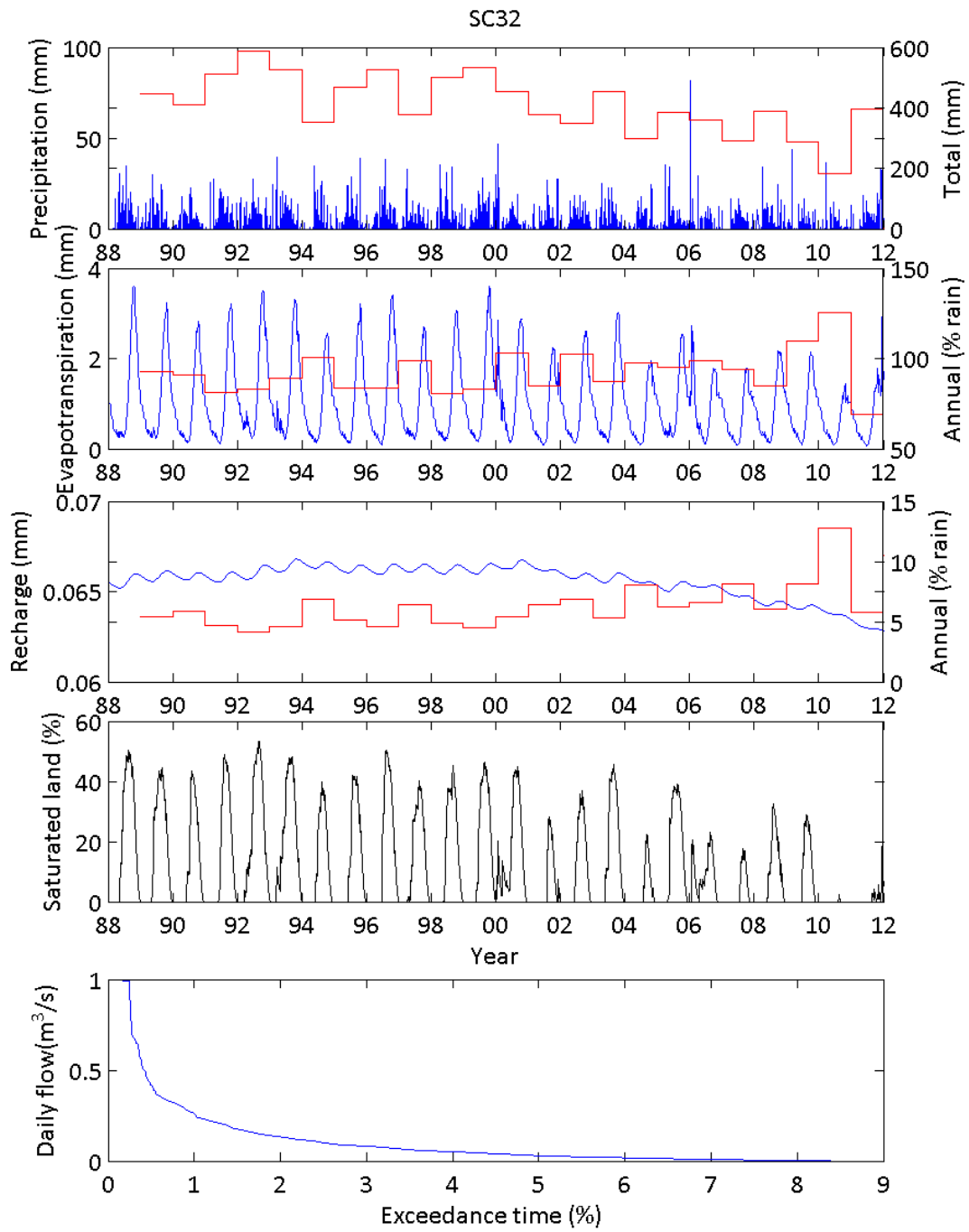


Figure 117: Long term trend surface water, recharge and evapotranspiration – S32.

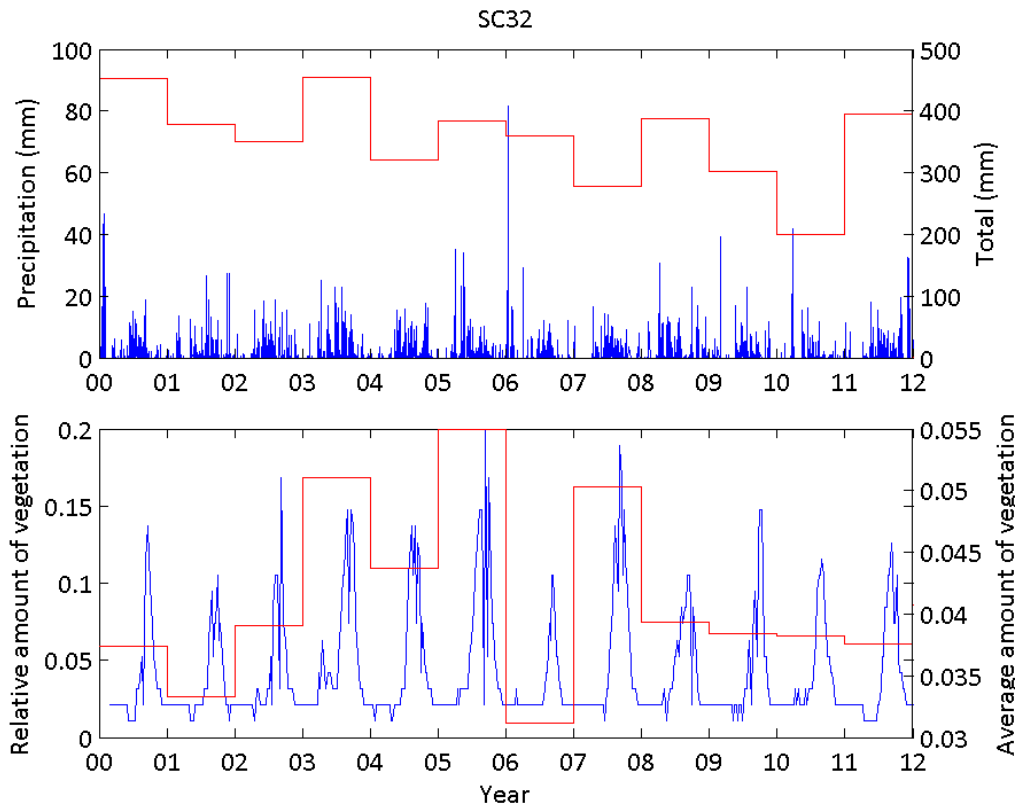


Figure 118: Long term trend vegetation – SC32.

Appendix H: Monthly Comparison of Surface Flows

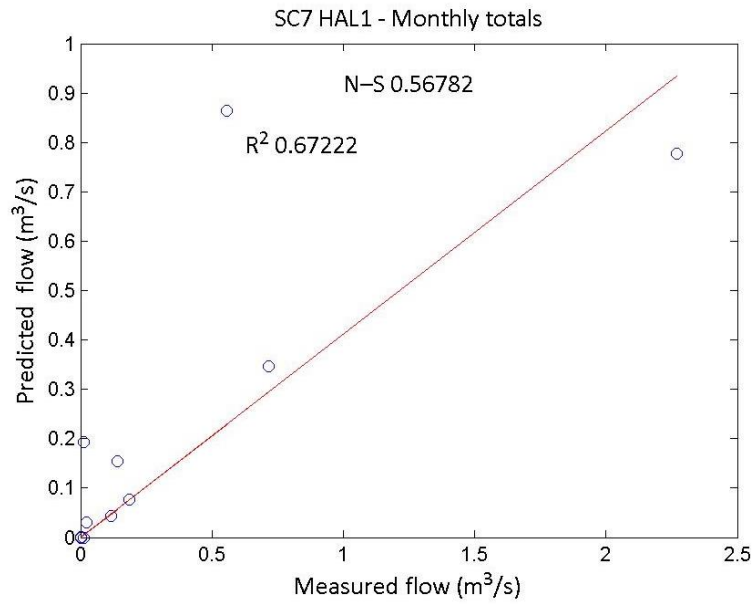


Figure 119: Monthly totals of surface runoff measured versus predicted at SC7.

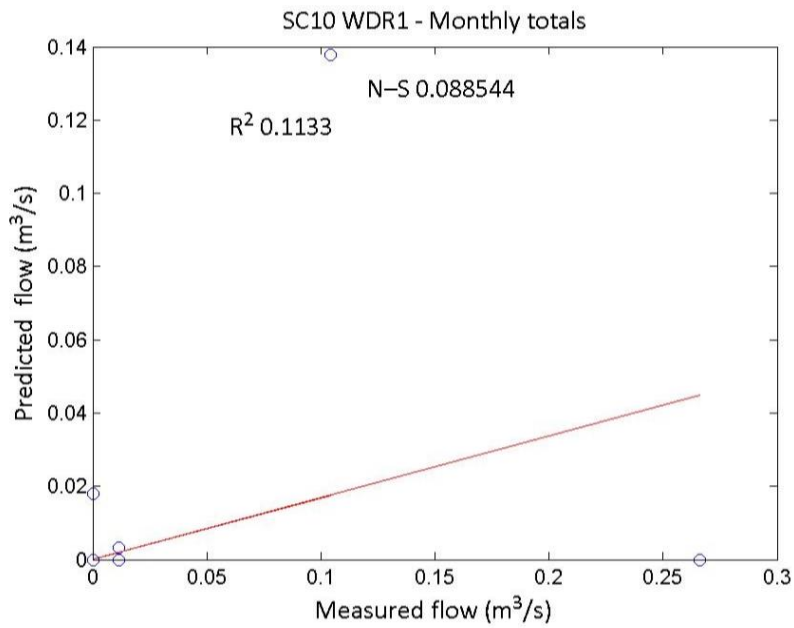


Figure 120: Monthly totals of surface runoff measured versus predicted at SC10.

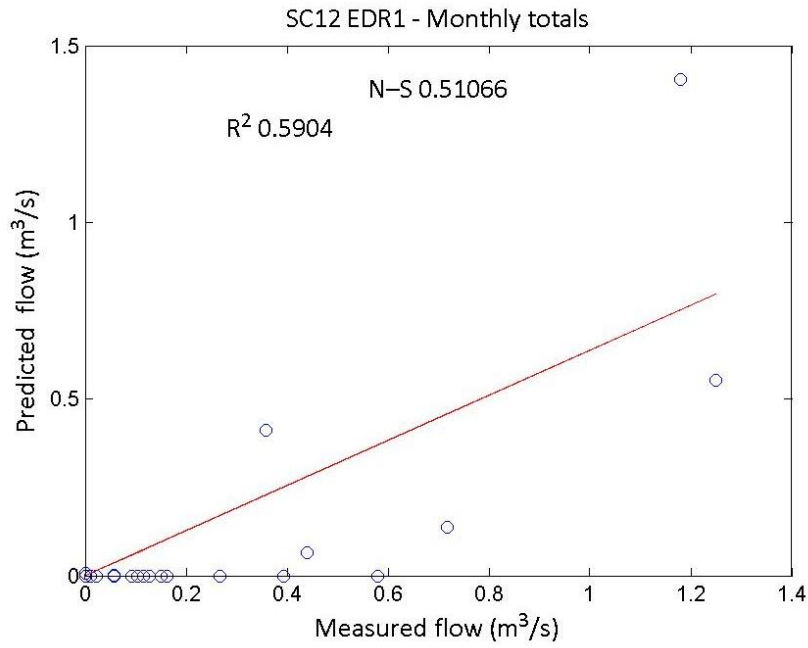


Figure 121: Monthly totals of surface runoff measured versus predicted at SC12.

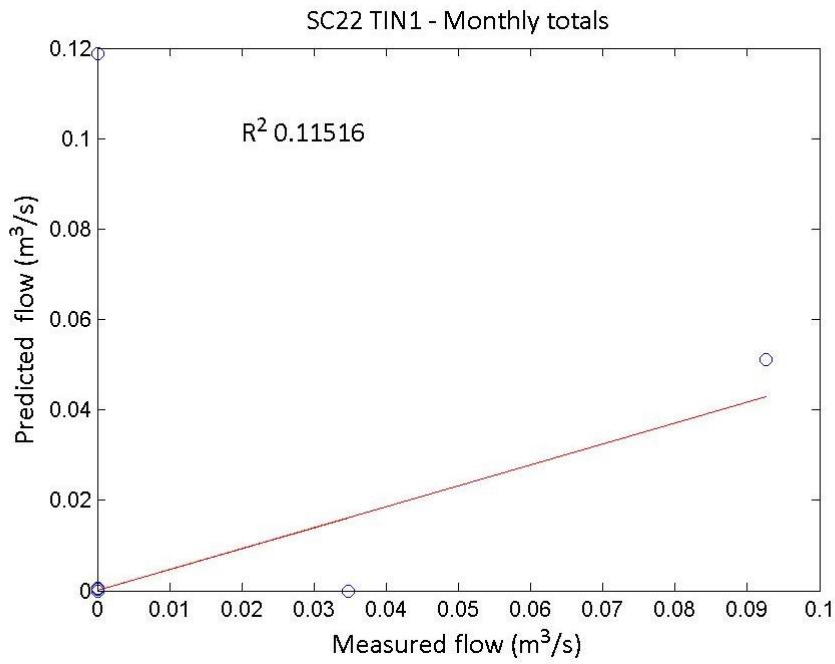


Figure 122: Monthly totals of surface runoff measured versus predicted at SC22.

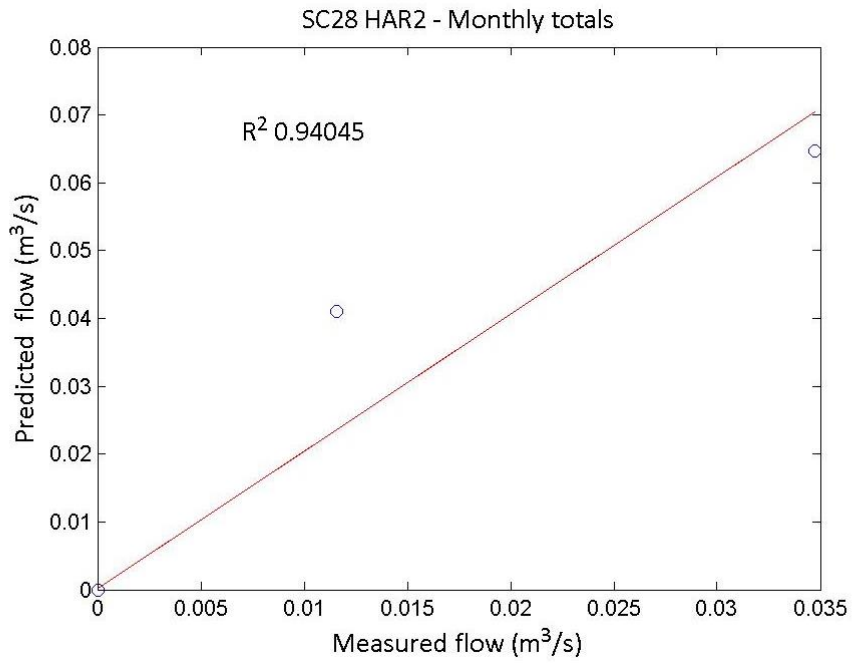


Figure 123: Monthly totals of surface runoff measured versus predicted at SC28.

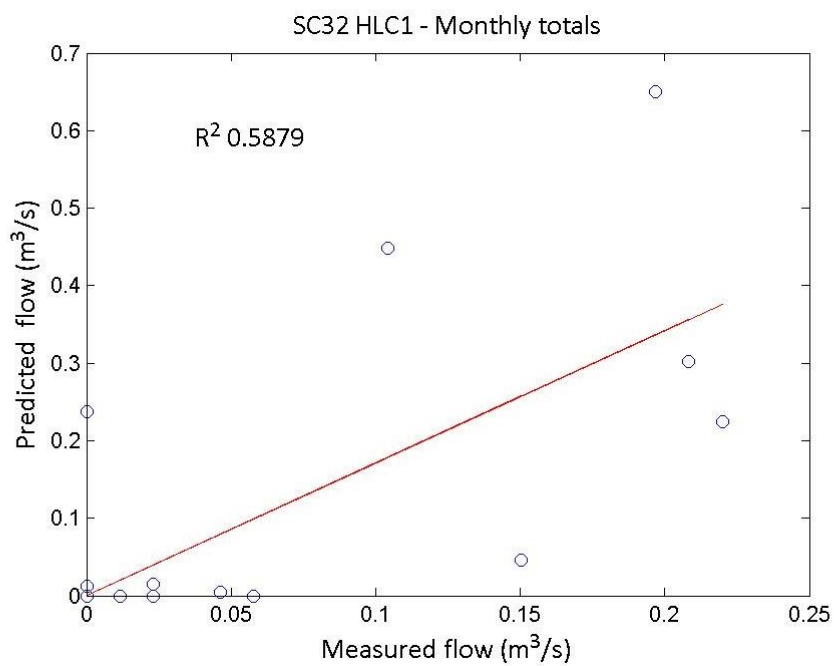


Figure 124: Monthly totals of surface runoff measured versus predicted at SC32.

Appendix I: Operation Summary of the Integrated Model

To allow the use of the integrated model system in an optimized way and to accelerate the workflow related to model settings and results processing, additional scripts were developed using Matlab® version 2011. Matlab is a high-level language and interactive environment for technical computing developed by Mathworks. The Matlab scripts help translating the inputs stored in spreadsheets (csv files) into the integrated model system input files, as well as processing model's results and generating ready-to-use outputs such as charts and time-series.

The integrated model and an example set up (including input files and parameters) can be downloaded from the Aquatic EcoDynamics website, URL: <http://aed.see.uwa.edu.au/research/projects/toolibin.php>. The input files, Matlab scripts and the integrated model system executables were built in an enclosed folder structure as illustrated below (Figure 125). The structure contains 3 main folders, namely input, matlab and output. The input folder contains the input files created by the user. The folder matlab contains scripts, the input files translated to the integrated model system format (once the input files are translated) and the integrated model system executable, while the folder output contains the post-processed the integrated model system results. The steps to prepare the input files ready to be used by the model are:

1. Prepare sub-catchment delineation and calculate:
 - a. area of each (km²);
 - b. distance to outfall (km);
 - c. Drainage density - length of stream per area (km stream per km²);
 - d. Centroid coordinates.

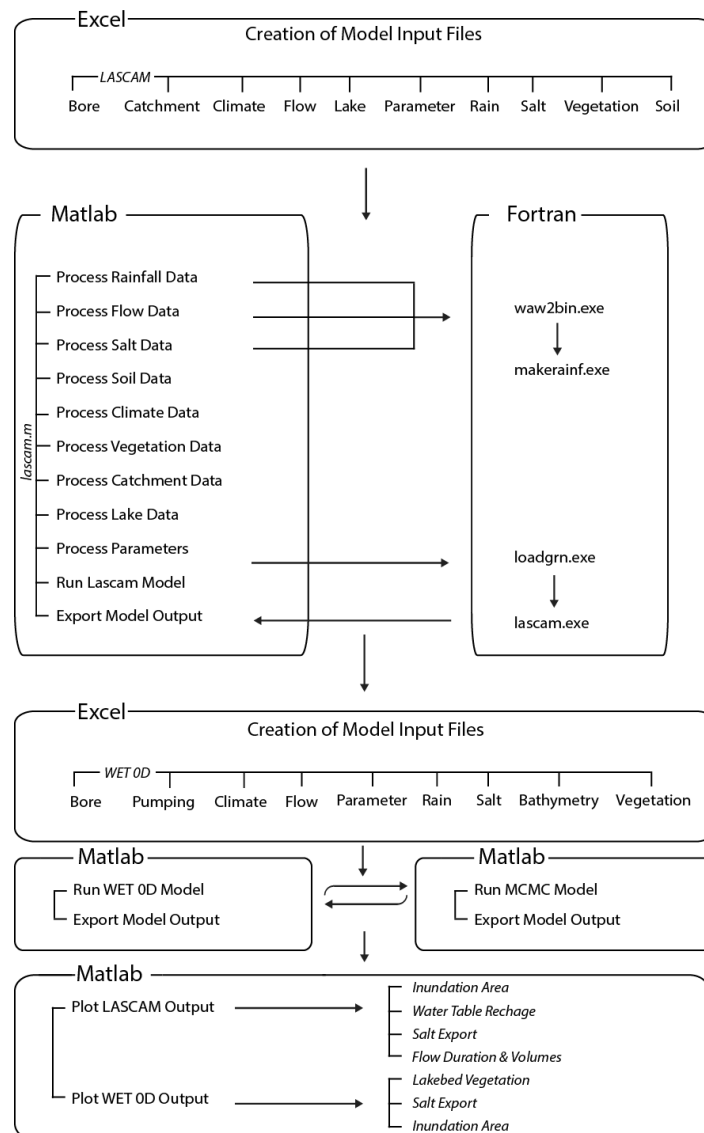


Figure 125: The integrated model system configuration.

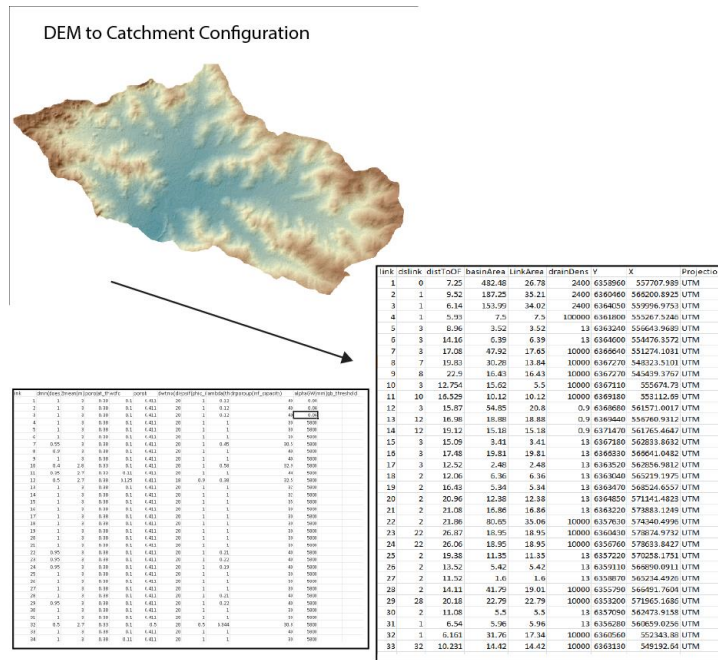


Figure 126: Data necessary for the catchment input file.

2. Prepare general climate files:
 - a. RAI: Long term mean annual rainfall (MAR) values for each catchment;
 - b. EVP: Long term mean potential evapotranspiration values for each catchment.

Rain.csv

X	Y	Station_Number	Date_Time	Year	Month	Day	Precip
551437.1	6359652	200	2/05/2007	2007		5	0.2
551437.1	6359652	200	3/05/2007	2007		5	0
551437.1	6359652	200	4/05/2007	2007		5	0
551437.1	6359652	200	5/05/2007	2007		5	0
551437.1	6359652	200	6/05/2007	2007		5	0
551437.1	6359652	200	7/05/2007	2007		5	0
551437.1	6359652	200	8/05/2007	2007		5	0
551437.1	6359652	200	9/05/2007	2007		5	0
551437.1	6359652	200	10/05/2007	2007		5	0

SiteSelection.xls

Site ID	Y	X	Projection
200	6367660	554657.4852	UTM
200	6356936	565520.2932	UTM
300	6364815	549217.9	UTM
400	6360244	562482.7795	UTM
500	6358857	557651.8904	UTM
1000	6372748	546747.67	UTM
400	6358557	562945.8013	UTM
400	6360806	568369.7705	UTM
200	6366483	556780.7707	UTM
200	6368388	551991.8028	UTM
200	6359218	566115.6069	UTM

climate.csv

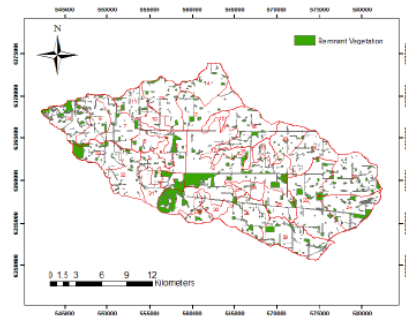
link	Evap	Rai
1	2000	480
2	2000	480
3	2000	480
4	2000	480
5	2000	480
6	2000	480
7	2000	480
8	2000	480
9	2000	480
10	2000	480

Figure 127: Data necessary for the climate input file.

3. Prepare rainfall station time series files:
 - a. For each rain gauge, compile daily data (mm) in csv/txt file.
4. Prepare streamflow gauging station files:
 - a. For each stream gauge, compile daily flow data (ML/day) in csv/txt file.

5. Prepare sub-catchment vegetation properties:
 - a. Identify % of deep-rooted (tree) species in each sub-catchment;
 - b. Identify Leaf Area Index (LAI) of crops in each;
 - c. Identify Leaf Area Index of deep rotted veg in each;
 - d. Impervious area fraction.

GRN % Coverage		RIP % Coverage	
Number	Value	Catchment	Value
1	2	1	1.2
2	2	2	1.2
3	2	3	1.2
4	2	4	1.2
5	2	5	1.2
6	2	6	1.2
7	0.5	7	2
8	0.5	8	2
9	0.5	9	2
10	1	10	1.2
11	1	11	1.2
12	0.5	12	2



Catchment	LAI	
	GRN	RIP
1	0.2	0.5
2	0.6	0.5
3	0.2	0.5
4	0.2	0.5
5	0.2	0.5
6	0.2	0.5
7	0.6	0.5
8	0.6	0.5
9	0.6	0.5
10	0.8	0.5
11	0.9	0.5
12	0.6	0.5

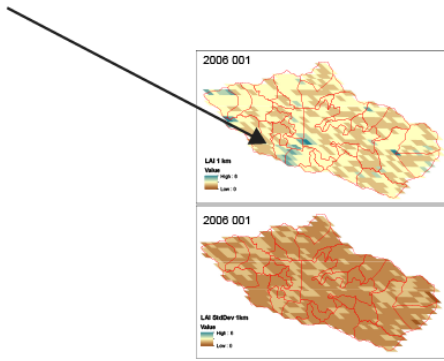


Figure 128: Data necessary for the vegetation input file.

6. Prepare sub-catchment soil properties:
 - a. Define 'average' soil types (porosity, hydraulic conductivity);
 - b. Soil depth (and depth to horizon of duplex);
 - c. Depth to bedrock.

7. Identify storages in stream network (dams, weirs) and:
 - a. volume-area-height storage relationship;
 - b. discharge – height relationship, above base invert.

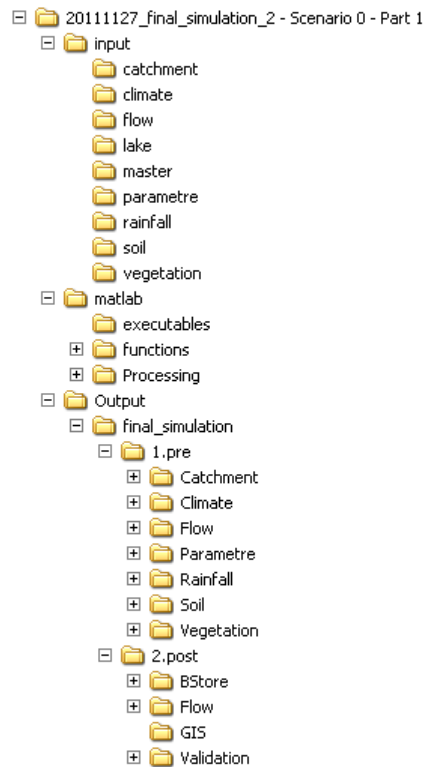


Figure 129: SWWAN-DSS folders creation.

All the inputs of the LASCAM model are saved in the folder **Input**. The several inputs are divided in subfolders according to its nature, as follows:

- **Catchment** – this subfolder contains information about sub-catchments;
- **Climate** – this subfolder contains climate information, such as rainfall and evaporation;
- **Flow** – this folder contains flow observations used in the model calibration;
- **Lake** – this folder contains information about lakes and reservoirs;
- **Master** – this folder contains inputs that control running time and outputs;
- **Parameter** – this folder contains parameter inputs that are common to all sub-catchments;
- **Rainfall** – this folder contains rainfall data;
- **Soil** – this folder contains information regarding soil parameters; and
- **Vegetation** – this folder contains information on the vegetation and impervious surfaces.
- **Bore** – this folder contains both the raw bore data and sub-catchment locations (plotting only, not used by **lascam**)

The files in the folder **matlab** relate to internal operation of the models and therefore must not be modified in any way.

Domain and Sub-catchment Selection

The LASCAM model domain and sub-catchment selection is defined in the file **catchment.csv** located in the **Catchment** folder. The file consists of a header line containing the column identifiers followed by one line per sub-catchment in the model. The sub-catchment input consists of 9 parameters, namely:

- **Link** – indicates the sub-catchment ID, starting from 1 for the most downstream catchment up to the total number of catchments;
- **Dslink** – indicates the ID of the downstream sub-catchment. For the most downstream sub-catchment, Dslink must be assigned as 0;
- **DistToOF** – distance along the river from the centroid of the sub-catchment to the most downstream point of the basin;
- **BasinArea** – total area of all sub-catchments located upstream of the current sub-catchment;
- **LinkArea** – area of the sub-catchment;
- **DrainDensity** – ratio between stream length within the sub-catchment and its corresponding area;
- **Y** – northern coordinate of the sub-catchment centroid;
- **X** – eastern coordinate of the sub-catchment centroid; and

- **Projection** – coordinate projection system used to define the centroid coordinates.

Important: Downstream sub-catchments must always have a lower index than those located upstream, and the most downstream sub-catchment must have an index of 1. Therefore users must ensure the indexing of sub-catchments is conducted to ensure water flow follows a path of decreasing sub-catchment index values.

Soil

Soil settings can be accessed and modified in the CSV file **soil.csv** in the **soil** folder. This file consists of one header line with column names followed by one line per sub-catchment where the parameters are set.

The required parameters are:

- **Link** – corresponds to the sub-catchment ID;
- **Dmin** – minimum soil depth (m);
- **Dmean** – average soil depth (m);
- **Poroup** – top-soil porosity (-);
- **FieldCap** – top-soil field capacity (-);
- **PoroZNS** – deep soil porosity (-);
- **DepthBR** – depth to bedrock (m);
- **Psif** – bubbling pressure (mm);
- **Lambda** – soil index;
- **SpecYield** – specific yield (-); and
- **AlphaGW** – fraction of the sub-catchment underlain by contributing aquifers.

The sub-catchment lines have to be in ascending order by ID. A typical soil file format is shown below.

link	dmin	dmean	poroup	fieldCap	poroZNS	depthBR	psif(mm)	lambda	specYield	alphaGW
1	0.2	2.1	0.313901	0.06805	0.213901	20	100	0.33	0.245851	0.01
2	0.2	2.1	0.289161	0.080419	0.189161	20	100	0.33	0.208742	0.01
3	0.2	2.1	0.322461	0.06377	0.222461	20	100	0.33	0.258691	0.01
4	0.2	2.1	0.295236	0.077382	0.195236	20	100	0.33	0.217854	0.01
5	0.2	2.1	0.338372	0.055814	0.238372	20	100	0.33	0.282557	0.01
6	0.2	2.1	0.272875	0.088563	0.172875	20	100	0.33	0.184312	0.01
7	0.2	2.1	0.303253	0.073374	0.203253	20	100	0.33	0.229879	0.01
8	0.2	2.1	0.28909	0.080455	0.18909	20	100	0.33	0.208634	0.01
9	0.2	2.1	0.315647	0.067177	0.215647	20	100	0.33	0.24847	0.01
10	0.2	2.1	0.3257	0.06215	0.2257	20	100	0.33	0.26355	0.01
11	0.2	2.1	0.268375	0.090812	0.168375	20	100	0.33	0.177563	0.01
12	0.2	2.1	0.254548	0.097726	0.154548	20	100	0.33	0.156822	0.01
13	0.2	2.1	0.262164	0.093918	0.162164	20	100	0.33	0.168246	0.01
14	0.2	2.1	0.282027	0.083986	0.182027	20	100	0.33	0.198041	0.01
15	0.2	2.1	0.278619	0.085691	0.178619	20	100	0.33	0.192928	0.01
16	0.2	2.1	0.251348	0.099326	0.151348	20	100	0.33	0.152022	0.01
17	0.2	2.1	0.260748	0.094626	0.160748	20	100	0.33	0.166122	0.01
18	0.2	2.1	0.324071	0.062964	0.224071	20	100	0.33	0.261107	0.01

Figure 130: Example of soil parameters file.

Surface Water Storage

Parameters of surface water storage such as lakes and reservoirs are defined in the CSV file **lake.csv** located in the **lake** folder. Similar to the soil file, the lake file consists of one header line followed by one line per lake/storage structure. Required parameters are described as follows:

- **Sub** – Id of the sub-catchment where the lake/storage is located;
- **LakAMax** – Maximum area of storage (km²);
- **LakvA** – Exponent parameter relating storage volume and area;
- **LakVDead** – Dead volume of storage (ML);
- **LakVAMax** – Storage volume at maximum lake area, LakAMax (ML);
- **LakVMax** – Maximum storage volume (ML);
- **LakQMax** – Discharge rate at maximum storage (ML/day);
- **LakvQ** – Parameter relating downstream discharge to storage level (-);

- **NAME** – Text containing the name of the storage (optional).

An example of the lake.csv file is presented below:

SUB	LakAMax	LakvA	LakVDead	LakVAmx	LakVMax	LakQMax	LakvQ	NAME
1	0.345501	0.5	345.5	5182.5	5182.5	259.1	1	Storage
2	0.774878	1.5	774.9	11623.2	11623.2	581.2	1	Storage
4	1.1775	1.5	1177.5	17662.5	17662.5	883.1	1	Storage
8	0.344112	1.5	344.1	5161.7	5161.7	258.1	1	Storage
10	0.170432	1.5	170.4	2556.5	2556.5	127.8	1	Storage
11	0.215963	1.5	216	3239.4	3239.4	162	1	Storage
12	0.142023	1.5	142	2130.3	2130.3	106.5	1	Storage
17	0.019627	1.5	19.6	294.4	294.4	14.7	1	Storage
24	0.771532	1.5	771.5	11573	11573	578.6	1	Storage
25	0.632395	1.5	632.4	9485.9	9485.9	474.3	1	Storage
27	0.29937	1.5	299.4	4490.6	4490.6	224.5	1	Storage
28	1.100976	1.5	1101	16514.6	16514.6	825.7	1	Storage
30	0.244616	1.5	244.6	3669.2	3669.2	183.5	1	Storage
31	1.151989	1.5	1152	17279.8	17279.8	864	1	Storage
33	82.68657	1.5	82686.6	1240299	1240299	62014.9	1	Storage
37	1.585266	1.5	1585.3	23779	23779	1188.9	1	Storage

Figure 131: Example of “lake”/storage parameters file.

Land Use

Land use settings are restricted to vegetation parameters in LASCAM. Vegetation parameters are defined in six CSV files located in the **vegetation** folder, namely:

- **grn.csv** – contains information on the deep-rooted vegetation fraction;
- **rip.csv** – contains information on riparian vegetation fraction;
- **imp.csv** – contains information on the sub-catchment impervious area fraction;
- **max.csv** – contains the maximum LAI values for each sub-catchment;
- **sc.csv** – contains sub-catchment leaf area indices (LAI’s); and
- **sea.csv** – contains scaling factor describing seasonal variation of LAI.

The file **grn.csv** consists of two columns, one for the sub-catchment ID and the second for the fraction of deep rooted (ie. remnant) vegetation (%). The first line is a header with the column identifiers with one additional line for each simulated sub-catchment. An example of this file is presented below:

Number	Value
1	14.9
2	6.4
3	16.7
4	0.1
5	50.9
6	4
7	30.3
8	0.1
9	10.4
10	34.4
11	0.2
12	0
13	2.5
14	0

Figure 132: Example of remnant vegetation parameter file.

The **imp.csv** file has a similar structure to the **grn.csv** file, with the first column containing the sub-catchment identifier and the second column containing the impervious fraction (%). A column identifier header is followed by one additional line per sub-catchment, as illustrated below:

Catchmen	Value
1	2
2	2
3	2
4	2.7
5	2
6	2
7	2
8	2
9	2
10	2

Figure 133: Example of percentage of impervious area vegetation parameter file.

The files **max.csv** and **rip.csv** have the same formats of **imp.csv** files. The **sc.csv** file contains the spatially distributed values for Leaf Area Index (LAI). It consists of one header line with the column identifier and one additional line for each sub-catchment, containing the following parameters:

- **Catchment** – refers to the sub-catchment ID;
- **GRN** – Leaf Area Index for the deep-rooted vegetation; and
- **RIP** – Leaf Area Index for the riparian vegetation.

An example of the **sc.csv** file is present below:

Catchmen	GRN	RIP
1	1.08	1.08
2	0.81	0.81
3	0.87	0.87
4	0.77	0.77
5	1.9	1.9
6	0.87	0.87
7	0.88	0.88
8	0.92	0.92
9	0.92	0.92
10	0.96	0.96
11	0.74	0.74
12	0.83	0.83

Figure 134: Example of percentage of deep and riparian vegetation parameter file.

Rainfall

Rainfall data is defined in three files. The first two files are **rain.csv** and **siteselection.xls** and are located in the folder rainfall. The file **rain.csv** contains the raw observed data from rainfall stations and consists of one header line with one additional line per rainfall record. Inputs required for each rainfall record are:

- **X** – eastern coordinate of the rainfall station;
- **Y** – northern coordinate of the rainfall station;
- **Station_Number** – rainfall station identification number;
- **Date_Time** – date and time of the rainfall record;
- **Year1** – year of the rainfall record;
- **Month1** – month of the rainfall record;
- **Day1** – day of the rainfall record; and
- **Precip** – recorded precipitation in mm.

Rainfall records are required to be in a daily basis. The records must also be ordered by station number and date. An example of the file is included below:

X	Y	Station_Number	Date_Time	Year1	Month1	Day1	Precip
757756.6	6649898	53026	01/01/1990	1990	1	1	0
757756.6	6649898	53026	02/01/1990	1990	1	2	0
757756.6	6649898	53026	03/01/1990	1990	1	3	0
757756.6	6649898	53026	04/01/1990	1990	1	4	0
757756.6	6649898	53026	05/01/1990	1990	1	5	0
757756.6	6649898	53026	06/01/1990	1990	1	6	0
757756.6	6649898	53026	07/01/1990	1990	1	7	0
757756.6	6649898	53026	08/01/1990	1990	1	8	0
757756.6	6649898	53026	09/01/1990	1990	1	9	0
757756.6	6649898	53026	10/01/1990	1990	1	10	0
757756.6	6649898	53026	11/01/1990	1990	1	11	0
757756.6	6649898	53026	12/01/1990	1990	1	12	0
757756.6	6649898	53026	13/01/1990	1990	1	13	0
757756.6	6649898	53026	14/01/1990	1990	1	14	0
757756.6	6649898	53026	15/01/1990	1990	1	15	0
757756.6	6649898	53026	16/01/1990	1990	1	16	0
757756.6	6649898	53026	17/01/1990	1990	1	17	0

Figure 135: Example rainfall input file.

The file **siteselection.xls** contains the stations that will be used by LASCAM, if only a sub-set of the rainfall record is planned to be used. This file is redundant if the option **Use User Defined Rain** in the file **runtime.xls** is set to "no".

The format of **siteselection.xls** consists of a header line with column identifiers, followed by one line per rainfall station that will be used in model. The followed inputs are required for each station:

- **Site ID** – Rainfall station Id. It must match the **Station_Number** field present in the **rain.csv** file;
- **Y** – northern coordinate of the rainfall station;
- **X** – eastern coordinate of the rainfall station;
- **Projection** – coordinate system used for the rainfall station coordinates

An example of the site selection file is presented in the following figure:

Site ID	Y	X	Projection
53026	6649898	757757	UTM
53034	6665784	723831	UTM
54003	6633786	846923	UTM
55000	6573844	868771	UTM
55006	6494862	806880	UTM
55024	6562915	812045	UTM
55043	6486439	823514	UTM
55045	6546590	788897	UTM
55049	6508161	849470	UTM
55069	6516630	787454	UTM
55136	6565924	915140	UTM
55140	6563356	854517	UTM
55143	6561153	888231	UTM
55176	6534680	889005	UTM
55239	6499982	830297	UTM
55274	6589907	828862	UTM
55276	6578158	833950	UTM
55311	6540048	863834	UTM
56075	6558148	924005	UTM

Figure 136: Example rainfall gauge location input file.

The file **climate.csv** is present in the climate folder and contains annual averages for rainfall and evaporation for each sub-catchment. The format of the **climate.csv** file is described in the following section.

Evaporation

Parameters required for evaporation are restricted to a single value of average annual evaporation per sub-catchment. These parameters are set in the **climate.csv** file (same file where average rainfall per catchment is defined) located in the **climate folder**. The file consists of one header line, followed by one line for each sub-catchment, with the following parameters:

- **Link** – represents the sub-catchment ID;
- **Evap** – average annual evaporation (mm);
- **Rai** – average annual rainfall (mm);

The following figure illustrates the **climate.csv** format:

link	Evap	Rai
1	2000	592.96
2	2000	567.7
3	2000	611.3
4	2000	533.35
5	2000	831.23
6	2000	570.51
7	2000	554.82
8	2000	572.2
9	2000	642.43
10	2000	663.65
11	2000	625.02

Figure 137: Example rainfall gauge location input file.

Time Settings

LASCAM models are simulated using a daily time step. Time settings are restricted to the beginning and end of the simulation dates. These settings can be accessed and modified in the spreadsheet **runtime.xls** located in the **master** folder.

The fields **StartDate** and **EndDate** (displayed in yellow in the next figure) control the dates for beginning and end of the simulation, respectively. The fields **Start Flow Input** and **End Flow Input** control the period in which observation data will be used for calibration purposes. The use of sub-sets is useful in some situations where an initial simulation period is assigned to the model stabilize numerically to initial conditions before sensible results can be provided, or for assigning calibration versus validation periods.

Runtime				
StartDate	EndDate			
01/01/2006	31/12/2009			
Start Flow Input				
End Flow Input				
01/01/1990	01/01/2010			
OutputDirectory				
final_simulation				
Convert Raw Data	Use User Defined Rain	Run Calibrator	Monthly B Store	Run Validation
yes	no	no	yes	yes
Zone				
55H				

Figure 138: Example master input file.

Specific Settings

Other specific run settings can also be found in the **runtime.xls** file and are highlighted in yellow in the screen print below. The specific run settings are:

- **OutputDirectory** – defines the name of the output directory which is created (when it does not exist) during the LASCAM run from Matlab;
- **Convert Raw Data** – defines whether the rainfall and observation inputs need to be converted to LASCAM binary format prior to the model run. The raw data conversion can be time consuming depending on the amount of data involved in the simulation, so if the data has been previously converted, it is recommended to set this option to “no”;

- **Use User Defined Rain** – defines the rainfall data to be used in the simulation. If this option is set as “no”, LASCAM will use the entire rainfall dataset for generation of spatially distributed values. If the option is set as “yes”, only the rainfall stations specified in the **siteselection.xls** spreadsheet will be used;
- **Run Calibrator** – defines whether the calibrator is to be used. When set to “no”, LASCAM will conduct one single run with the specified parameters. When set to “yes”, LASCAM will be run many times and attempt to obtain the best match between the model results and observation data varying the parameters specified in the file **calibration.dat**;
- **Monthly B Store** – defines whether a specific output containing infiltration, evaporation and net balance for each sub-catchment is to be written. If set to “yes” Matlab post-processing will generate a series of charts and spreadsheets for each sub-catchment. If set to “no”, output will be ignored; and
- **Run Validation** – defines whether additional plots comparing observed and simulated flow rates are generated.

Runtime				
StartDate	EndDate			
01/01/2006	31/12/2009			
Start Flow Input End Flow Input				
01/01/1990	01/01/2010			
OutputDirectory				
final_simulation				
Convert Raw Data	Use User Defined Rain	Run Calibrator	Monthly B Store	Run Validation
yes	no	no	yes	yes
Zone				
55H				

Figure 139: Example configuration input file.

LASCAM Post Processing Results

Once the input files are set, the model can be run from Matlab. Firstly the current folder of Matlab must be set to the **matlab** folder described in section 3.1. To change the current folder, type the folder location in the **Current Folder**: combo box located at the top of Matlab Window, or press the button  located next to it, as presented in the following figure.

After selecting the current folder, go to the **Command Window** in Matlab, type **lascar** and press Enter. This command starts the Matlab scripts that will translate the input files and call the LASCAM executable. Charts and plots will be displayed showing the observation data as the simulation goes and, once the run is finished, another series of plots will be displayed.

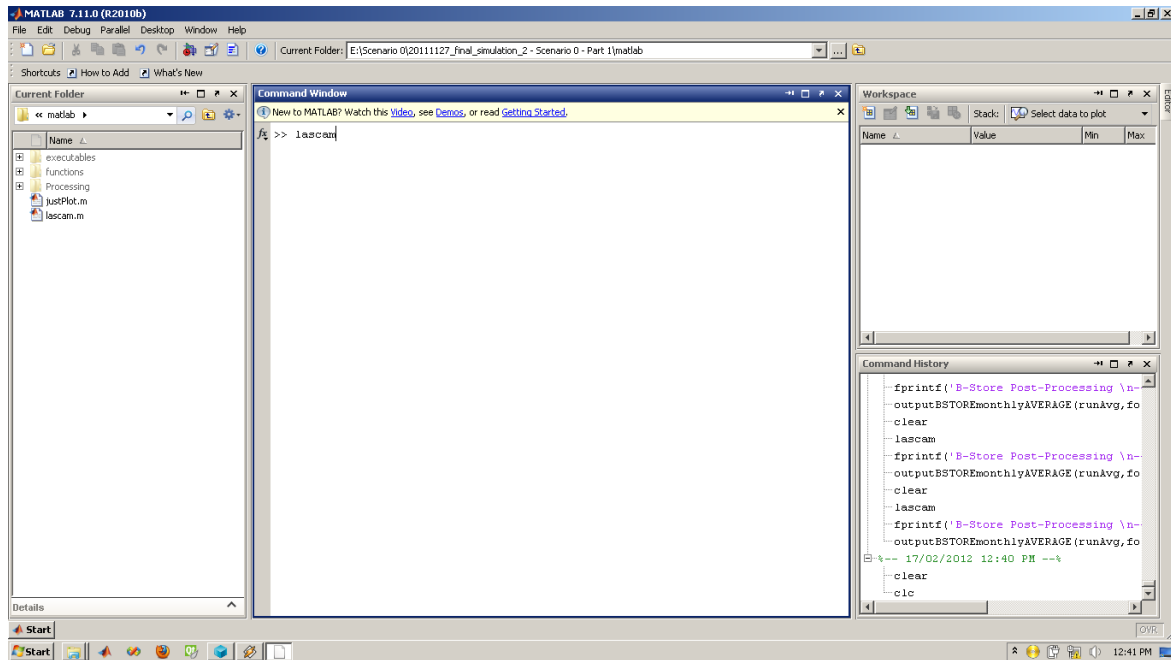


Figure 140: MatLab command window.

All the plots and spreadsheets generated by Matlab post processing scripts are saved in the subfolder **2.post** located within the **Output** folder. The **2.post** folder contains 3 subfolders, namely:

- BStore;
- Flow; and
- Validation.

The **BStore** folder stores the results regarding infiltration and evaporation rates into the deep aquifer. The **CSV** subfolder contains a series of spreadsheets. The **Master_Bstore.xlsx** file contains monthly average values for evaporation and recharge into the aquifer. This file contains the data for all the catchments and entire simulated period. An example of the file is illustrated below.

Subcatchment	Year	Month	Recharge	Evaporation	Recharge - Evaporation
1	1990	1	1.1569	54.5519	-53.395
1	1990	2	1.0381	19.1689	-18.1308
1	1990	3	1.1419	27.8544	-26.7125
1	1990	4	1.0982	1.866	-0.7678
1	1990	5	1.1281	1.8352	-0.7071
1	1990	6	1.0852	0.0117	1.0735
1	1990	7	1.1149	0.0071	1.1078
1	1990	8	1.108	0.0202	1.0878
1	1990	9	1.066	4.8537	-3.7877
1	1990	10	1.0949	36.2512	-35.1563
1	1990	11	1.0533	54.6288	-53.5755
1	1990	12	1.0821	53.9222	-52.8401
1	1991	1	1.0763	30.0574	-28.9811
1	1991	2	0.9673	29.8007	-28.8334
1	1991	3	1.0658	30.0377	-28.9719
1	1991	4	1.0269	15.5213	-14.4944
1	1991	5	1.0559	2.1266	-1.0707
1	1991	6	1.0177	0.0062	1.0115
1	1991	7	1.0467	0.0057	1.041
1	1991	8	1.0424	0.0382	1.0042
1	1991	9	1.004	15.1126	-14.1086
1	1991	10	1.033	51.2204	-50.1874
1	1991	11	0.9949	48.756	-47.7611

Figure 141: Example of an output file showing monthly averages of relevant hydrological processes.

In addition to the **Master_Bstore.xlsx** file, additional files containing individual values of recharge and evaporation for each sub catchment are created. The general file name is **scXXX_store.xlsx**, where XXX is the corresponding catchment number. These files have the same format as the master file.

The **Flow** folder contains charts and spreadsheets comparing results from LASCAM against observation data. The subfolder **Plots** contain charts with hydrographs of simulated and observed flow rates, as illustrated below. One plot for each observation point is generated.

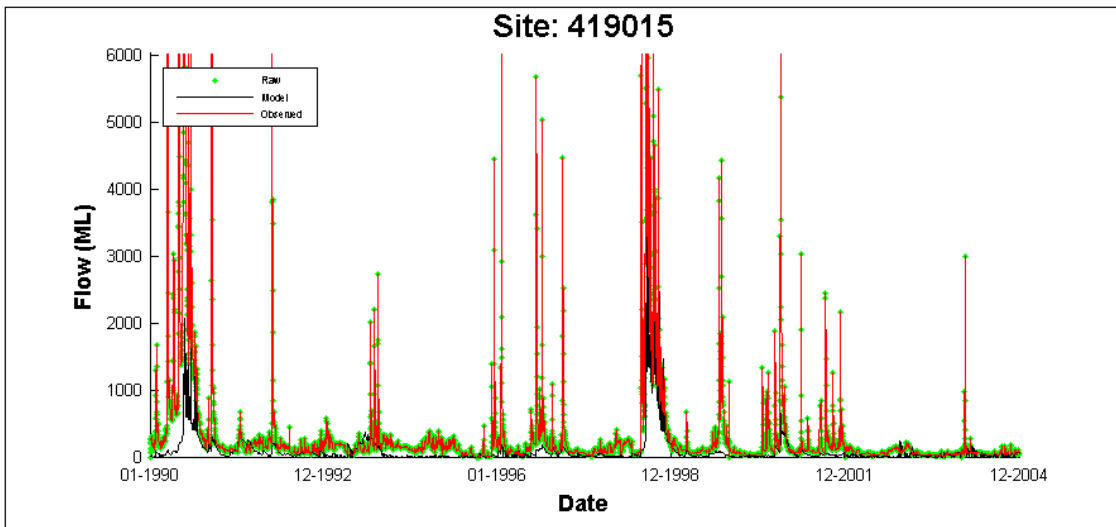


Figure 142: Example of output chart (daily values).

The **CSV** folder within **Flow** contains spreadsheets containing the data used to generate the plots. The file **masterFlow.xlsx** contains all the observation data and corresponding LASCAM result values. The spreadsheet contains 5 columns namely:

- **StationID**: contains the name of the observation point;
- **X**: contains the eastern coordinate of the observation;
- **Y**: contain the northern coordinate of the observation;
- **Raw**: contains the observation data (in ML/day);
- **Model**: contains the model results (ML/day);

Additional files with the same format are generated individually for each station. The file name corresponds to the station ID. The format of the flow files is illustrated below:

StationID	X	Y	Date	Raw	Model
419015	887628.7	6543187	01/01/1990	0	0
419015	887628.7	6543187	02/01/1990	60.6	0
419015	887628.7	6543187	03/01/1990	127.6	0
419015	887628.7	6543187	04/01/1990	278.2	0
419015	887628.7	6543187	05/01/1990	201.6	0
419015	887628.7	6543187	06/01/1990	226	0
419015	887628.7	6543187	07/01/1990	226	0
419015	887628.7	6543187	08/01/1990	248.6	0
419015	887628.7	6543187	09/01/1990	320	8.1216
419015	887628.7	6543187	10/01/1990	202.4	13.77216
419015	887628.7	6543187	11/01/1990	174.6	22.00608
419015	887628.7	6543187	12/01/1990	184.2	20.89152
419015	887628.7	6543187	13/01/1990	180.6	20.66688
419015	887628.7	6543187	14/01/1990	177.6	19.63872
419015	887628.7	6543187	15/01/1990	172	18.84384
419015	887628.7	6543187	16/01/1990	187.2	18.37728
419015	887628.7	6543187	17/01/1990	198.6	18.46368
419015	887628.7	6543187	18/01/1990	144.2	18.16128
419015	887628.7	6543187	19/01/1990	137	18.13536
419015	887628.7	6543187	20/01/1990	137	17.68608
419015	887628.7	6543187	21/01/1990	141	16.75296
419015	887628.7	6543187	22/01/1990	145	15.84576
419015	887628.7	6543187	23/01/1990	144.6	14.9904
419015	887628.7	6543187	24/01/1990	143.2	0
419015	887628.7	6543187	25/01/1990	161.2	0

Figure 143: Additional output files.

The **validation** folder contains additional plots used to assess the consistency of model results at catchments where observations are present. The subfolder **Plots** contains the following plots:

- **Annual Runoff** – which compares simulated and observed runoff values in an yearly basis;
- **Cumulative Total** – plotting cumulative observed and simulated runoff rates;
- **Flow Duration** – which compares simulated and observed values of runoff against percentage of time equalled or exceeded;
- **Monthly Average** – which plot monthly averaged values for observed and simulated runoff rates;
- **Monthly Flow** – which plot monthly simulated runoff values against corresponding monthly averaged observations;
- **Monthly Average Recharge** – which presents monthly average infiltration values (mm).
- **Stores** – which present time series of storage volumes for the A, B, D and F stores (as defined in LASCAM) in millimetres;

These 7 plots are generated for each observation station. The files are names as mentioned above, with the station name append at the end. Illustrative examples of the **Annual Runoff** and **Stores** plot are presented below.

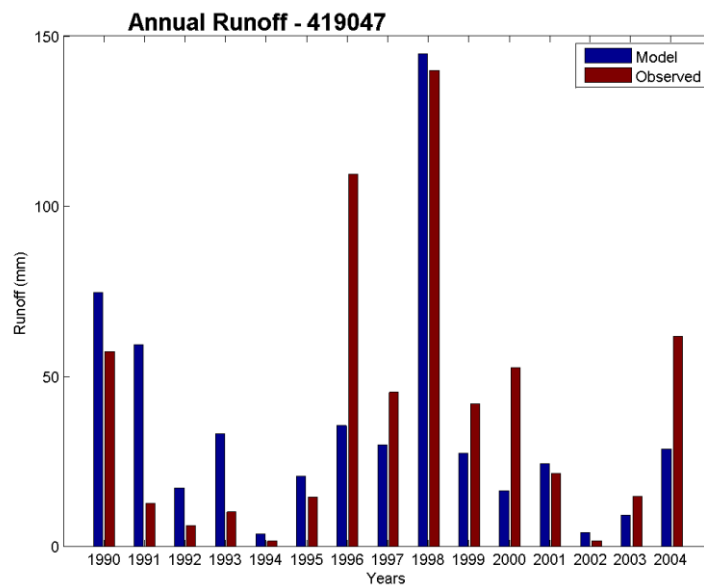


Figure 144: Example of output chart (monthly values).

Appendix J: Example of Input Files

Future Climate

To test the hydrological response of predicted changes in rainfall.

Rain.csv

X	Y	Station_Number	Date_Time	Year	Month	Day	Precip
551437.1	6359652	200	2/05/2007	2007	5	2	0.2
551437.1	6359652	200	3/05/2007	2007	5	3	0
551437.1	6359652	200	4/05/2007	2007	5	4	0
551437.1	6359652	200	5/05/2007	2007	5	5	0
551437.1	6359652	200	6/05/2007	2007	5	6	0
551437.1	6359652	200	7/05/2007	2007	5	7	0
551437.1	6359652	200	8/05/2007	2007	5	8	0
551437.1	6359652	200	9/05/2007	2007	5	9	0
551437.1	6359652	200	10/05/2007	2007	5	10	0

SiteSelection.xls

Site ID	Y	X	Projection
200	6367660	554657.4852	UTM
200	6356936	565520.2932	UTM
300	6364815	549217.9	UTM
400	6360244	562482.7795	UTM
500	6358857	557651.8904	UTM
1000	6372748	546747.67	UTM
400	6358557	562945.8013	UTM
400	6360806	568369.7705	UTM
200	6366483	556780.7707	UTM
200	6368388	551991.8028	UTM
200	6359218	566115.6069	UTM

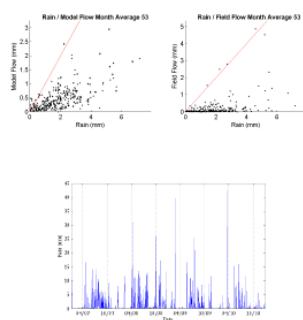


Figure 145: Example climate input csv files.

Re-vegetation

To test the percentage of area allocated to deep-rooted vegetation. The period for total establishment of plant biomass and water consumption is user-defined. In all simulations, this period was 10 years (Figure 146).

Runtime		Mallee Set-up	
StartDate	EndDate	StartDate	EndDate
1/01/2005	2/02/2012	01/01/1979	01/01/1999
Start Flow Input		GRN Increase %	RIP Increase %
2/01/2005	2/01/2013	0	0

$$F_{\text{deeprooted}}(t) = F_{\text{revegetat}} + (1 - F_{\text{revegetat}}) \times D_{\text{mallee}} \times I(t)$$

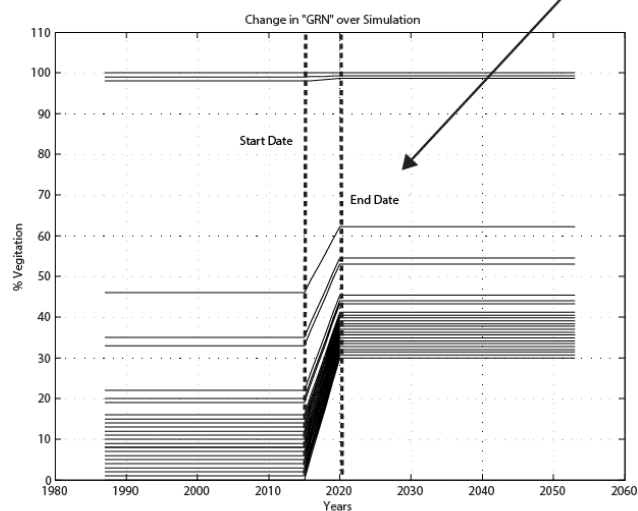


Figure 146: Re-vegetation input file showing how a user can set rate and extent of revegetation.

Appendix L: List of Acronyms

Acronym	Description
DEC	Department of Environment and Conservation
BoM	Bureau of Meteorology
DoW	Department of Water
DPaW	Department of Parks and Wildlife
SWWA	South-west of Western Australia
AEP	Annual Exceedance Probability
EC	Electrical Conductivity
DBH	Diameter at Breast Height
IFD	Intensity–Frequency–Duration
IC	Initial Condition
ASL	Above Sea Level
OM	Organic Matter
DI	Dryness Index
GHG	Greenhouse Gas
TEC	Threatened Ecological Communities
SW-GW	Surface Water - Groundwater
GCM	General Circulation Model
TDS	Total Dissolved Salts
LAI	Leaf Area Index